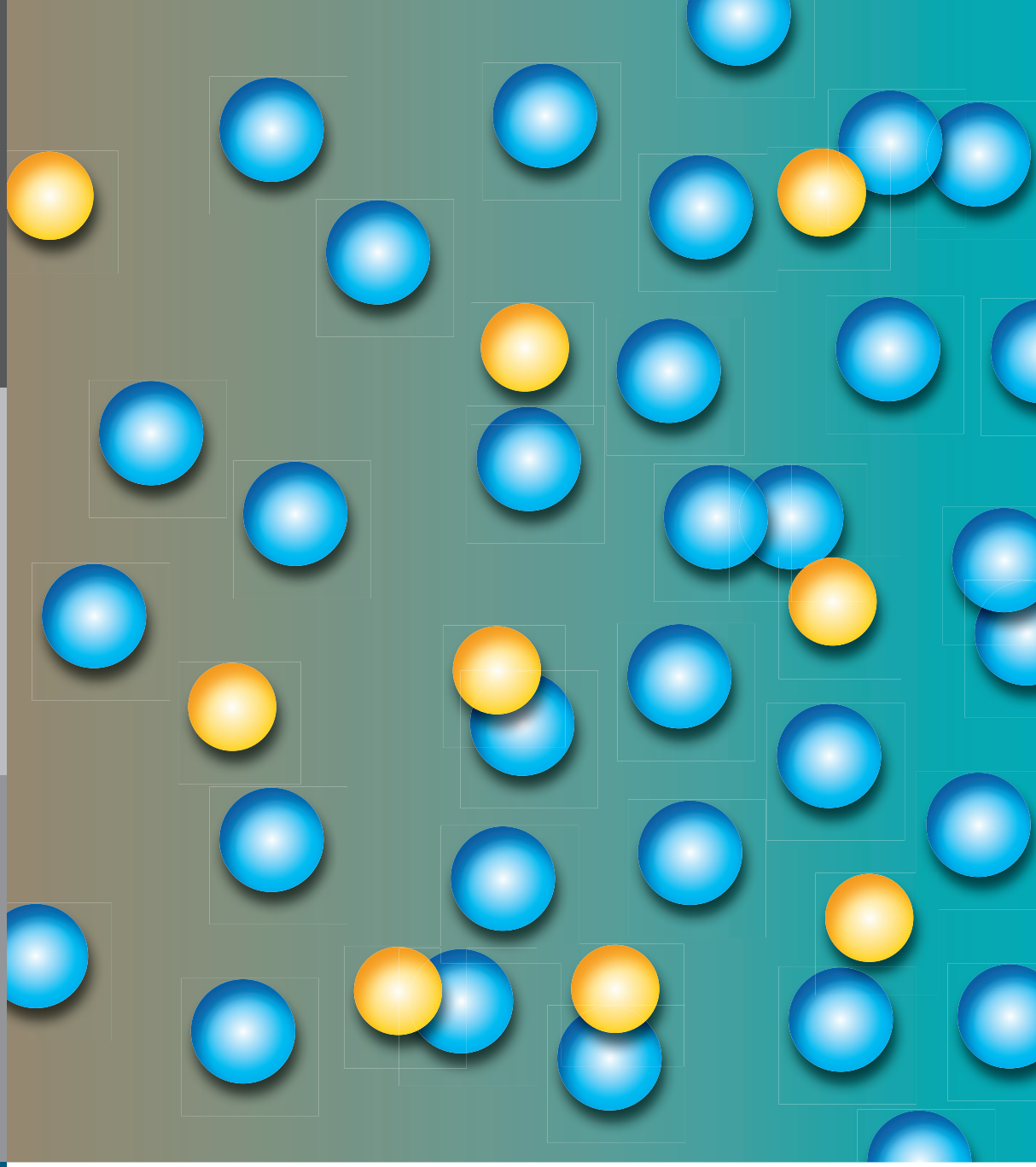

8th International Meeting on Thermodiffusion

Thermal Nonequilibrium

Lecture Notes

Mitglied der Helmholtz-Gemeinschaft

JÜLICH
FORSCHUNGSZENTRUM

Schriften des Forschungszentrums Jülich
Reihe Schlüsseltechnologien / Key Technologies Band / Volume 3

Forschungszentrum Jülich GmbH
Institute of Solid State Research
Soft Matter

Lecture Notes of the
8th International Meeting on Thermodiffusion

S. Wiegand, W. Köhler, J.K.G. Dhont (Eds.)

Thermal Nonequilibrium

This Thermodiffusion Meeting has been organized
by the Institute of Solid State Research
and the University of Bayreuth
in Bonn at the Gustav-Stresemann-Institute
9 – 13 June 2008.

In collaboration with
European Group on Thermodiffusion Research and
Deutsche Forschungsgemeinschaft (DFG)

Schriften des Forschungszentrums Jülich
Reihe Schlüsseltechnologien / Key Technologies Band / Volume 3

ISSN 1866-1807 ISBN 978-3-89336-523-4

Bibliographic information published by the Deutsche Nationalbibliothek.
The Deutsche Nationalbibliothek lists this publication in the Deutsche Nationalbibliografie; detailed bibliographic data are available in the Internet at http://dnb.d-nb.de.

Publisher and Distributor:	Forschungszentrum Jülich GmbH Zentralbibliothek, Verlag D-52425 Jülich phone:+49 2461 61-5368 · fax:+49 2461 61-6103 e-mail: zb-publikation@fz-juelich.de Internet: http://www.fz-juelich.de/zb
Cover Design:	Grafische Medien, Forschungszentrum Jülich GmbH
Printer:	Grafische Medien, Forschungszentrum Jülich GmbH
Copyright:	Forschungszentrum Jülich 2008

Schriften des Forschungszentrums Jülich
Reihe Schlüsseltechnologien / Key Technologies Band / Volume 3

ISSN 1866-1807
ISBN 978-3-89336-523-4

Preface

This book, “Thermal Nonequilibrium”, is a compilation of the papers presented during the Eighth International Meeting on Thermodiffusion (IMT8) from June 9 to June 13, 2008, at the Gustav-Stresemann-Institut in Bonn, Germany. The conference is jointly organized by the Forschungszentrum Jülich and the University of Bayreuth.

IMT8 is the eighth conference in the IMT series that started out in 1994 in Toulouse with IMT1 and then continued on a biannual basis: IMT2 (Pau 1996), IMT3 (Mons 1998), IMT4 (Bayreuth 2000), IMT5 (Lyngby 2002), IMT6 (Varenna 2004), and IMT7 (San Sebastian 2006). While the first meetings originated from Francophone countries, the conference quickly became international. Now, the objective of the IMT conferences is to bring together researchers in the field of thermodiffusion from all over the world and to provide a regular platform for scientific discussion and exchange.

The participating researchers represent a substantial fraction of the scientific community currently working in the field of thermodiffusion, and this compilation gives an overview of the current state of research in these active groups. Following the structure of the meeting, the book is organized into sections that loosely define the topics of the contributions: simple fluids, polymers, colloids, convection, and simulation.

We want to thank all authors for timely submitting well formatted contributions required for the compilation of this book. We also express our thanks to many people who helped during the preparation of the conference, especially Ursula Funk-Kath, Marie Göcking and Dorothea Henkel, who shouldered much of the organizational burden such as the design of the WEB pages, preparation of the abstract book and this proceeding volume. The reasonable conference fee with a reduction for young researchers would not have been possible without financial support from the Forschungszentrum Jülich and the Deutsche Forschungsgemeinschaft (DFG).

Simone Wiegand
Werner Köhler
Jan K. G. Dhont

Contents

1 Simple Fluids **1**

1.1 New approach in the prediction of the thermal diffusion factor in associating mixtures 3
Alireza Abbasi, M. Ziad Saghir and Masahiro Kawaji

1.2 Development of a new high pressure thermodiffusion cell 9
H. Bataller, C. Miqueu, F. Plantier, J.L. Daridon, Z. Saghir, F. Dubois and S. Van Vaerenbergh

1.3 Thermal diffusion values for some alkane mixtures: A comparison between thermogravitational column and thermal diffusion forced Rayleigh scattering 15
P. Blanco, P. Polyakov, M. M. Bou-Ali and S. Wiegand

1.4 Determination of the thermal diffusion coefficient in n-alkane mixtures: empirical correlations 23
P. Blanco, M. M. Bou-Ali, J. K. Platten, P. Urteaga, J. A. Madariaga and C. Santamaría

1.5 Thermal diffusion in multicomponent mixtures: theoretical modeling and experiments 29
A. Firoozabadi

1.6 Isotope and isomer effect in thermal diffusion of binary liquid mixtures 35
S. Hartmann, A. Königer and W. Köhler

1.7 The theory of the thermodiffusion column with arbitrary cross-section 41
I. Hodor

1.8 Comparison between theoretical model and experimental data of thermodiffusion coefficients for binary and ternary hydrocarbon mixtures and water-alcohol mixtures 49
T. J. Jaber, Y. Yan, A. Abbasi and M.Z. Saghir

1.9 Study of the thermal diffusion behavior of simple and associated mixtures 57
P. Polyakov and Simone Wiegand

1.10 Phase demixing in non-isothermal binary liquids 63
S. N. Semenov and M. E. Schimpf

1.11 Thermogravitational technique at high pressure for liquid mixtures 71
P. Urteaga, M.M. Bou-Ali and P. Blanco

1.12 Thermodiffusion coefficient (D_T) for binary hydrocarbon mixtures at high pressures 77
P. Urteaga, F. Plantier, M.M. Bou-Ali and H. Bataller

1.13 Theoretical modeling and experimental measurement of thermodiffusion coefficients in binary n-alkane mixtures 83
Y. Yan, P. Blanco, M.Z. Saghir and M. Bou-Ali

2 Polymers **89**

2.1 Numerical model of unsteady flows of melt polymer in cylindrical ducts 91
K. Gueraoui, M. Taibi, S. Chtioui, Y. M. Haddad and G. Zeggwagh

2.2 Ludwig-Soret Effect for Aqueous and Non-aqueous Solutions of Polysaccharide 97
Yuki Kishikawa, Rio Kita, Hartmut Kriegs and Simone Wiegand

2.3 Thermodiffusion Driven Patterns in a Polymer Blend Close to the Critical Point 103
A. Krekhov, F. Schwaiger, S. Frank, A. Voit and W. Köhler

2.4 On thermodynamic approach to mass transport 109
S. N. Semenov and M. E. Schimpf

2.5 Theory of strong temperature dependence in thermophoresis 117
S. N. Semenov and M. E. Schimpf

2.6 The crossover of transport properties of polymer solutions from the high polymer limit to finite chain length 125
D. Stadelmaier, T. Pollak, J. Rauch, M. Hartung and W. Köhler

3 Complex fluids and ternary systems **131**

3.1 The thermodiffusion coefficients in the ternary mixture THN-IBB-nC12 with mass fraction c_i =1/3 and molar fraction x_i =1/3 at 25°C 133
P. Blanco, M. M. Bou-Ali, J. K. Platten, D. Alonso de Mezquia, P. Urteaga, J.A. Madariaga and C. Santamaría

3.2 Remarks on the analysis method for determining the mass fractions in ternary mixtures of alkanes 141
P. Blanco, M. M. Bou-Ali, J. K. Platten, D. Alonso de Mezquia and P. Urteaga

3.3 Soret effect of nonionic surfactants in water studied by different transient grating setups 147
S.Datta, H.Ning, T.Sottmann and S.Wiegand

3.4 Soret-driven concentration fluctuations in a chemically reacting liquid mixture 153
José M. Ortiz de Zárate, Jan V. Sengers, Dick Bedeaux and Signe Kjelstrup

4 Convection and confinement **161**

4.1 Localized steady states in binary fluid convection 163
Oriol Batiste, Isabel Mercader, Arantxa Alonso and Edgar Knobloch

4.2 Thermoosmotic transfer of ferrocolloids through a capillary porous layer in the presence of transversal magnetic field 169
Elmars Blums, Gunars Kronkalns and Michail Maiorov

4.3 Quasiperiodic gravitational modulation of convection in magnetic fluid 175
T. Boulal, S. Aniss and M. Belhaq

4.4 Theoretical determination of effective thermodiffusion coefficients, application to the description of mass transfer in porous media 181
H. Davarzani, J. Chastanet, M. Marcoux and M. Quintard

4.5 Thermal convection of binary mixes in thin channels 187
V.A. Demin and A.F. Glukhov

4.6 Linear stability analysis of the Soret-driven monocellular flow in a horizontal porous layer subjected to vertical vibrations 197
B. Elhajjar, A. Mojtabi and M. C. Charrier-Mojtabi
4.7 Diffusive mass transport under vibrations 203
Yu. Gaponenko and V. Shevtsova
4.8 Numerical modeling of two-dimensional natural convection 209
K. Gueraoui, M. Taibi, N. Dahmani, A. Mrabti, Y. M. Haddad and G. Zeggwagh
4.9 Theoretical and Numerical Model for the Lowest Layers of the Atmosphere 215
K. Gueraoui, M. Taibi, I. Aberdane, A. Dhiri, Y. M. Haddad and G. Zeggwagh
4.10 Gain of Soret separation in binary mixture due to vibrations 223
D. E. Melnikov and V.M. Shevtsova
4.11 Spatio-temporal dynamics near the onset of convection for binary mixtures in cylindrical containers 229
Isabel Mercader, Arantxa Alonso and Oriol Batiste
4.12 Marangoni convection in binary and nano-fluids in the presence of the Soret effect 235
Alla Podolny, Alex Nepomnyashchy and Alex Oron
4.13 Anomalous diffusion in porous media 243
J. Prehl, K. H. Hoffmann, M. Hofmann, G. Rünger and S. Tarafdar
4.14 Stability of multicomponent convection in vertical layer with thermal diffusion 249
I. Ryzhkov and V. Shevtsova

5 Colloids **255**

5.1 Single-particle thermal diffusion of charged colloids: double-layer theory in a temperature gradient 257
J.K.G. Dhont and W.J. Briels
5.2 What Soret can learn from Seebeck 261
E. Bringuier
5.3 The Dynamics for the Soret Motion of a Charged Spherical Colloid 269
S. N. Rasuli and R. Golestanian

6 Simulations **275**

6.1 New theoretical model for thermal diffusion: Prigogine's approach revisited! 277
P.-A. Artola, B. Rousseau and G. Galliéro
6.2 Molecular description: influence on thermodiffusion in non-polar simple mixtures 283
Guillaume Galliero
6.3 Non-isothermal gravitational segregation by molecular dynamics simulations 291
Guillaume Galliero and François Montel
6.4 Single particle thermodiffusion by molecular dynamics simulations: application to simple Lennard-Jones mixtures and nanofluids 299
Guillaume Galliero and Sebastian Volz

Simple Fluids

New approach in the prediction of the thermal diffusion factor in associating mixtures

Alireza Abbasi[1,2], M. Ziad Saghir[1] and Masahiro Kawaji[2]

[1]Department of Mechanical and Industrial Engineering, Ryerson University, 350Victoria St.,Toronto, Ontario M5B2K3, Canada
[2]Department of Chemical Engineering, University of Toronto, Toronto, Ontario, M5S3E5, Canada

E-mail: zsaghir@ryerson.ca

Abstract

The PCSAFT equation of state, by using two adjustable parameters calculated from experimental data, is used for evaluating thermodiffusion coefficient for different water-alcohol mixtures. One of the adjustable parameters, the binary interaction parameters for the mixture of interest under a range of temperatures has been optimized by availability of experimental vapor–liquid equilibrium. A new equation was developed for predicting ratio of evaporation energy to viscous energy (second adjustable parameter) based on proposed viscous energy equation. Particularly, this approach is implemented to predict the sign change of thermal diffusion factor in associating mixtures, which has been a major step forward in thermodiffusion studies for associating mixtures. Firoozabadi's thermodiffusion model combined with PCSAFT equation of state was applied to calculate the Soret coefficient, as well as the thermodiffusion coefficient.

1 Introduction

For years, various attempts have been made to generate reliable thermodiffusion coefficient models for binary mixtures. However the prediction of the diffusion coefficient in associating mixture system is still a new subject. Firoozabadi et al. [1] developed an analytical expression for the thermal, molecular, and pressure diffusion coefficients for multicomponent mixtures. Their model has been widely applied in hydrocarbon mixtures as well as associating mixtures such as water–ethanol, water–methanol and water–isopropanol [2]. In the case of hydrocarbon system, the properties of the fluid mixture at equilibrium were calculated using the Peng–Robinson (PR) equation of state as well the cubic plus association (CPA) equation of state.

In this paper we calculate the molecular diffusion and thermodiffusion coefficients for binary mixtures of water-acetone, water-methanol, water-ethanol and water-isopropanol at different temperature with a newly proposed modified mixing rule. This approach relies on the calculation of the ratio of evaporation energy to viscous energy (second adjustable parameter).

2 Ratio of evaporation energy to viscous energy

One of the major difficulties of predicting thermal diffusion factor is finding τ_i, the ratio of evaporation energy and viscous energy. Under the non-equilibrium thermodynamics framework, the thermodiffusion phenomenon in associating liquid mixtures has been studied by Pan et al. [2] and Saghir et al. [3]. In their first attempt, they simply used Cubic Plus Association (CPA) and PC-SAFT equations of state which are suitable for associating mixtures. It has been found that in aqueous alcohol solutions, the choice of τ_i = 4 proposed by Shukla and Firoozabadi [4] for hydrocarbon mixtures along with Dougherty and Drickamer's [5] did not give a good agreement with experimental results. By increasing the value of τ_i to 10 and above appears to provide a good match with experiment at low water concentration but failed to detect the change in the sign of thermal diffusion factor.

These findings encouraged Pan et al [2] to suppose that τ_i may be a variable rather than constant over the entire concentration range. By suggesting that $\tau_{1\to 0}$ and $\tau_{2\to 1}$, respectively, are the values for τ_1 and τ_2 when $x_1 \to 1$ respectively and, similarly $\tau_{1\to 1}$ and $\tau_{2\to 0}$ when $x_1 \to 0$, a new expression for τ_1 and τ_2 as a function of $x_1, \tau_{1\to 0}, \tau_{2\to 1}, \tau_{1\to 1}$ and $\tau_{2\to 0}$ is proposed. Here $\tau_{1\to\infty}$ and $\tau_{2\to\infty}$ represent the effect of unlike intermolecular interactions and $\tau_{1\to 0}$ and $\tau_{2\to 0}$ represent the effect of alike intermolecular interactions. Pan et al. [2] proposed a simple mixing rule for calculation of the energy ratio τ_i having the following expression;

$$\tau_i = \frac{x_i \tau_{i\to 0} + x_{3-i}\tau_{3-i\to 1}}{1+\dfrac{d\,ln\,\gamma_1}{d\,ln\,x_1}},\quad i=1,2 \tag{1}$$

In general, predicting thermal diffusion factor with PC-SAFT EOS depends on two adjustable parameters. The first one is the binary interaction parameters for the mixture of interest which is optimized by the availability of experimental vapor–liquid equilibrium. The second one is the ratio of the energy of evaporation to the viscous energy that can be obtained by fitting the model with available experimental data.

The energy of evaporation $\Delta U_{evap,i}$ is the difference between internal energy of gas and liquid phase at equilibrium condition. Using PC-SAFT equation of sate, equilibrium condition for specific temperature and pressure can be achieved. Thus $\Delta U_{evap,i}$ calculation for each mole fraction is manageable.

However calculation of viscous energy $\Delta U_{vis,i}$ as a function of mole fraction doesn't have any specific model. It can be calculated knowing the following energy ratios $\tau_{1\to 0}$, $\tau_{2\to 0}, \tau_{1\to 1}$ and $\tau_{2\to 1}$ based on Shu's simple mixing rule 1. We propose a modified mixing rule for estimating viscous energy as a function of mole fraction as follows

$$\Delta U_{vis,i} = \left(x_2 \Delta U_{vis,i\to 0} + x_1 \Delta U_{vis,i\to 1}\right) * \left(1+\frac{d\,ln\,\gamma_1}{d\,ln\,x_1}\right),\ i=1,2 \tag{2}$$

Where

$$\Delta U_{vis,i\to 0} = \frac{\Delta U_{evap,i\to 0}}{\tau_{i\to 1}},\ \Delta U_{vis,k\to\infty} = \frac{\Delta U_{evap,i\to 1}}{\tau_{i\to 0}},\ i=1,2 \tag{3}$$

Estimating value of $\Delta U_{vis,i}$ using Equation 2 and predicting $\Delta U_{evap,i}$ leads to the calculation of τ_i. By using Equation 2 the modified ration of energy τ_i becomes

$$\tau_i = \frac{x_i \tau_{i\to 0}^{\exp\left(a_1 x_i^{y_{11}} x_{3-i}^{y_{12}}\right)} + x_{3-i}\tau_{3-i\to 1}^{\exp\left(a_2 x_i^{y_{11}} x_{3-i}^{y_{12}}\right)}}{1+\dfrac{d\,ln\,\gamma_1}{d\,ln\,x_1}},\quad |a_1| = |a_2|,\ i=1,2 \tag{4}$$

Where γ_1 is the activity coefficient of component one. The required thermodynamic properties for thermodiffusion models, including $\left(d\,ln\,\gamma_1 / d\,ln\,x_1\right)$, $\left(\partial\mu_1/\partial x_1\right)$, U_i, and V_i can be derived easily using PC SAFT equation of state.

Table 1: Modified mixing rule parameters for water – alcohol mixtures

	τ_1 **(organic compound)**				τ_2 **(water)**			
Mixtures	a_1	a_2	y_{11}	y_{12}	a_1	a_2	y_{11}	y_{12}
Water -acetone	3.2	-3.2	0.77	2.0	1.6	1.6	1.6	0.9
Water methanol-	-0.17	-0.17	0.1	3	-0.17	-0.17	1	1
Water ethanol	0.8	-0.8	0.5	1.2	-0.7	-0.7	1	1.5
Water isopropanol	-1	-1	0.9	-1.6	-1	-1	1.2	0.9

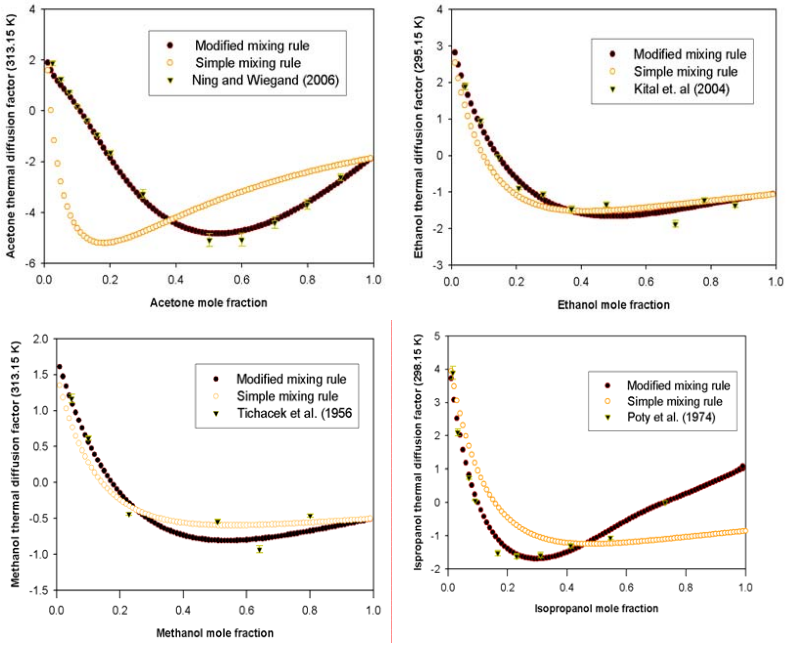

Fig. 1: *Evaluation of thermal diffusion factor in a) acetone-water mixture. b) ethanol-water mixture. c) Methanol-water mixture c) isopropanol-water mixture.*

3 Results and discussion

Figure 1 show the thermal diffusion factor calculated with modified and simple mixing rules and experimental result. Modified mixing rule was implemented to predict thermal diffusion factor for four different water – alcohol mixtures Results show modified mixing rule has very good agreement with experimental result.

4 Conclusion

A new theoretical approach in the calculation of viscous energy and the ratio of evaporation energy to viscous energy was presented to evaluate the thermal diffusion factor in associating solutions. The Firoozabadi model combined with the PC-SAFT achieved in calculation thermal diffusion factor. It accomplished very good agreement between the experimental data and the calculated values.

Acknowledgements

The authors acknowledge the financial support of the European Space Agency contract number 20690/07/NL/VJ and NSERC for supporting this research.

References

[1] Ghorayeb, K., Firoozabadi, A., Molecular, pressure, and thermal diffusion in nonideal multicomponent mixtures, AlChE J., 46 (2000), 883–891

[2] Pan, S., Jiang, C., Yan, Y., Kawaji, M., Saghir, Z., Theoretical prediction of thermal diffusion in water–methanol, water–ethanol, and water– isopropanol mixtures using the PC-SAFT equation of State, J. Non-Equilib. Thermodyn., 31 (2006), 47–71

[3] Faruque, D., Saghir, M.Z., Chacha, M., Ghorayeb, K., Compositional variationconsidering di¤usion and convection for a binary mixture in a porous medium, J. Por. Med., 2 (2004), 1–19

[4] K. Shukla, A. Firoozabadi, A new model of thermal diffusion. coefficients in binary hydrocarbon mixtures, Ind. Eng. Chem. Res. 37. (1998) 3331

[5] Dougherty, E.L, Drickamer H.G., A theory of thermal diffusion in liquids, J. Chem. Phys., 23-2(1955), 295-309

Development of a new high pressure thermodiffusion cell

H. Bataller[1], C. Miqueu[1], F. Plantier[1], J.L. Daridon[1], Z. Saghir[2], F. Dubois[3], S. Van Vaerenbergh[3]

[1]Laboratoire des Fluides Complexes - UMR 5150, Université de Pau et des Pays de l'Adour, BP 1155, 64013 Pau, France
[2]Ryerson University, 350 Victoria St, Toronto, ONT, M5B 2K3
[3]Microgravity Research Center, Université Libre de Bruxelles, CP165/62, B-1150 Bruxelles, Belgium

E-mail: henri.bataller@univ-pau.fr

Abstract

In this work we present a new thermodiffusion cell designed to measure thermal and molecular diffusion coefficients of binary systems under high pressure. The cell is a horizontal cylinder closed by two plugs connected to two thermoregulated baths that impose a horizontal thermal gradient. To avoid the convection, a monolithic porous medium fills the almost-totality of the cell. At each extremities of the porous medium, two dead volumes are let to permit the passage of two laser beams through windows sapphires. The cell, connected to the circuit of filling and of setting under pressure, is installed in a Mach-Zender interferometer, each beam crossing one of the dead volumes.
With short time experiments with pure ethanol and the binary 1,2,3,4-tétrahydronaphtalène (THN)/dodécane (C12) at the mass fraction of 50% we have validated the design of the cell and have permitted to develop a procedure of determination of the variation of the refractive index between the hot and the cold side of the cell.

1 Introduction

Several experimental methods have been developed on ground and in microgravity to measure with precision both thermal diffusion and Soret coefficients of binary mixtures at atmospheric pressure [1, 2, 3, 4, 5] in order to provide understanding of separation processes and molecular interaction.

Recently high pressure measurements of thermal diffusion coefficients have been made with a thermogravitational column [6, 7]. In this work we present a new thermodiffusion high pressure cell with the ability to measure thermal diffusion coefficient as well as molecular diffusion coefficient of binary systems.

2 Experimental setup and principle of the analysis

The cell is a horizontal cylinder closed by two plugs connected to two thermoregulated baths that impose a horizontal thermal gradient. To avoid the convection, a monolithic porous medium fill the almost-totality of the cell. At each extremities of the porous medium, two dead volumes are let to permit the passage of two laser beams through windows sapphires. The cell, connected to the circuit of filling and of setting under pressure, is installed in a Mach-Zender interferometer, each beam crossing one of the dead volumes.

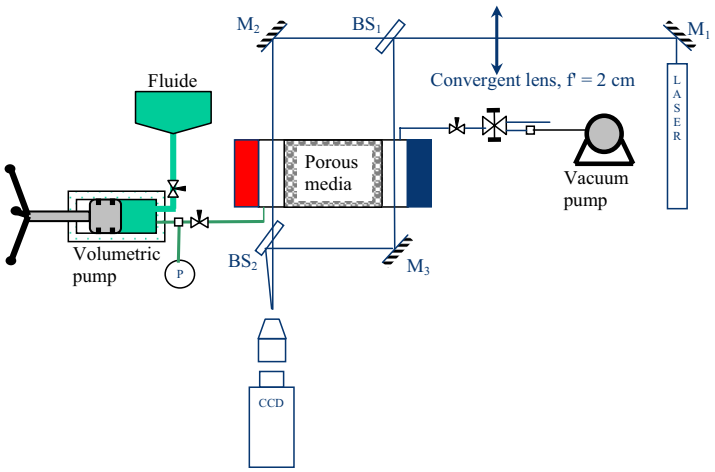

Fig. 1: *Experimental setup*

The inner diameter of the cell is e = 1 cm. The working P-T ranges are [1; 1000 bar] and [278,15; 313,15K]. Two thermocouples in the dead volumes give the value of the temperature difference at each side of the porous medium. A He-Ne laser (λ_0 = 632,8 nm)

is used. The interferometer is set to obtain vertical delocalised fringes (by rotating the beam-splitter BS2). The interferogram (fig. 3) is displayed by a CCD video camera and recorded.
At the beginning, each side of the cell is maintained at the low temperature T_1. Only the bath connected to the plug of the left on figure 1 is put to the high temperature T_2. ΔT is the difference of temperature between the hot and the cold side. The variation of the phase difference between the beam having crossed the hot side and the beam having crossed the cold side is given by:

$$\Delta\Phi = -\frac{2\pi e}{\lambda_0}\Delta n \qquad (1)$$

where Δn is the total variation of the refractive index between the hot side and the cold side. For binary systems, the variation of refractive index is :

$$\Delta n = \frac{\partial n}{\partial T}\Delta T + \frac{\partial n}{\partial c}\Delta c \qquad (2)$$

where Δc is the concentration difference of the densest component between the hot and the cold side. Coefficients $\partial n/\partial T$ and $\partial n/\partial c$ are the so-called contrast factors [3]. The kinetics of thermal and molecular diffusion have a huge magnitude of difference [4, 8]. Hence their effects are completely decoupled.

The phase difference is deduced from the analysis of the interferogram on a single line converted in term of intensity (gray levels, see figure 2).

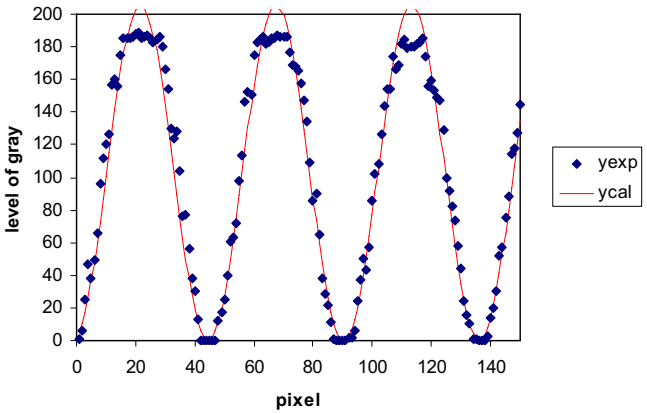

Fig. 2: *Gray level and adjustment of the first 150 pixels of the ligne 500 of an interferogram (THN/C12 mixture = 50% mass fraction; T_{mean} = 25°C; ΔT = 3°C; time = 511,95 s).*

Light intensity is fitted by:

$$I(x) = a\cos^2(bx - c) \tag{3}$$

a, b and c being computed by a least-square method. $c = \Phi/2$ at $x = 0$. As adjustment constraint we impose that values of c must to be bounded between $-\pi/2$ et $+\pi/2$. c is corrected to take into account the progressive scrolling of fringes.
Then the phase difference evolution is fitted by:

$$\Phi(t) = a' \times \{1 - exp(-b' \times t)\} + c' \tag{4}$$

The total variation of the phase difference $\Delta\Phi$ due to the thermal effect is then a'.

3. Results

3.1. Pure ethanol

The interferograms obtained with and without porous medium are compared in figure 3.

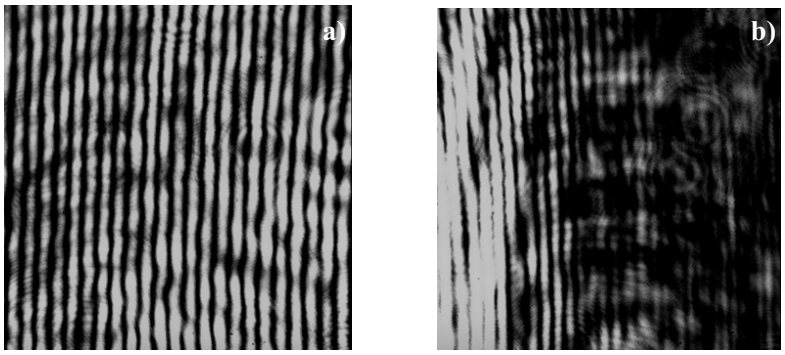

Fig. 3: *Interferogram of ethanol at T_{mean} = 25 °C and ΔT = 5 °C after 300 s a) with porous media and b) without porous medium.*

Without porous medium the bending is so important that beams do not interfere anymore. The behaviour is assigned to convection that clearly demonstrates the important role of the porous medium to avoid convection.

3.2. Binary mixture THN/C12

In figure 4 are plotted the phase difference of 1,2,3,4-tétrahydronaphtalène (THN)/ dodecane (C12) (50/50 weight fraction) at T_{mean} = 25 °C, pressure P = 1 bar and P = 100 bar for several thermal gradients.

Δn is computed for each ΔT from eq. (1) and ΔΦ plotted in figure 4. By neglecting the concentration effect in eq. (2) (short times), one can compute contrast factor $\partial n / \partial T$.

At 25 °C and atmospheric pressure, for THN/C12 mixture we obtain until ΔT =5°C an good agreement with the value of $-4{,}39\times10^{-4}$ K^{-1} established in the literature[3]. For ΔT ≥ 7°C, the value of contrast factor $\partial n / \partial T$ calculated is a little high. Convection in dead volumes can not be neglected from this ΔT and eq. (2) is not suitable anymore.

Finally, we can see that in figure 4 the measurement under pressure (P= 100 bar, ΔT =5°C) affects thermal diffusion.

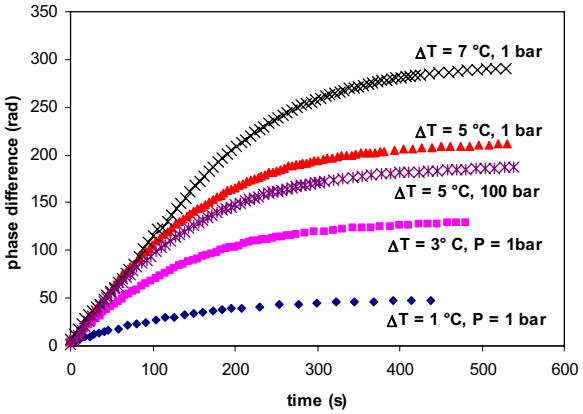

Fig. 4: *Phase difference versus time for THN/C12 for differents pressures P and temperature differences ΔT.*

4 Conclusions

The good agreement of the contrast factor $\partial n / \partial T$ with the literature value for the THN/C12 mixture at 25 °C and at the atmospheric pressure is the first step for the validation of the experimental setup.

The second step of this validation will consist in the check of the molecular diffusion effect on the separation process that involves long times experiments (several weeks) and will be presented at the meeting if obtained on time.

Acknowledgment

This work was financially supported by the European Spatial Agency and the Conseil Régional d'Aquitaine. The authors would like to thank Valentina Shevtsova, Jean-Claude Legros and Alexander Mialdun for the impulsion given to the work at the meeting of Biarritz and for valuable discussions.

References

[1] Platten J.K, Bou-Ali M.M., Costesèque P., Dutrieux J.F., Köhler W., Leppla C., Wiegand S., Wittko G., Phil. Mag., **83**, 1965 (2003)

[2] Bou-Ali M.M., Valencia J.J, Madariaga J.A.., Santamaria C., Ecenarro O., Dutrieux J.F., Phil. Mag., **83**, 2011 (2003)

[3] Wittko G., Köhler W., Phil. Mag., **83,** 1973 (2003)

[4] Zhang K.J., Briggs, Gammon R.W., Sengers J.V., J. Chem Phys., **104**, 6881 (1996)

[5] Van Vaerenbergh S., Legros J.C., J. Phys. Chem., **102**, p. 4426 (1998)

[6] Urteaga P., Bou-Ali M.M., Platten J.K., Madariaga J.A., Santamaria C., in M.M. Bou-Ali, J.K. Platten (Ed.), Thermodiffusion: Basics and Applications, Mondragon Unibertsitateko Zerbitzu Editoriala: Mondragon (Spain), 449 (2006)

[7] Urteaga P., oral presentotion at the 8th international meeting on thermodiffusion, Bonn (2008)

[8] Mialdun A., Shevtsova V.M., Int. J. Heat and Mass Transfer, in Press

Thermal diffusion values for some alkane mixtures: A comparison between thermo-gravitational column and thermal diffusion forced Rayleigh scattering

P. Blanco[1], P. Polyakov[2], M. M. Bou-Ali[1] and S. Wiegand[2]

[1]MGEP Mondragon Goi Eskola Politeknikoa, Manufacturing Department. Loramendi 4, Apdo. 23, 20500 Mondragon, Spain.
[2]Forschungszentrum Jülich GmbH, IFF-Weiche Materie, D-52428 Jülich, Germany.

E-mail: pblanco@eps.mondragon.edu

Abstract

In the present study we measured and analyzed *n*-decane/*n*-alkane mixtures by thermogravitational column (TC) and thermal diffusion forced Rayleigh scattering (TDFRS) method. We studied the thermal diffusion behaviour of the *n*-decane/*n*-pentane binary mixture at different mass concentrations at 27ºC. In addition, we studied the *n*-decane in other *n*-alkanes from *n*-pentane to *n*-eicosane at a mass concentration of 50% at 25ºC. The deviations of the results of both techniques agreed within the error bars. Compared to the recently published data we found deviations in the order of 30%. We analyze and discuss the possible reasons for the discrepancies for the present and the past publications.

1 Introduction

The phenomenon of thermal diffusion was discovered by C. Ludwig [1] and later more deeply analyzed by C. Soret [2]. The magnitude that describes this phenomenon is known nowadays as the Ludwig-Soret or Soret coefficient. Since its discovery, numerous investigations have been attributed to this phenomenon and observations in diverse fields such geology, biology, industry, physiology, environment and even the origin of the life [3] have been made.

In the recent years due the limited energy resources mainly the characterization of petroleum reservoirs gained a lot of interest [4]. In this context especially the knowledge of transport properties of hydrocarbon mixtures such as linear alkanes and organic ring compounds are very important [5]. Different techniques exist to determine the thermal diffusive properties of liquid mixtures [6] and optical techniques such as thermal diffusion forced Rayleigh scattering (TDFRS) and thermogravitational columns (TC) have been validated in a benchmark test for three binary hydrocarbon mixtures [7].

In a recent work [8], the transport properties of water mixtures published latterly in the literature [9] have been compared with new experimental results obtained by three different thermogravitational columns. The differences reach more than 300% in some mixtures and sometime even different signs for the Soret coefficient are found. Presently, we repeat measurements for the thermal diffusion properties of binary *n*-alkane mixtures with *n*-decane as first component. Some of the *n*-decane/*n*-alkane mixtures have already been studied in the past by TDFRS method [10] and by thermogravitational technique [11]. Compared to the literature we found deviations up to 30%. In the present study we measured and analyzed *n*-decane/*n*-alkane mixtures by thermogravitational column and TDFRS method. Even for the volatile *n*-pentane/*n*-decane mixture the deviations agreed within the error bars of both techniques.

2 Experimental

In this experimental work we have used the thermogravitational technique and the thermal diffusion forced Rayleigh scattering method. Next we present briefly the experimental setup of each technique. For more details of each technique operation we refer to the literature (Refs. [12,13])

2.1 Thermogravitational column:

The TC theory provides a relation between the stationary separation Δc and the thermodiffusion coefficient D_T . For more details see Ref. [14]:

$$\Delta c = -\frac{504 L_z}{g L_x^{\,4}} \frac{D_T \nu}{\alpha} c_0 (1 - c_0) \tag{1}$$

where

$$\Delta c = \frac{L_z}{\beta \rho} \frac{\partial \rho}{\partial z} \tag{2}$$

being Δc the mass fraction difference between the top and the bottom of the thermogravitational column, $\alpha = -\frac{1}{\rho}\frac{\partial \rho}{\partial T}$ the thermal expansion coefficient, $\beta = \frac{1}{\rho}\frac{\partial \rho}{\partial c}$ the mass expansion coefficient, $\frac{\partial \rho}{\partial z}$ the vertical density gradient along the column at the stationary state, ν the kinematic viscosity, L_z the height of the column, L_x the gap of the column, c_0 the initial mass fraction of the reference component and g the gravity acceleration. Combining Eqs. (1) and (2) we obtain the expression which is used experimentally:

$$D_T = -\frac{g L_x^4}{504} \frac{\alpha}{c_0 (1 - c_0) \beta \mu} \frac{\partial \rho}{\partial z} \tag{3}$$

being μ the dynamic viscosity.

All the products used in the TC were purchased from Merck with a purity of over 99%. First we always filled in the less volatile component, i.e., the alkane with higher molecular weight; then the corresponding amount of the second alkane is added. The concentrations of the binary mixtures were adjusted by weighting both components separately. We used two scales for the preparation of the mixtures with a capacity up to 310 g and an accuracy of 0.0001 g. and with a capacity up to 4500 g and an accuracy of 0.01 g. The thermal expansion α, the mass expansion β and the density ρ of all the mixtures have been measured with an Anton Paar DMA 5000 vibrating quartz U-tube densimeter. It has a reproducibility of $1 \cdot 10^{-6}$ g/cm^3 with a temperature accuracy of 0.001ºC. The sample volume needed to make one density measurement is roughly 1.5 ml. Dynamic viscosity has been determined by a HAAKE falling ball viscosimeter with an estimated accuracy of ±1%. The temperature stability is ±0.1ºC. The volume needed to make one viscosity measurement is approximately 40 ml. The TC used in this work has been validated previously with experiments well documented in the bibliography [15], and also some experimental results of this TC have been contrasted with different installations [16]

2.2 Thermal diffusion forced Rayleigh scattering

The thermal diffusion auxiliary of the solutions was investigated by thermal diffusion forced Rayleigh scattering (TDFRS). A detailed description of the set-up can be found elsewhere [13]. The heterodyne diffraction signal ζ_{het} is evaluated by the equation:

$$\zeta_{het}(t) = 1 + \left(\frac{\partial n}{\partial T}\right)^{-1}\left(\frac{\partial n}{\partial c}\right) S_T c(1-c)\left(1 - e^{-q^2 Dt}\right) \tag{4}$$

with the refractive index increment with concentration at constant pressure and temperature $\partial n/\partial c$, the derivative of the refractive index with temperature at constant pressure and concentration $\partial n/\partial T$ and the collective diffusion coefficient D.

The alkanes *n*-pentane (>99%), *n*-hexane (>99%), *n*-heptane (>99.5%), *n*-octane (>99.5%), *n*-octadecane (>99%) and *n*-tetradecane (>99%) were purchased from Fluka; *n*-decane (>99%), *n*-heptadecane (99%) and *n*-eicosane (99%) were ordered from Aldrich. The alkane mole fraction of all mixtures was adjusted by weighing the components. The TDFRS experiments require a small amount of dye in the sample. In this work, all samples contained approximately 0.002 wt% of the dye Quinizarin (Aldrich). This amount ensures a sufficient optical modulation of the grating but is small enough to avoid convection and contributions of the dye to the concentration signal.

Before each TDFRS experiment, approximately 2 ml of the freshly prepared solution were filtered through 0.2 µm filter (hydrophobic PTFE) into an optical quartz cell with 0.2 mm optical path length (Helma) which was carefully cleaned from dust particles before usage. After each measurement we checked carefully by monitoring the change of the meniscus height in the two filling capillaries of the sample cell whether the volatile solvent evaporated during the measurement. The accuracy of this method is certainly better than 1%. The total volume of the sample cell is in the order of 0.6 ml. Even for the n-decane/n-pentane mixture with the lowest pentane content, the concentration change should be less than $\Delta x \approx c \approx 0.01$.

An Anton Paar RXA 156 refractometer has been used to measure the refractive index increments with the mass concentration ($\partial n/\partial c$). It has a repeatability of $2 \cdot 10^{-5}$ and the temperature accuracy is ±0.01ºC. The volume needed to make one measurement is less than 1 ml. For all mixtures except for the system *n*-decane/*n*-pentane ($\partial n/\partial T$) was directly measured by an interferometer. In the case of *n*-decane/*n*-pentane ($\partial n/\partial T$) the reliability of the refractometer was better, because due to the long measurement time in the interferometer pentane evaporated partly, which lead to concentration changes in during the measurement.

3 Results and Discussion

3.1 Mixtures *n*-decane/*n*-pentane

Figure 1 shows the thermal diffusion coefficient D_T of the *n*-decane for the *n*-decane/*n*-pentane mixtures at different molar fractions of *n*-decane. We estimated the error bars for the TC by error propagation taking into account the experimental uncertainties of the auxiliary quantities such as viscosity (<1%), mass expansion (<1%), thermal expansion (<0.5%), variation of the density with height in the column (<2%) and geometrical parameters (≈2%). The error bars for the TDFRS data correspond to one standard deviation of the mean for repeated measurements. The highest deviation in comparison with the TDFRS data has been found for the lowest pentane content. This concentration is also most sensitive to evaporation of pentane. The same absolute loss of pentane leads to a much larger relative concentration change compared to concentrations with a higher pentane content.

The old TDFRS measurements [10] are systematically 10-20% lower than the present TDFRS data and the deviation with the TC data are in the order of 5-15%. The deviations between the two sets of TDFRS data can probably be explained by the fact that at that time the data had not been corrected by the so-called excitation function which accounts for time delays in the electrical switching of the Pockels cell. A detailed description of the procedure can be found in Ref. [13]. A comparison of the new TC and TDFRS data with simulation results for the system *n*-decane/*n*-pentane by Perronace et al. [10] leads to systematic deviations in the order 15-40%, which is slightly better than the agreement in the past and for the equimolar mixture the data almost agree within the error bars.

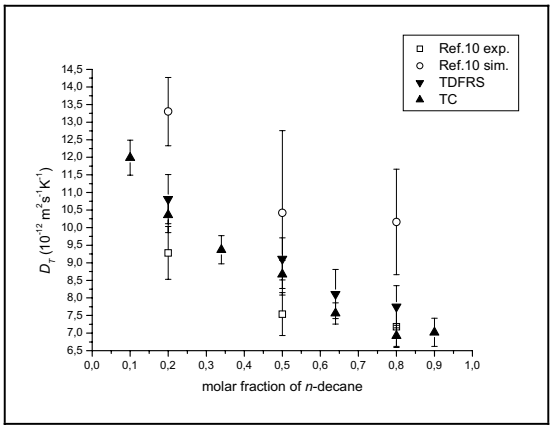

Fig. 1: *Thermal diffusion coefficient D_T for n-decane in n-pentane in dependence of the molar fraction of n-decane at 27ºC. Results obtained by TC (▲) and TDFRS (▼). For comparison we show also the previous experimental (□) and simulation results in the center–of–volume–reference frame (○)[10].*

3.2 Mixtures n-decane/n-alkane

In addition we performed measurements for *n*-decane with various shorter and longer linear alkanes. Figure 2 shows the thermal diffusion for the experimental tests of the TC and the TDFRS as function of the number of carbon atoms of the second component. The mass fraction is 50% and the temperature is 25ºC. For comparison we show also the previous data [11] which have been recorded under the same experimental conditions. In this case, we do not show the error bars because of clarity of the figure. As expected, the thermal diffusion coefficient D_T of *n*-decane in shorter alkanes is positive, and therefore the *n*-decane goes towards the cold region (*n*-decane is the densest), while it becomes negative when the mass of the second component becomes larger, which implies that *n*-decane migrates to the warm side (*n*-decane is the less dense). We can observe the good agreement between the TC and the TDFRS data. The new data deviate from the previous data [11] between 10-30%. Compared to the previous TC [11], the TC used in this work allows a more accurate analysis of the mass separation between the top and the bottom of the TC due to the smaller gap and a better precision of the gap of $L_x = 1.0 \pm 0.005$ mm [15]. The TC used in [11] had a gap of 1.6 ± 0.02mm. This low precision of the gap dimensions causes an uncertainty of 5% in the determination of the thermal diffusion coefficient, not regarding the propagating errors due to uncertainties in the thermophysical properties, which are required to calculate the thermal diffusion coefficient (see Eq 3). For the TC used in this work the steady mass separation is 6.55 times greater compared to the TC used in Ref. [11]. Therefore, the difference in D_T determined with those two columns becomes larger for mixtures with a small mass separation. For instance, this tendency can be observed for the mixtures *n*-decane/*n*-heptane and *n*-decane/*n*-hexadecane where the differences are around of 30% between the average values of both techniques used in this study and previous data [11].

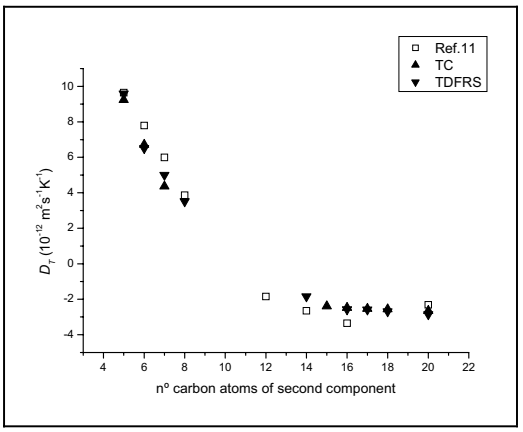

Fig. 2: *Thermal diffusion coefficient D_T for n-decane in some n-alkanes in function of the number of carbon atoms of the second n-alkane component at 25ºC andwith equal mass ratio. Results obtained by TC (▲) and TDFRS (▼) and compared with previously published experimental data (□) [11].*

4 Conclusions

In this paper, we have studied some binary *n*-alkane mixtures by two different techniques, a convective method as thermogravitational columns (TC) and a non-convective method thermal diffusion forced Rayleigh scattering (TDFRS). In general we found a very good agreement between these two methods. However we found some discrepancies with data published in the literature. The observed disagreement between the published TDFRS [10] data for the binary mixture *n*-decane/*n*-pentane is probably caused by an improved data analysis algorithm, which accounts for finite rising times and slow drifts of the electro-optic devices used in the experiment. Additionally we found discrepancies with recently published TC data [11]. We assume that the cause is the bigger gap L_x in their TC [11] compared to the TC used in this work. The bigger gap decreases the accuracy of determining the steady mass separation between the two ends of the TC. This is especially important for the binary *n*-alkane mixtures which both components are similar in mass and in length of the chain, because more similar they are less mass separation they have between the two ends of the TC.

Acknowledgment

This work was partially supported by the Deutsche Forschungsgemeinschaft grant Wi 1684, the Basque Government grant BFI05.449 and project GOVSORET (PI2008-14) and Spanish Government project TESBLUR (CTQ2005/09389/C02/01/PPQ).

References

[1] Ludwig C., Sitz. Ber. Akad. Wiss. Wien Math-Naturw. Kl., **20**, 539 (1856).

[2] Soret C., Archives des Sciences Phyiques et Naturelles de Geneve, **2**, 48-61 (1879).

[3] Gaeta F., Mita D., Perna G. And Scala G., Nuovo Cimento, **30**, 153, (1975).

[4] Montel F., Entropie, **214**, 7-10 (1998).

[5] Van Vaerenbergh S., Shapiro A., Galliero G., Montel F., Legros J., Caltagirone J., Daridon J. and Saghir Z., European Space Agency, (Special Publication) ESA SP, **1290**, 202-213 (2005).

[6] Wiegand S., Journal of Physics: Condensed Matter, **16**, R357-R379 (2004).

[7] Platten J., Bou-Ali M., Costesèque P., Dutrieux J., Köhler W., Leppla C., Wiegand S. and Wittko G., Philosophical Magazine, **83**, 1965-1971 (2003).

[8] Platten J. K., Bou-Ali M. M., Blanco P., Madariaga J. A., Santamaría C., J. Phys. Chem. B, **111**, 11524-11530 (2007).

[9] Van Vaerenbergh S. and Legros J.C., J. Phys. Chem. B, **102**, 4426-4431 (1998).

[10] Perronace, A.; Leppla, C.; Leroy, F.; Rousseau, B. & Wiegand, S., Journal of Chemical Physics, **116**, 3718-3729 (2002).

[11] Leahy-Dios, A. & Firoozabadi, A., J. Phys. Chem. B, **111(1)**, 191 – 198 (2007).

[12] Bou-Ali, M.; Ecenarro, O.; Madariaga, J.; Santamar¡a, C. & Valencia, J., Journal of Physics: Condensed Matter, **10**, 3321-3331 (1998)

[13] H. Ning, R. Kita, H. Kriegs, J. Luettmer-Strathmann, and S. Wiegand, J. Phys. Chem. B **110**, 10746 (2006).

[14] J. Dutrieux, J. Platten, G. Chavepeyer, and M. Bou-Ali, J. Phys. Chem. B **106**, 6104 (2002)

[15] P. Urteaga, M. Bou-Ali, J. Madariaga, C. Santamaría, P. Blanco, and J. Platten, in Thermodiffusion: Basics and Applications, edited by M.M. Bou-Ali and J.K. Platten, (Mondragon Unibertsitateko Zerbitzu Editoriala, Spain, 2006), p.449.

[16] P. Blanco, M. Bou-Ali, J. Platten, J. Madariaga, P. Urteaga, and C. Santamara, J. Non-Equilib. Thermodyn. **32**, 309 (2007).

Determination of the thermal diffusion coefficient in n-alkane mixtures: empirical correlations

P. Blanco[1], M. M. Bou-Ali[1], J. K. Platten[1], P. Urteaga[1], J. A. Madariaga[2] and C. Santamaría[2]

[1]MGEP Mondragon Goi Eskola Politeknikoa, Manufacturing Department. Loramendi 4, Apdo. 23, 20500 Mondragon, Spain.

[2]UPV University of Basque Country, Department of Applied Physics II, Apdo. 644, 48080 Bilbao, Spain.

E-mail: pblanco@eps.mondragon.edu

Abstract

In this experimental work we present a primary relationship between the thermal diffusion coefficient D_T and the molecular weight of the mixture's components for equimolar mixtures of n-alkanes. On the other hand, an empirical quantitative correlation has been obtained between D_T, the molecular weights of the components, the viscosity and the thermal expansion coefficient of the mixtures.

1 Introduction

Numerous researchers have studied the particular transport property of thermal diffusion, starting with C. Ludwig and C. Soret, respectively its discoverer and the first researcher of this phenomenon in the XIX century. Some researchers pointed out that [1] the study of thermodiffusion might help in a better understanding of intermolecular forces, although nowadays we still do not know which parameters are the most important in the thermodiffusion phenomenon or to what extent [2]. These parameters could be chemical interactions and physical properties like mass, moment of inertia and size of the molecules or particles [3]. In relation to this, recently a lot of work has been done, for instance, the work [4] in which a study of the influence of the molecular architecture on the Soret effect in binary mixtures of benzene in n-alkanes and in branched alkanes or the work [5] which studied the dependency of the Soret coefficient with the mass and moment of inertia difference and a chemical contribution in mixtures of benzene and cyclohexane. Also in n-alkane binary mixtures some attempts have been made to show the dependency of the thermal diffusion coefficient with the chain length of the mixture's components [6,7].

In the last few years, the oil industry has been one of the industrial fields that have shown most interest in the thermal diffusion phenomenon, because of its implication in the distribution of the species in hydrocarbon reservoirs [8]. One example of this are the experiments realized in microgravity and on earth to determine the Soret coefficients in crude oils [8, 9], highlighting an increasing demand on experimental results of this transport property for hydrocarbon mixtures [8, 10] in order to be able to use the numerical codes [11] in non equilibrium thermodynamics [12] or in the field of molecular dynamics [13].

Therefore, this work has been carried out to study the influence of the molecular weight (or length of the chain) in the thermodiffusion coefficient for liquid binary mixtures. The chosen mixtures are normal alkanes which are of interest to the oil industry because they are derived from petroleum. The thermodiffusion coefficient has been determined for different equimolar mixtures of n-alkanes at a temperature of 25ºC. These mixtures correspond to the following three series:

- nC12-nCi ; i = 5, 6, 7, 8, 9, 17, 18
- nC10-nCi ; i = 5, 6, 7, 15, 16, 17, 18
- nC6-nCi ; i = 10, 12, 14, 16, 18

To determine the thermodiffusion coefficient the thermogravitational technique has been used, whose thermo-hydro dynamical behaviour is very well documented [14-16] both experimentally and analytically. The obtained results together with the previously published ones [6] for the series nC18-nCi have made it possible to establish a relation showing that the main parameter that determines D_T in each series is in relation to the molecular weights of the mixture's components.

2 Experimental

2.1 Materials and Equipment

The liquids used in this work are normal alkanes and were purchased from Merck with a purity of over 99%. An Anton Paar DMA 5000 vibrating quartz U-tube densimeter having a repeatability of $1 \cdot 10^{-6}$ g/cm^3 has been used to determine the density of the studied mixtures. The mixtures have been prepared using a 310 g capacity scale with an accuracy of 0.0001 g. Dynamic viscosity has been determined by a falling ball viscosimeter HAAKE with a ±1% precision. In this work a cylindrical thermogravitational column developed to work at high pressures has been used, although in the present work all the experimental tests have been carried out at atmospheric pressure. This thermogravitational column has been validated by several experimental tests realized for binary mixtures widely used in the literature. We invite the reader to see [17] for a general description of this thermogravitational column.

2.2 Mathematical formulation

Next we summarize the equation typically used to determine the thermal diffusion coefficient using the thermogravitational technique and which can be found elsewhere [18]:

$$\Delta c = -\frac{504 L_z}{g L_x^{\,4}} \frac{D_T \nu}{\alpha} c_0 (1 - c_0) \tag{1}$$

where

$$\Delta c = \frac{L_z}{\beta \rho} \frac{\partial \rho}{\partial z} \tag{2}$$

being Δc the mass fraction difference between the top and the bottom of the thermogravitational column, $\beta = \frac{1}{\rho}\frac{\partial \rho}{\partial c}$ the mass expansion coefficient, $\alpha = -\frac{1}{\rho}\frac{\partial \rho}{\partial T}$ the thermal expansion coefficient, $\frac{\partial \rho}{\partial z}$ the vertical density gradient along the column at the stationary state, ν the kinematic viscosity, L_z the height of the column, L_x the gap, c_0 the initial mass fraction of the reference component and g the gravity acceleration. According to our signs convention D_T >0 when the reference component migrates towards cold regions. In fact, experimentally we use the next expression which is the result of the combination of Eqs. (1) and (2):

$$D_T = -\frac{g L_x^4}{504} \frac{\alpha}{c_0 (1 - c_0) \beta \mu} \frac{\partial \rho}{\partial z} \tag{3}$$

being μ the dynamic viscosity.

3 Results and Discussion

The thermophysical parameters like β and α are lineal for all the mixtures studied in this work as we can observe as an example for the mixture nC12-nC5 in Figs.1a and 1b respectively. In the steady state $\frac{\partial \rho}{\partial z}$ is also linear for all the mixtures as we can see as an example in Fig. 1c.

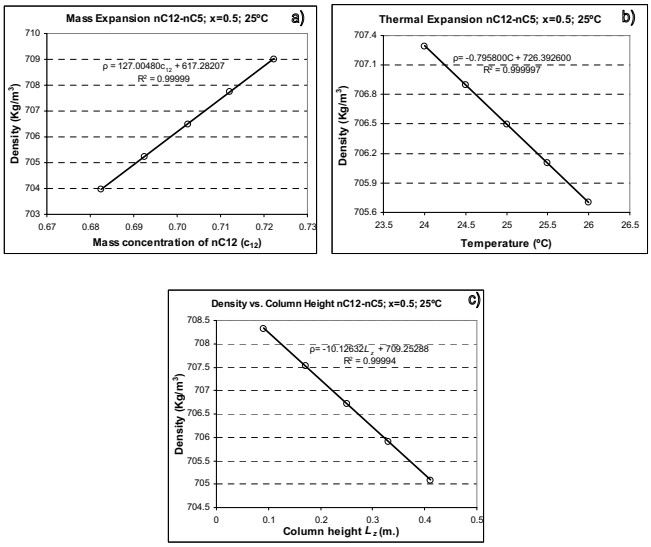

Fig. 1: *a)Mass expansion b) Thermal expansion c) Density gradient with elevation in the column of the mixture nC12-nC5 at 25ºC and molar fraction x = 0.5.*

We have found a correlation between the thermal diffusion coefficient D_T and the relative molecular weight difference $\delta M = (M_j - M_i)/(M_j + M_i)$, being M_j the molecular weight of the reference component and M_i the molecular weight of the second component. This correlation allows predicting the thermodiffusion coefficient of any equimolar mixture of two n-alkanes knowing only their molecular weights. The correlation is:

$$D_T = D_{T0}\delta M(1 + \lambda \delta M) \tag{4}$$

where D_{T0} and λ are constant parameters which depend on the reference component. In Fig. 2a we present as an example the thermodiffusion coefficient for the series of mixtures nC18-nCi.

As well, we have also found a linear correlation between the group $c_0(1-c_0)\frac{D_T\nu}{\alpha}$ and the molecular weight difference $\Delta M = (M_j - M_i)$. The good linear correlation of the experimental results shown in Fig 2b can be observed. An even better linear correlation is obtained when instead of kinematic viscosity ν, we take the dynamic viscosity μ. The group $c_0(1-c_0)\frac{D_T\mu}{\alpha}$ shows a quite better linearity of the experimental results as can be observed in Fig.3. In order to facilitate the visualization of the results we plot the quantity $-c_0(1-c_0)\frac{D_T\mu}{\alpha}$ instead of the positive one. Both straight lines pass through the origin. We still ignore why this unexpected behaviour happens with equimolar binary mixtures of n-alkanes but it seems to be related to the viscosity and thermal expansion of the mixtures.

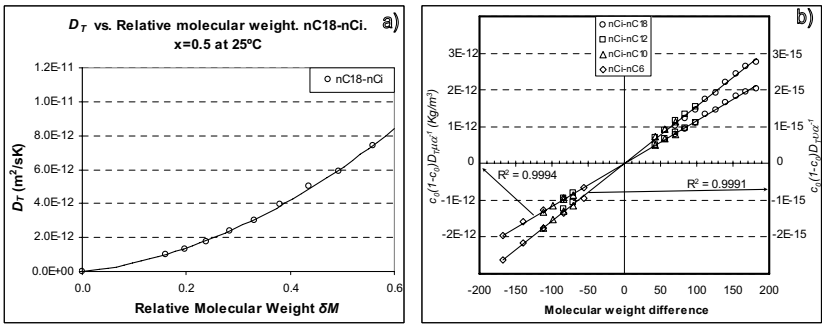

Fig. 2: *a) Thermal diffusion coefficient D_T of the series nC18-nCi with molar fraction x=0.5 and at 25ºC. b) The group $c_0(1-c_0)\frac{D_T\nu}{\alpha}$ and the group $-c_0(1-c_0)\frac{D_T\mu}{\alpha}$ in function of the molecular weight difference $\Delta M = (M_j - M_i)$.*

4 Conclusions

This is a first report of an accurate correlation for D_T in liquid mixtures. The results of this work allow predicting with accuracy the thermodiffusion coefficient D_T of any binary equimolar n-alkane mixture. A first correlation allows determining D_T only knowing the molecular weights of the mixture's components. A better quantitative correlation let to determine accurately D_T knowing some parameters like the viscosity and the thermal expansion coefficient of the mixtures.

Acknowledgment

This paper presents results partly obtained in the framework of the following projects, GOVSORET (PI2008-14) and the grant (BFI05.449) of the Basque Government, and TESBLUR (CTQ2005/09389/C02/01/PPQ) of the Spanish Government.

References

[1] W. Furry, R. Jones, and Onsager, L., Phys. Rev. E 55, 1083 (1939).

[2] G. Wittko and W. Köhler, J. Chem. Phys. **123**, 014506-1 (2005).

[3] S. Wiegand, J. Phys.: Condensed Matter **16**, R357 (2004).

[4] P. Polyakov, J. Luettmer-Strathmann, and S. Wiegand, J. Phys. Chem. B **110**, 26215 (2006)

[5] C. Debuschewitz and W. Köhler, Phys. Rev. Lett. **87**, 055901-1 (2001)

[6] Blanco P., Bou-Ali M., Platten J., Madariaga J., Urteaga P. and Santamaría C., J. Non-Equilib. Therm., **32**, 309 (2007).

[7] A. Leahy-Dios, A. Firoozabadi, J. Phys. Chem. B **111**, 191 (2007)

[8] P. Georis, F. Montel, S. Van Vaerenbergh, Y. Decroly, and J. Legros, in Proceedings of the European Petroleum Conference, **1**, 57. (1998)

[9] P. Costesèque, D. Fargue, and Ph. Jamet, Lectures Notes in Physics **584**, 389 (2002).

[10] S. Van Vaerenbergh, A. Shapiro, G. Galliero, F. Montel, J. Legros, J. Caltagirone, J. Daridon, and Z. Saghir, European Space Agency, (Special Publication) ESA SP **1290**, 202 (2005).

[11] B. Lacabanne, S. Blancher, R. Creff, and F. Montel, in Thermal Nonequilibrium Phenomena in Fluid Mixtures, edited by W. Köhler and S. Wiegand, (Springer Berlin/Heidelberg, 2002), p. 448.

[12] M. Khawaja, C.G. Jiang, S. Van Vaerenbergh, and M. Saghir, J. Non-Equilib. Therm. **30**, 359 (2005).

[13] C. Nieto-Draghi, J. Avalos, and B. Rousseau, J. Chem. Phys. **122**, 114503-1 (2005).

[14] J. Dutrieux, J. Platten, G. Chavepeyer, and M. Bou-Ali, J. Phys. Chem. B **106**, 6104 (2002).

[15] M. Bou-Ali, O. Ecenarro, J. Madariaga, C. Santamaría, and J. Valencia, J. Phys.: Condensed Matter **10**, 3321 (1998).

[16] J. Valencia, M. Bou-Ali, O. Ecenarro, J. Madariaga, and C. Santamaría, in Thermal Nonequilibrium Phenomena in Fluid Mixtures, edited by W. Köhler and S. Wiegand, (Springer Berlin/Heidelberg, 2002), p.233.

[17] P. Urteaga, M. Bou-Ali, J. Madariaga, C. Santamaría, P. Blanco, and J. Platten, in *Thermodiffusion: Basics and Applications,* edited by M.M. Bou-Ali and J.K. Platten, (Mondragon Unibertsitateko Zerbitzu Editoriala, Spain, 2006), p.449.

[18] J. Dutrieux, J. Platten, G. Chavepeyer, and M. Bou-Ali, J. Phys. Chem. B **106**, 6104 (2002)

Thermal diffusion in multicomponent mixtures: theoretical modeling and experiments

A. Firoozabadi

Yale University, New Haven, Connecticut, and RERI, Palo Alto, California

E-mail: abbas.firoozabadi@yale.edu

Abstract

There has been much progress on thermal diffusion in two-component mixtures in recent years. The work on multicomponent (more than two species) mixtures is, however, limited. The focus of this presentation will be on the mathematical link between thermal diffusion, pressure diffusion, and Fickian diffusion, as well as promising measurement techniques for multicomponent diffusion coefficients.

1 Introduction

Thermal diffusion is the selective movement of species due to temperature gradient. There are two other main diffusion processes: 1) Fickian diffusion caused by concentration gradient, and 2) pressure diffusion driven by pressure gradient. Thermal diffusion is the least understood and the most complicated form of diffusion.

All of the three main diffusion processes have broad applications in nature and in industry. We will briefly review three of the fascinating examples. In two examples, all three diffusion processes may occur simultaneously. In one example, pressure diffusion is absent.

Dating of Abrupt Climate Changes – The understanding of the coupling between the atmosphere and climate can be made by studying ice-cores from the large glaciers in Greenland and Antarctica. Both temperature and atmospheric condition are recorded in the air bubbles. All three diffusion processes are used in dating abrupt climate changes with composition.[1,2]

Origin of Life – One of the issues in the understanding of the origin of life relates to the mechanism for establishing highly concentrated solutions of biomolecules.[3,4] An abstraction of the problem can be made by studying transport processes in a short and narrow cleft-like geometry with a closed bottom and an open top. The biomolecule concentration is fixed at the top in a highly dilute condition in the ocean. The hydrothermal emergence of life is suggested by the combined effect of thermal diffusion and natural convection when a large temperature difference is applied across the walls. Accumulation grows exponentially with molecular size of the biomolecule in the brine solution.

Species Distribution in Hydrocarbon Reservoirs and Hydrocarbon Flowlines - In the subsurface where hydrocarbon reservoirs are found, there exists always a vertical thermal gradient. In some reservoirs, there is also a horizontal temperature gradient. These temperature gradients may have profound effects on distribution of various species in oil and gas reservoirs including salinity variation in the aqueous phase. There are cases in which one encounters a heavy phase floated on top of a light phase. Interestingly, the floatation of a heavy fluid on top of a light fluid in a large cavity was first predicted from theory[5] in 1998. It was later confirmed from data in a gas reservoir in Japan[6].

Another important observation from theory has been a significant effect of a small horizontal temperature gradient of the order of 4-6 K/km on species and phase distribution. All the three diffusion processes and natural convection affect the distribution of the species[7,8].

Very recently, we have demonstrated that thermal diffusion has a significant effect on wax deposition and aging in flowlines[9,10]. When thermal diffusion is accounted for, the radial distribution of some of the species shows a maximum at the interface between the liquid and the gel region. This maximum is confirmed with measurements.

2 Modeling

In some of the problems in industry and in nature, there may be three and higher components which participate in diffusion. The general expression for diffusion flux in such media is given by:

$$\vec{J}_i = -c\left[\sum_{j=1}^{n-1} D_{ij}^M \nabla x_j + D_i^T \nabla T + D_i^P \nabla P\right] \qquad i = 1,...,n-1 \tag{1}$$

In the above expression, n is the number of components, c is the mixture molar density, x_j is the mole fraction of species j, T is absolute temperature, P is pressure, and D_{ij}^M, D_i^T and D_i^P are Fickian, thermal, and pressure diffusion coefficients, respectively. D^P can be computed based on measurements of D^M and D^T because it does not have its own phenomenological coefficients. The expressions for D_{ij}, D_i^T and D_i^P are given by[11,12]:

$$D_{il}^M = a_{in} D_{in} \frac{M_i x_i}{L_{ii}} \sum_{k=1}^{n-1} L_{ik} \sum_{j=1}^{n-1} \frac{M_j x_j + M_n x_n \delta_{jk}}{M_j} \frac{\partial \ln f_i}{\partial x_l}\bigg|_{T,P,\mathbf{x}_l} \tag{2}$$

$$i,l = 1,...,n-1$$

$$D_i^T = a_{in} D_{in} M \frac{k_{Ti}}{T} \qquad i = 1,...,n-1 \tag{3}$$

$$D_i^P = a_{in} D_{in} \frac{M_i x_i}{RTL_{ii}} \sum_{k=1}^{n-1} L_{ik} \left[\sum_{j=1}^{n-1} x_j \bar{V}_j + \frac{M_n x_n}{M_c} - \frac{1}{c}\right] \qquad i = 1,...,n-1 \tag{4}$$

where

$$D_{in} = \frac{M^2 RL_{ii}}{cM_i^2 M_n^2 x_i x_n} \qquad i = 1,...,n-1 \tag{5}$$

and

$$k_{Ti} = \frac{M_i M_n x_i x_n L_{iq}}{MRL_{ii}} \qquad i = 1,...,n-1 \tag{6}$$

In the above expressions, L_{ij} and L_{iq} are the phenomenological coefficients of Fickian diffusion and thermal diffusion, respectively. k_{Ti} is the thermal diffusion ratio of component i. Other symbols are defined in Refs. 11 and 12.

The following remarks may set the stage for understanding and for future research.

- In a mixture composed of three components, four Fickian diffusion coefficients describe Fickian diffusion flux. The three pairs of Fickian diffusion coefficients from two-component mixtures cannot describe the flux in a three-component mixture. This is true even for an ideal gas mixture. An example is the mixture of CO_2, N_2 and H_2 at 35 °C and 1 atmosphere[13].

- The Soret coefficient commonly measured in a two-component mixture does not have meaning in multicomponent mixtures. The ratio of D^T/D, even in a two-component mixture, is a measure of two vastly different processes (molecular mobility and molecular disparity)[14]. Sign convention for thermal diffusion coefficients is neither necessary nor useful. Thermodynamic stability provides a sound framework in predicting the sign[12].

- There are two alternative approaches to describe Fickian diffusion and its coefficients. Momentum balance has been in a clear way to derive Maxell-Stephen (MS) diffusion coefficients[15]. The effect of nonideality is, however, inserted in the flux expression. MS diffusion coefficients have simple features. Classical irreversible thermodynamics leads to general expressions for all three diffusion coefficients[11]. It also provides the link between various diffusion coefficients. The irreversible thermodynamic approach also allows to break down the diffusion coefficients in terms of various effects.

- There are two main approaches to formulate thermal diffusion coefficients. In one approach, the formulation is based on equilibrium thermodynamics[16]. The other approach is based on non-equilibrium phenomena. Because of strong correlation of thermal diffusion coefficients with viscosity[14], one may see the advantage from the non-equilibrium approach.

3 Measurements

There have been much data on thermal diffusion coefficients in two-component mixtures in the last decade[17-19]. There have been much more data on two-component Fickian diffusion coefficients. The number of data points for three-component mixtures are very limited for Fickian diffusion coefficients. The accuracy of cross diffusion coefficients for these limited data is low. For thermal diffusion coefficients, there are perhaps no more than two papers in the literature for three-component mixtures[20]. For improved oil recovery processes and CO_2 sequestration, the need for such data is urgent.

There are perhaps three methods for measuring multicomponent Fickian and thermal diffusion coefficients. For two methods, the theory is well established. For the third method, the work is in progress for Fickian diffusion. We briefly discuss these three methods.

Thermogravitational column – Leahy-Dios, et al. [20] report both Fickian and thermal diffusion coefficients for ternary mixtures consisting of two normal alkanes and one aromatic. Data indicate that depending on concentration, the sign of the thermal diffusion coefficient of one of the species may change. Because of the issues with analysis, the method is currently limited to three species. Haugen and Firoozabadi[21] present working equations to measure both Fickian and thermal diffusion coefficients from transient and steady state separation data.

Laser beam deflection technique – Haugen and Firoozabadi[22] have established the theory to measure both Fickian and thermal diffusion coefficients in multicomponent mixtures. The deflection of a beam of (n–1) wavelengths would provide data for an n-component mixture. No data has yet been reported. The advantages of using optical methods include speed and limited analytical efforts.

Use of non-equilibrium phases in constant volume cell - We have made progress in formulating the problem of pressure and level evolution when non-equilibrium gas and liquid phases in a multicomponent mixture are brought into contact. We use a constant temperature and constant volume cell to measure simultaneously diffusion coefficients of gas and liquid phases in nonideal multicomponent phases. We hope as the work is published, various groups will embark on its extension to non-isothermal conditions to obtain both Fickian and thermal diffusion coefficients. A major complexity in the methodology has been the formulation of a moving fluid boundary with three and higher species. When there are two species, the formulation becomes less complicated.

Acknowledgments

The work of one of the past post-docs, Dr. Kassem Ghorayeb, and two recent PhD students at Yale University, Dr. Kjetil Haugen and Dr. Alana Leahy-Dios, has helped the author in the understanding of thermal and other diffusion processes. Member companies of the Reservoir Engineering Research Institute and the Petroleum Research Fund of the American Chemical Society (Grant PRF 45927-AC9) to Yale University have supported the work of our group.

References

[1] Severinghaus, J.P., Sowers, T., Brook, E.J., Alley, R.B., and Bender, M.L. *Nature* (1998) **391**, 141.

[2] Severinghaus, J.P. and Brook, E.J. *Science* (1999) **286**, 930.

[3] Braun, D. and Libchaser, A. *Phys. Bio* (2004) **1**, 1-8.

[4] Baaske, P., Weinert, F.M., Duhr, S., Lemke, K.H., Russell, M.J. and Braun, D. *PNAS* (2007) **104**, 9346-9351.

[5] Riley, M. F. and Firoozabadi, A. *AIChE Journal* (Feb. 1998) 452-464.

[6] Ghorayeb, K., Firoozabadi, A., and Anraku, T. *SPE Journal* (June 2003)114-123.

[7] Ghorayeb, K., and Firoozabadi, A. *SPE Journal* (June 2000) 157-171.

[8] Nasrabadi, H., Ghorayeb, K. and Firoozabadi, A. *SPE Reservoir Evaluation and Engineering* (Oct., 2006) 530-542.

[9] Banki, R., Hoteit, H. and Firoozabadi, A. *International Journal of Heat and Mass Transfer* (to appear).

[10] Hoteit, H., Banki, R. and Firoozabadi, A. *Energy & Fuels* (to appear).

[11] Ghorayeb, K., and Firoozabadi A. *AIChE Journal* (May 2000) 883-891.

[12] Firoozabadi, A., Ghorayeb, K., and Shukla, K. *AIChE Journal* (May 2000) 892-900.

[13] Duncan, J.B. and Toor, H.L. *AIChE Journal* (1962) **8**, 38-41.

[14] Leahy-Dios, A., Zhou, L. and Firoozabadi, A. *Journal of Physical Chemistry B* (to appear).

[15] Taylor, R. and Krishna, R.: Multicomponent Mass Transfer (Wiley, New York, 1993).

[16] Astumian, R.D. *PNAS* (2007) 104, 3.

[17] Platten, J. K., Bou-Ali, M. M., Costèsèque, P., Dutrieux, J. F., Köhler, W., Leppla, C., Weigand, S. and Wittko, G. *Phil. Mag.* (2003) 83, 1965.

[18] Wiegand *J Phys: Cond. Matter* (2004) 16, 357.

[19] Platten, J. K. *Trans. ASME, J. Appl. Mech* (2006) 73, 5.

[20] Leahy-Dios, A., Bou-Ali, M., Platten, J.K., and Firoozabadi, A. *Journal of Chemical Physics* (2005) **122**, 254502, 1-12.

[21] Haugen, K., and Firoozabadi, A. *Journal of Chemical Physics* (Oct. 2007) 127, 154507.

[22] Haugen, K. and Firoozabadi, A. *Journal of Physical Chemistry B* (2006) **110**, No. 35, 17678-17682.

Isotope and isomer effect in thermal diffusion of binary liquid mixtures

S. Hartmann, A. Königer and W. Köhler

Physikalisches Institut, Universität Bayreuth, Germany

Contact: werner.koehler@uni-bayreuth.de

Abstract

We have investigated the effect of isotopic substitution and of isomerism in cyclohexane/decalin mixtures on the Soret coefficient at room temperature over the entire concentration range. As already observed for other mixing partners of cyclohexane, the Soret coefficient S_T of cyclohexane increases upon perdeuteration (C_6D_{12}) by $\Delta S_T \approx 0.84 \times 10^{-3} K^{-1}$ in case of *cis*-decalin and by $\Delta S_T \approx 0.83 \times 10^{-3} K^{-1}$ in case of *trans*-decalin. In either case ΔS_T is independent of concentration. Perdeuteration of the other component, *cis*-decalin ($C_{10}D_{18}$), reduces the Soret coefficient of cyclohexane in *cis*-decalin by $0.81 \times 10^{-3} K^{-1}$. In all systems investigated, the sign change is such that perdeuteration renders the respective component more thermophobic. This observation is in agreement with results from MD simulations. Contrary to isotopic substitution, the replacement of *cis*-decalin by its configurational isomer *trans*-decalin results in a slightly concentration dependent increase of S_T of cyclohexane. This corresponds to a more thermophobic tendency of the *cis*- than of the *trans*-form of decalin, which is also recovered in the direct comparison of mixtures of *cis*- and *trans*-decalin, showing a positive S_T. The isotope and the isomer effect in cyclohexane/decalin mixtures are mutually independent and additive. The Soret coefficients have been measured by means of a transient holographic grating technique and, in some cases, a Soret cell with optical beam deflection.

1 Introduction

Experiments where molecular parameters of a binary liquid mixture are varied in a systematic manner are of crucial importance for a better understanding of the Soret effect. One route for well-defined changes on the molecular level is isotopic substitution, where the mass of a molecule and the mass distribution within a molecule can be changed while leaving the chemistry unaffected and not or only slightly altering the intermolecular potentials. Early experiments on H_2O/D_2O have already been performed by Prigogine [1]. Binary isotopic mixtures of organic liquids were investigated by Ma and Beyerlein and Rutherford. These authors studied, among others, mixtures of benzene of various degrees of deuteration, isotopically substituted mixtures of halogenated benzenes, mixtures of partly and fully deuterated methanol, and isotopic mixtures of carbon disulfide by means of the thermogravitational column technique (for references see [2]). Recent molecular dynamics simulations of Lennard-Jones liquids have shown that the differences in molecular mass, moment of inertia, diameter, and interaction strength contribute additively to the Soret coefficient S_T in such a manner that the molecules with the higher mass, the higher moment of inertia, the smaller diameter, and the stronger interaction prefer the cold side [3–7]. In order to obtain a systematic study of isotopic substitution, we have performed studies on isotopically substituted benzene [8] and cyclohexane, the latter in a number of different organic liquids [2]. The major result of these studies was a constant isotope effect of the Soret coefficient of cyclohexane ($\Delta S_T \approx -1.0 \times 10^{-3}\,\mathrm{K}^{-1}$), independent of both the second component and the concentration of the mixture. With good approximation the Soret coefficient can be decomposed into three contributions: $S_T = S_T^0 + a_m \Delta M + b_i \Delta I$. ΔM is the difference of the molecular masses and ΔI the difference of the molecular moments of inertia of the two components. S_T^0 is the so-called chemical contribution. It accounts for the concentration dependence, and MD simulation have shown that it is due to the interaction between unlike particles [9]. Besides isotopic substitution, the substitution of one compound by an isomer is the second subtle change that can be made to a binary mixture. Polyakov et al. have performed a systematic study of alkanes in benzene, where they could show that the alkanes become more thermophobic with an increasing degree of branching [10].

Motivated by the question about the effect of configurational isomerism, as compared to the structural isomerism of the alkanes, and by the question about the interplay between isotopic and isomeric substitution, we report about experiments on mixtures of cyclohexane with the two configurational isomers *cis*- and *trans*-decalin. Both cyclohexane and *cis*-decalin have also been used in the perdeuterated, besides the protonated, form.

2 Experimental

The experimental data shown here have been obtained by thermal diffusion forced Rayleigh scattering (TDFRS) [11]. The contrast factors $(\partial n/\partial T)_{p,c}$ and $(\partial n/\partial c)_{p,T}$ have been measured interferometrically or with an Abbe refractometer, respectively. The typical diffusion length in TDFRS experiments is 10 µm, resulting in short diffusion time constants of the order of 10 ms. Although TDFRS combines a number of experimental advantages, like the short diffusion times and the high sensitivity, there is the need to add some dye for optical absorption. Especially for aqueous systems suitable dyes are scarce, and even

in organic mixtures a possible influence of a dye is occasionally difficult to rule out [12]. Wiegand et al. [13] have employed an IR laser, which is directly absorbed by water to circumvent the dye problem in aqueous systems.

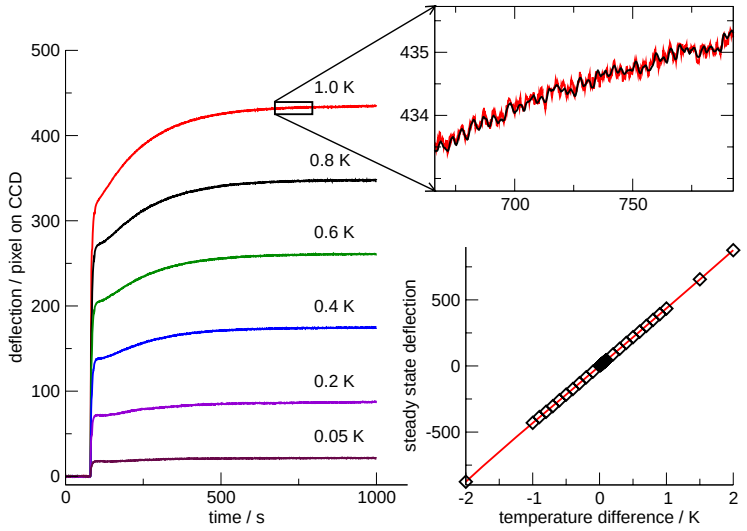

Fig. 1: *Beam deflection signal for ethanol/water (15 weight percent ethanol, $T = 20\,^{\circ}\mathrm{C}$) The left figure shows the beam deflection after switching for various temperature differences between top and bottom plate. The upper right insert shows an enlarged part of the measured curve (red) and the numerical solution (black). Note that the oscillations result from measured temperature jitters caused by the temperature controller. They propagate through the numerical integration and are part of the signal and not noise. The lower figure on the right side shows the long time steady state deflection as a function of the applied temperature difference.*

In order to have an alternative experimental technique available, we have built a beam deflection setup with optical readout, which relies on heating from the boundary instead by optical absorption in the volume. Following the works of Meyerhoff [14], optical Soret cells have been used by a number of authors [15–17]. Our instrument has been built, with some modifications, according to the one operated in the group of Piazza [18]. The first very promising results, obtained with a cell of 1 mm spacing and 40 mm path length, are shown in Fig. 1.

Chemicals were obtained from Aldrich and Acros Organics (purity $> 99\%$). Cyclohexane has been used in its protonated (C_6H_{12}) and perdeuterated (C_6D_{12}) form. Decalin (decahydronaphthalene, $C_{10}H_{18}$) exists both in a *cis* and in a *trans* form. Both isomers have been investigated as protonated and cis-decalin additionally as perdeuterated ($C_{10}D_{18}$) compounds (Fig. 3).

3 Results and Discussion

3.1 Isotope effect

Fig. 2 shows the effect of isotopic substitution for decalin/cyclohexane mixtures as a function of the cyclohexane mole fraction. S_T of cyclohexane is negative in either decalin isomer (open squares and triangles in Fig. 2), meaning that cyclohexane migrates to the hot side.

As already observed in case of other mixtures [2, 8], deuteration renders a compound more thermophobic: the Soret coefficient of C_6D_{12} both in *cis*- and in *trans*-decalin is larger than the one of C_6H_{12}. This shift (arrows *a* in Fig. 2) is independent of concentration and amounts to $\Delta S_T \approx 0.84 \times 10^{-3}\,\mathrm{K}^{-1}$ in case of *cis*-decalin and $0.83 \times 10^{-3}\,\mathrm{K}^{-1}$ in case of *trans*-decalin. These almost identical values are, albeit more towards the lower end of the variation, in reasonable agreement with the isotopic shift of the Soret coefficient of cyclohexane found in other mixtures [2].

In agreement with the increase of S_T upon deuteration of cyclohexane, S_T decreases in case of deuteration of *cis*-decalin (filled diamonds on Fig. 2, arrow *b*). The absolute value of the change is $0.81 \times 10^{-3}\,\mathrm{K}^{-1}$ and, surprisingly, almost identical to the one in case of deuteration of cyclohexane.

Due to the strong correlation between molecular mass and moment of inertia, both in case of cyclohexane and decalin, a separation into distinct contributions as done in Refs. [2,8] has not been possible. Additional measurements at different temperatures have shown that all data can be well described by a common fit function

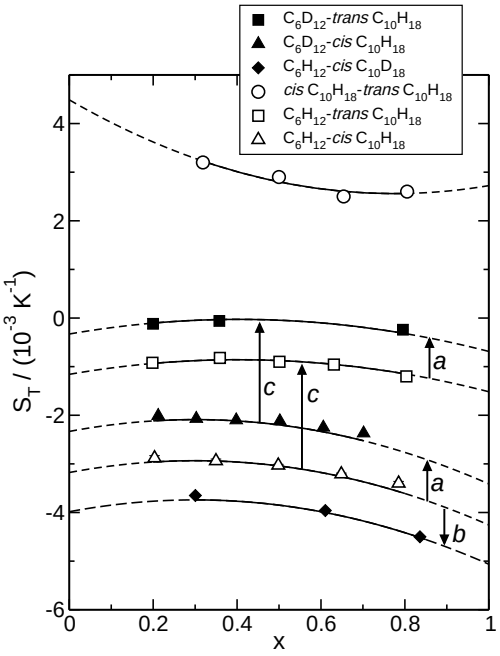

Fig. 2: *Soret coefficients S_T of cyclohexane and the two configurational isomers of decalin, respectively, as a function of cyclohexane mole fraction x at temperature $T = 25^\circ$. The lines are polynomial fits. The filled symbols correspond to mixtures with perdeuterated compounds. Upper curve (open circles):* cis-*decalin in* trans-*decalin as function of* cis-*decalin mole fraction. The arrows are explained in the text.*

$$S_T = \alpha(x)\beta(T) + c_M \frac{M_y - M_z}{M_y M_z} \tag{1}$$

with $c_M = 0.627\,\mathrm{uK}^{-1}$. M_y and M_z are the molecular masses of the two components.

Expression 1 differs slightly from the ones used in Refs. [2, 12], but a detailed discussion is beyond the scope of this contribution. The solid lines in Fig. 2 result from a common fit of Eq. 1 to all concentrations and temperatures between 10 °C and 55 °C.

3.2 Isomer effect

Isomers are ideally suited for the study of the influence of structural properties on the Soret coefficient. While Polyakov et al. have investigated the effect of branching for the structural isomers of heptane [10] in benzene, *cis*- and *trans*-decalin differ only by their configuration (Fig. 3), thus representing a more subtle change of the molecules.
Fig. 2 also shows the effect of isomeric substitution of decalin for mixtures with protonated and perdeuterated cyclohexane (arrows *c*). In either case, the isomeric substitution of decalin leads to the identical change of S_T. Contrary to the isotope effect, the isomer effect is, albeit only weakly, concentration dependent and increases slightly with increasing cyclohexane concentration. When comparing the absolute values, one finds that the isomer effect exceeds the isotope effect by more than a factor of two.

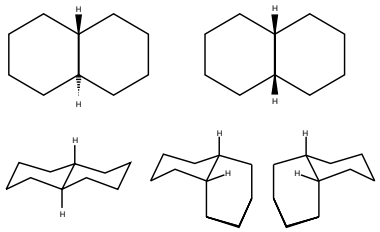

Fig. 3: *Trans (left) and cis (right) isomers of decalin.*

From the mixtures with cyclohexane it can be seen that *cis*-decalin is more thermophobic than *trans*-decalin. This property is retained in the mixtures of the two decalin isomers (open circles in Fig. 2). There, the Soret coefficient of *cis*-decalin in *trans*-decalin is positive, corresponding to *cis*-decalin migrating to the cold side (being more thermophobic).
As a result, we find that the change of S_T upon isotopic substitution of cyclohexane is independent of the decalin isomer and, vice versa, the change of S_T upon replacement of *cis*- by *trans*-decalin is independent of the deuteration of cyclohexane. Hence, isotope and isomer effect are mutually independent and additive. The interesting question, as to whether perdeuteration of the two decalin isomers leads to an identical shift of the Soret coefficient, still awaits an answer.

Acknowledgement We thank R. Piazza for help with the beam deflection setup, B. Meier for building the first version of this instrument in our lab, and the Deutsche Forschungsgemeinschaft (DFG) for financial support (Ko 1524/5-2).

References

[1] I. Prigogine, L. de Brouckère, and R. Buess, Physica **18**, 915 (1952).
[2] G. Wittko and W. Köhler, J. Chem. Phys. **123**, 014506 (2005).
[3] B. Hafskjold, T. Ikeshoji, and S. K. Ratkje, Molec. Phys. **80**, 1389 (1993).
[4] D. Reith and F. Müller-Plathe, J. Chem. Phys. **112**, 2436 (2000).
[5] P. Bordat, D. Reith, and F. Müller-Plathe, J. Chem. Phys. **115**, 8978 (2001).
[6] G. Galliero, B. Duguay, J.-P. Caltagirone, and F. Montel, Fluid Phase Equilibria **208**, 171 (2003).

[7] G. Galliero, B. Duguay, J.-P. Caltagirone, and F. Montel, Philos. Mag. **83**, 2097 (2003).
[8] C. Debuschewitz and W. Köhler, Phys. Rev. Lett. **87**, 055901 (2001).
[9] P.-A. Artola and B. Rousseau, Phys. Rev. Lett. **98**, 125901 (2007).
[10] P. Polyakov, J. Luettmer-Strathmann, and S. Wiegand, J. Phys. Chem. B **110**, 26215 (2006).
[11] G. Wittko and W. Köhler, Philos. Mag. **83**, 1973 (2003).
[12] G. Wittko and W. Köhler, Europhys. Lett. **78**, 46007 (2007).
[13] S. Wiegand, H. Ning, and H. Kriegs, **submitted**, (2007).
[14] G. Meyerhoff and K. Nachtigall, J. Polym. Sci. **57**, 227 (1962).
[15] M. Giglio and A. Vendramini, Phys. Rev. Lett. **34**, 561 (1975).
[16] P. Kolodner, H. Williams, and C. Moe, J. Chem. Phys. **88**, 6512 (1988).
[17] K. J. Zhang, M. E. Briggs, R. W. Gammon, and J. V. Sengers, J. Chem. Phys. **104**, 6881 (1996).
[18] R. Piazza and A. Guarino, Phys. Rev. Lett. **88**, 208302 (2002).

The theory of the thermodiffusion column with arbitrary cross-section

I. Hodor

National Institute for R&D of Isotopic and Molecular Technologies,
Cluj-Napoca, Romania

E-mail: *hodor@itim-cj.ro*

Abstract

The cylindrical thermodiffusion column with an arbitrary cross-section is theoretically treated as a particular application of a general theory of the separation column previously developed by the author. The expression of the species-transport through the column is deduced and some applications are discussed.

1 Introduction

The thermodiffusion (TD) column has been theoretically studied only for simple column cross-sections so far: Furry-Jones-Onsager (FJO) [1] and Marcoux-Costeseque [2] considered rectangular cross-sections with one side much greater than the other one, and Furry-Jones [3] considered the annular cross-section. The treatment of the general cross-section case is useful for it can be specialised for any geometry of practical interest. For instance it can be particularised for squared cross-section with comparable sides, which is more realistic than the limit cases studied so far. In this paper the TD column with an arbitrary cross-section, for a binary fluid mixture, is treated by applying a general theory of the separation column developed previously [4-7].

2 Assumptions and preliminaries

(a) The TD column is essentially cylindrical, upright and with an arbitrary cross-section as suggested by Fig. 1. Impermeable walls limit the fluid mixture. A transversal temperature gradient gives rise to a TD separation effect and a countercurrent laminar convection. Thermodynamic equilibrium is locally attained and let (T, p, w_1)= (temperature, pressure, mass fraction of the component 1) be the local independent state parameters. The mass flux of the species 1 is given by

$$\mathbf{J}_1 = \rho w_1 \mathbf{v} - \rho D(\nabla w_1 - \alpha w_1 w_2 \nabla \ln T) \tag{1}$$

where ρ is the mass density, $\mathbf{v}$ the local mass average velocity, $w_2 = 1 - w_1$ the mass fraction of component 2, D the mutual diffusion coefficient, and α the thermal diffusion factor. In principle, ρ, D, and α are state parameters depending on (T, p, w_1).

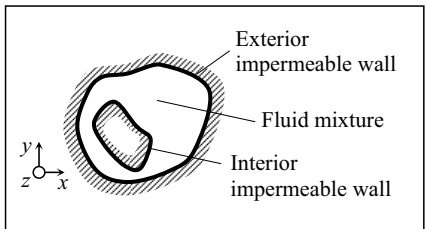

Fig. 1: Sketch of column cross-section.

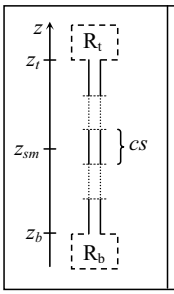

Fig. 2: A sketch of the column.
R_b, R_t, infinite reservoirs.
cs, column segment of length l_s.
z_{sm} middle coordinate of *cs*.

(b) Assume α is small and denote $\alpha = \varepsilon\widetilde{\alpha}$ where ε is an infinitesimal constant and $\widetilde{\alpha} = \widetilde{\alpha}(T, p, w_1)$ a finite function. Let $L = z_t - z_b$ be the column length and $S = (w_{1t} / w_{2t})/(w_{1b} / w_{2b})$ the separation, where *t* and *b* indicate the *t*op and the *b*ottom of the column, Fig. 2. Assume $S - 1$ is finite, which involves $L \to \infty$ when $\varepsilon \to 0$.

(c) Denote by z_{sm} the coordinate z for which $(z_{sm}-z_b)/L=s$ and consider a column segment of length l_s having the center in z_{sm}. Denote by z_s the coordinate z for which $z_s=z\in(z_{sm}-\frac{1}{2}l_s,z_{sm}+\frac{1}{2}l_s)$ and by S_s the separation between the ends of the segment s. Now, assume that l_s is chosen so that the following not exclusive conditions are satisfied: if $\varepsilon\to 0$ and $L\to\infty$ then $l_s\to\infty$, $l_s/L\to 0$, $S_s-1\to 0$, and $\varepsilon/(S_s-1)\to 0$. Corollary: If $\varepsilon\to 0$ then: $z_s/L\to s$, the segments are disjoint, and the set of segments is an infinite of Cantor's cardinality $\aleph_1$. Note that a position along column can be given either by z or by the pair (s, z_s).

(d) The boundary conditions that can be imposed at $z=z_b$ and $z=z_t$ are of an infinite variety. However, these conditions have a strong effect only upon the end segments $s=0$ and $s=1$, while the effect is very limited for $s\in(0,1)$. Since only the theory for $s\in(0,1)$ is treated here, it is assumed without any restriction on generality that the column ends are connected to infinite reservoirs containing mixture of concentration w_{1t} at the top and w_{1b} at the bottom, and between which there is a pressure difference that gives rise to a net mass flow through the column $\tau=\iint_\sigma \rho v_z\,dxdy$, where σ is the cross-section of the working space.

(e) The column can either separate or mix. Here we treat the separation, and in this case the following **theorem** is valid: *If ε is infinitesimal then (i) ∇w_1 and τ are infinitesimal of the ε-order and (ii) $\partial w_1/\partial z=\beta\widetilde{w}_{1z}$ where β is of ε-order and $\widetilde{w}_{1z}$ is a finite function*. **Proof**:

- In Eq. 1, $\alpha w_1 w_2\nabla\ln T$ is the source and ∇w_1 the sink of separation. As the source is small, of the ε-order, the sink ∇w_1 should also be of the ε-order; otherwise the separation can neither be produced nor maintained.
- In the steady state, if $w_{1t}=w_{1b}$ then $\partial w_1/\partial z=0$, which means that $\partial w_1/\partial z=\beta\widetilde{w}_{1z}$, where β is an arbitrary constant determinable from boundary conditions. Since ∇w_1 is of ε-order, β can be treated as an arbitrary constant of ε-order and $\widetilde{w}_{1z}$ as a finite function.
- Since ∇w_1 is of the order of ε one can write $w_1(x,y,z)=\overline{w}_1(z)+\varepsilon\widetilde{w}_1(x,y,z)$ where $\overline{w}_1(z)$ and $\widetilde{w}_1(x,y,z)$ are finite functions. Using this expression of w_1, the integration of Eq. 1 gives

$$\tau_1=\overline{w}_1(z)\tau+\varepsilon\widetilde{\tau}_1(z) \tag{2}$$

where $\tau_1=\iint_\sigma \mathbf{J}_1\,dxdy$ is the mass transport of species 1 through the column and $\widetilde{\tau}_1(z)$ is a finite function of z. Since in a steady state τ_1 and τ are independent of z and the

variation of $\overline{w}_1(z)$ along the whole column is larger than the ε-order, Eq. 2 is possible if and only if τ_1 and τ are small of ε-order.

3 Transport equation

We have discovered the group or vector (τ,ε,β) composed of three independent parameters that, ideally, are infinitesimal and of the same order of magnitude; ε is a property of the working fluid while τ and β are arbitrary constants determinable from the boundary conditions imposed at the two column ends. Any process function F can be expanded into a power series and truncated by the model,

$$F = \sum_{i,j,k=0}^{\infty} \tau^i \varepsilon^j \beta^k F_{(ijk)}\,, \qquad F_{(n)} = \sum_{i,j,k=0}^{i+j+k<n+1} \tau^i \varepsilon^j \beta^k F_{(ijk)} \tag{3}$$

The main purpose of the column theory is to derive a working expression for τ_1. The series (2) are extremely convergent, so that it is sufficient to find only the first order truncation $\tau_{1(1)}$ in order to obtain what other authors have aimed. When $(\tau,\varepsilon,\beta)\to(0,0,0)$ then $\tau_{1(1)}$ is the exact solution of the problem and in this case we will say that the column is *ideal.*

The mathematical model of the TD column can always be written as $\mathbf{S}=\mathbf{S}(\arg)=\mathbf{0}$ where $\mathbf{S}$ is a column-vector whose elements are mathematical expressions and $(\arg)$ stands for arguments of interest. The system $\mathbf{S}$ is composed of three subsystems, $\mathbf{S}=[\mathbf{M},\mathbf{L},\mathbf{E}]^{\mathrm{T}}=\mathbf{0}$, where $\mathbf{M}=\mathbf{0}$, $\mathbf{L}=\mathbf{0}$, and $\mathbf{E}=\mathbf{0}$ are material, momentum and energy equations, respectively.

Using the series expansion (3) for every vector component, the equation $\mathbf{S}=\mathbf{0}$ becomes

$$\mathbf{S} = \sum_{i,j,k=0}^{\infty} \tau^i \varepsilon^j \beta^k \mathbf{S}_{(ijk)} = \mathbf{0} \quad \Rightarrow \quad \mathbf{S}_{(ijk)} = \mathbf{0} \tag{4}$$

The expression for $\tau_{1(1)}$ can be deduced by using the equations of a segment $s\in(0,1)$. For this purpose, assume the segment has *column symmetry* in the sense that $\mathbf{S}$ is invariant to any finite translation along the z-axis, that is $\mathbf{S}(x,y,s,z_s+\Delta z_s)\equiv\mathbf{S}(x,y,s,z_s)$. Note that this is a global assumption, which includes particular assumptions; as for instance *the compressibility of the fluid in the segment s is assumed to be negligible.* Now, we have to solve successively the system of equations $\mathbf{S}_{(ijk)}=\mathbf{0}$. The equation $\mathbf{S}_{(000)}(x,y,s,z_s)=\mathbf{0}$ gives: (i) a constant field of concentration $w_{1(0)}(s)$, (ii) a temperature field $T_{(0)}(x,y,s)$ that does not depend on z_s, and (iii) a velocity field having the components $\mathrm{v}_{x(0)}=\mathrm{v}_{y(0)}=0$ and $\mathrm{v}_{z(0)}(x,y,s)$. The next truncation of the concentration field is of the general form

$$w_{1(1)} = w_{1(0)}(s) + \tau w_{1(100)} + \varepsilon w_{1(010)} + \beta w_{1(001)} \tag{5}$$

The fields $w_{1(100)}$, $w_{1(010)}$, and $w_{1(001)}$ are solutions of the equations $\mathbf{M}_{(100)} = \mathbf{0}$, $\mathbf{M}_{(010)} = \mathbf{0}$, and $\mathbf{M}_{(001)} = \mathbf{0}$ respectively. It is easy to show that $w_{1(100)} \equiv 0$. The field $w_{1(010)}$ does not depend on z_s and can be expressed by

$$w_{1(100)} = w_{1(100)}(x, y, s) = \frac{w_{1(0)} w_{2(0)}}{\varepsilon} \int_{T^*}^{T_{(0)}} \frac{\alpha_{(0)}}{T} dT \tag{6}$$

where T^* is an arbitrary constant temperature independent of x and y. A key point of the present theory is that the field $w_{1(001)}$ has the following special form derived in [6, 4]:

$$w_{1(001)}(x, y, s, z_s) = \psi_0(x, y, s) + z_s \tag{7}$$

By substituting this field in $\mathbf{M}_{(001)} = \mathbf{0}$ one obtains the equation for ψ_0

$$\rho_{(0)} \mathrm{v}_{z(0)} - \nabla_{xy} \left[\rho_{(0)} D_{(0)} (\nabla_{xy} \psi_0)\right] = 0 \tag{8}$$

$$(\nabla_{xy} \psi_0)_{(\mathrm{w}\perp)} = 0 \tag{8a}$$

where ∇_{xy} stands for the operator ∇ in the xy-plane. Eq. 8a represents the boundary condition at the wall and the subscript $(\mathrm{w}\perp)$ indicates the normal vector projection on the wall.

Using the obtained expression for $w_{1(1)}$, one obtains the transport

$$\tau_{1(1)} = w_{1(0)} \tau + w_{1(0)} w_{2(0)} H - (K_c + K_d)(\partial w_{1(1)} / \partial z_s) \tag{9}$$

$$H = \iint_{\sigma} \left(\int_{T^*}^{T_{(0)}} \frac{\alpha_{(0)}}{T} dT \right) \rho_{(0)} \mathrm{v}_{z(0)} \, dx \, dy \tag{9a}$$

$$K_c = -\iint_{\sigma} \psi_0 \rho_{(0)} \mathrm{v}_{z(0)} \, dx \, dy \tag{9b}$$

$$K_d = \iint_{\sigma} \rho_{(0)} D_{(0)} \, dx \, dy \tag{9c}$$

4 Discussion

It needs to be emphasized that Eq. 9 is the exact expression for the transport τ_1 when α approaches zero. Generally, one should use numerical methods in order to calculate some

integrals and equations. However, the numerical methods are much simplified by the fact that the z-coordinate is absent.

The velocity field $v_{z(0)}$ entering Eqs. 9a and 9b is produced by the temperature gradient alone. This is a proof that the influence of the concentration gradient upon the velocity field, called *forgotten effect*, is of second order. Hence, ***the forgotten effect should be forgotten***. A special treatment of the forgotten effect was previously given [7].

Eq. 9 can be adapted and used in many ways, according to circumstances.

The concentration $w_{1(0)} = w_{1(0)}(s)$ is constant in the segment s but varies from one segment to another. We can drop the iteration subscripts and use the coordinate z instead of the pair (s, z_s) and Eq. 9 becomes

$$\tau_1 = w_1\tau + w_1 w_2 H - (K_c + K_d)(\partial w_1 / \partial z) \tag{10}$$

Here w_1 is a function of z. If $w_t - w_{1b}$ is great and the state parameters ($\rho, D, ...$) strongly depend on concentration, then H, K_c, and K_d should be treated as functions of concentration.

If $\alpha = \overline{\alpha}$ can be treated as constant, then $H = \overline{\alpha} \iint_\sigma \rho_{(0)} v_{z(0)} \ln T_{(0)} dx\, dy$, and Eq. 10 leads to a working equation for the computation of $\overline{\alpha}$ from experimental concentration data.

Eq. 9 is established in the assumption that $\mathbf{S}(s, z_s + \Delta z_s) \equiv \mathbf{S}(s, z_s)$. It means that one can consider that $\mathbf{S}(s + \Delta s, z_s) \neq \mathbf{S}(s, z_s)$ in which case Eq. (10) describes a cascade. Moreover, although τ_1 does not depend on z_s, one can consider that it depends on s, in which case one can write the equation for the unsteady state of the column/cascade,

$$h \frac{\partial w_1}{\partial t} = -\frac{\partial}{\partial z}\left(w_1\tau + w_1 w_2 H - (K_c + K_d)\frac{\partial w_1}{\partial z} \right) \tag{11}$$

where h is the holdup of the liquid mixture per unit length of column.

References

[1] W. H. Furry, R. C. Jones, and L. Onsager, Phys. Rev. **55**, 1083 (1939**)**

[2] M. Marcoux, P. Costeseque, *Thermodiffusion: Basics&Applications* (Proc. of

IMT7-2006, eds. M. M. Bou-Ali & J. K. Platten, Mondragon Univ., 307)

[3] W. H. Furry and R. C. Jones: Phys. Rev., **69**, 459 (1946)

[4] I. Hodor, Isotopenpraxis, **20(9)**, 330 (1984)

[5] I. Hodor, Sep. Sci. Technol., **38(5)**, 1229 (2003)

[6] I. Hodor, *Thesis* (Univ. Babeş-Bolyai, Romania, 1971)

[7] I. Hodor, *Thermodiffusion: Basics&Applications* (Proc. of IMT7-2006, eds. M. M. Bou-Ali & J. K. Platten, Mondragon Univ., 67)

Comparison between theoretical model and experimental data of thermodiffusion coefficients for binary and ternary hydrocarbon mixtures and water-alcohol mixtures

T. J. Jaber[1], Y Yan[1], A. Abbasi[1,2] ,M.Z. Saghir[1]

[1] Department of Mechanical Engineering, Ryerson University, Canada
[2]Department of Chemical Engineering and Applied Chemistry, University of Toronto, Canada

E-mail: zsaghir@ryerson.ca

Abstract

Thermodiffusion coefficients were measured experimentally using a space hardware developed by the European Space Agency (ESA) and flown on board FOTON Soyuz rocket in September 2007 in collaboration with TOTAL France. Six different mixtures (Methane, Dodecane and n-Butane) were used to measure the thermal diffusion factor. The mixtures were maintained at a pressure of 35 MPa at an average temperature of 328 K. On the theoretical aspect, using the irreversible thermodynamics theory, theoretical calculations were performed on different hydrocarbon and water alcohol mixtures using Peng Robinson, volume translated Peng Robinson and PCSAFT equation of state. This theory was used in determining the thermodiffusion coefficients for different binary water-alcohol mixtures and hydrocarbon mixtures (nC_5-C_{12}) and then compared successfully with experimental data.

1 Introduction

Since its discovery by Carl Ludwig and Charles Soret in 1800s, thermodiffusion has attracted great interest from a wide range of areas including petroleum engineering, biology, environmental studies, material science and metallurgy. Comprehensive thermodiffusion theories and accurate thermodiffusion experiments are of great importance to the understanding and optimization of diffusion-dominant industrial processes. The kinetic theory considers thermodiffusion as a stepwise activated process relying on the activation energy to break down cohesive bonds [1]. The lattice model uses a thermostatic approach to relate the Soret coefficient with the canonical partition function of a "two-chamber" system [2]. The theory of non- equilibrium thermodynamics models has provided a general definition of the thermal diffusion factor as a function of the net heat of transport and chemical potential. In the past, many researchers applied the theory of non-equilibrium thermodynamics in their thermodiffusion studies including Dougherty et al [3], Firoozabadi et al [4] and Pan et al [5].

In this paper, a comparison has been made for modelled and measured thermodiffusion coefficients for different binary n-alkane mixtures and water alcohol mixtures. The ground base experimental data are obtained through the technique of thermogravitational column. A theoretical model based on the theory of non-equilibrium thermodynamics is used to calculate the thermal diffusion factor α_T. Results revealed a good agreement with experimental data. Then estimated thermodiffusion coefficients of ternary hydrocarbon mixtures are revealed in preparation for comparison with experimental data from FOTON Soyuz rocket.

2 Theoretical Model

According to the theory of non-equilibrium thermodynamics, molar diffusion flux can be expressed in terms of phenomenological coefficients. In a binary mixture at a constant pressure, only molecular diffusion and thermodiffusion contribute to the diffusion flux, therefore

$$\vec{J}_1^{mol} = -L_{11}^* \frac{Q_1^* - Q_2^*}{T^2} \vec{\nabla} T - \frac{1}{T x_2} L_{11}^* \left(\frac{\partial \mu_1}{\partial x_1} \right)_{T,p} \vec{\nabla} x_1 \tag{1}$$

where $\vec{J}_1^{mol}$ is the molar diffusion flux of component 1 with respect to a molar average reference velocity. Q_i^* is the net heat of transport of component *i*, and μ_1 is the chemical potential. x_1 and x_2 are the molar fraction of component 1 and 2, respectively. L_{11}^* is the phenomenological coefficient. Conventionally, diffusion flux can also be expressed in terms of molecular diffusion coefficient (or Fick's coefficient) and thermodiffusion coefficient as follows:

$$\vec{J}_1^{mol} = -\rho^{mol} (D^{mol} \vec{\nabla} x_1 + D_T^{mol} x_1 x_2 \vec{\nabla} T) \tag{2}$$

A general equation for thermal diffusion factor α_T for binary mixtures can be derived:

$$\alpha_T = \frac{Q_1^* - Q_2^*}{x_1\left(\frac{\partial \mu_1}{\partial x_1}\right)_{T,p}} \tag{3}$$

It can be seen from eq. (3) that accurate thermodiffusion modelling relies on accurate prediction of the net heat of transport Q_i^*. By applying Eyring's viscosity theory, Dougherty et al [3] followed by Shukla and Firoozabadi [4] presented an expression Eq. (4) for thermal diffusion factor for binary mixtures;

$$\alpha_T = -\left(\frac{\left(\overline{U}_1 - \overline{U}_{1g}^0\right)/\tau_1 - \left(\overline{U}_2 - \overline{U}_{2g}^0\right)/\tau_2}{x_1\left(\frac{\partial \mu_1}{\partial x_1}\right)_{T,p}} + \frac{\overline{V}_2 - \overline{V}_1}{\overline{V}_1 x_1 + \overline{V}_2 x_2} \cdot \frac{x_1\left(\overline{U}_1 - \overline{U}_{1g}^0\right)/\tau_1 + x_2\left(\overline{U}_2 - \overline{U}_{2g}^0\right)/\tau_2}{x_1\left(\frac{\partial \mu_1}{\partial x_1}\right)_{T,p}} \right) \tag{4}$$

where $\overline{U}_i$ is the partial molar internal energy of component i $\overline{U}_{ig}^0$ is the internal energy of the ideal gas at the same temperature. τ_i is a parameter to represent the ratio of viscous energy to the cohesive energy. Eq. (4) requires accurate thermodynamics properties, namely, $\left(\overline{U}_i - \overline{U}_{ig}^0\right)$, $x_1\left(\partial \mu_1/\partial x_1\right)$ and $\overline{V}_i$. Therefore, U_i, $x_1\left(\partial \mu_1/\partial x_1\right)$ and $\overline{V}_i$ can all be calculated accurately through equations of state. The choice of EOS depends on the nature of the fluid mixtures.

3 Results and Discussion

Different binary and ternary mixtures are investigated in this study. These mixtures are binary hydrocarbon mixtures nC_i–nC_{12} (i=5~9), binary water-alcohol mixtures and ternary hydrocarbon of Dodecane-nButane-Methane.

3.1 Thermal Diffusion Coefficient for Binary Hydrocarbon Mixtures

A comparison of thermodiffusion coefficient obtained through modelling and experiments are listed in Table 1. Note that the thermodiffusion coefficients D_{T2} shown in these tables are for the second component, nC_{12}.

The positive thermodiffusion coefficients indicates that the second components, nC_{12}, moves in a direction opposite to the temperature gradient.

Table 1: *Thermal diffusion coefficient D_T for nC_i (1) – nC_{12} (2) at 25°C*

$nC_i - nC_{12}$ (50:50 wt%) i=5-9	D_{T2} , 10^{-12} m^2/sK			
	Measurement	Calculation	Comparison	
			$abs(D_{T\_cal} - D_{T\_exp})$	Relative Error (%)
5	10.94	13.56	2.62	23.93
6	7.45	7.61	0.16	2.17
7	5.15	5.13	0.02	0.33
8	3.39	4.21	0.82	24.29
9	2.15	2.29	0.14	6.44

3.2 Thermal Diffusion factor for Binary Water-alcohol Mixture

Predicting thermal diffusion factor with PC-SAFT equation of state depends on two adjustable parameters. One is the binary interaction parameters for the mixture of interest which can be optimized through available experimental vapor–liquid equilibrium data under a range of temperatures. The second one is the ratio of the energy of vaporization to the viscous energy. The energy of vaporization $\Delta U_{evap,i}$ is considered the difference between the internal energy of gas and liquid phase in equilibrium. Using PC-SAFT EoS, equilibrium condition for specific temperature and pressure can be achieved. Thus $\Delta U_{evap,i}$ calculation for each mole fraction is manageable. However calculation of the viscous energy $\Delta U_{vis,i}$ as a function of mole fraction doesn't have any specific model. Figure 1 shows a comparison between the calculated thermal diffusion factors calculated with modified and simple mixing rules and the experimental results. The calculation based on the modified mixing rule show very good agreement with the experimental result.

3.3 Thermodiffusion Coefficients for Ternary Hydrocarbon Mixtures

Using Peng-Robinson and volume translated Peng Robinson equations of state, the thermodiffusion coefficients at a pressure of 350 bar has been evaluated for six ternary mixture made of dodecane, n-butane and methane.

As shown in Table 2, Methane the lightest component has a mole fraction of 20% and is maintained constant during the proposed six mixtures. In this calculation, methane is defined as the carrier (component 3), dodecane is the component 1 and n-butane is the component 2. Therefore D_{T1} is the thermodiffusion coefficient of dodecane in the mixture and D_{T2} is the thermodiffusion coefficient of n-Butane in the mixture. Figure 2 shows the calculated thermodiffusion coefficients for mixture 1 at different average temperature using PR EoS and vt-PR EoS.

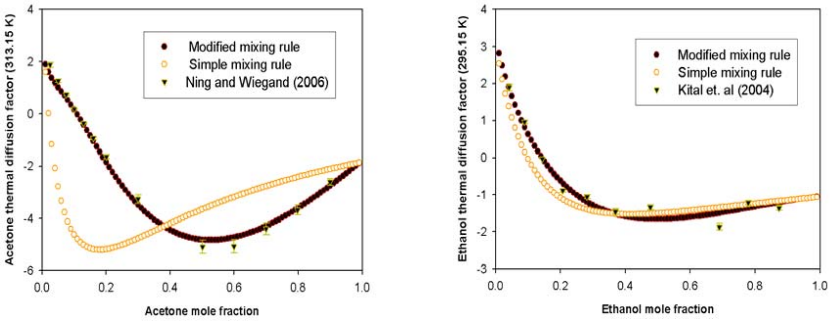

(a) Water-acetone system (50%-50%)

(b) Water-ethanol system (90%-10%)

(c) Water-isopropanol system (90%-10%)

Fig. 1: *Evaluation of thermal diffusion factor.*

Table 2: *Hydrocarbon Mixtures Composition in Mole Fraction*

Mixture	Methane	n-Butane	Dodecane
1	20%	10%	70%
2	20%	20%	60%
3	20%	30%	50%
4	20%	40%	40%
5	20%	50%	30%
6	20%	60%	20%

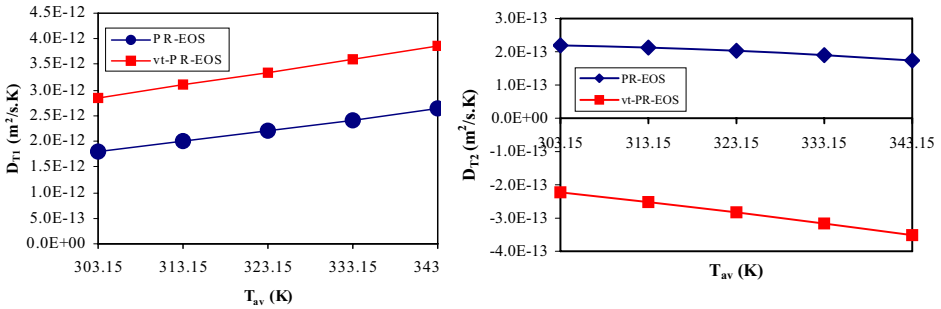

(a) D_{T1} versus T_{av} **(b) D_{T2} versus T_{av}**

Fig. 2: *Variation of the thermal diffusion coefficients as function of average temperatures.*

4 Conclusions

This paper presents the theoretical calculations for thermodiffusion in both binary and ternary mixtures. The binary mixture includes n-alkane mixtures of nC_i-nC_{12} (i =5~9), water-isopropanol, water-ethanol and water-acetone. The calculated results for those binary mixtures show very good agreement with the experimental data. The theoretical model verified through binary mixtures is then used to estimate the thermodiffusion coefficients in the ternary flight mixtures on board FOTON M3.

Acknowledgment

The authors wish to acknowledge the support of the European Space Agency (ESA) and the Natural Science and Engineering Council, Canada (NSERC).

References

[1] I. Prigogine, L. Debrouckere L., and R. Amand, Recherches sur la thermodiffusion en phase liquide .1. PHYSICA, **16**(7-8):577-598, 1950.

[2] J. Luettmer-Strathmann, Lattice model for thermodiffusion in polymer solutions. Int. J. Thermophysics, **26**(6):1693-1707, November 2005.

[3] E. L. Dougherty, H. G Drickamer , A theory of thermal diffusion in liquids, J. Chem. Phys. **23**(2): 295-309,1955.

[4] A. Firoozabadi, K. Ghorayeb, K Shukla, Theoretical model of thermal diffusion factors in multicomponent mixtures. AIChE J., **46**(5):892-900, 2000.

[5] S. Pan, M.Z. Saghir, M Kawaji, C Jiang, Y Yan, Theoretical approach to evaluate thermodiffusion in aqueous alkanol solutions, J. Chem. Phys., **126(1)**, 014502, 2007.

Study of the thermal diffusion behavior of simple and associated mixtures

P. Polyakov and S.Wiegand

IFF, Forschungszentrum Jülich, Germany

Contact: p.polyakov@fz-juelich.de

Abstract

We performed systematic temperature and concentration measurements of the Soret coefficient for two different groups of mixtures using Thermal diffusion Rayleigh scattering method. The mixtures from the first group (carbon tetrabromide, tetraethylsilane and di-tert-butylsilane in carbon tetrachloride) can be treated as ideal solutions. The Soret coefficient of CBr_4 in CCl_4 is positive and S_T of both silanes in CCl_4 is negative, which implies that the heavier component always moves to the cold side. This is the expected behavior for unpolar simple molecules. The results are discussed in the framework of thermodynamic theories and the Hildebrand parameter concept. Additionally, the Soret coefficients for both silane/CCl_4 systems were determined by nonequilibrium molecular-dynamics calculations. The simulations predict the correct direction of the thermophoretic motion and reflect the stronger drive toward the warm side for di-tert-butylsilane compared to the more symmetric tetraethylsilane. The values deviate systematically between 9% and 18% from the experimental values. The mixtures from the second group (dimethyl sulfoxide (DMSO), methanol, ethanol, acetone, methanol, 1-propanol, propionaldehyde in water) are not ideal due to their ability to form hydrogen bonds. It was found, that for some of the mixtures such as ethanol/water, acetone/water, DMSO/water and propionaldehyde/water the concentration at which the Soret coefficient changes its sign does not depend on temperature and is equal to the concentration where the Soret coefficient isotherms intersect. While for propanol/water mixtures the sign change concentration is temperature dependent. The dependence of the sign concentration of S_T was analyzed in terms of the ratio of the vaporization enthalpies of the pure components. The obtained results are related to hydrophilic and hydrophobic interactions of the solute molecules with water.

1 Introduction

Conceptually, binary mixtures of simple molecules can be divided into three groups: mixture of spherical molecules without specific interactions, mixtures of non-spherical molecules without specific interactions and associated mixtures. In the first group of mixtures the component with the larger mass or higher density moves to the cold side, and this effect becomes stronger if the components are less miscible [1–3]. This empirical observations still hold for some mixtures from the second group [1]. Associated mixtures often show a sign change of the Soret coefficient with concentration [4] so that the direction of the thermal diffusion process is predominantly guided by excess properties and not by the properties of the mixing partners like the difference in mass or moment of inertia. On the other hand it was observed that the sign change concentration correlates with the concentration at which the hydrogen bond network breaks down [4] and the concentration dependence of the Soret coefficient in aqueous systems seems to be universal [5]. Therefore it might be possible to relate the sign change concentration with properties of the pure components and the structure of the mixture.

In this paper we investigated two groups of mixtures. For the first group we have chosen rather simple tetrahedral, non-polar molecules, which can be well approximated by a spherical shape: carbon tetrachloride (CCl_4), slightly heavier carbon tetrabromide (CBr_4) and two isomers tetraethylsilane and di-tert-butylsilane. For the second group we have chosen polar molecules like water, deuterated water, dimethyl sulfoxide (DMSO), ethanol, acetone, methanol, 1-propanol, 2-propanol and propionaldehyde. Particular attention has been given to the sign change concentrations. The Soret for all systems was measured using Thermal diffusion Rayleigh scattering technique. For two mixtures of isomers with CCl_4 from the first group nonequilibrium molecular dynamic simulations were performed additionally.

2 TDFRS experiment and NEMD simulations

Experimental details about the sample preparation and the description of the TDFRS experiment can be found in [6] and references therein. A detailed description of reverse nonequilibrium molecular dynamics method (NEMD) can be found elsewhere [7, 8]. The force field for carbon tetrachloride was taken from the work by Rey at al. [9]. For the alkane chains of both silanes we applied the force field from Wescott [10]. A detailed description of the composed force field can be found in Polyakov et al [6]. In the case of tetraethylsilane, the Lennard Jones parameters σ and ε of Si, and for di-tert-butylsilane those of SiH_2 have been adjusted to reproduce experimental density and heat of vaporization. The cell was elongated in z-direction, which is the direction of the heat flow (L_x=L_y=$L_z/3 \approx 4$ nm). The cutoff length for nonbonded interactions was 1.2 nm. The time step was 2 fs. All NEMD simulations were performed at constant NVT conditions (densities: 1047.2 and 1009.9 kg/m^3 for equimolar mixtures of tetraethylsilane and di-tert-butylsilane in carbon tetrachloride, respectively) with 960 molecules in the simulation box. The average temperature was kept constant by the thermostat of Berendsen, with the temperature coupling time being T = 1 ps.

3 Results and Discussion

3.1 Mixture of spherical molecules

Fig 1 shows the experimental measured Soret coefficient of CBr_4, $Si(C_2H_5)_4$ and $[C(CH_3)_3]_2SiH_2$ in CCl_4 at different temperatures as a function of concentration. The corresponding values determined by simulations at around 303 K for a binary equimolar mixtures of $Si(C_2H_5)_4$ and $[C(CH_3)_3]_2SiH_2$ in CCl_4 are: $-5 \pm 0.3\times\ 10^{-3}$ and $-5.5 \pm 0.3\times\ 10^{-3}$ K^{-1}. The simulation results are larger than the experimental values and their magnitude is smaller by 9 and 18 $\%$.

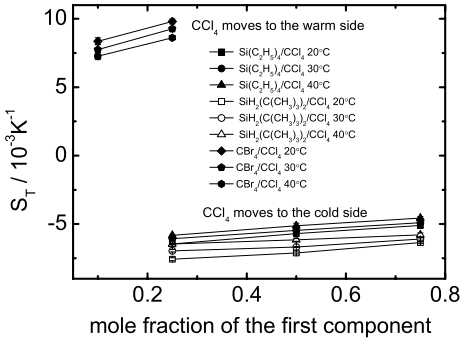

Fig. 1: *Soret coefficient S_T of CBr_4, $Si(C_2H_5)_4$, $[C(CH_3)_3]_2SiH_2$ in CCl_4 as a function of concentration.*

Those small systematic errors are probably due to the force field parameters, which were developed to reproduce the density and heat of vaporization of the pure components but not any transport coefficient. Another reason might be the sensitivity of the Soret coefficient to the chosen mixing rule.

Galliero et al [3] investigated the thermodiffusion behavior of equimolar mixtures of "super methane" in methane. The parameters mass, m, diameter, σ, and depth of the interaction potential, ε of super methane were different from those of methane. They obtained three additive contributions S_T^m, S_T^σ and S_T^ε to S_T stemming from the mass, diameter and interaction strength, respectively. We calculated these contributions for all three investigated mixtures. The ratios of the diameter and the depths of the interaction potential were estimated using the experimental molar volumes V_{mol} (at room temperature) and enthalpies of vaporization H_{vap} (at boiling point) for the different components. The mass contribution for CBr_4/CCl_4 mixture is positive 1.77 $10^{-3}K^{-1}$ while for tetraethylsilane/CCl_4 and di-tert-butylsilane/CCl_4 it is negative -0.15 $10^{-3}K^{-1}$. This implies that the component with the higher molar mass moves to the cold side. At the same time the difference in size -0.36 $10^{-3}K^{-1}$ (-0.33 $10^{-3}K^{-1}$) and even more pronounced the difference in the interaction potential 0.26 $10^{-3}K^{-1}$ (0.382 $10^{-3}K^{-1}$) leads to a stronger (weaker) drive of di-tert-butylsilane (tetraethylsilane) to the hot side. The obtained S_T

values reproduce the correct direction of thermodiffusion motion for all three mixtures, but they are one order of magnitude too small. As it is expected in our case the component with the larger Hildebrand parameter (18.1MPa^{-1} for CBr_4; 13.4MPa^{-1} for $Si(C_2H_5)_4$; 12.7MPa^{-1} for $(CH_3C)_2SiH_2$ and 17.0MPa^{-1} for CCl_4) carbon tetrabromide (mixed with carbon tetrachloride) and carbon tetrachloride (mixed with one of the silanes) accumulates in the cold region.

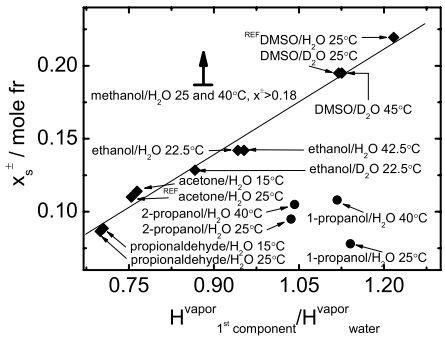

Fig. 2: *Sign change concentration $x_s^{\pm}$ plotted versus the ratio of the vaporization enthalpies of the pure components. For aqueous systems where the solvent has two carbons (⧫) $x_s^{\pm}$ increases linearly with the ratio $H_s^{\mathrm{vapor}}/H_w^{\mathrm{vapor}}$, while solvents with three carbon atoms (•) do not follow the line. Some data for DMSO/H_2O and acetone/H_2O have been taken from the literature [4].*

3.2 Mixtures of associated molecules

Experimental details about the associated mixtures studied can be found in [11]. For aqueous solutions of ethanol, DMSO, acetone it was observed that the sign change concentration correlates with the concentration at which the hydrogen bond network breaks down [4]. The sign change concentration can be determined by the hydrophilic (dipole moment) and hydrophobic (number of carbon atoms in hydrophobic part) parts of the solute molecules. In Fig. 2 the sign change concentration is plotted versus the ratio of the vaporization enthalpies $H_s^{\mathrm{vapor}}/H_w^{\mathrm{vapor}}$ of the pure components. Data for aqueous solutions of solutes with a similar hydrophobic part (propionaldehyde, acetone, DMSO, ethanol) follow the straight line, which indicates for those systems the importance of hydrophilic interaction rather than effect of mass or moment of inertia. The isotopic substitution of water decrease $x_s^{\pm}$, but the roughly 10% larger vaporization energy for heavy water compensates this effect so that also those systems follow the line. At the same time decreasing (or increasing) the hydrophobic part of the solute increases in case of methanol (or decrease in case of propanol) the concentration at which the sign change occurs. A similar trend has been observed for the break down of the hydrogen bond network [12].

4 Conclusions

The observed thermophoretic motion for three unpolar mixtures follows the common rules, which state that the component with the larger molar mass and the larger Hildebrandt parameter accumulates in the cold region. We found a fairly good agreement between the simulated and experimentally determined Soret coefficients for the systems tetraethylsilane and di-tert-butylsilane in carbon tetrachloride. Both methods found that di-tert-butylsilane accumulates slightly stronger in the warm region than the more symmetric tetraethylsilane. The dependence of the sign change concentration for associated mixtures versus the ratio of the vaporization enthalpies of the pure components is explained by the hydrophobic and hydrophilic interactions of the solute with water molecules.

Acknowledgment

We thank the Deutsche Forschungsgemeinschaft and the John von Neumann Institute for Computing at the Forschungszentrum Juelich, which provided the computer time for this study and Deutsche Forschungsgemeinschaft for the financial support (WI 1684).

References

[1] S. Wiegand. *J.Phys.:Condens. Matter*, 16:R357–R379, 2004.

[2] D. Reith and F. Müller-Plathe. *J. Chem. Phys.*, 112(5):2436–2443, 2000.

[3] G. Galliero, B. Duguay, J. P. Caltagirone, and F. Montel. *Fluid Phase Equilibr.*, 208(1-2):171–188, 2003.

[4] H. Ning and S. Wiegand. *J. Chem. Phys.*, 125:221102, 2006.

[5] S. Wiegand, R. Kita, and H. Ning. *J. Noneq. Thermod*, 32:193–201, 2007.

[6] P. Polyakov, M. Zhang, F. Müller-Plathe, and S Wiegand. *J. Chem. Phys.*, 127:014502, 2007.

[7] M. Zhang and F. Müller-Plathe. *J. Chem. Phys.*, 123:124502, 2005.

[8] F. Müller-Plathe. *Comput. Phys. Commun.*, 78:77, 1993.

[9] R. Rey, L.C. Pardo, E. Llanta, K. Ando, D.O. Lopez, J.Li. Tamarit, and M. Barrio. *J. Chem. Phys.*, 112:7505, 2000.

[10] J.T. Wescott, P. Kung, and S.K. Nath. *Fluid Phase Equilibr.*, 208:123, 2003.

[11] P. Polyakov and S. Wiegand. *J. Chem. Phys.*, 128:034505, 2008.

[12] T. Takamuku, H. Maruyama, K. Watanabe, and T. Yamaguchi. *J. Solution Chem.*, 33:641, 2003.

Phase demixing in non-isothermal binary liquids

S.N. Semenov[1] and M.E. Schimpf[2]

[1]*Institute of Biochemical Physics RAS, Moscow, Russia*
[2]*Boise State University, Boise, ID USA*

E-mail: sem@triniti.ru; mschimpf@boisetstate.edu

Abstract

The two-phase and critical behavior in non-isothermal binary liquid mixtures is examined using the mass transport equations obtained previously. Hydrodynamic approach developed earlier is used to calculate the necessary dynamic parameters. The stationary concentration distribution in the temperature gradient is calculated. At certain critical temperature and below, the resulting expression predicts a critical behavior and the layering of liquid phases in the mixture. At the critical temperature, the inflection point appears at the concentration distribution at the respective coordinate point. With decrease of temperature, this inflection is transformed into a jump in the concentration, which corresponds to the thermodynamically equilibrium concentrations of the components at the temperature established at this point.

1 Introduction

The aim of this article is the analysis of critical and two-phase behavior in binary liquid systems placed in a temperature gradient using the mass transport equations obtained previously. When a liquid mixture is placed in a temperature gradient, there is movement of the components, generating a concentration gradient, what is known as thermodiffusion or the Ludwig-Soret effect. Experimental and theoretical results on thermodiffusion can be found in Ref. [1].

As the thermodiffusion experiments are based on the data on the temperature-induced concentration distribution, equations describing the mass transport are necessary. In our previous paper (Ref. [2]) the equations of the mass transport in thermodiffusion were obtained. This approach uses the standard form of the mass conservation equations for the components

$$\frac{\partial \phi_i}{\partial t} = -\nabla \vec{J}_i \tag{1}$$

where ϕ_i is the volume fraction of the ith component, $\vec{J}_i$ is its mass flux, and t is time. The dynamic parameters (mass diffusion, cross-diffusion and thermodiffusion coefficients) are calculated by the hydrodynamic approach suggested in Ref. [3].
This hydrodynamic approach considers the flow of liquid around the particle caused by a local pressure gradient, as defined by the Navier-Stokes equation

$$\eta \Delta \vec{u} = -\nabla \Pi_{loc} + \vec{f}_{loc} \tag{2}$$

where $\vec{u}$ is the velocity of the liquid, Π_{loc} is the local pressure distribution around the particle, η is the dynamic viscosity of the liquid, and $\vec{f}_{loc}$ is the local volume force in the surrounding liquid.

Modifying the approach used in the theory of particle diffusiophoresis [4], we showed [3] that the local pressure distribution can be obtained from the condition of hydrostatic equilibrium in the uniform liquid taken together with condition of the local equilibrium in temperature gradients. These conditions give the local pressure gradient in a liquid around the molecule of ith kind

$$\nabla \Pi^i_{loc} = \frac{\Phi_{ij}}{v_j} \sum_{j=1}^{N} \alpha_j \phi_j \nabla T - \nabla \phi_j \tag{3}$$

where α_j is the cubic thermal expansion coefficient of the liquid of molecules of type j, ϕ_j is the volume fraction of these molecules, v_j is the specific molecular volume for the molecule of the j^{th} kind, and Φ_{ij} is the interaction potential between molecules of the i^{th} and j^{th} kind.

For liquids with low electrical conductivity

$$\Phi_{ij}(r) = -16\sqrt{A_i A_j}\left(r_i r_j\right)^3 \Big/ 9r^6 \tag{4}$$

where A_i and A_j are the respective Hamaker constants, r is the radial coordinate for a spherical molecule, and r_i and r_j are the molecular radii. Solving Eq. (2) for a spherical particle and calculating the respective hydrodynamic stresses, we have the following expressions for the partial cross-diffusion coefficient and the partial thermodiffusion coefficient defined as the velocity of a selected particle of the i^{th} kind per unit concentration gradient of the j^{th} component and per the unit temperature gradient, respectively:

$$b_{Dij} = 8r_{iH}^2\sqrt{A_i A_j}\Big/ 27\eta v_j \tag{5}$$

$$b_{Tij} = -\alpha_j b_{Dij} \tag{6}$$

where r_{iH} is the hydrodynamic radius of the particle.

Substituting the drift flux of the considered component into respective Eq. (1), we obtain the mass transport equations. In a system, where a temperature and/or concentration gradient exist, a macroscopic pressure gradient should be established to keep the hydrostatic equilibrium in the system. The respective barophoretic mass fluxes also are included in the mass transport equations. In general case, the macroscopic pressure gradient is derived from the mass transport equations. For the closed steady-state systems it can be described by the Gibbs-Duhem equation (Ref. [5]).

In a temperature gradient, the mass transport equations for the components can be written as

$$-\frac{\partial\phi}{\partial t} = \nabla\left\{D_1\left\{-\nabla\phi + (1-\phi)\left[\frac{\overline{v}_1}{kT}\nabla P - \sigma(\delta-1)\nabla\phi\right] + \sigma\left[\alpha_1(1-\phi) + \delta\alpha_2\phi\right]\nabla T\right\}\right\} \tag{7}$$

$$\frac{\partial\phi}{\partial t} = \nabla\left\{D_2\left\{\nabla\phi + \phi\left[\frac{\overline{v}_2}{kT}\nabla P - \delta_H\sigma(\delta-1)\nabla\phi\right] + \delta_H\sigma\left[\alpha_1(1-\phi) + \delta\alpha_2\phi\right]\nabla T\right\}\right\} \tag{8}$$

where $\phi_2 = \phi$ and $\phi_1 = 1-\phi$ are the volume fractions of the respective components, D_1, D_2 are their diffusion coefficients, $\overline{v}_1$, $\overline{v}_2$ are the partial volumes of the components, which are about the same as their specific molecular volumes v_1, v_2, $v_{1,2H} = 4\pi r_{1,2H}^3/3$, $\sigma = b_{D11}/D_1 = 4v_{1H}A_1/3v_1kT$, $\delta = v_1\sqrt{A_2}/v_2\sqrt{A_1}$, and $\delta_H = v_{1H}\sqrt{A_2}/v_{2H}\sqrt{A_1}$. Excluding the pressure gradient from Eqs. (7, 8), we obtain the equation for the concentration distribution

$$\frac{\partial\phi}{\partial t}=\nabla\left\{\frac{D_2}{1-\phi+\Delta\phi}\left\{\left[1-\phi+\frac{v_2}{v_1}\phi-\frac{v_2}{v_1}\sigma(\delta-1)(1-\phi)\phi\right]\nabla\phi-\sigma\left(\frac{v_2}{v_1}-\delta_H\right)(1-\phi)\phi\left[\alpha_1(1-\phi)+\delta\alpha_2\phi\right]\nabla T\right\}\right\} \quad (9)$$

where $\Delta = v_2 D_2 / v_1 D_1$ is the parameter related to the dynamic pressure gradient established in the non-stationary system. In Eq. (9), the parameter σ characterizes the value of the intermolecular interaction in one component, and the parameter δ characterizes the ratio in the intermolecular interactions between the components. It is equal to the ratio of the respective solubility parameters (Ref. [6]).

2 Results and Discussion

The term

$$D_{eff}=\frac{D_2}{1-\phi+\Delta\phi}\left[1-\phi+\frac{v_2}{v_1}\phi-\frac{v_2}{v_1}\sigma(\delta-1)(1-\phi)\phi\right] \quad (10)$$

in Eq. (9) is the effective diffusion coefficient. In stable systems, $D_{eff}>0$ (Ref. [5]). However, at $\delta>1$, the diffusion coefficient becomes zero at the point

$$\phi_c=\left(1+\sqrt{v_2/v_1}\right)^{-1} \quad (11)$$

$$T_c=4v_{1H}(\delta-1)A_1/3v_1k\phi_c^2 \quad (12)$$

At $T<T_c$, there is the two-phase domain described by the equilibrium curve

$$T/T_c=\phi(1-\phi)/\left[(1-2\phi_c)\phi+\phi_c^2\right] \quad (13)$$

which separates stable equilibrium concentrations $\phi\le\phi_{e1}(T), \phi\ge\phi_{e2}(T)$ from unstable region where $D_{eff}<0$, at the temperature *T*. The equilibrium concentrations are obtained from Eq. (13).

Near the critical point, the stationary mass transport equation [Eq. (9)] can be written as

$$(\phi-\phi_c)^2\nabla\phi=(1-\phi_c)\phi_c\left[\alpha_1(1-\phi_c)+\delta\alpha_2\phi_c\right]\varepsilon\nabla T \quad (14)$$

where $\varepsilon=\left[\delta(v_{2H}/v_{1H})-1\right]/(\delta-1)$. This parameter can be both positive and negative, what corresponds for negative and positive thermodiffusion, respectively. The solution of Eq. (14) is

$$\phi(x)=\phi_c+\sqrt[3]{3(1-\phi_c)\phi_c\left[\alpha_1(1-\phi_c)+\delta\alpha_2\phi_c\right]\varepsilon\left[T_c-T(x)\right]} \quad (15)$$

The concentration distribution described by Eq. (15) is the continuous function and it has the inflection point at the position x_c, where $\phi = \phi_c$ and $T = T_c$. The similar conclusion on the critical behavior of the concentration distribution was made in [7] on the base of thermodynamics.

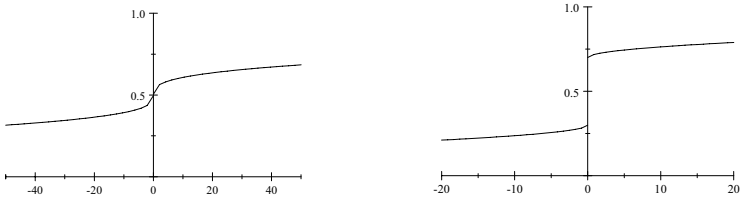

(a) $\varepsilon\left[T(x)-T_c\right]$ (b) $\varepsilon\left[T(x)-T_0\right]$

Fig. 1: *A typical concentration distribution in binary mixture* **(a)** *around the critical point and* **(b)** *in the two-phase domain.*

The typical critical concentration distribution is shown in Fig. 1a. The condition of the mass conservation

$$\int_0^L \phi(x)dx = \overline{\phi} L \tag{16}$$

imposes some limitations on the concentration range, where critical concentration distribution with the inflection point can be established. Here, $\overline{\phi}$ is the mean volume fraction of the second component in the uniform mixture, and L is the dimension of the measurement cell.

Using Eq. (15), Eq. (16) for the determination of the critical point position x_c can be written as

$$\overline{\phi} - \phi_c = \frac{3}{4}\left\{\left[1-\frac{x_c}{L}\left(T_c - T_0\right)\right]^{\frac{4}{3}} - \left[\frac{x_c}{L}\left(T_L - T_c\right)\right]^{\frac{4}{3}}\right\}\left\{3\left(1-\phi_c\right)\phi_c\varepsilon\left[\alpha_1\left(1-\phi_c\right)+\delta\alpha_2\phi_c\right]\right\}^{\frac{4}{3}} \tag{17}$$

Here, T_0 and T_L are the temperatures at the respective walls. Eq. (17) may give the limits of the uniform concentration, where the critical point can exist. They correspond to $x_c = 0, L$, when the critical temperature is established at the respective walls. These limits are:

$$\overline{\phi} = \phi_c \pm \frac{3}{4}\left\{3\left(1-\phi_c\right)\phi_c\varepsilon\left[\alpha_1\left(1-\phi_c\right)+\delta\alpha_2\phi_c\right]\Delta T\right\}^{\frac{4}{3}} \tag{18}$$

where ΔT is the temperature drop across the cell. For the liquids, the values of the thermal expansion coefficients are about $10^{-3}\ K^{-1}$ (see Ref. [6]). When the critical temperature is about the room temperature (about $3\cdot10^{2}\ K$), the temperature drops about $10^{2}\ K$ are available. According to Eq. (18), the maximal deviation in the initial mean volume fraction from the critical volume fraction $\phi_c \approx 1/2$ is about several percent.

This situation possesses the characteristic "critical" features. It is realized only at the unique temperature and the concentration, and within narrow range of the initial uniform concentrations.

When temperatures in the system are decreased below the critical point, the effective diffusion coefficient D_{eff} [Eq. (10)] becomes negative for two volume fractions ϕ_{e1}, ϕ_{e2}, which are the equilibrium concentrations in the two-phase system at the temperature corresponding to some point x_0 (see Fig. 1). In the depth of the two-phase domain, where $T << T_c$,

$$\phi_{e1} \approx \phi_c^2 T / T_c \tag{19}$$

$$\phi_{e2} \approx 1 - \phi_c^2 v_2 T / v_1 T_c \tag{20}$$

In this diluted two-phase system, the stationary Eq. (9) can be written in two different forms:

$$\left(\phi_{e1} - \phi\right)\frac{\partial \phi}{\partial x} = \alpha_1 \phi_{e1} \varepsilon \nabla T, \quad \text{at } \phi \approx \phi_{e1} \tag{21}$$

$$\left(\phi - \phi_{e2}\right)\frac{\partial \phi}{\partial x} = \delta\alpha_2 \varepsilon \nabla T, \quad \text{at } \phi \approx \phi_{e2} \tag{22}$$

The solution of Eqs. (21, 22) is:

$$\begin{gathered}\phi_{-}(x) = \phi_{e1} - \sqrt{2\alpha_{T1}\phi_{e1}\varepsilon\left[T(x) - T_0\right]}, \\ \text{at } \varepsilon\left[T(x) - T_0\right] \geq 0; \quad \phi_{-}(x) = 0, \text{ at } \varepsilon\left[T(x) - T_0\right] < 0\end{gathered} \tag{23}$$

$$\begin{gathered}\phi_{+}(x) = \phi_{e2} + \sqrt{2\alpha_{T2}(1 - \phi_{e2})\varepsilon\left[T_0 - T(x)\right]}, \\ \text{at } \varepsilon\left[T(x) - T_0\right] \leq 0; \quad \phi_{+}(x) = 0, \text{ at } \varepsilon\left[T(x) - T_0\right] > 0\end{gathered} \tag{24}$$

The designations $\phi_{-}(x)$, $\phi_{+}(x)$ are used for the domains with the lower and higher concentration, respectively. The typical concentration distribution is illustrated in Fig. 1b.

The position of the point x_0 and temperature $T_0(x_0)$ can be found by the condition of the mass conservation

$$\int_0^{x_0} \phi_-(x)dx + \int_{x_0}^{L} \phi_-(x)dx = \bar{\phi} L \tag{25}$$

For systems, which are far from the critical point, Eq. (25) takes the form

$$\frac{x_0}{L} = \frac{1-\phi_c^2 v_2 T_0(x_0)/v_1 T_c - \bar{\phi}}{1-(1+v_2/v_1)\phi_c^2 T_0(x_0)/T_c} \tag{26}$$

In the raise of the mean volume fraction $\bar{\phi}$ from ϕ_{e1} to ϕ_{e2}, the position x_0 changes gradually from L to zero, respectively, and the layers of different thickness may be obtained.

In two-phase domain, the position x_0 of the concentration jump corresponding to the phase boundary may be controlled in a wide range. It may be done by the gradual change in the mean uniform concentration $\bar{\phi}$ and by the scanning the temperature profile in the cell, while maintaining the same temperature drop between the walls. This situation allows for the control of the position of suspended particles in the two-phase mixture. It is possible, when the sign of the thermodiffusion coefficient of the particle is changed in the particle transition from one component to another. This sign change was seen in numerous experiments and predicted theoretically in [8]. Then particles may be focused around the phase boundary and be shifted together with it. It provides a method for the manipulations with the suspended particles.

3 Conclusions

The critical behavior and phase layering in non-isothermal binary liquid mixtures are examined using the kinetic mass transport equations. The stationary concentration distribution in the temperature gradient is calculated. Close to critical temperature and below, the resulting expression predicts a critical behavior and the layering of liquid phases in the mixture. At the critical temperature, the inflection point appears in the concentration distribution at the corresponding coordinate point. This situation may be seen in an experiment in a very narrow range of the concentrations, about several percent, around the critical concentration. With decrease of temperature, this inflection is transformed into a jump in the concentration, which corresponds to the thermodynamically equilibrium concentrations of the components at the temperature established at this point. At temperatures significantly lower than the critical one, the phase layering with the controllably changed position of the phase boundary can be obtained. This situation can be used to manipulate the suspended particles in the predetermined manner.

References

[1] *Thermal Nonequilibrium Phenomena in Liquid Mixtures*, edited by W. Köhler and S. Wiegand (Springer, Berlin, 2002).

[2] S. N. Semenov, M. E. Schimpf, *Phys. Rev. E*, 72, 041202 (2005).

[3] M. E. Schimpf and S. N. Semenov, *J. Phys. Chem. B* **104**, 9935 (2000).

[4] J. L. Anderson, *Ann. Rev. Fluid Mechanics* **21**, 61 (1989).

[5] D. Kondepudi and I. Prigogine, *Modern Thermodynamics* (Wiley, New York, 1999).

[6] *Organic Solvents. Physical Properties and Methods of Purifications*, 4th Edition, edited by J. A. Riddik, W. B. Bunger, and T. K. Sakano (Wiley, New York, 1986)

[7] K. Ghoraeb, A. Firoozabadi, *AIChE*, 46 883 (2000).

[8] S. N. Semenov and M. E. Schimpf, *Phys. Rev. E* **69**, 011201 (2004).

Thermogravitational technique at high pressure for liquid mixtures

P. Urteaga, M.M. Bou-Ali, P. Blanco

Manufacturing Department, MGEP Mondragon Goi Eskola Politeknikoa
Loramendi 4, Apartado 23, 20500 Mondragon, Spain.

E-mail: purteaga@eps.mondragon.edu

Abstract

A thermogravitational column that makes possible to carry out experimental measurements of a stationary separation produced in a mixture under high pressures has been built. The new device is able to work at pressures up to 50 MPa.

The column was validated at atmospheric pressure working with liquid mixtures which thermodiffusion and molecular diffusion coefficients are well known in literature, like, water-ethanol (60.9% mass fraction of water, at an average temperature of 22.5ºC); toluene-nhexane (51.67% mass fraction of toluene, at 25ºC); 1,2,3,4-Tetrahydronaphthalene(THN)-Isobutylbenzene(IBB), THN-n-Dodecane(*n*C12) and IBB-*n*C12 (50% mass fraction of each component, at 25ºC). The stationary separation and thermodiffusion coefficient (D_T) obtained with the new column show a repeatability of 98% and the difference between the obtained data and data from the literature is within the experimental error.

In this paper some experimental data for stationary separation at pressures up to 14 MPa., mean temperature of 25 ºC and 50% mass fraction, for the following mixtures: THN-*n*C12 and IBB-*nC12* will be presented.

1 Introduction

Throughout last years, the importance of thermodiffusion coefficient and transport properties knowledge in very different sectors has been stated, and the oil industry is the one which greatest interest has shown, in order to optimize the exploration and the exploitation of the oilfields [1], even some experiments for determining the transport properties have been carried out in microgravity [2] in collaboration with the European Space Agency (ESA) and the Oil Industry. Up to now, these expensive experiments have not offered conclusive results. There are some theoretical [3], numerical [4] and experimental [5] studies that confirm a dependency of transport properties with pressure, temperature and concentration. In addition the lack of experimental data for these coefficients in working conditions blocks further theoretical, numerical and industrial development [6,7].

Recently, in *Benchmark values for the Soret, thermal diffusion and diffusion coefficients* [8], the efficiency of the themogravitational technique and the corresponding experimental method have been demonstrated for determining the transport properties of liquid mixtures. Up to now, the thermogravitational technique has been used, only at atmospheric pressure. Nevertheless, the conditions in which the hydrocarbons are found in oilfields, depending on the systems, imply high pressures. For all this, it was decided, to design and to build a new themogravitational installation that allows determining the thermodiffusion coefficient at various pressures, up to 50 MPa, for both liquid and liquefied mixtures.

2 The new thermogravitational installation

The new themogravitational installation (TGC-HP) has a cylindrical configuration and as it can be seen in figure 1 it is constituted by the following modules:

1) Thermogravitational column
2) Load system.
3) Pressure generation system.
4) Sample extraction and analyzing system.

The key factors to have in mind when designing and manufacturing a thermogravitational column are: the dimensional, geometric and surface finish tolerances, compatibility of materials, structural calculation of the components that work under pressure, the materials and the whole column's thermal behaviour, being hermetically closed up to pressures of 50 MPa. The main features of the TGC-HP are: height 500 mm, it is made of stainless steel, it has five equidistant sample extraction taps and its gap width is 1 ± 0.005 mm.
This installation has two external water thermostatic baths to create the temperature gradient between the gap's two walls.

To collect reliable information about the gap's outer and inner walls temperatures, the previously described installation has four "J" type thermocouples, of 1 mm diameter. Two of them are in the top and the other two in the bottom of the column. In addition, it has a pressure transducer in the top part of column in order to know the pressure inside the gap.

To guarantee a totally hermetic closing of the gap, single acting, spring-energized, PTFE seals are used. The spring supplies the load required for sealing at low pressures. The ”U” shaped jacket allows fluid pressure to energize the sealing lips, so total sealing pressure rises with increasing operating pressure.

Once the steady state is reached the sample extraction for being analyzed can be done across the valves which are integrated in the outer tube of the column. Thanks to the valves design the extraction can be done, both, at atmospheric pressure and at high pressure. The valves assure hermetic closing while it eliminates all the possible dead volumes.

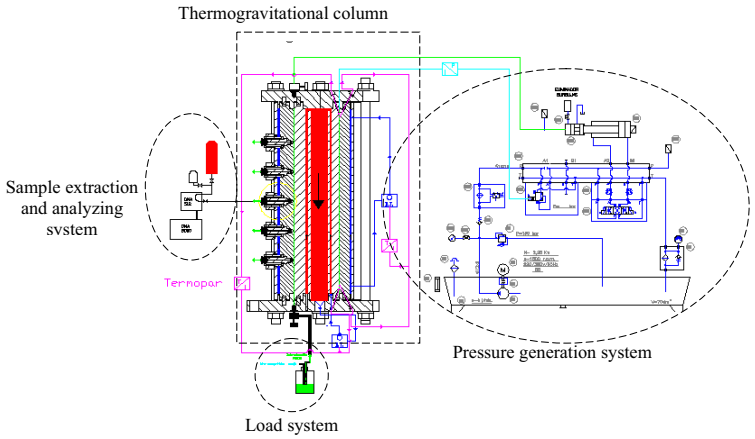

Fig. 1: *High pressure thermogravitational device*

The mixture's loading is realized from the bottom of the column at controlled speed, due to compressed air’s pressure. This way, the liquid will evacuate all the air inside the gap, managing to eliminate all the possible bubbles that might try to remain into the gap. For liquid loading, two different types of fluids can be acknowledged, on one hand there are the fluids that at atmospheric pressure and temperature are in liquid state and on the other hand those fluids that in these conditions are in gaseous state. In this work, liquids have been studied at different pressures.

The working pressure is generated by pressure generation system, see figure 1, and the maximum pressure it can work is 50 MPa. This module is formed by a hydraulic system and a pressure intensifier, which can store 120 cm^3 of liquid and its pressure ratio is 1 to 5.

The extracting liquid's volume is controlled by means of cylinder displacement. In order to do this, the hydraulic cylinder has a displacement transducer which provides continuous information about the cylinder's position.

3 Experimental results

The validation of the TGC-HP was realized [9, 10] at atmospheric pressure by means of tests of liquid binary mixtures which transport properties are sufficiently verified in the bibliography.

The used mixtures were: Water-ethanol (W-E): c_{H_2O} = 0.6088; T = 22.5ºC and T = 25ºC; Toluene–n-hexane (Tol-*n*C6): $c_{tolueno}$ = 0.5167; T = 25ºC; 1,2,3,4-Tetrahydronaftaleno-Isobutylbencene (THN-IBB): c = 0.5; T = 25ºC; 1,2,3,4-Tetrahydronaftalene–n-dodecane (THN-*n*C12): c = 0.5; T = 25ºC; Isobutylbencene–n-dodecane (IBB- nC12): c = 0.5; T = 25ºC.

3.1 Experimental test at high pressure

Once the correct operation of TGC-HP installation at atmospheric pressure was demonstrated, experimental test at a range of high pressure were carried out. To perform these experimental tests the following two binary hydrocarbons mixtures were chosen: IBB-nC12 y THN-nC12, in an identical conditions of mass concentration, mean temperature and thermal gradient, which were used in the validation process of the TGC-HP column, (c= 0.5; T = 25 ºC).

The relative pressure range at which the test has been carried out is between 0 y 14 MPa. 8 tests for each mixture have been carried out, at following pressures 0, 2, 4, 6, 8, 1, 12, 14 MPa., and each test has been repeated several times. Once the stationary state is reached the pressure is removed and the five samples are extracted for been analyzed measuring its density by means of a DMA 5000 ANTON PAAR's densimeter.

In table 1 the obtained values of stationary mass separation between the two ends of TGC-HP are shown for the different tested pressures. It can be observed that the obtained separation decreases as the working pressure rises. The concentration varies 3,96% for IBB-nC12 and 7,85 % for THN-nC12 when relative pressure goes from 0 to 14 MPa.

The mixtures concentration variation values along the columns from table 1 have been plotted in a Concentration variation-Pressure graph in figure 2, it can be appreciate that the variation of stationary separation with the pressure fits quite well to a straight line.

Pressure (MPa)	Δc IBB-nC12	Δc THN-nC12
0,1013	0,0381	0,0792
2	0,0376	0,0781
4	0,0374	0,0763
6	0,0372	0,0756
8	0,0365	0,0749
10	0,0364	0,0739
12	0,0363	0,0730
14	0,0361	0,0720

Table 1: *Concentration variation (Δc) of IBB-nC12 and THN-nC12 for various working pressures*

4 Conclusions

It is the first time that the steady state separation for liquid mixtures THN-*n*C12 and IBB-*n*C12 at high pressure has been determined. The variation of stationary separation with working pressure depends on the studied mixture. A greater influence of pressure on THN-*n*C12 mixtures than on the other studied mixture IBB-*n*C12 can be appreciated on the chart 2, at least at pressures up to 14 MPa.

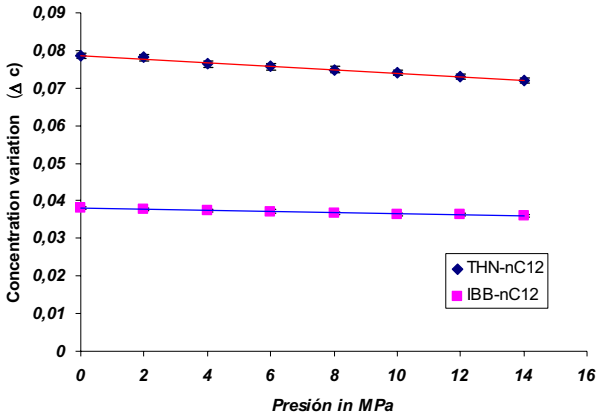

Fig. 2: *Stationary separation in TGC-HP vs. working pressure*

Acknowledgment

This work has been financed by MONDRAGON CORPORATION COOPERATIVA and the following projects: GOVSORET (PI2008-14), TESBLUR (CTQ2005/09389/C02/01/PPQ) and the Grant (BFI05.449) of Basque Government.

References

[1] Montel F., *Report*, Elf Aquitane, Pau, CSTJF, France, Septembre (1994).

[2] Van Vaerenbergh S., Shapiro A., Galliero G., Montel F., Legros J., Caltagirone J., Daridon J., Saghir Z., *European Space Agency, (Special Publication) ESA SP,* **1290**, (2005) 202-213.

[3] Firoozabadi A. Thermodynamics of hydrocarbon Reservoirs *McGraw-Hill Professional* (1999).

[4] Faruque D., Saghir M.Z., Chacha M., Ghorayeb K., *Journal of Porous Media* v7.**2**.10 (2004)

[5] W.M Rutherford. *J. Chem. Phys*. **58**, 1613-8, (1973).

[6] Shapiro, A., *Physica A,* 2004, **332**, 151-175

[7] Khawaja, M.; Jiang, C.G.; Van Vaerenbergh, S. & Saghir, M., *Journal of non-equilibrium Thermodynamics,* 2005, **30**, 359-374.

[8] Platten JK., Bou-Ali MM., Costesèque P.,Dutrieux JF., Köhler W.,Leppla C.,Wiegand S.and Wittko G. *Philosophical Magazine* **Vol. 83**, P. 1965 (2003)

[9] Urteaga, P.; Bou-Ali, M.; Madariaga, J.; Santamaría, C.; Blanco, P. & Platten, J., *Mondragon Unibertsitateko Zerbitzu Editoriala: Mondragon (Spain)*, 2006, 449-458

[10] Blanco P.; Bou-Ali M.M.; Platten J.K.; Alonso de Mezquia D.; Urteaga P.; Madariaga J. A; Santamaria C.; *IMT8 Proceeding*. 2008.

Thermodiffusion coefficient (D_T) for binary hydrocarbon mixtures at high pressures

P. Urteaga[1], F. Plantier[2], M.M. Bou-Ali[1], H. Bataller[2]

[1] Manufacturing Department, MGEP Mondragon Goi Eskola Politeknikoa Loramendi 4, Apartado 23, 20500 Mondragon, Spain.
[2] University of Pau, Avenue de l'université, BP 1155, 64013 Pau, France

E-mail: purteaga@eps.mondragon.edu

Abstract

In this study the thermal diffusion coefficient at high pressure has been determined for first time. The binary liquid mixtures that have been studied are n-dodecane (*n*C12), isobutylbenzene (IBB) and 1,2,3,4-tetrahydronaphtalene (THN) for pressures going from the atmospheric pressure up to 14 MPa. The tests were carried out at 50 % of mass concentration and at a mean temperature of 25 °C.

The chosen binary mixtures are the ones which were studied in the benchmark of Fontainebleau. They were also used in the calibration process at atmospheric pressure of the new themogravitational device (TGC-HP) developed in the University of Mondragon Unibertsitatea.

1 Introduction

In the last decades many experimental works have been carried out to study the transport properties of binary liquid mixtures at atmospheric pressure by means of different techniques [1].
Having in mind that recently the oil industry has showed great interest to study the transport properties [2] and that the conditions under which the crude oil is found underground implies high pressure, it is considered very important to analyze the influence that pressure has on transport properties of liquid mixtures in order to be able to achieve a major reliability of the algorithms used for crude oil's simulation in the oilfields. In fact, the pressure in oil fields would be over 100 MPa. [2]. There are some theoretical [3] and numerical [4] works that confirm a dependency of transport properties with pressure [5], temperature and concentration. In addition, the lack of experimental data for these coefficients in working conditions represent a difficulty for further development in the industrial sector from the theoretical, numerical and experimental point of view [6].

2 Experimental determination of the thermodiffusion coefficient at high pressure

Since K. Clusius has proposed the possibility to use the thermogravitational column as a method to measure the thermodiffusion coefficient D_T [7], many theoretical and experimental works have been carried out with both, liquid and gaseous mixtures.
In agreement with thermogravitational theory the stationary separation, Δc, between the ends of the column is given by:

$$\Delta c = 504 \frac{\upsilon}{\alpha g} \frac{L_z}{L_x^4} c_0 (1 - c_0) D_T \tag{1}$$

where: υ: is the kinematics' viscosity; α: thermal expansion coefficient; L_x: gap's width; L_z: total length of the column; c_0: is the initial concentration of mixture; g: is the gravity acceleration; D_T: is the thermodiffusion coefficient.

In the thermogravitational column the variation of the density along the column's height $\partial\rho/\partial z$ is measured, and steady state mass separation Δc is determined by means of equation (2):

$$\Delta c = \frac{L_z}{\beta \rho_0} \frac{\partial \rho}{\partial z} \tag{2}$$

where β: is the mass expansion coefficient; ρ_0: is the mixture's initial density. Considering equations 1 and 2 we get equation 3 to determine D_T,

$$D_T = \frac{1}{504}\frac{\alpha g}{\mu\beta}\frac{L_x^4}{c_0(1-c_0)}\frac{\partial\rho}{\partial z} \tag{3}$$

where μ is the dynamic viscosity. From equation 3 can be deduced that to determine D_T it is necessary to carry out experimental measurement of following properties α, β, μ, $\partial\rho/\partial z$. In this work the liquid mixtures of IBB-*n*C12 and THN-*n*C12 has been carried out, at a mass fraction of 50 %, mean temperature of 25 ºC and relative pressures of : 0.1013, 2, 4, 6, 8, 10, 12, 14 MPa.

2.1 Thermophysical properties

a) Thermal expansion coefficient

The experimental method consists of measuring the density of a given liquid mixture in a small interval of temperatures around the testing temperature and at certain pressure. Tables 1 and 2 show the thermal expansion coefficients calculated by means of $\alpha = -\rho_0^{-1}(\partial\rho/\partial T)$ for the liquid mixtures studied in this work at different working pressures. As it can be observed in the table 1 and 2 the thermal expansion coefficient goes down slightly as the working pressure rises.

b) Mass expansion coefficient

The experimental method consists of measuring the density of a given mixture in a small interval of concentrations around the concentration which is going to be studied, at constant temperature and at a certain pressure. Tables 1 and 2 show respectively the mass expansion coefficient's values calculated with $\beta = \rho_0^{-1}(\partial\rho/\partial c)$ for the liquid mixtures THN-*n*C12 and IBB-*n*C12. The mass expansion coefficient does not vary with pressure, at least up to 14 MPa.

c) Dynamic viscosity

To measure the viscosity a needle falling viscosimeter commercialized by Irvine-Park is used with an external thermostatic bath in order to control the test temperature (25 ºC). The fluid mixture in an inner tube of the viscosimeterr was compressed by a pump. Afterwards a needle of known density is dropped through the testing fluid, and the drop time between two marked points is measured. All the measurements were preformed three times and the mean value was calculated. The dynamic viscosity of the fluid is derived from:

$$\mu = K(\rho_N - \rho_F)\overline{\Delta t} \tag{4}$$

where, K is a calibration constant, ρ_N is the needle density, ρ_F the fluid density and $\overline{\Delta t}$ is the average value of the three measured times. The uncertainty of measured viscosity is estimated in 0.03 mPa.s. From the tables 1 and 2 it can be stated that the dynamic viscosity is rising when working pressure is increasing.

d) Density variation along the column

The TGC-HP has been used to determine the stationary separation in terms of working pressure. The experimental method to measure $\partial\rho/\partial z$ is described in [8]. In figure 1 it can be observed an example of the values obtained in one experimental set for THN-*n*C12 liquid mixture at a pressure of 10 MPa.

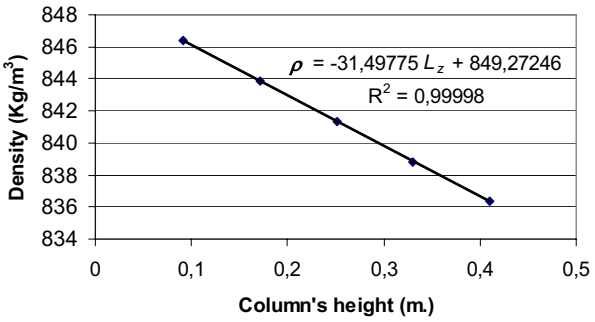

Fig. 1: *Density variation through the column's height for THN-nC12 with c_0=0.5, at mean temperature of 25 ºC and pressure of 10 MPa.*

In tables 1 and 2 are shown the mean values of $\partial\rho/\partial z$ for all the tests performed for each working pressure. From the tables we can realize that it decreases when working pressure rises. It decrease 8,3 % for the mixture THN-*n*C12 and 4,9 % for IBB-*n*C12, when the working pressure varies between atmospheric pressure and 14 MPa.

Pressure (MPa)	α (10^{-4} K^{-1})	β	μ (mPa.s)	$\partial\rho/\partial z$
0,1013	8,6	0,27	1,46	33,9331
2	8,5	0,27	1,50	33,7663
4	8,3	0,27	1,53	32,9975
6	8,2	0,27	1,57	32,7018
8	8,4	0,27	1,60	32,3807
10	8,4	0,26	1,64	31,9700
12	8,2	0,26	1,66	31,5466
14	8,1	0,26	1,71	31,1112

Table 1: *Thermophysical properties α, β, μ and $\partial\rho/\partial z$ for THN-nC12 with c_0=0,5 (mass fraction), at 25 ºC and various pressures from atmospheric to 14 MPa.*

Pressure (MPa)	α (10^{-4} K^{-1})	β	μ (mPa.s)	$\partial\rho/\partial z$
0,1013	9,3	0,13	1,09	7,8500
2	9,0	0,14	1,11	7,7973
4	8,9	0,13	1,14	7,7224
6	8,8	0,13	1,16	7,7062
8	9,0	0,13	1,19	7,5476
10	9,0	0,13	1,22	7,6321
12	8,9	0,13	1,24	7,5145
14	8,8	0,13	1,26	7,4591

Table 2: *Thermphysical properties α, β, μ and $\partial\rho/\partial z$ for IBB-nC12 with c_0=0,5 (mass fraction), at 25 ºC and various pressures from atmospheric to 14 MPa.*

3 Discussion and Conclusions

Considering equation 3, D_T has been determined for the liquid mixtures THN-*n*C12 and IBB-*n*C12 at mass fraction of 50 %, mean temperature of 25 ºC and working relative pressures from 0 to 14 MPa. The obtained values are plotted in Pressure-D_T graph (Fig. 2).

From the figure 2 it can be stated that for both mixtures the variation of D_T with working pressure fits rather well to a linear variation. For first time the thermodiffusion coefficient (D_T) of THN-*n*C12 and IBB-*n*C12 at high pressure has been determined experimentally.

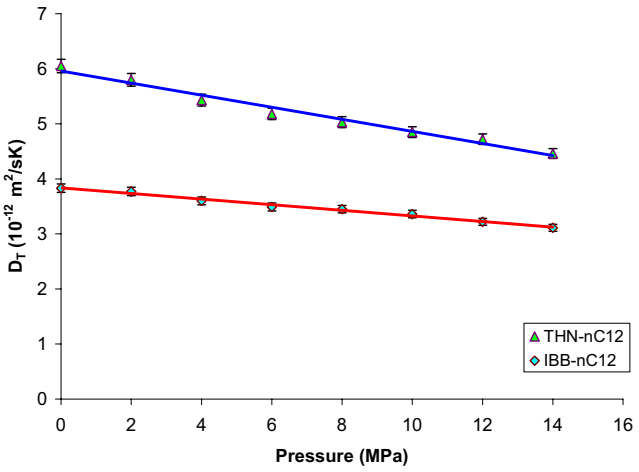

Fig. 2: *D_T variation in function of working pressure of mixtures THN-nC12 and IBB-nC12, at mass fraction of c=0.5 and mean temperature of 25ºC.*

Acknowledgment

This work has been financed by MONDRAGON CORPORATION COOPERATIVA and the following projects: GOVSORET (PI2008-14), TESBLUR (CTQ2005/09389/C02/01/PPQ)

References

[1] Platten J., Bou-Ali M., Costesèque P., Dutrieux J., Köhler W., Leppla C., Wiegand S. and G. Wittko, *Philos. Mag*. 83, (2003) 1965-1971

[2] Ghorayeb K., Firoozabadi A., Anraku *T. SPE Journal*, **8 (2)**, (2003) 114-123

[3] Firoozabadi A. *McGraw-Hill Professional* (1999)

[4] Faruque D., Saghir M.Z., Chacha M., Ghorayeb K., *Journal of Porous Media* v**7**.2.**10** (2004)

[5] W.M Rutherford. *J. Chem. Phys*. **58**,1613-8, (1973).

[6] Van Vaerenbergh S., Shapiro A., Galliero G., Montel F., Legros J., Caltagirone J., Daridon J., Saghir Z., *European Space Agency, (Special Publication) ESA SP*, **1290**, (2005) 202-213.

[7] Clusius. Huber M. Z. *Naturforch.* **10 a**. 230, (1955).

[8] Urteaga P.; Bou-Ali M.M.; Blanco P.; *Proceeding of IMT8.* (2008)

Theoretical modeling and experimental measurement of thermodiffusion coefficients in binary n-alkane mixtures

Y. Yan[1], P. Blanco[2], M.Z. Saghir[1], M. Bou-Ali[2]

[1]*Ryerson University, Department of Mechanical & Industrial Engineering, Canada*
[2]*Manufacturing Department, MGEP Mondragon Goi Eskola Politeknikoa, Spain*

E-mail: zsaghir@ryerson.ca

Abstract

Thermodiffusion or Soret effect is a phenomenon of mass transport in fluid mixtures driven by temperature gradients. In this paper, we have studied thermodiffusion coefficients for different binary n-alkane mixtures (equal mass fraction) through both theoretical and experimental methods. The theoretical model is based on the theory of non-equilibrium thermodynamics. The experimental data is obtained through a thermogravitational column. A good agreement is found between the theoretical results and the experimental data

1 Introduction

Thermodiffusion has been studied through various theories. In the past, many researchers applied the theory of non-equilibrium thermodynamics in their thermodiffusion studies including Doughty and Drickamer [1, 2], Kempers [3], Firoozabadi et al [4] and Pan et al [5]. After decades of improvement, this line of theoretical development has made a great progress. Pan et al [5] model is capable in predicting sign change in thermal diffusion factors for binary small-molecule associating mixtures. Many techniques have been developed such as diffusion cell, laser Doppler velocimetry, Rayleigh-Benard configuration, thermogravitational column, laser beam deflection, thermal diffusion forced Rayleigh scattering (TDFRS) and microgravity method. These methods either create a convection-free condition thus to reduce the effect of convection or make use of the coupling with convection and then determine thermodiffusion coefficients through fluid mechanics analyses. Platten [6] has provided complementary reviews for current experimental techniques. In this paper, a comparison has been made for modelled and measured thermodiffusion coefficients for different binary n-alkane mixtures. The experimental data are obtained through the technique of thermogravitational column. A theoretical model based on the theory of non-equilibrium thermodynamics is used to calculate the thermal diffusion factor α_T.

2 Theoretical Model

According to the theory of non-equilibrium thermodynamics, molar diffusion flux can be expressed in terms of phenomenological coefficients. In a binary mixture at a constant pressure, only molecular diffusion and thermodiffusion contribute to the diffusion flux, therefore

$$\vec{J}_1^{mol} = -L_{11}^* \frac{Q_1^* - Q_2^*}{T^2} \vec{\nabla} T - \frac{1}{Tx_2} L_{11}^* \left(\frac{\partial \mu_1}{\partial x_1} \right)_{T,p} \vec{\nabla} x_1 \tag{1}$$

where $\vec{J}_1^{mol}$ is the molar diffusion flux with respect to a molar average reference velocity. Q_i^* is the net heat of transport. μ_1 is the chemical potential. x_1 and x_2 are the molar fraction of component 1 and 2, respectively. L_{11}^* is the phenomenological coefficient.

Conventionally, diffusion flux can also be expressed in terms of molecular diffusion coefficient (or Fick's coefficient) and thermodiffusion coefficient as follows:

$$\vec{J}_1^{mol} = -\rho^{mol} (D^{mol} \vec{\nabla} x_1 + D_T^{mol} x_1 x_2 \vec{\nabla} T) \tag{2}$$

Compare eqs (1) and (2) and use the relation $\alpha_T = TS_T = TD_T / D$, a general equation for thermal diffusion factor α_T for binary mixtures can be derived:

$$\alpha_T = \frac{Q_1^* - Q_2^*}{x_1\left(\frac{\partial \mu_1}{\partial x_1}\right)_{T,p}} \tag{3}$$

It can be seen from eq. (3) that accurate thermodiffusion modelling relies on accurate prediction of the net heat of transport Q_i^*. Many researches have been concentrated on interpreting Q_i^* through physically meaningful and practically achievable ways. In Dougherty and Drickamer [12, 13], the net heat transport Q_i^* was related to partial molar volumes ($\overline{V}_i$), and two energies – the energy needed to detach a molecule from its neighbors and the energy released when one molecule fills a hole. By further applying Eyring's viscosity theory, they presented an expression, eq. (4), for thermal diffusion factor for binary mixtures.

$$\alpha_T = -\left(\frac{\left(\overline{U}_1 - \overline{U}_{1g}^0\right)/\tau_1 - \left(\overline{U}_2 - \overline{U}_{2g}^0\right)/\tau_2}{x_1\left(\frac{\partial \mu_1}{\partial x_1}\right)_{T,p}} + \frac{\overline{V}_2 - \overline{V}_1}{\overline{V}_1 x_1 + \overline{V}_2 x_2} \cdot \frac{x_1\left(\overline{U}_1 - \overline{U}_{1g}^0\right)/\tau_1 + x_2\left(\overline{U}_2 - \overline{U}_{2g}^0\right)/\tau_2}{x_1\left(\frac{\partial \mu_1}{\partial x_1}\right)_{T,p}} \right) \tag{4}$$

where $\overline{U}_i$ is the partial molar internal energy of component *i*. $\overline{U}_{ig}^0$ is the internal energy of the ideal gas at the same temperature. τ_i is a parameter to represent the ratio of viscous energy to the cohesive energy. Eq. (4) requires accurate thermodynamics properties, namely, $\left(\overline{U}_i - \overline{U}_{ig}^0\right)$, $x_1\left(\partial \mu_1 / \partial x_1\right)$ and $\overline{V}_i$.

3 Experiment

Thermodiffusion coefficients of binary mixtures composed of n-alkane hydrocarbons, namely n-C_iH_{2i+2} (i=5, 6, 7, 8, 9, 12, 18) are measured at the temperature of 25°C and the pressure of 1 atm. This column has a height of 50 cm and a gap of 1 mm and has been previously tested with other binary mixtures [24]. In this thermogravitational column, the evaluation of thermodiffusion coefficients is through the following relation:

$$D_T = \frac{g \cdot \alpha \cdot L_x^4}{504 \cdot \beta \cdot \eta \cdot c_0 \cdot (1 - c_0)} \cdot \frac{\partial \rho}{\partial z} \tag{5}$$

where $\frac{\partial \rho}{\partial z}$ is the density gradient along the column at the steady state; L_x is the gap of the column (1mm in this study); α and β are the thermal and mass expansion coefficients, respectively; η is the dynamic viscosity; g is the gravitational acceleration and c_0 is the initial mass concentration.

4 Results and Discussion

Seven n-alkane hydrocarbons are used to form binary mixtures in this study. They are *n*-Pentane (C_5H_{12}), *n*-Hexane (C_6H_{14}), *n*-Heptane (C_7H_{16}), *n*-Octane (C_8H_{18}), *n*-Nonane (C_9H_{20}), *n*-Dodecane ($C_{12}H_{26}$) and *n*-Octadecane ($C_{18}H_{38}$). Two groups of binary mixtures $nC_i - nC_{18}$ (i=5~9, 12) and $nC_i - nC_{12}$ (i=5~9) at 25ºC, 1 atm will be investigated.

4.1 Molecular diffusion coefficient

Fick's diffusion coefficients are calculated and listed in Table 1. In our model, these coefficients are calculated with the method recommended by Taylor and Krishna [22] and Hayduk–Minhas correlation was used to estimate the molecular diffusion coefficients in infinite dilution solutions.

Table 1: Calculated molecular diffusion coefficient *D* at 25ºC

$nC_i - nC_{18}$ (50:50 wt%) i=	D 10^{-10} m^2/s	$nC_i - nC_{12}$ (50:50 wt%) i=	D 10^{-10} m^2/s
5	12.14	5	23.90
6	13.12	6	19.22
7	10.34	7	15.70
8	8.57	8	13.68
9	7.13	9	12.04
12	4.48	18	4.48

4.2 Thermodiffusion coefficient

A comparison of thermodiffusion coefficient obtained through modelling and experiments are listed in Tables 2 and 3. Note that the thermodiffusion coefficient $D_{T,2}$ shown in these tables are for the second component, i.e., $D_{T,2}$ in Table 2 represents the thermodiffusion coefficient of nC_{18}; and $D_{T,2}$ in Table 3 represents the thermodiffusion coefficient of nC_{12}. For both mixtures $nC_i - nC_{18}$ and $nC_i - nC_{12}$, $D_{T,2}$ are positive, which indicate that the second components, nC_{18} and nC_{12}, respectively, move in a direction opposite to the temperature gradient. For the mixture $nC_{12} - nC_{18}$, the experimental result shows that nC_{18} moves to the cold side of the cavity; while the calculation shows a contradictory result. This discrepancy may be resulted from the state of nC_{18} at 25ºC. The triple point of nC_{18} is 301.3K (28.15 ºC). The current operating temperature 25ºC is below the triple point. This means that nC_{18} at 25ºC is not stable and either gas phase or liquid phase or solid phase may be present. This uncertainty makes it very difficult to obtain thermodynamic properties required in the modeling at this temperature. In fact, some thermodynamic properties of nC_{18} under the triple point are not available therefore the properties slightly above the triple point are used instead. This approximation may be a source of the discrepancy as it is already known that thermodiffusion coefficients are sensitive to the

temperature (as the temperature increases, the Soret effect lessens). This may also explain why the calculated $D_{T,2}$ for mixtures of nC_i – nC_{18} are consistently smaller than the measured ones. The comparison with experimental data has suggested that the theoretical thermodiffusion model as detailed in Section 2 may be used in a temperature and pressure range where the mixture components are in stable states, i.e. the range away from the triple point and critical point. In such range, the thermodiffusion model can achieve moderate to good performance, as shown in the calculations for the mixtures of nC_i – nC_{12}; the average relative error is about 11% for this group of mixtures. With in mind the small magnitude of thermodiffusion coefficients, this accuracy can be regarded as very good.

Table 2: Thermodiffusion coefficient D_T for nC_i (1) – nC_{18} (2) at 25ºC

nC_i – nC_{18} (50:50 wt%) i=	$D_{T,2}$, 10^{-12} m^2/sK			
	Measurement	Calculation	Comparison	
			abs(D_{T_cal} - D_{T_exp})	Relative Error (%)
5	11.86	10.63	1.23	10.33
6	8.90	7.08	1.82	20.43
7	6.28	5.32	0.96	15.21
8	4.69	3.56	1.13	24.06
9	3.57	1.81	1.76	49.26
12	1.49	-0.92	2.41	161.77

Table 3: Thermodiffusion coefficient D_T for nC_i (1) – nC_{12} (2) at 25ºC

nC_i – nC_{12} (50:50 wt%) i=	$D_{T,2}$, 10^{-12} m^2/sK			
	Measurement	Calculation	Comparison	
			abs(D_{T_cal} - D_{T_exp})	Relative Error (%)
5	10.94	13.56	2.62	23.93
6	7.45	7.61	0.16	2.17
7	5.15	5.13	0.02	0.33
8	3.39	4.21	0.82	24.29
9	2.15	2.29	0.14	6.44

5 Conclusions

Thermodiffusion coefficients of binary n-alkane mixtures, namely nC_i - nC_{12} and nC_i - nC_{18} (i = 5~9), have been investigated both theoretically and experimentally. It is found that the calculated results agree very well with the experimental data obtained through the thermogravitational method.

Acknowledgment

The authors wish to acknowledge the support of the Canadian Space Agency (CSA), European Space Agency (ESA) and the Natural Science and Engineering Council, Canada (NSERC). The authors also wish to acknowledge that the experimental results are partly obtained in the framework of the following projects: GOVSORET2, TESBLUR (CTQ2005/09389/C02/01/PPQ) and the grant of the Department of Education, Universities and Investigation of the B.G. (BFI05.449).

References

[1] Dougherty E.L., Drickamer H.G., A theory of thermal diffusion in liquids, J. Chem. Phys. 23, 295 (1955)

[2] Dougherty E.L., Drickamer H.G., Thermal diffusion and molecular motion in liquids, J. Phys. Chem. 59, 443 (1955)

[3] Kempers L.J.T.M., A comprehensive thermodynamic theory of the Soret effect in a multicomponent gas, liquid, or solid. J. Chem. Phys., 115(14): 6330-6341, October 2001

[4] Firoozabadi A., Ghorayeb K., Shukla K., Theoretical model of thermal diffusion factors in multicomponent mixtures. AIChE J., 46, 892 (2000)

[5] Pan S., Saghir M.Z., Kawaji M., Jiang C., Yan Y., Theoretical approach to evaluate thermodiffusion in aqueous alkanol solutions, J. Chem. Phys., 126, 014502 (2006)

[6] Platten J.K., The Soret effect: A review of recent experimental results. J. Applied Mechanics – Transactions of the ASME, 73(1):5-15, January 2006

Polymers

Numerical model of unsteady flows of melt polymer in cylindrical ducts

K. Gueraoui[1,2], M. Taibi[1], S. Chtioui[1], Y. M. Haddad[2] and G. Zeggwagh[3]

[1] *Équipe de modélisation numérique et théorique en mécanique des fluides et en environnement, LPT, Faculté des Sciences, Rabat, Maroc.*
[2] *Département de Génie Mécanique, Université d'Ottawa, Ottawa, Canada, K1N 6N5*
[3] *Laboratoire de Mathématiques Appliquées, Faculté des Sciences Rabat-Agdal, B.P. 1014, Rabat, Maroc*

E-mail: kgueraoui@yahoo.fr

Abstract

In the present work we report on progress in the development of software tools for fluid flow prediction in the polymer processing industry. This involves state-of-the-art numerical techniques, in order to investigate realistic transient problems relevant to industrial processes. Particularly we study the effects of rheological parameters of fluid and heat transfer properties of the flowing materials in the flow, in a conical duct.

1 Introduction

This work is aimed at developing a computer code to simulate the types of flow which are important in the polymer processing industry [1-4]. In particular finite difference methods for incompressible viscous flows have been implemented for dealing with non-Newtonian materials under transient and thermal conditions.

The originality of this study is to investigate the effects of some rheological parameters of fluid and some thermal properties of the flowing material [5].

2 Theoretical model

The generalized equations of motion and energy for incompressible fluids are adopted. In conventional notation, the dimensional form of the momentum and mass conservation equations for the axisymmetric problem can be written as:

$$\rho\frac{\partial w}{\partial t} = -\frac{\partial P}{\partial z} + \frac{\eta_a}{r}\frac{\partial w}{\partial r} + \frac{\partial \eta_a}{\partial r}\frac{\partial w}{\partial r} + \eta_a\frac{\partial^2 w}{\partial r^2} - \rho u\frac{\partial w}{\partial r} - \rho w\frac{\partial w}{\partial z} \tag{1}$$

$$\frac{1}{r}\frac{\partial (ru)}{\partial r} + \frac{\partial w}{\partial z} = 0 \tag{2}$$

Where radial and axial coordinates are r and z, the fluid velocity is $\vec{V} = (u, w)$, P is the fluid pressure, ρ is the density and η_a is the fluid viscosity.

Likewise the energy equation for the axisymmetric problem can be expressed as:

$$\rho c_p\frac{\partial T}{\partial t} = \left[\frac{1}{r}\frac{\partial}{\partial r}\left(Kr\frac{\partial T}{\partial r}\right)\right] - \rho c_p\left(u\frac{\partial T}{\partial r} + w\frac{\partial T}{\partial z}\right) + \eta_a\left(\frac{\partial w}{\partial r}\right)^2 \tag{3}$$

Where T is the fluid temperature, c_p is the thermal heat capacity at constant pressure, K is the thermal conductivity.

The thermal power-law model is of Arrhenius form for the capillary flow where the viscosity function η_a is prescribed as [6]:

$$\eta_a = \eta_0\, \mathrm{e}^{-\beta(T-T_0)}\left|\frac{\partial w}{\partial r}\right|^{m-1} \tag{4}$$

Where T_0 is a reference temperature, m is the power-law index, η_0 is a reference viscosity value (associated with a unit shear rate and the reference temperature T_0) and β is a material constant.

The pressure gradient is unknown dimension in the duct, since we complete the above equations, which we cannot solve separately by a pressure equation:

$$\frac{\partial^2 P}{\partial z^2} - \frac{2tg\psi}{R}\frac{\partial P}{\partial z} + \frac{2tg\psi}{R^2}\tau_p - \frac{2}{R}\frac{\partial \tau_p}{\partial z} + \frac{\rho}{R^2}\frac{\partial^2 H}{\partial z^2} = 0 \tag{5}$$

With:

$$\tau_p = \left(\eta_a \frac{\partial w}{\partial r}\right)_{r=R}$$
$$H = 2\int_0^R rw^2 dr \tag{6}$$

Where R is the radius of the duct, ψ is the half-angle at the duct top, τ_p is the parietal stress.

3 Method and process of solution

3.1 Method of solution

The system of equations of energy and flow are solved by using a finite differences scheme [7].

3.2 Process of solution

Calculations start with an initial profile which can be whatever provided that it satisfies the boundaries conditions. However, and to reduce the calculating time, we choose an initial profile which is enough close to the exact one.

The solution of the flow equations, then the pressure equation, allow having in all section and at every moment the values of radial and axial velocity and the gradient of pressure. From the solution of the energy equation, we determine the temperature profile; the process is repeated until convergence of the solution.

The test of convergence is related to the temperature. Let ζ the cycles' number of calculation and ε_1 a small quantity fixed beforehand, we impose:

$$Sup\left|\frac{T_{\zeta}(r,z,t)-T_{\zeta+1}(r,z,t)}{T_{\zeta+1}(r,z,t)}\right|<\varepsilon_1 \qquad (7)$$

4 Results

The figure 1 shows the axial velocity profiles for a generalized Bingham fluid (m = 0.5) and a Bingham fluid (m = 1). We can verify that a diminution of m, which is translated by a more accented pseudo-plasticity, is accompanied by a decrease of the apparent viscosity that involves an increase in the velocity amplitudes. We obtain some qualitatively similar results to those of other authors in either the supple duct case [8-9] or rigid duct one [10].

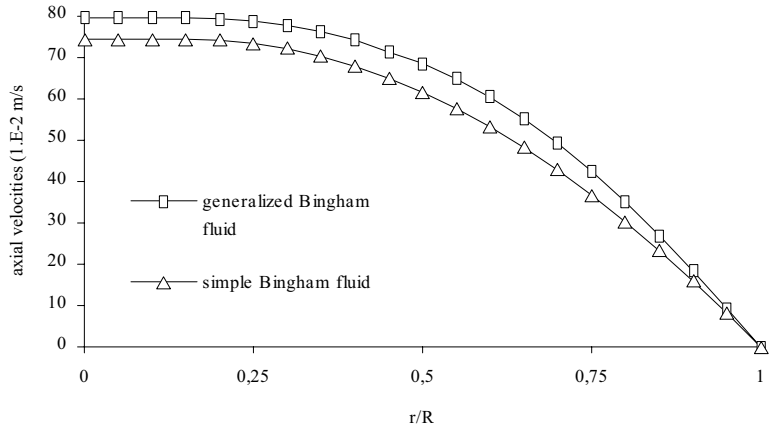

Fig 1: *Axial velocity profiles at z =L/2 and t =T/2 for 2 power law index values m.*

5 Conclusions

This study allowed us to analyze the influence and the evolution of the phenomena bounded to the power law index and the viscoelasticity of the wall pipe. The results show the importance of taking into account the nature of the fluid and the arterial wall.

References

[1] R.M. Turian, Viscous heating in the cone-and-plate viscometer-III. Non Newtonian fluids with temperature-dependent viscosity and thermal conductivity, Chem. Eng. Sci., 20 771-781, (1965).

[2] B. Martin, Some analytical solutions for viscometric flows of power-law fluids with heat generation and temperature dependent viscosity, Int. J. Non-linear Mechanics, 2(4) 285-301, (1967).

[3] L.T. Lindt, Flow of a temperature dependent power-law model fluid between parallel plates: an approximation for flow in a screw extruder, Polym. Eng. Sci. 29(7), 471-478, (1989).

[4] R.M.Griffith, Fully developed flow in screw extruders, Ind. Eng. Chem. Fundam., 1 180-187, (1962).

[5] H.H.Winter, Temperture fields in extruder dies with circular annular or slit cross-section, Polym. Eng. Sci., 15(2), 84-89, (1975).

[6] D. Ding, P. Townsend and M.F. Webster, On computation of two and three-dimensional unsteady thermal non-Newtonian flows, Int. J. Num. Meth. Heat Fluid Flow, 5, 495-510, (1995).

[7] J.P. Nougier, Méthodes de calcul numérique, Masson, 3ème édition, Paris, (1989).

[8] M. Zagzoule, J. Khalid-Naciri and J. Mauss, Unsteady wall shear stress in a distensible tube, Journal of Biomechanics, 24(6), 435-439, (1991).

[9] Z. Doulfoukar, M. Ouazzani Touhami, J. Khalid Naciri, M. Zagzoule, Méthode numérique pour la résolution de l'écoulement d'un fluide viscoélastique en conduite à paroi déformable, Journal Physique III, 433-442, (1996).

[10] G. Zeggwagh. Modélisations théorique et expérimentale de l'hémodynamique en microcirculation. Thèse de Doctorat ès-Sciences, I. N. P Toulouse, (1988).

Ludwig-Soret Effect for Aqueous and Non-aqueous Solutions of Polysaccharide

Yuki Kishikawa[1], Rio Kita[1], Hartmut Kriegs[2] and Simone Wiegand[2]

[1] Department of Physics, Tokai University, Japan
[2] IFF, Forschungszentrum Jülich, Germany

Contact: rkita@keyaki.cc.u-tokai.ac.jp

Abstract

The Ludwig-Soret effect was studied for aqueous and non-aqueous solutions of polysaccharides, pullulan and dextran, in the temperature range of $15 < T < 55$ °C by means of thermal diffusion forced Rayleigh scattering (TDFRS). The thermally induced sign change of the Soret coefficient was observed for these aqueous solutions. The sign of the Soret coefficient is positive at high temperatures ($T > 41$ °C for pullulan and $T > 45$ °C for dextran). While for low temperatures, a negative Soret coefficient has been observed, which corresponds to a migration of the polymers to the warm side. For solutions of pullulan in dimethyl sulfoxide (DMSO) and of dextran in 5 M urea water, the Soret coefficient is only positive in the same temperature range. The result indicates that the interactions via hydrogen bondings play a key role for the heat induced sign change of the Soret coefficient in aqueous polysaccharide solutions. Additionally, we studied the effect of the addition of sodium chloride to aqueous solutions of pullulan using an infrared laser to write the optical grating in the TDFRS experiment. The results indicate that the existence of NaCl tends to weaken the amplitude of the concentration gradient. Additionally, we performed light scattering experiments for the dilute solutions of pullulan and dextran at a homogeneous temperature of 25 °C. The obtained solution properties such as second virial coefficient, radius of gyration and hydrodynamic radius did not show any pronounced correlation with the sign change behavior of the Soret coefficient.

1 Introduction

The Ludwig-Soret effect of water-soluble polymers in dilute concentration regime often exhibits peculiar transport phenomena. One representative case is the sign change behavior of the Soret coefficient S_{T} and thermal diffusion coefficient D_{T} of the polymers [1–4]. It has also been observed that the sign change behavior of S_{T} depends on the solvent quality [5–7]. Recently, we reported the thermally induced sign change of S_{T} for the solution of dextran in water in the presence and absence of urea [7]. Dextran is a physiologically inactive polysaccharide utilizing extensively for pharmaceutical and industrial applications. It is composed of α-(1,6)-linked glucose as the backbone with a minor amount of branches by α-(1,3) linkage. It was observed at room temperature that the S_{T} of dextran is negative corresponding to the migration direction of dextran towards warm side in temperature gradient. While in the high temperature range ($T > 45$ °C), dextran moves to the cold side of the fluid. To our best knowledge, this is the first observation of the sign change of S_{T} as a function temperature occurring in a binary system composed of polymer and water. Studies of the effect of polar substance, urea, to the aqueous solution of dextran revealed that the modification of local structure of water is associating to the sign change of S_{T}. However, the numbers of the studies for aqueous polysaccharide solutions are limited. Systematic studies are then desired for better understanding of the thermal diffusion of polysaccharide solutions.

In this report, we show the experimental results of thermal diffusion forced Rayleigh scattering (TDFRS) for the solutions of pullulan and dextran. Pullulan is composed of α-(1,6)-linked maltotriose, which is a trimer made up of α-(1,4)-linked glucose. This means pullulan and dextran are composed of glucose as the basic constituent unit. However glucose is the monomer only for dextran but not for pullulan because the repeating unit of pullulan is maltotriose. Thus these polymers are different from each other in molecular structure although the basic constituent molecule is identical. Additionally, we determined the Soret coefficient of glucose and maltotriose in water by means of IR-TDFRS, which is the optimized setup for aqueous systems using an infrared-laser to write the optical grating [8]. With the IR-TDFRS setup, studies of the effect of sodium chloride to the aqueous pullulan solution was employed as well. Moreover, dimethyl sulfoxide (DMSO) is used as the solvent of pullulan in order to compare with the results of aqueous solution. While DMSO is polar solvent able to dissolve pullulan, it does not form hydrogen bonds. These systems could give a new insight for the mechanisms of thermal diffusion of polysaccharides. The solution properties of pullulan and dextran at a homogeneous temperature are investigated by light scattering which yields fundamental properties such as the mass and size of polymers and thermodynamic parameters of the solutions.

2 Experimental

Pullulan (Hayashibara Co., PF20) was purified three times by a methanol precipitation. The weight-averaged molecular weight of pullulan was obtained as M_w = 3.55×10^5 g/mol by light scattering. Dextran (Polymer Standard Service, GmbH) was purified and fractionated with methanol and the molecular weight was M_w = 8.67×10^4 g/mol. The details of the sample preparation of dextran was reported elsewhere [7]. Water is distilled and deionized one by a Milli-Q system (Millipore). Other chemicals were an analytical grade

purchased from Sigma-Aldrich and Wako and used without further purification.
The experimental details of classical TDFRS and the IR-TDFRS have been described elsewhere [8, 9]. Sample solutions for TDFRS measurements contain basantol yellow (BASF) as a dye to create the temperature gradient [7], whereas solutions were prepared without dye for IR-TDFRS measurements. The concentration of samples and the other experimental conditions will be stated in each experimental result. The refractive index increment with respect to the concentration, $(\partial n/\partial c)_{T,P}$, and the temperature, $(\partial n/\partial T)_{c,P}$, were measured individually for analyzing data of TDFRS [10].

3 Results and Discussion

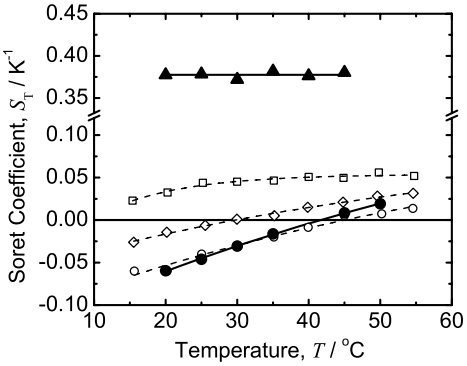

Fig. 1: *Soret coefficients of pullulan and dextran solutions as a function of temperature. The concentration of polysaccharide is 5.0 g/L for all solutions. Symbols are assigned as pullulan in water (●), pullulan in DMSO (▲), dextran in water(○), dextran in 2M urea water (◇), and dextran in 5M urea water (□). The lines are drawn to guide eyes.*

Figure 1 shows the Soret coefficient S_{T} (= D_{T}/D) of polysaccharide solutions as a function of temperature obtained by TDFRS. Here, D_{T} and D indicate the thermal diffusion coefficient and the mass diffusion coefficient, respectively. The filled and open symbols refer to the pullulan solutions and dextran solutions [7], respectively. The S_{T} of pulluan in water (●) increases with increasing the temperature, where a sign change is observed at T = 41 °C. At lower temperatures ($T < 41$ °C) the S_{T} of pullulan is negative which corresponds to a migration of pullulan to the warm side. This behavior is similar to that of the solution of dextran in water (○). The good agreement of S_{T} could be originated from chemical contributions of glucose as the basic constituent of pullulan and dextran. However, the mechanism leading to the sign change of these systems is not easy to understand. For instance S_{T} for solutions of glucose in water and of maltotriose in water is always positive and does not show a sign change [11]. These results indicate that the thermal diffusion behavior of polysaccharides is associated with not only chemical contributions but also intrinsic properties of polymers such as nonideal solution nature arising

from the context of long flexible chain of polymers. There are still arguments for the relationship between polymers and the monomer/oligomer unit on thermal diffusion of polymer solutions [12]. Further systematic studies for these systems are required.
As shown with open symbols in Fig. 1, the sign change behavior of the dextran solution is affected by the addition of urea; that is, the value of S_{T} increases and the sign change temperature shifts to lower values for dextran in 2 M urea/water (◇). In 5 M urea/water (□) S_{T} of dextran does not change the sign in the investigated temperature range. The negative S_{T} of dextran tends to being positive with decreasing the strength of hydrogen bondings by heating as well as by the addition of urea. The results imply a key role of hydrogen bonding for the sign change behavior.
The filled triangle in Fig. 1 denotes the result of pullulan in DMSO. It is found that the sign of S_{T} is always positive and shows no temperature dependence. It might be worthwhile to note the absolute value of S_{T} for pullulan in DMSO is larger than that of pullulan in water roughly 8 times at 25 °C. Measurements of the second virial coefficient by static light scattering indicate that the solubility of pullulan in DMSO is good and similar to the solubility in water. As mentioned above DMSO is a non-hydrogen bonding solvent. Consequently, it is expected that the negative sign of S_{T} of pullulan in water might be governed by the interactions via hydrogen bondings which is analogous to the results for dextran solutions.

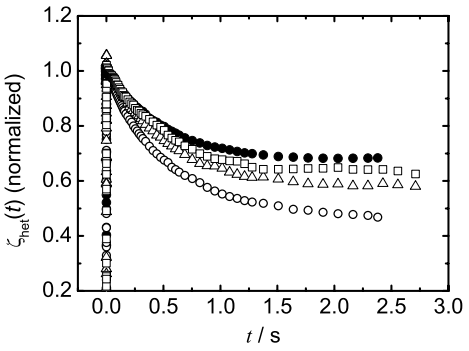

Fig. 2: *Normalized heterodyne signal of conventional TDFRS for pullulan in water (●) with the dye, basantol yellow. As well as signal of IR-TDFRS for pullulan in water (○), pullulan in 0.1 M NaCl water (△), and pullulan in 0.2 M NaCl water (□) measured without dye. The concentration of polysaccharide is 5.0 g/L for all solutions. The sample temperature was kept at 25 °C.*

Figure 2 shows the normalized heterodyne signal $\zeta_{\mathrm{het}}(t)$ for the solution of pullulan in water (●) measured by TDFRS. It also includes the signal obtained by IR-TDFRS for the solutions of pullulan in water (○), pullulan in 0.1 M NaCl water (△), and pullulan in 0.2 M NaCl water (□). The concentration of polymer is constant in all samples but the NaCl content is varied. The decay signals correspond to the diffusion of pullulan under the temperature gradient and the amplitude of the signal relates to the magnitude of

the concentration gradient. As seen from open symbols the signal amplitude decreased with increase the NaCl concentration. The aqueous solution of pullulan prepared with the dye, basantol yellow, (•) showed the smallest amplitude, although it does not contain NaCl. The result indicates that the dye possesses a charge effect. Indeed the dye basantol yellow is a trivalent salt, which influences the solution in a similiar way as the addition of NaCl [13]. Further considerations are necessary to reveal the effect of the ionic dye especially for studies of aqueous system investigated by the classical TDFRS. The results demonstrate that studies with the IR-TDFRS in aqueous systems are necessary to investigate the influence of charge effects on the systems.

4 Conclusions

The Ludwig-Soret effect for the solutions of pullulan and dextran is investigated in terms of temperature, the effect of addition of urea, and different solvents (water and DMSO). It is revealed that the heat induced sign change of S_{T} for solutions of pullulan and dextran in water are identical due to the chemical contributions of glucose as the basic constituent molecule. It is also suggested that the sign change of S_{T} depends on the intrinsic properties of polymers. In a non-hydrogen bonding solvent, DMSO, the S_{T} is always positive. These results imply that the thermal diffusion of polysaccharide is associated with the strength of hydrogen-bonding of polysaccharide solutions.

Acknowledgment

The authors are indebted to Jan Dhont at Forschungszentrum Jülich, GmbH, for his kind support. This work was partially supported by the Ministry of Education, Science, Sports and Culture, Japan and by the Deutsche Forschungsgemeinschaft (WI 1684).

References

[1] B.-J. de Gans, R. Kita, S. Wiegand, and J. Luettmer Strathmann, Phys. Rev. Lett. **91**, 245501 (2003).

[2] S. Iacopini and R. Piazza, Europhys. Lett. **63**, 247 (2003).

[3] R. Kita, S. Wiegand, and J. Luettmer-Strathmann, J. Chem. Phys. **121**, 3874 (2004).

[4] R. Kita, G. Kircher, and S. Wiegand, J. Chem. Phys. **121**, 9140 (2004).

[5] S. Wiegand, N. Hui, and R. Kita, J. Non-Equilib. Thermodyn. **32**, 193 (2007).

[6] R. Kita, P. Polyakov, and S. Wiegand, Macromolecules **40**, 1638 (2007).

[7] R. Sugaya, B. A. Wolf., and R Kita, Biomacromolecules **7**, 435 (2006).

[8] S. Wiegand, N. Hui, and H. Kriegs, J. Phys. Chem. B **111**, 14169 (2007).

[9] W. Köhler and R. Schäfer, In *Advances in Polymer Science*, Vol. 151, Pages 1-59 (Springer, Berlin, 2000).

[10] A. Becker, W. Köhler, and B. Müller, Ber. Bunsen-Ges. Phys. Chem. Chem. Phys. **99**, 600 (1995).

[11] Y. Kishikawa, R. Kita, H. Kriegs, and S. Wiegand, (to be submitted).

[12] J. Rauch and W. Köhler, Macromolecules **38**, 3571 (2005).

[13] N. Hui, R. Kita, H. Kriegs, J. Luettmer-Strathmann, and S. Wiegand, J. Phys. Chem. B **110**, 10746 (2006).

Thermodiffusion Driven Patterns in a Polymer Blend Close to the Critical Point

A. Krekhov, F. Schwaiger, S. Frank, A. Voit and W. Köhler

Physics Department, University of Bayreuth, Germany

Contact: alexei.krekhov@uni-bayreuth.de, werner.koehler@uni-bayreuth.de

Abstract

We have studied the effects of thermal diffusion on the formation of compositional patterns in a thin layer of a polymer blend. The coupling between the order parameter (composition) and the temperature gradient which is described by the Soret effect becomes especially effective near the critical point. In the experiments on a PDMS-PEMS polymer blend it has been found that the Soret coefficient is four orders of magnitude larger than the values known for small molecules. Due to such strong coupling a polymer blend in an inhomogeneous temperature field cannot be treated in terms of a quasi-equilibrium system and even UCST-systems can be quenched into the two phase region by a local heating. We discuss the formation of composition patterns both in the one- and in the two-phase region. The quantitative theoretical description of the laser induced structures in the one-phase region is based on the heat and the diffusion equations taking into account both thermal diffusion and advection. The analysis of phase separation in the two-phase region is based on the Cahn-Hilliard model including the thermal diffusion.

1 Introduction

The influence of external fields on phase separation and structuring of thin polymer films has received growing attention because of the possibility of controlling the demixing morphology. It has been found that thin films of incompatible polymers resemble the structure of the underlying pre-patterned substrate, if the characteristic wavelength of the pre-patterning is compatible with the intrinsic length scale of the free spinodal demixing morphology [1]. Small filler particles can trigger composition waves in phase-separating polymer blends [2]. A variation of the morphology of thin PMMA/SAN films has been achieved by changing the PMMA content [3]. Naturally, such an approach is not suitable for the formation of, e.g., a single linear structure within an otherwise homogeneous film. In the present work we show that local heating of a polymer blend in the vicinity of the critical point by a focused laser beam can be utilized to create almost arbitrary two-dimensional structures in a thin polymer layer both in the one- and in the two-phase regime. The local composition variation is caused by the Soret effect, which accounts for a concentration gradient that develops in a multicomponent mixture subjected to an inhomogeneous temperature field.

2 Experimental Setup

The large Soret coefficients for polymer blend near a critical point can be utilized to write almost arbitrary composition patterns into a layer of the polymer blend by localized heating [4–6]. A sketch of the experimental setup is shown in Fig. 1. It consists of an inverted phase contrast microscope with a laser port. Two mirrors mounted on magnet closed loop galvano scanners are situated in a conjugate confocal plane with a scanning point in the sample. The conjugate planes are formed with the help of two lenses (telecentric system) and an objective. The latter serves both for focusing of the laser beam and for observation of the sample. The laser can be focused down to below $1\,\mu\mathrm{m}$ and typical power values are between 0.1 and $100\,\mathrm{mW}$. The cell is mounted horizontally in a temperature-controlled *xyz*-stage in the focal plane of a phase contrast microscope. It has a layer thickness of $100\,\mu\mathrm{m}$ and is sealed with two component epoxy resin (Torr Seal).

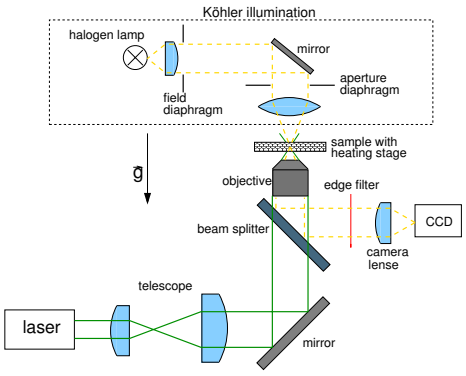

Fig. 1: *Experimental setup.*

3 Pattern Writing in the One-Phase Region

For the patterning experiments an almost symmetric PDMS(16.4 kg/mol)/PEMS(15.9 kg/mol) polymer blend with a critical composition $c = c_{\mathrm{crit}} = 0.48\,\mathrm{g/g}$ and a convenient critical

temperature $T_c = 290.15\,\mathrm{K}$ has been chosen. Micrographs of the time evolution of the pattern at two different temperatures of the sample ($\Delta T = 1\,\mathrm{K}$ and $\Delta T = 11.5\,\mathrm{K}$) above T_c are shown in Fig. 2.

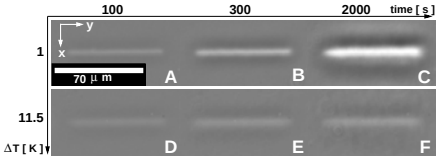

Fig. 2: *Spatial modulation of concentration by scanning a laser along the y-axis with a scanning frequency of* $20\,\mathrm{Hz}$ *and a laser power of* $1\,\mathrm{mW}$ *at two different temperatures above the critical temperature. Pictures A-C taken at* $\Delta T = 1\,\mathrm{K}$ *after* $t = 100\,\mathrm{s}$, $t = 300\,\mathrm{s}$, *and* $t = 2000\,\mathrm{s}$. *Pictures D-F taken at same time intervals but at* $\Delta T = 11.5\,\mathrm{K}$. *The intensity is normalized to the one of the undisturbed sample (picture at* $t = 0\,\mathrm{s}$*). To display positive and negative changes, 127 is added to the 8-bit grey values. Grey values greater than 127 represent an increase of intensity, values smaller than 127 a decrease.*

Due to the positive phase contrast technique, bright regions in the picture represent a lower refractive index (PDMS enriched) compared to the dark regions. Until $100\,\mathrm{s}$ there is hardly a difference in the amplitudes of the concentration modulations, indicating an almost constant thermal diffusion coefficient D_T, which governs the early stage of the formation of the concentration pattern. At such short times, back diffusion as competing process is still irrelevant. After $300\,\mathrm{s}$ this is no longer the case for the higher temperature. The growth of the structure becomes progressively limited by Fickian diffusion and solutal convection of the polymer, which aims at restoring the homogeneous state and, eventually, the Soret coefficient $S_T = D_T/D$ determines the maximum modulation depth. Close to T_c the structure is still within the initial linear growth regime after 300 s. After $2000\,\mathrm{s}$ the line for $\Delta T = 1\,\mathrm{K}$ becomes even more intense, whereas the line for $\Delta T = 11.5\,\mathrm{K}$ remains almost unchanged.

The description of an incompressible binary mixture in the one-phase regime under inhomogeneous temperature field produced by light absorption is based on the heat equation for the temperature $T(\boldsymbol{r}, t)$ and the diffusion equation for the concentration $c(\boldsymbol{r}, t)$.

The Navier-Stokes equation for the velocity $\boldsymbol{v}(\boldsymbol{r}, t)$ is included to account for convection due to local heating. To describe the temperature and concentration distributions in the cross section of the polymer layer ($x - z$ plane) located in the middle of the written line, we consider a two-dimensional model supposing the line to be infinitely extended in the y direction. Consequently, T, c and $\boldsymbol{v}$ are independent of y. Details of the simulation technique can be found in Ref. [6]. We have used the measured values for the material parameters $D(T, c)$, $D_T(T)$ [6] and all others were taken from the literature. The results of the simulations are shown in Fig. 3 in comparison with the experimental data.

4 Pattern Writing in the Two-Phase Region

Fig. 4(I) shows the time evolution of one single line written into a PDMS(16.4 kg/mol)/PEMS (22.0 kg/mol) blend ($c = 0.512\,\mathrm{g/g}$, $T_c = 314.7\,\mathrm{K}$, $\alpha \approx 500\,\mathrm{m}^{-1}$) at a temperature 1.3 K below T_c and a laser power of 1 mW. The width of the laser focus is about $1.6\,\mu\mathrm{m}$, the length of the line is almost $140\,\mu\mathrm{m}$. Obviously, it is not possible to write a stable line into the sample. After approximately 1000 s surface tension effects lead to a pearling

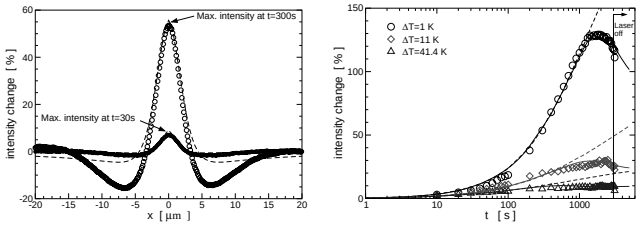

Fig. 3: *(left) Intensity profile along the x-axis, averaged over the length of the written line, taken from images (Fig. 2) at* $t = 300\,\mathrm{s}$ *and* $t = 30\,\mathrm{s}$ *for* $\Delta T = 1\,\mathrm{K}$*. The open symbols show the result from the experimental pictures. The dashed lines show the numerical simulation. An increase of intensity represents accumulation of PDMS. Far away from the written line the sample remains unchanged. (right) Maximum intensity change obtained from averaged images plotted versus time at a laser power of* $1\,\mathrm{mW}$ *(open symbols) for different temperatures* ΔT *above the critical temperature. The vertical solid line indicates the switch-off time of the laser. The solid lines show numerical simulations with convection, the dashed lines without.*

instability that eventually dominates the structure formation.

Fig. 4(II) shows the result if multiple parallel lines are written instead of a single one. A grid pattern evolves with a period comparable to the length scale of the already coarsened spinodal pattern. This grid pattern is stable as long as the writing process continues (A). Turning the laser off for 360 s leads to a beginning degradation (B), but continued writing again stabilizes the imposed structure (C). After turning the laser off again, some deformation due to bulging of the left- and rightmost grid lines is observable (D). Continued writing of only the outermost (longer) lines allows for a continued stabilization of the central grid pattern (E). After switching the laser off, surface tension takes over and all parallel lines eventually decay into spherical structures.

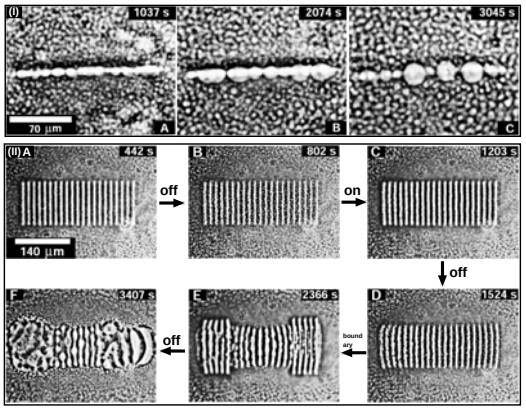

Fig. 4: *Temporal evolution of one single line (I) (written from* $t = 0\,\mathrm{s}$ *until* $t = 2074\,\mathrm{s}$ *at 1.3 K below* T_c*, laser-power* $1\,\mathrm{mW}$*). 21 parallel lines (II) (written from* $t = 0\,\mathrm{s}$ *with 8 mW at 1.5 K below* T_c*; "on" and "off" refer to switching of the laser; "boundary" means that only the outermost lines are written in order to stabilize the central part of the pattern; see text for details).*

To model the effect of phase separation we use the Cahn-Hilliard equation taking into account an inhomogeneous tem-

perature distribution which couples to concentration variation via the Soret effect (see [7] for details). We have found that under spatially periodic temperature modulation $T = T_0 + \delta T \cos(qx)$ there exist a critical modulation amplitude δT above which the spinodal decomposition ends up in the stationary periodic solution with the period of the driving $2\pi/q$. In Fig. 5 typical snapshots of 2D simulations are shown for the modulation amplitude slightly above the critical one.

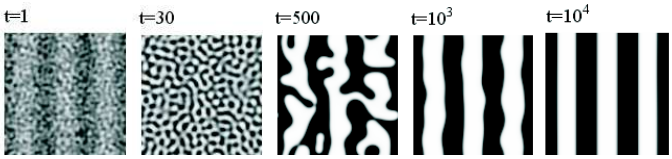

Fig. 5: *Snapshots of the phase separation under the spatially periodic temperature modulation slightly above the critical modulation amplitude. Time is given in the dimensionless units.*

Acknowledgment

This work was supported by the *Deutsche Forschungsgemeinschaft* (SFB 481/A8).

References

[1] M. Böltau, S. Walheim, J. Mlynek, G. Krausch, and U. Steiner, Nature **391**, 877 (1998)
[2] B. P. Lee, J. F. Douglas, and S. C. Glotzer, Phys. Rev. E **60**, 5812 (1999)
[3] H. J. Chung, H. Wang, and R. J. Composto, Macromolecules **39**, 153 (2006)
[4] A. Voit, A. Krekhov, W. Enge, L. Kramer, and W. Köhler, Phys. Rev. Lett. **94**, 214501 (2005)
[5] A. Voit, A. Krekhov, and W. Köhler, Macromolecules **40**, 9 (2007)
[6] A. Voit, A. Krekhov, W. Köhler, Phys. Rev. E., **76**, 011808 (2007)
[7] A. P. Krekhov and L. Kramer, Phys. Rev. E **70**, 061801 (2004)

On thermodynamic approach to mass transport

S.N. Semenov[1] and M.E. Schimpf[2]

[1]*Institute of Biochemical Physics RAS, Moscow, Russia*
[2]*Boise State University, Boise, ID USA*

E-mail: *mschimpf@boisetstate.edu* *sem@triniti.ru*

Abstract

A thermodynamic approach to mass transport is applied to liquid mixtures in a temperature gradient. The consistency of the Onsager equations for the component mass flux is evaluated with the resulting conclusion that heats of transport are equal to the chemical potentials of the components to eliminate thermodiffusion in pure liquids. In an open and/or non-stationary system, consistency between the Gibbs-Duhem equation and the Onsager equations is impossible. Using the original approach, the dynamic pressure gradient is calculated. Coefficients of thermodiffusion and mass diffusion are described over the entire compositional range of a mixture. It is shown that barodiffusion changes the second virial coefficient calculated from diffusion measurements, and that dynamic barodiffusion can explain the size dependence in the thermal diffusion of DNA.

1 Introduction

Certain refinements in non-equilibrium thermodynamics are necessary for non-isothermal mixtures when more than one of the components is not dilute. In order to simplify the problem, we examine here a binary mixture. Our motivation is based on three observations:

1. Current non-equilibrium thermodynamics approaches to mass transport fail to provide an unambiguous description of concentrated systems, in that component behavior depends on which component is considered to be the solvent.

2. In the Onsager formulation, the component mass fluxes are expressed through kinetic coefficients. In thermodynamic theories of thermal diffusion, the heat of transfer is formulated into equations for the Soret coefficient. We argue that a component's heat of transfer must equal its chemical potential. Without such equality, certain consequences follow that violate the condition of hydrostatic equilibrium.

Usually, the Gibbs-Duhem equation is used to derive the pressure gradient. We will show that viscous drag in an open or/and non-stationary system causes additional dynamic pressure gradient.

2 Consistency Conditions for Onsager Mass Fluxes

The thermodynamic approach is based on the rate of entropy production σ [1, 2]:

$$\sigma = \vec{J}_e \cdot \nabla\left(\frac{1}{T}\right) - \vec{J}_1 \cdot \nabla\left(\frac{\mu_1}{T}\right) - \vec{J}_2 \cdot \nabla\left(\frac{\mu_2}{T}\right) \tag{1}$$

Here, $\vec{J}_e$ is the energy flux, $\vec{J}_1$ and $\vec{J}_2$ are the mass fluxes of the two components, μ_1 and μ_2 are their chemical potentials, and T is temperature. The energy flux and temperature profile are defined by the difference in temperature at the system boundaries ([2], Ch. 16), while the mass flux is defined by the following continuity equation:

$$\frac{\partial n_i}{\partial t} = -\nabla \vec{J}_i \tag{2}$$

Here n_i is the numeric volume concentration of the i^{th} component and t is time. The mass flux is further defined by non-equilibrium thermodynamics as [1, 2]:

$$\vec{J}_i = -n_i L_i \nabla \frac{\mu_i}{T} - n_i L_{iQ} \nabla \frac{1}{T} \tag{3}$$

where L_i and L_{iQ} are the Onsager coefficients.
In order to utilize Eq. (3) in a predictive capacity, it is transformed into a form that contains component concentrations and other physically measurable system parameters:

$$\nabla \mu_\kappa = \sum_{l=1}^{2} \frac{\partial \mu_k}{\partial n_l} \nabla n_l - \overline{v}_k \nabla P + \frac{\partial \mu_k}{\partial T} \nabla T \tag{4}$$

where P is the internal macroscopic pressure of the system and $\overline{v}_k =$ is the partial molecular volume. Substitution of Eq. (4) into Eq. (3) yields

$$\vec{J}_i = \frac{n_i L_i}{T} \left\{ -\sum_{k=1}^{2} \frac{\partial \mu_i}{\partial n_k} \nabla n_k + \overline{v}_i \nabla P + \left[\left(\frac{\mu_i}{T} - \frac{\partial \mu_i}{\partial T} \right) - \frac{L_{iQ}}{T L_i} \right] \nabla T \right\} \tag{5}$$

The term in square brackets on the right-hand side of Eq. (5) can be related to the enthalpy h_i, entropy s_i, and heat of transport q_i as follows: $h_i = \mu_i - T s_i$; $s_i = \partial \mu_i / \partial T$; and $q_i = L_{iQ} / L_i$ [1, 2].

The thermodynamic approach utilizes the Gibbs-Duhem equation [4, 5]:

$$\nabla P = \sum_{i=1}^{2} n_i \left(\sum_{k=1}^{2} \frac{\partial \mu_i}{\partial n_k} \nabla n_k + \frac{\partial \mu_i}{\partial T} \nabla T \right) \tag{6}$$

Eq. (6a) defines the pressure gradient required to maintain hydrostatic equilibrium. An equation similar to Eq. (6a) has been used to calculate diffusion and thermal diffusion coefficients [6], where the osmotic pressure Π is introduced as $\delta \Pi = \delta P - \delta \left(\mu_1 / v_1 \right) = n_2 \delta \left(\mu^* \right)$, where δ is the difference between two isothermal cells connected by a thin conduit, and $\mu^* = \mu_2 - \left(v_2 / v_1 \right) \mu_1$ is the combined chemical potential. Substituting Eq. (6) into Eq. (5) we obtain

$$\vec{J}_1 = \frac{L_1 v_1}{T v_2} \left[\phi (1 - \phi) \left(2 \frac{\partial \mu^*}{\partial \phi} \nabla \phi + \frac{\partial \mu^*}{\partial T} \nabla T \right) - (1 - \phi)(\mu_1 - q_1) \frac{\nabla T}{T} \right] \tag{7}$$

$$\vec{J}_2 = -\frac{L_2}{T} \left[\phi (1 - \phi) \left(2 \frac{\partial \mu^*}{\partial \phi} \nabla \phi + \frac{\partial \mu^*}{\partial T} \nabla T \right) + \phi (\mu_2 - q_2) \frac{\nabla T}{T} \right] \tag{8}$$

In formulating Eqs. (7) and (8) we have introduced the volume fractions $\phi_2 = n_2 v_2 = \phi$ and $\phi_1 = n_1 v_1 = 1 - \phi$, and substituted specific molecular volumes v_1 and v_2 for the partial molecular volumes used in Eqs. (4) and (5). We have also utilized the equality $\partial \mu^* / \partial \varphi_1 = -\left(\partial \mu^* / \partial \varphi_2 \right)$.

Equations (7) and (8) are two non-equivalent expressions that relate mass flux to the volume fraction ϕ of a component in a non-isothermal system. Consequently, the result will depend on which equation is used. In practice Eq. (8) is used to define the transport of the dilute component in a mixture, while transport of the solvent is defined through conservation of mass. In mixtures where more than one component is concentrated, the result will differ depending on which component is selected as the solvent.

In order for Eqs. (7) and (8) to be made consistent, the following conditions must be met:

$$\mu_1 = q_1 \tag{9}$$

$$\mu_2 = q_2 \tag{10}$$

$$\vec{J}_1 = \vec{J}_2 = 0 \tag{11}$$

The conditions defined by Eqs. (9) and (10) eliminate the motion of pure liquid in a temperature gradient, which would inconsistent with the Gibbs-Duhem equation.

While the condition defined by Eqs. (9) and (10) should be accepted for any system, Eq. (11) is fulfilled only in a closed system that is stationary. Consequently, Eqs. (7) and (8) are incompatible with the Gibbs-Duhem equation for any system that is open and non-stationary.

Combining either of Eqs. (7) and (8) with Eqs. (9-11), we obtain the equation:

$$\phi(1-\phi)\left(2\frac{\partial\mu^*}{\partial\phi}\nabla\phi+\frac{\partial\mu^*}{\partial T}\nabla T\right)=0 \tag{12}$$

which can be used to obtain the stationary concentration distribution and any related parameters.

In a dilute solution ($\phi << 1$) the chemical potentials can be written as [7]

$$\mu_1(\phi)=\mu_1^0-kT\left(\phi/v_2N_a\right) \tag{13}$$

$$\mu_2(\phi)=\mu_2^0+kT\ln\phi \tag{14}$$

where μ_1^0 and μ_2^0 are the chemical potentials of the pure component and the isolated specie of the second component in the solvent, respectively, and N_a is Avogadro's number. Then, we obtain the following expression for the Soret coefficient:

$$S_T=-\frac{\nabla\phi}{\phi(1-\phi)\nabla T}\approx\frac{s_0^*}{2kT} \tag{15}$$

Here, $\mu_0^* = \mu_2^0 - \mu_1^0 \left(v_2 / v_1 \right)$, and $s_0^* = \partial \mu_0^* / \partial T$ is the combined molecular entropy.

Duhr and Braun used a priori a similar expression [8]. The analysis of results of Duhr and Braun says that: a) the entropy term in Eq. (15) is not the entropy of a single dissolved molecule or suspended particle. b) A factor of 2 is missing from the denominator in their work. c) The only term μ_2^0 in μ_0^* is proportional to the particle surface area for large particles. It makes the explanation of the size dependence given in [8] less acceptable.

3 The Dynamic Pressure Gradient and Barodiffusion

In an open or non-stationary system, the total mass flux or the component fluxes can be non-zero.
Here, the mass transport equations can be obtained, calculating the pressure gradient using Eqs. (7) and (8), and considering ∇P and ϕ as unknown functions:

$$\nabla P = \frac{-\frac{\vec{J}}{L_1} + 2[(1-\phi)\frac{\partial \mu_1}{\partial \phi} + \frac{L_2}{L_1}\phi \frac{\partial \mu_2}{\partial \phi}]\nabla \phi + [(1-\phi)\frac{\partial \mu_1}{\partial T} + \frac{L_2}{L_1}\phi \frac{\partial \mu_2}{\partial T}]\nabla T}{v_1 \left[1 - \phi + \left(D_2 v_2 / D_1 v_1 \right)\phi \right]} \tag{16}$$

$$\frac{\partial \phi}{\partial t} = \frac{L_2}{T} \nabla [\frac{\phi(1-\phi)\left(2\frac{\partial \mu^*}{\partial \phi}\nabla \phi + \frac{\partial \mu^*}{\partial T}\nabla T \right) - \phi \frac{\vec{J}}{L_1}}{1 - \phi + \left(D_2 v_2 / D_1 v_1 \right)\phi}] \tag{17}$$

Eq. (16) described the dynamic pressure gradient established in open and non-stationary systems. It is different of the Gibbs-Duhem pressure gradient predicted by Eq. (6).

Similar equations were obtained using a kinetic approach [9, 10]. Compared to Eq. (12), the mass flux in Eq. (17) contains the term $\vec{J}$ responsible for the solute drift in the open system. When the molecules entering through one boundary may leave the system through another, the component meets viscous resistance, which creates a dynamic pressure gradient and barodiffusion in the system. This situation is not considered in the Gibbs-Duhem equation.

For ideal solutions, the effective diffusion coefficient given by Eq. (17) can be expressed as

$$D_{eff} = D_2(\phi) \frac{1 - \phi + \left(v_2 / v_1 \right)\phi}{1 - \phi + \left(D_2 v_2 / D_1 v_1 \right)\phi} \tag{18}$$

where $D_i(\phi)$ is the Stokes-Einstein diffusion coefficient in the real liquid mixture. Eq. (18) accurately predicts the diffusion coefficient at any concentration. For dilute systems, the dynamic barodiffusion factor $\left[1-\phi+\left(D_2v_2/D_1v_1\right)\phi\right]^{-1}$ allows the effective diffusion coefficient described by Eq. (18) to be transformed into the Stokes-Einstein expression. Without such a factor the model of Dhont [6] fails to provide this physically reasonable behavior, even in ideal solutions.

Eqs. (17) and (18) predict the concentration dependence of the effective diffusion coefficient measured by dynamic light scattering. In semidilute systems, the concentration dependence of the effective diffusion coefficient is typically described by the virial expansion coefficient B [11].

$$D_{eff} \approx D_2\left(\phi=0\right)\left[1-\left(\frac{2B}{v_2}-\frac{D_2v_2}{D_1v_1}-\frac{3}{2}\right)\phi\right] \tag{19}$$

When barodiffusion in the dynamic pressure gradient is ignored, the term D_2v_2/D_1v_1 in concentration dependence of the effective diffusion coefficient is absent [11].
By comparing Eq. (19) and its simplified form, we can evaluate the relative contribution of dynamic barodiffusion to the effective diffusion coefficient as $\left(2/27\right)\left|\left(D_2v_2/D_1v_1\right)-1\right|$. In a mixture of methanol and ethanol with molar volumes of 41 and 58 cm^3, respectively [12], and similar Stokes-Einstein diffusion coefficients [13], the contribution of dynamic barodiffusion is about 3%. For methanol/n-propanol, where $v_1/v_2 \approx 41/75$, the contribution is about 6%. In concentrated mixtures of methanol and ethanol, for example, the relative barodiffusion change in the diffusion coefficient is about 17%; for methanol/n-propanol it is 30%.

The effect of dynamic barrodiffusion on measurements of diffusion and thermodiffusion is even more significant for polymers and colloidal particles because parameter D_2v_2/D_1v_1, which reflects the role of the dynamic pressure gradient, can be quite large. For example, in a study by Duhr and Braun of DNA molecules [8], the thermodiffusion coefficient of DNA was reported to decrease with chain length. To date there is no theoretical explanation for this observation.
For dilute systems ($\phi << 1$), the expression for the thermodiffusion coefficient is

$$D_T = \frac{D_2}{1-\phi+\left(D_2v_2/D_1v_1\right)\phi}\frac{s_0^*}{2kT} \tag{20}$$

According to Eq. (20), the thermodiffusion coefficient may decrease with increasing particle size, provided $\left(D_2v_2/D_1v_1\right)\phi \approx 1$. Therefore, Eq. (20) is consistent with the behavior of diluted DNA solutions reported by Duhr and Braun [8].

4 Conclusions

When the thermodynamic approach is evaluated, we find that the equations for mass flux are inconsistent unless the heats of transport are equal to the respective chemical potentials. Then, the unacceptable effect of motion in pure non-isothermal liquids is eliminated. This approach also verifies the dominance of entopic forces in the thermodiffusion.

Our analysis also demonstrates that the Gibbs-Duhem equation is inadequate for open and non-stationary systems. By defining the dynamic pressure gradient, a distinction is made between the equilibrium pressure gradient predicted by the Gibbs-Duhem equation and the dynamic pressure gradient in an open and/or non-steady state system. Application of the model to semidilute systems indicates that dynamic barodiffusion should be incorporated into calculations of the second virial coefficient based on fluctuation dynamics.

Highly structured macromolecules and colloidal particles suspended in a solvent can create large dynamic pressure gradients. It is found that such effects may qualitatively explain the measured size dependence of thermodiffusion in DNA experiments.

References

[1] S. R. De Groot, P. Mazur, *Non-equilibrium Thermodynamics* (North-Holland, Amsterdam, 1962).

[2] D. Kondepudi, I. Prigogine, *Modern Thermodynamics* (Wiley, New York, 1999).

[3] L. D Landau, E. M. Lifshitz, *Fluid Mechanics* (Pergamon, London, 1959);

[4] K. Ghoraeb, A. Firoozabadi, *AIChE*, 46 883 (2000).

[5] S. Pan, M. Z. Sahgir, M. Kawaji, C. G. Jiang, Y. Yan, *J. Chem. Phys*. **126**, 014502 (2007).

[6] J. K. G. Dhont, *J. Chem. Phys*. **120**, 1632 (2004).

[7] L. D. Landau, E. M. Lifshitz, Statistical Physics, Part 1, Chapter IX, "Nauka" Publishing, Moscow 1976 (In Russian)

[8] S. Duhr, D. Braun, *PNAS published online*, Dec 12, 2006. doi:10.1073/pnas. 0603873103.

[9] M. E. Schimpf, S. N. Semenov, *Phys. Rev. E*, 70, 031202 (2004).

[10] S. N. Semenov, M. E. Schimpf, *Phys. Rev. E*, 72, 041202 (2005).

[11] *Photon Correlation and Light Beating Spectroscopy*, edited by H. Z. Cummings and E. R. Pike (Plenum Press, New York), 1974.

[12] *Organic Solvents. Physical Properties and Methods of Purifications*, 4th ed. J. A. Riddik, W. B. Bunger, and T. K. Sakano, Eds. (Wiley, New York), 1986.

[13] E. J. W. Welsink, A. C. Hoffmann, P. J. van Maaren, D. van der Spoel, *J. Chem. Phys.*, 119, 7308 (2003). J. K. G. Dhont et al, *Langmuir,* **23**, 1674 (2007).

Theory of strong temperature dependence in thermophoresis

S.N. Semenov[1] and M.E. Schimpf[2]

[1]*Institute of Biochemical Physics RAS, Moscow, Russia*
[2]*Boise State University, Boise, ID USA*

E-mail: *sem@triniti.ru*; *mschimpf@boisetstate.edu*

Abstract

The strong temperature dependence in thermal diffusion is examined. An effective interaction potential is calculated by averaging the standard interaction potential for the isolated molecules using the Boltzmann factor and accounting steric limitations. The strong temperature dependence is expected when the solute-solvent interactions are weak, and the hydrodynamic radius of the solvent is smaller than of the dissolved monomer or molecule. The theoretical results are used to obtain these parameters for poly(N-isopropyl acrylamide) in methanol, ethanol, and 1-propanol with the error about 5%. This result is used to calculate the respective parameters in 1-butanol, which are consistent with data for the other three alcohols.

1 Introduction

The goal of these studies is the qualitative explanation of the experimental data on the poly(N-isopropyl acrylamide) (PNiPAM) thermal diffusion in monohydric alcohols, where unusually strong temperature dependence of thermal diffusion and even the change in the direction of thermophoretic motion is observed [1]. The respective experimental data will be discussed further, when the basic theoretical expressions will be obtained and discussed.

In the hydrodynamic approach, the flow of liquid around an isolated particle is caused by a local pressure gradient around the particle, as defined by the Navier-Stokes equation [2]:

$$\eta \nabla \vec{u} = \vec{f}_{loc}^{2} - \nabla \Pi_{loc} \tag{1}$$

Here $\vec{u}$ is the velocity of the liquid, Π_{loc} is the local pressure distribution around the particle, $\vec{f}_{loc}^{2}$ is the volume force that results from the particle's interaction with molecules of the liquid, and η is the dynamic viscosity of the liquid. In a temperature or concentration gradient, the pressure distribution becomes non-uniform due to the local interaction of a particle with non-uniformly arranged molecules of the surrounding liquid.

The local pressure distribution can be obtained from the condition of hydrostatic equilibrium in the surrounding liquid (local equilibrium), in the absence of temperature gradient, using the assumption of uniform density in the surrounding liquid [3, 4]:

$$\Pi_{loc} - \Pi_0 = -\Phi_{21} / v_1 \tag{2}$$

where Π_0 is the macroscopic pressure, which is not changed significantly at the molecular lengths, but should not be macroscopically constant, v_1 is the specific molecular volume of the solvent, and Φ_{21} is the interaction potential between the dissolved molecule and the solvent. For liquids with low ion concentration:

$$\Phi_{21}(r) = -16\sqrt{A_1 A_2}\left(r_1^H + r_2^H\right)^3 \Big/ 9r^6 \tag{3}$$

where A_i and A_j are the Hamaker constants, and r_1^H and r_2^H are the molecular hydrodynamic radiuses of the dissolved particle or monomer and the solvent molecule, r is the radial coordinate [5].

Using Eq. (3), we calculate the local pressure gradient around the selected molecule as

$$\nabla \Pi_{loc} = \Phi_{21} \alpha_T \nabla T / v_1 \tag{4}$$

where α_{Tj} is the cubic thermal expansion coefficient in the solvent [3, 4].

Using the condition of steady-state motion, we obtain the general expression for the molecular velocity U_2:

$$U_2 = \frac{\alpha_T}{6\pi\eta r_2^H v_1} \int_0^\pi Sin\vartheta d\vartheta \int_{r_2^H}^\infty 2\pi r^2 dr \Phi_{21} \nabla T \cdot \vec{U}_{1(2)} \tag{5}$$

Here ϑ is the angle between $\vec{r}$ and the outer temperature gradient ∇T, and

$$\vec{U}_{1(2)}(\vec{r}) = \left(3r_2^H/4r\right)\left[\vec{u}_0 + \vec{n}_0\left(\vec{u}_0 \cdot \vec{n}_0\right)\right] + \left(r_2^H/64r\right)^3\left[\vec{u}_0 - 3\vec{n}_0\left(\vec{u}_0 \cdot \vec{n}_0\right)\right] \tag{6}$$

where $\vec{u}_0$ and $\vec{n}_0$ are the unit vectors along $\vec{U}_{1(2)}$ and the radius vector $\vec{r}$, respectively.

These reasonings can be applied to the solvent molecule in the temperature gradient, and the volume force should be established in the solvent with v_1^{-1} molecules in the unit volume

$$\vec{F}_1 = \frac{\alpha_T}{v_1^2} \int_0^\pi Sin\vartheta d\vartheta \int_{r_1^H}^\infty 2\pi r^2 dr \Phi_{11} \nabla T \cdot \vec{U}_{1(1)} \tag{7}$$

where Φ_{11} is the solvent-solvent molecular interaction potential. In hydrodynamically stable t liquid, this volume force is cancelled by the respective macroscopic pressure gradient $\nabla\Pi_0 = -\vec{F}_1$. In this pressure gradient, the barodiffusion force $-v_2\nabla\Pi_0$ acts on the dissolved particle making the respective contribution to its thermophoretic velocity. Together, these factors give the thermodiffusion coefficient of the dissolved molecule or monomer

$$D_T = \frac{8\alpha_T v_{1H}}{9\pi\eta r_{1H} v_1} \sqrt{A_1 A_2} F_1(\beta) \tag{8}$$

where

$$v_{1H} = \frac{4\pi}{3}\left(r_{1H}\right)^3, \quad \beta = 2r_1^H/\left(r_1^H + r_2^H\right), \quad F_1(\beta) = \frac{2-5\beta}{2\beta^2} - \frac{3}{5}\frac{v_2}{v_1}\sqrt{\frac{A_1}{A_2}}\frac{\beta}{2-\beta}$$

2 Thermal motion of molecules and cooperative intermolecular interaction potential

The molecular interaction potential given by Eq. (3) is for the isolated couple of freely rotating and/or induced dipoles. In order to consider the effect of adjacent molecules, we calculate the effect on the force that acts on solvent molecule "1" when it is placed in a force field of a dissolved (solute) molecule "0". The complete force acting on molecule "1" is [6]

$$-\frac{\partial \Phi^{*}_{n_1"}}{\partial \vec{r}_{n_1"}} = -\frac{\partial \Phi_{n_1"}}{\partial \vec{r}_{n_1"}} - \sum_{"i"=2}^{N_{\text{int}}} \frac{\partial \Phi_{n_1""i"}}{\partial \vec{r}_{n_1"}} \tag{9}$$

where $\Phi^{*}_{n_1"}$ is the effective potential of the pair interaction between molecules "0" and "1" after taking into account collective effects, $\Phi_{n_1"}$ is the dipole-dipole interaction potential for the isolated pair of these molecules, operator $\frac{\partial}{\partial \vec{r}_{n_1"}}$ represents the gradient operator, N_{int} is the number of molecules taking part in the interaction, and $\Phi_{n_1""i"}$ is the potential of the interaction between molecules "1" and another solvent molecule "*i*". In this section molecule "0" is the dissolved molecule or monomer, all molecules designated as "1", "2"…"*i*" are solvent molecules, and the subscript "*i*" designates position.

Thermal motion of the solvent is considered by introducing a Boltzmann factor:

$$e^{-\frac{\Phi_{i"}\left(\vec{r}_{n_{i"}}\right)+\Phi_{1""i"}\left(\vec{r}_{n_{i"}}-\vec{r}_{n_1"}\right)}{kT}} \Bigg/ \int_{V_{\text{int}}} dv_{n_{i"}} e^{-\frac{\Phi_{i"}\left(\vec{r}_{n_{i"}}\right)+\Phi_{1""i"}\left(\vec{r}_{n_{i"}}-\vec{r}_{n_1"}\right)}{kT}}$$

where V_{int} is the volume of the entire system. Using this approach, Eq. (15) can be written as

$$-\frac{\partial \Phi^{*}_{n_1"}}{\partial \vec{r}_{n_1"}} = -\frac{\partial \Phi_{n_1"}}{\partial \vec{r}_{n_1"}} - N_{\text{int}} \int_{V_{\text{int}}} dv_{n_2"} \frac{\partial \Phi_{1""2"}\left(\vec{r}_{n_2"}-\vec{r}_{n_1"}\right)}{\partial \vec{r}_{n_1"}} \left[e^{-\frac{\Phi_{2"}\left(\vec{r}_{n_2"}\right)+\Phi_{1""2"}\left(\vec{r}_{n_2"}-\vec{r}_{n_1"}\right)}{kT}} \Bigg/ \int_{V_{\text{int}}} dv_{n_2"} e^{-\frac{\Phi_{2"}\left(\vec{r}_{n_2"}\right)+\Phi_{1""2"}\left(\vec{r}_{n_2"}-\vec{r}_{n_1"}\right)}{kT}} \right] \tag{10}$$

where $\Phi_{n_2"}$ and $\Phi_{1""2"}$ are dipole-dipole interaction potentials between particles "0" and "2", and "1" and "2", respectively. After some algebra, we obtain

$$\frac{\partial \Phi^{*}_{1}}{\partial \vec{r}_{1}} \approx \frac{\partial \Phi_{1}}{\partial \vec{r}_{1}} - \frac{2\pi r_{11}^{2} kT}{v_1} \int_0^{\vartheta_m} Sin\vartheta Cos\vartheta d\vartheta \left\{ 1 - \frac{\partial \left\{ \Phi_{2"}[\rho_{n_2"}\left(r_{11}, \rho_{n_1"}, Cos\vartheta'\right)] \right\}}{\partial \rho} \Bigg/ \frac{\partial \Phi_{1""2"}\left(r_{11}\right)}{\partial \rho} \right\} \tag{11}$$

Incorporating a maximum angle ϑ_m precludes the impossibility of inserting any additional solvent molecule between particles "0" and "1" when $\rho_{n_1"} < r_{11} + r_{12}$, where $r_{11} = 2r_1^H$ and $r_{12} = r_1^H + r_2^H$ are the closest approach radiuses. Considering the triangle with sides of length $\rho_{n_1"}$, $\rho = r_{11}$, and $\rho_{n_2"} = r_{12}$, we obtain

$$Cos\vartheta_m = \left(r_{12}^2 - r_{11}^2 - \rho_{n_1"}^2\right) \Big/ \left(2r_{11}\rho_{n_1"}\right) \tag{12}$$

$$\text{at } \rho_{"1"} < r_{11} + r_{12}\,; \quad Cos\vartheta_m = -1 \text{ at } \rho_{"1"} \geq r_{11} + r_{12}$$

Using Eqs. (11), (12), we obtain the equation for the pair interaction potential between a dissolved molecule or mer and a solvent molecule:

$$\frac{\partial \Phi_1^*}{\partial \vec{r}_1} = \frac{\partial \Phi_1}{\partial \vec{r}_1} - \frac{\pi r_{11}^2 kT}{v_1}\left(1 - Cos^2\vartheta_m\right) \tag{13}$$

$$\text{at } \rho_{"1"} < r_{11} + r_{12}\,; \quad \frac{\partial \Phi_1^*}{\partial \vec{r}_1} = \frac{\partial \Phi_1}{\partial \vec{r}_1} \text{ at } \rho_{"1"} \geq r_{11} + r_{12}$$

Solving Eq. (13), we obtain

$$\Phi_{21}^* = \Phi_{21} + 2\pi kT \frac{r_{11}^2 r_{12}}{v_1} \frac{1}{4\beta^2}\left[\frac{\xi^3}{6} - \frac{\left(1-\beta^2\right)^2}{2\xi} - \left(1+\beta^2\right)\xi + \frac{\left(1-\beta^2\right)^2}{2(1+\beta)} - \frac{(1+\beta)^3}{6} + \left(1+\beta^2\right)(1+\beta)\right] \tag{14}$$

$$\text{at } \xi < 1+\beta$$

$$\Phi_{12}^* = \Phi_{12} \quad \text{at} \quad \xi \geq 1+\beta$$

where $\xi = \frac{r}{r_{12}}$. The respective effective interaction potential Φ_{11}^* for solvent molecules is obtained from Eq. (14) using $\beta = 1$ and $r_{12} = r_{11}$.

3 Effective interaction potential and temperature dependence of thermophoresis

Using Eqs. (3), (14), (5), (6) and making the same derivations that led to Eq. (9), we obtain

$$D_T = \frac{16\alpha_T}{6\pi\eta r_{1H}} \frac{3v_{1H}}{v_1}\left[\frac{\sqrt{A_1 A_2}}{9} F_1(\beta) - kT \frac{3v_{1H}}{v_1} F_2(\beta)\right] \tag{15}$$

$$F_2(\beta) = \frac{1}{8\beta^5}\left[\frac{\beta^3}{4} - \frac{\beta^2}{2} + \frac{11\beta^4}{6} + \ln(1+\beta)\left(\frac{\beta}{2} - \beta^3 + \frac{\beta^5}{2}\right)\right] - 0.055\frac{v_2}{v_1}\frac{\beta}{2-\beta} \tag{16}$$

Eq. (15) contains two terms that can be conditionally referred to as the temperature-independent thermal diffusion coefficient (proportional to $\sqrt{A_1 A_2}$), and the temperature-dependent thermal diffusion coefficient (proportional to *kT*).

4 Thermophoresis of PNiPAM

For PNiPAM dissolved in alcohols, the direction of thermophoresis changes as the carbon numbers is increased [1]. Using Eq. (15), we can represent the temperature dependence by

$$D_T(T) = D_{0T}\left[1-(T/T_0)\right] \tag{17}$$

where D_{0T} is the thermodiffusion coefficient at T_0, and T_0 is the temperature of zero thermodiffusion. The parameters in Eq. (17) can be related to those in Eq. (15) as follows:

$$27kT_0\left[v_{1H}F_2(\beta)/v_1F_1(\beta)\right] = \sqrt{A_1A_2} \tag{18}$$

$$\frac{D_{0T}}{16\alpha_T D_{01}}\left(\frac{v_1}{3v_{1H}}\right)^2 = F_2(\beta) \tag{19}$$

where $D_{01} = kT_0/6\pi\eta r_{1H}$ is the solvent self-diffusion coefficient at the temperature of thermal diffusion sign change T_0. The literature physical parameters necessary to calculate β and $\sqrt{A_1A_2}$ in several alcohols are shown in Table I, where only the literature parameters and the experimental results from [1] are set forth.

The numeric theoretical values are representing in Table II. The available literature data allow for the calculation of the PNiPAM hydrodynamic radiuses r_{2H} in methanol, ethanol, and 1-propanol. As Table II shows, these values of the PNiPAM hydrodynamic radius for the alcohols are about the same, with the error ≈ 5%. This is an evidence of the validity of the theory.

Table I: Literature Physical Parameters of the PNiPAM/Alcohol Systems

Alcohol	D_{0T}, 10^{-7} cm^2/s.K, [1]	T_0, K, [1]	D_{01}, 10^{-5} cm^2/s, [7]	r_{1H}, 10^{-8} cm, [7]	α_T, 10^{-3} K^{-1}, [8]	η, 10^{-2} g/s.cm, [7]	v_1, 10^{-23} cm^3, [8]
MeOH	2.83	353	2.3	1.8	1.20	0.60	6.81
EtOH	1.23	308	1.2	2.0	1.12	1.2	9.80
1-PrOH	0.643	283	0.95	2.1	0.96	0.97	12.53
1-BuOH	0.387	284		0.28*	0.95	2.95	15.34

Table II: Calculated Theoretical Parameters of the PNiPAM/Alcohol Systems

Alcohol	β	$F_1(\beta)$	$F_2(\beta)$	$3v_{1H}/v_1$	D_{02}, 10^{-6}cm^2/s	r_{2H}, 10^{-8} cm	$\sqrt{A_1A_2}$, $\times10^{-14}$ erg
MeOH	0.189	26	0.56	1.07		**17.2**	**0.85**
EtOH	0.195	24	0.55	1.02		**18.5**	**0.88**
1-PrOH	0.197	23	0.53	0.92		**19.2**	**0.85**
1-BuOH	0.268**	13**	0.38**		0.95**	**1.83±0.10***	**0.65**

*Average value in methanol, ethanol and 1-propanol with the standard deviation;
**Calculated by Eq. (21) and the average value of r_{2H}

The hydrodynamic radii of methanol, ethanol and 1-propanol are similar (*0.18, 0.2*, and *0.21 nm*, respectively [7]). The hydrodynamic radius of a spheroid-like particle is [2].

$$1/r_H = \left[\left(1/r_{\square H}\right) + \left(2/r_{\perp H}\right)\right]/3 \tag{20}$$

where $r_{\square H}$ and $r_{\perp H}$ are the respective equivalent half axes of the spheroid. This expression is valid when the particle can rotate freely. When the motion in some direction is hindered, the appropriate "partial" hydrodynamic radius should be removed from Eq. (20). The transverse and longitudinal dimensions of the PNiPAM monomer, based on the bond lengths taken from Ref. [9], are approximately *0.7 nm* and *0.9 nm*, respectively. The estimated hydrodynamic radius, [Eq.(20)] is about *0.9 nm*, and the associated value of $r_{1H}/r_{2H} \approx 0.2$ which is greater than the value about 0.1 calculated from experimental data. The discrepancy can be further reduced by assuming that the motion of solvent is hindered in the transverse direction, due to the presence of adjacent monomers in the polymer chain. In that case, one obtains: $r_{1H}/r_{2H} \approx 0.15$. Thus, the value of the parameter β obtained by the present theory can be explained by the molecular shapes. As we have the reliable value for the monomer hydrodynamic radius, we could calculate the relevant physical parameters for 1-butanol. In this approach, we could use the known results on thermal diffusion to obtain the parameters for new solvents with the same dissolved PNiPAM molecule, using Eq. (19) in the form

$$\left(D_{0T}/16\alpha_T D_{02}\right)\left(v_1/3v_{2H}\right)^2 = \beta^5 F_2(\beta)/(2-\beta)^5 \tag{21}$$

where $D_{02} = kT_0/6\pi\eta r_{2H}$ and v_{2H} are the monomer diffusion coefficient and the hydrodynamic volume, respectively. Obtaining the value of the parameter β from Eq. (21), we can calculate the hydrodynamic radius for the 1-butanol.

This value is present in Table I. Using the obtained dynamic parameters, we calculated energetic parameters $\sqrt{A_1A_2}$ for PNiPAM in alcohols. The results are present in Table II and are in the range consistent with the physical nature of the considered system.

5 Conclusions

The hydrodynamic approach to thermophoresis has been refined to account for cooperative interaction and thermal motion. When the model is applied to dilute solutions of PNiPAM in alcohols, it gives qualitative agreement with the experimental data. Strong temperature dependence occurs when the solute-solvent interaction is low and the respective ratio of hydrodynamic radii is large. The measurement of parameters related to the temperature dependence of thermal diffusion may provide new possibilities for the characterization of solvent mixtures and polymer solutions.

References

[1] R. Kita, P. Poliakov, S. Wiegand, *Macromol.* 40, 1638 (2007).

[2] Landau, L. D., Lifshitz, E. M., *Fluid Mechanics* (Pergamon, London), 1959.

[3] Semenov, S. N., Schimpf, M. E., *Phys. Rev. E*, 69, 011201 (2004).

[4] Semenov, S. N., Schimpf, M. E., *Phys. Rev. E.,*71, 041202 (2005)

[5] Kojima, K., Kato, N., Nomura, H., *J. Solution Chem.,* 13, 151(1984).

[6] R. J. Hunter, *Foundations of Colloid Science*, Vol. II (Oxford Press, Oxford, UK, 1992), chapter 11.

[7] E. J. W. Welsink, A. C. Hoffmann, P. J. van Maaren, D. van der Spoel, *J. Chem. Phys,* 119, 7308 (2003).

[8] *Organic Solvents. Physical Properties and Methods of Purifications*, 4th ed. Riddik, J. A., Bunger, W. B., and Sakano, T. K., Eds. (Wiley, New York), 1986.

[9] http://www.bbc.co.uk/dna/h2g2/A791246.

The crossover of transport properties of polymer solutions from the high polymer limit to finite chain length

D. Stadelmaier, T. Pollak, J. Rauch, M. Hartung and W. Köhler

Physikalisches Institut, Universität Bayreuth, Germany

Contact: werner.koehler@uni-bayreuth.de

Abstract

We have studied the crossover from small-molecule to polymer behavior in the Soret effect of dilute solutions of polystyrene with molar masses ranging from the monomer to $M \approx 10^3\,\mathrm{kg/mol}$ in the seven solvents cyclooctane, cyclohexane, tetrahydrofuran, ethyl acetate, toluene, methyl ethyl ketone, and ethylbenzene. The thermal diffusion coefficient D_T is molar mass independent in the high polymer regime and the quantity ηD_T is approximately constant and independent of the solvent. For shorter chains below $M \approx 10\,\mathrm{kg/mol}$, D_T decreases monotonously with M and ηD_T does no longer follow a common master curve. For the two 'monomers' ethylbenzene and 3,3'-dimethyl-butylbenzene there is even a sign change in several solvents. We conclude that the thermal diffusion coefficient, albeit being molar mass independent in the high polymer limit, is not a property of the monomer but rather of correlated segments of the order of the Kuhn segment. Hydrodynamic interactions dominate the behavior of the Soret coefficient for sufficiently long chains, where swelling due to excluded volume interactions becomes important. For a given molar mass the Soret coefficient depends only on the effective hydrodynamic radius of the polymer coil and, hence, on the solvent quality.

1 Introduction

We discuss the interplay between isothermal and non-isothermal diffusion in dilute polymer solutions. These diffusion phenomena are of particular interest for the emergence of polymer properties, since isothermal diffusion is known to depend on the chain length, whereas thermal diffusion has traditionally been regarded as being more a monomer than a polymer property. Isothermal diffusion has extensively been studied and there exists a well established picture for the diffusion coefficient D. In the dilute limit hydrodynamic interactions play a dominant role and, according to the Zimm model, lead to a characteristic molar mass dependence $D \propto M^{-\nu}$. The scaling exponent ν is determined by the excluded volume interaction and ranges from $\nu = 0.5$ for ideal chains under theta conditions to $\nu \approx 0.6$ for expanded chains in good solvents.

Under non-isothermal conditions an additional thermal diffusion current $\vec{j}_T = -\rho c(1-c)D_T \nabla T$ is driven by a temperature rather than a concentration gradient. The thermal diffusion coefficient D_T has been found to be independent of the polymer molar mass [1, 2]. A theoretical explanation has been given by Brochard and de Gennes [3] based on the absence of long-range interactions between distant monomers. Würger has analyzed thermophoresis of colloids as originating from Marangoni forces [4]. Assuming slip boundary conditions, he obtained a flow field without hydrodynamic interactions between particles. Treating a polymer as a chain of spheres, he concluded that D_T should be molar mass and concentration independent. Zhang and Müller-Plathe investigated polymer thermal diffusion by means of reverse nonequilibrium molecular dynamics simulations (RNEMD) [5]. They found a molar mass independent D_T for polymer chains exceeding a few persistence lengths and interpreted their results as being in qualitative agreement with predictions by Schimpf and Semenov [6].

Here, we report on a systematic study of the molar mass and solvent dependence of the thermal diffusion and the Soret coefficient of polystyrene (PS) in the dilute limit. The work was partly motivated by own results for short polymer chains [7] and partly by the request for experimental data on the effect of solvents and end groups raised by Zhang and Müller-Plathe [5].

2 Experimental

All transport coefficients were measured by thermal diffusion forced Rayleigh scattering (TDFRS) [8]. Polystyrene of various degrees of polymerization and narrow molar mass distribution was obtained from Polymer Standards Service GmbH (Mainz). Ethylbenzene is a model compound for the repeat unit of PS. 3,3'-dimethyl-butylbenzene (PS162) is effectively a PS oligomer with degree of polymerization of unity, including the tert-butyl end-group (Fig. 1). The solvents were cyclooctane ($>$ 99%, Aldrich), cyclohexane (p.a., $>$ 99.5%, Acros), toluene ($>$ 99.9%, Merck), tetrahydrofuran (THF, $>$ 99%,

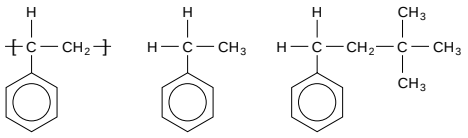

Fig. 1: *Repeat unit of the PS chain (left), ethylbenzene (middle), and 3,3'-dimethyl-butylbenzene (PS162) (right).*

Aldrich), ethyl acetate (> 99%, Merck) and methyl ethyl ketone (MEK, > 99.5%, Merck). The effective monomer ethylbenzene (> 99%, Fluka) also served as solvent from the dimer on. The dilute limit was obtained by extrapolation to $c = 0$. The temperature was $T = 295\,\mathrm{K}$ or, in some cases, 298 K.

3 Results

In Ref. [9] we have found that the high molar mass plateau of D_T is to a good approximation inversely proportional to the solvent viscosity. The proportionality constant only depends on the polymer and not on the solvent, which suggests to plot ηD_T as shown in Fig. 2.

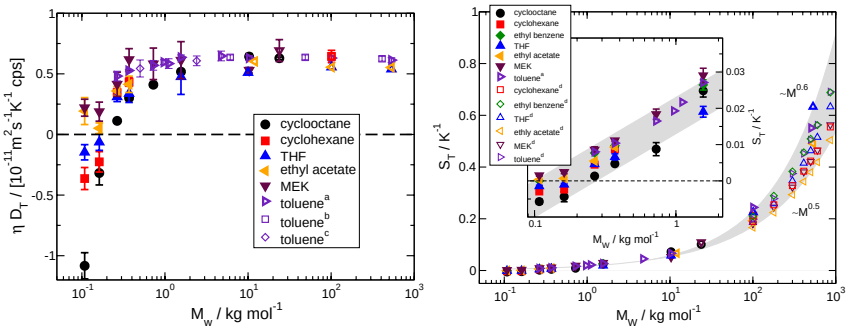

Fig. 2: ηD_T *(left) and Soret coefficient* S_T *(right) of PS in different solvents for* $T = 295\,\mathrm{K}$ *or* 298 K. *Included are data from [7] (a), [10] (b), [11] (c), [2] (d, computed from D and* D_T*).*

As expected, all curves collapse onto a common plateau for large M. For short chains this universality gets lost completely. As already known for small molecules, there is no simple theory to predict D_T (or ηD_T), except for some phenomenological rules like the more pronounced thermophobic behavior of heavier and more strongly interacting species [12–16]. More insight is obtained when looking at the Soret coefficient as plotted in Fig. 2. Again, two regimes can be identified. As shown in the insert, $S_T(\log M)$ increases with M for oligomers and short polymers up to a few kg/mol with a constant slope. Here, a change of the solvent always leads to approximately the same change of S_T as indicated by the gray band. Both the absolute values of S_T and the width of the band are of the order of $10^{-2}\,\mathrm{K}^{-1}$ which is typical for small molecules.
For molar masses above 10 kg/mol, where D_T has reached its constant plateau value, the solvent dependence of S_T becomes more pronounced. As indicated by the shaded area in the main part of the plot, all values now fall into a region whose boundaries are defined by power laws M^ν with the exponents $\nu = 0.5$ and $\nu = 0.6$.

4 Discussion

Let us now consider the same polymer in two different solvents s and s' in the dilute limit. The two solutions are characterized by (D, D_T, S_T) and (D', D'_T, S'_T), respectively. Let us

further assume that a change of the solvent from s' to s changes the Soret coefficient by δS_T:

$$S_T = S_T' + \delta S_T \tag{1}$$

The diffusion coefficient of the polymer can be expressed by the Stokes-Einstein relation $D = k_B T/(6\pi\eta R_h)$, where η is the solvent viscosity and R_h the effective hydrodynamic radius of the polymer. Hence, exchange of the solvent leads to a change of the diffusion coefficient

$$D = D' \frac{\eta' R_h'}{\eta R_h}. \tag{2}$$

R_h' is the hydrodynamic radius of the polymer in solvent s' of viscosity η'. Combining Eqs. 1 and 2, the thermal diffusion coefficients in s and s' are related by

$$D_T = S_T D = D_T' \frac{\eta' R_h'}{\eta R_h} + \delta S_T D. \tag{3}$$

Monomers, oligomers, and short chains $M \leq 10\,\mathrm{kg/mol}$ defines the regime where δS_T does not depend on M and is only a function of the solvent. Excluded volume interaction is not yet effective and the hydrodynamic radius of a polymer is solvent independent ($R_h = R_h'$). Eq. 3 reduces to

$$\eta D_T = \eta' D_T' + \delta S_T \frac{k_B T}{6\pi R_h}. \tag{4}$$

Eq. 4 reflects the scenario plotted in the left part of Fig. 2. For higher molar masses, but still below $M = 10\,\mathrm{kg/mol}$, the second term vanishes like $1/R_h$ and the left and right side become equal ($\eta D_T = \eta' D_T'$). For shorter chains with $M \ll 10\,\mathrm{kg/mol}$ the second term becomes increasingly important and eventually dominates D_T of oligomers and the two effective monomers.

High polymers The high polymer limit above 10 kg/mol is characterized by a molar mass independence of $D_T = D_T^\infty$ and by a molar mass and solvent independent value of $\eta D_T^\infty \equiv \Delta^\infty$. Together with Eq. 2, the ratio of the Soret coefficients in solvent s and s' becomes

$$\frac{S_T}{S_T'} = \frac{D_T}{D_T'} \frac{D'}{D} = \frac{\eta'}{\eta} \frac{\eta R_h}{\eta' R_h'} = \frac{R_h}{R_h'}. \tag{5}$$

This remarkable result tells us that the ratio of the Soret coefficients of a high polymer in two different solvents should only depend on the ratio of the hydrodynamic radii. The hydrodynamic radius of a flexible polymer follows a scaling law $R_h \propto M^\nu$. The exponent ν is determined by the quality of the solvent. $\nu = 0.5$ characterizes ideal chains in a theta solvent and $\nu \approx 0.6$ is typical for chains expanded by excluded volume interactions in a good solvent. Fig. 2 shows that above relation is fulfilled to good approximation. The shaded area indicates the range between the two limiting scaling laws corresponding to exponents of 0.5 and 0.6. Since chain expansion is only effective in the high polymer limit, the pre-factor has arbitrarily been chosen such that both curves start with a common value at $M = 10\,\mathrm{kg/mol}$. All Soret coefficients for high molar masses fall into this region. As expected, good solvents like toluene and THF can be found closer to the upper limit, corresponding to more chain expansion. Marginal and theta solvents like ethyl acetate

and cyclohexane tend towards the lower boundary defined by $\nu = 0.5$.

Crossover from the monomer to the polymer In a previous work we investigated the molar mass dependence of D_T [7] and interpreted the bending down for low M as being due to an end-group effect. The shortest oligomer investigated in Ref. [7] was the dimer, consisting of two C_8H_8 repeat units and a butyl end-group. Now, we have extended our investigations not only to a large number of different solvents but have also included ethylbenzene and PS162 on the 'polymer' side. Following the analysis in Ref. [7], a significantly smaller thermal diffusion coefficient would have to be expected for PS162 than for ethylbenzene, which is obviously not the case. In addition, Zhang and Müller-Plathe found a saturation of D_T for chains exceeding a few persistence lengths in their recent RNEMD simulations [5]. Based on this finding and on our new results with a continuous increase of D_T with increasing M for short chains, including the two monomers, we come to the conclusion that an end-group model with a linear superposition does not yield an adequate description.
Starting with ethylbenzene, the systematic increase of both D_T and S_T must be attributed to the increasing mass and/or size of the molecules. As long as the PS chains are shorter than the Kuhn segment, they may be regarded as rigid units. This increase of D_T is in accordance with the observation that heavier species are more thermophobic [12, 15, 16]. The Kuhn segment of PS comprises eight to ten monomers ($M \approx 1\,\mathrm{kg/mol}$) [17]. Indeed, a small number of such Kuhn segments defines the range between 1 and $10\,\mathrm{kg/mol}$ where the high polymer plateau value of D_T is reached. Hence, the molar mass independence of D_T observed in the high polymer limit does not imply that the thermal diffusion coefficient is a monomer property. From our data it rather follows that there are units of the size of the Kuhn segment that are the relevant entities for thermal diffusion. Within these segments monomers are correlated and act cooperatively. Over larger distances this correlation gets lost. Remarkably, the high polymer value of ηD_T is even independent of the solvent. However, the solvent quality determines the swelling of long polymer chains and the effective hydrodynamic radius. Since hydrodynamic interactions with a long-ranged flow field ($\propto r^{-1}$) are only effective for Fickian but not for thermal diffusion, where the flow field around a monomer decays like r^{-3} [4], a dependence on the solvent quality is introduced in $S_T = D_T/D$ according to Eq. 5 for longer chains.

5 Conclusion

Thermal diffusion of a flexible polymer is characterized by the presence of short-range cooperativity and correlation between the monomers. Long-range hydrodynamic interactions that dominate Fickian diffusion are absent in thermal diffusion. As a consequence, despite the molar mass independence of D_T, the units relevant for thermal diffusion of a PS chain are correlated segments with a size comparable to the Kuhn segment.

Acknowledgement This work was supported by the Deutsche Forschungsgemeinschaft (DFG, SFB481/A8).

References

[1] G. Meyerhoff and K. Nachtigall, J. Polym. Sci. **57**, 227 (1962).

[2] M. E. Schimpf and J. C. Giddings, J. Polym. Sci.: Part B: Polym. Phys. **27**, 1317 (1989).
[3] F. Brochard and P.-G. de Gennes, C. R. Acad. Sc. Paris, Ser. 2 **293**, 1025 (1981).
[4] A. Würger, Phys. Rev. Lett. **98**, 138301 (2007).
[5] M. Zhang and F. Müller-Plathe, J. Chem. Phys. **125**, 124903 (2006).
[6] M. E. Schimpf and S. N. Semenov, J. Phys. Chem. B **104**, 9935 (2000).
[7] J. Rauch and W. Köhler, Macromolecules **38**, 3571 (2005).
[8] G. Wittko and W. Köhler, Philos. Mag. **83**, 1973 (2003).
[9] M. Hartung, J. Rauch, and W. Köhler, J. Chem. Phys. **125**, 214904 (2006).
[10] W. Köhler, C. Rosenauer, and P. Rossmanith, Int. J. Thermophys. **16**, 11 (1995).
[11] R. Schäfer, Ph.D. thesis, Mainz, 1997.
[12] D. Reith and F. Müller-Plathe, J. Chem. Phys. **112**, 2436 (2000).
[13] P.-A. Artola and B. Rousseau, Phys. Rev. Lett. **98**, 125901 (2007).
[14] G. Galliero, B. Duguay, J.-P. Caltagirone, and F. Montel, Philos. Mag. **83**, 2097 (2003).
[15] G. Wittko and W. Köhler, J. Chem. Phys. **123**, 014506 (2005).
[16] C. Debuschewitz and W. Köhler, Phys. Rev. Lett. **87**, 055901 (2001).
[17] Y. Ding and A. P. Sokolov, J. Polym. Sci.: Part B: Polym. Phys. **42**, 3505 (2004).

Complex fluids and ternary systems

The thermodiffusion coefficients in the ternary mixture THN-IBB-nC12 with mass fraction $c_i = 1/3$ and molar fraction $x_i = 1/3$ at 25ºC

P. Blanco[1], M. M. Bou-Ali[1], J. K. Platten[1], D. Alonso de Mezquia[1], P. Urteaga[1], J.A. Madariaga[2] and C. Santamaría[2]

[1]MGEP Mondragon Goi Eskola Politeknikoa, Manufacturing Department. Loramendi 4, Apdo. 23, 20500 Mondragon, Spain.
[2]UPV University of Basque Country, Department of Applied Physics II, Apdo. 644, 48080 Bilbao, Spain

E-mai: pblanco@eps.mondragon.edu

Abstract

In the present study the thermogravitational technique has been used to determine the thermodiffusion coefficients of the three components in the ternary liquid mixture of 1,2,3,4-tetrahydronaphthalene-isobutylbencene-*n*-dodecane (THN-IBB-*n*C12) with equal mass and molar ratio (c = 1:1:1 and x = 1:1:1) at 25ºC. We have used two different thermogravitational columns (TC) with both configurations, parallepipedic and cylindrical. The results of both TCs agree within the experimental error. The comparison with recently published values shows that the differences are around 25%.

1 Introduction

A lot of work have been made in the study of binary liquid mixtures, showing even that different techniques, convective and non-convective, agree within the experimental error [1,2]. But on the contrary, to our knowledge, in ternary mixtures there is no any comparative study between different techniques because of the difficulty of the experimental setup and experimental analysis. The latest experimental works of ternary liquid mixtures [3,4] have been made by means of the thermogravitational technique showing experimentally its potentiality to determine the transport properties of multicomponent mixtures, although the analysis methodology presented in those experimental works may not be adequate for some mixtures such as *n*-alkane ternary mixtures [5].
Although in the last years the interest in the study of transport properties in ternary mixtures has increased, especially in the oil industry [6,7], there are only few experimental works in multicomponent liquid mixtures published in the literature [3,4]. Additionally, the demand of experimental results has grown in order to verify numerical codes [8,9].

Because of all these reasons, we present in this work the thermodiffusion coefficients of the three components in two different ternary mixtures made of THN-IBB-*n*C12 having successively mass fraction (c_i) and molar fraction (x_i) equal to 1/3, i.e, mass and molar ratio of 1:1:1. The mean temperature has been fixed at 25ºC. For the first time, in order to compare the results of ternary mixtures, two types of thermogravitational columns (TC) have been used, with both parallelepipedic and cylindrical configuration. The results between both columns have been contrasted and, in addition, the results of the ternary mixture with mass fraction c_i=1/3 have been compared with those previously published in [3] and presented for the first time at IMT6.

2 Experimental

2.1 Working equations

In the thermogravitational technique the determination of the component's concentrations after the thermodiffusion process is needed. This is made by means of a previous calibration. It consists on measuring the density and the refractive index of mixtures of known mass concentration previously prepared by weighing in a scale with a precision of 0.0001g. The mixture with molar fraction $x_i = 1/3$ corresponds to mass fractions of $c_{THN} = 0.3027$, $c_{IBB} = 0.3073$ and $c_{nC12} = 0.3900$. In this study we have carried out a calibration for both mixtures of THN-IBB-*n*C12 (mass and molar fraction $c_i = x_i = 1/3$). We have prepared 66 mixtures of known concentration around the corresponding average initial mass fractions of THN (from $c_{THN} = 0.265$ to $c_{THN} = 0.365$) and IBB (from $c_{IBB} = 0.265$ to $c_{IBB} = 0.365$) with increments of $c = 0.01$.

Next, we resume the working equations which are documented in previous studies of ternary mixtures [3,4]. As we are working with small variations of concentration we can assume that the density and refractive index as linear with the mass concentration of the components. We can state the density and the refractive index as:

$$\rho = a + b \cdot c_i + d \cdot c_j \tag{1}$$

$$n = a' + b' \cdot c_i + d' \cdot c_j \tag{2}$$

being a, b and d the constant parameters of the density as a function of the mass concentrations of the components i and j in the ternary mixture (i+j+k). a', b' and d' are the constant parameters of the refractive index as a function of the mass concentrations of the components i and j in the ternary mixture (i+j+k). Eqs. (1) and (2) must be independent to be able to determine the mass concentrations of each component from the measurements of the density and refractive index of the ternary mixtures [5]. The calibration planes of the mixtures of this study are shown in Fig.1. We chose THN and *n*C12 as components *i* and *j* respectively because they are the densest and the less dense components of the ternary mixtures.

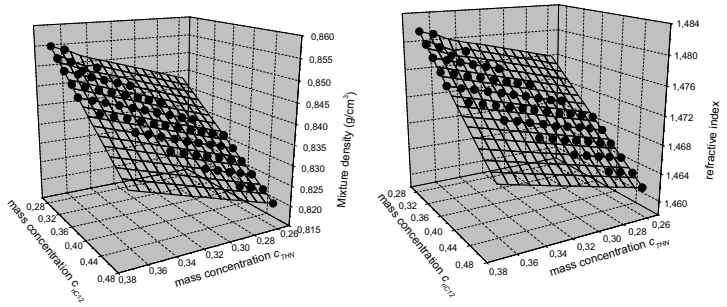

Fig. 1: *Calibration planes of density and refractive index for the mixture THN-IBB-nC12.*

The constant parameters of calibration planes are determined in such a way that the difference between the density and refractive index measured experimentally and the calculated ones from Eqs. 1 and 2 is minimised, considering all the mixtures of the calibration.

The thermodiffusion coefficient of component *i* in a multicomponent mixture is determined from the following relation:

$$D_T^i \approx -\frac{L_x^4}{504 L_z} \frac{\alpha g}{\nu} \Delta c_i \tag{3}$$

where $\Delta c_i = c_i^{top} - c_i^{bottom}$, being Δc_i the mass fraction difference of the component i between the top and the bottom of the TC, $\alpha = -\frac{1}{\rho}\frac{\partial \rho}{\partial T}$ the thermal expansion coefficient of the mixture, ν the kinematic viscosity of the mixture, L_z the height of the TC, L_x the gap of the TC and g the gravity acceleration.

2.2 Materials and Equipment

The three components used in this study were purchased from Merck with a purity of over 99%. An Anton Paar DMA 5000 vibrating quartz U-tube densimeter having a repeatability of $1 \cdot 10^{-6}$ g/cm^3 and an Anton Paar RXA 156 refractometer with a repeatability of $2 \cdot 10^{-5}$ nD have been used to determine the density and refractive index of the studied mixtures. A scale of 310 g capacity with an accuracy of 0.0001 g has been used to prepare the mixtures of the parallelepipedic TC. A scale of 4500 g capacity with an accuracy of 0.01 g has been used to prepare the mixtures of the cylindrical TC. The cylindrical TC has been previously validated with experiments well documented in the bibliography [11], and also some experimental results of this cylindrical TC have been contrasted with different installations [12,13]. In this study, both TCs have 500 mm. height, a gap of 1 mm and 5 taking points equidistantly separated along the TC. A falling ball viscosimeter HAAKE with a ±1% precision has been used to determine the dynamic viscosity of the mixtures.

3 Results and Discussion

3.1 Calibration of the parallelepipedic TC

The parallelepipedic TC has been designed and developed in MGEP. It has been also validated with experiments in binary mixtures well documented in the bibliography as it is shown in table I.

Mixture	D_T (10^{-12} m^2/sK) Parallelepipedic TC	D_T (10^{-12} m^2/sK) Cylindrical TC	D_T (10^{-12} m^2/sK) Published
H_2O/Etanol c=0.6088 at 25ºC	1.34	1.33	1.32 [ref.14] ; 1.34 [ref.15] 1.33 [ref.16] ; 1.36 [ref.17]
Tolueno/*n*C6 c=0.5167 at 25ºC	13.7	13.7	13.1 [ref.18] ; 13.7 [ref.19] 13.8 [ref.11] ; 14.1 [ref.17]
THN/IBB c=0.5 at 25ºC	2.93	2.90	2.8 ± 0.1 [ref.1] ; 2.81 [ref.15]
THN/*n*C12 c=0.5 at 25ºC	6.20	6.13	5.9 ± 0.3 [ref.1] ; 5.88 [ref.15]
IBB/*n*C12 c=0.5 at 25ºC	3.86	3.84	3.7 ± 0.2 [ref.1] ; 3.85 [ref.15]

Table I: *Comparison between experimental data of parallelepipedic and cylindrical TCs and published values.*

The differences in the experimental results between both TCs are in the order of 1%. The differences with published data are within the experimental error of 5%. Another example of its good operation is that the thermal diffusion coefficient D_T, according with the theory, is independent of the applied temperature gradient between the two vertical walls of the TC. To do this, we chose the mixture n-hexane/toluene with a toluene mass fraction of c=0.5167 at 25ºC and we repeated the test several times at different temperature gradients. A comparison between both TCs is shown in Fig.2a.

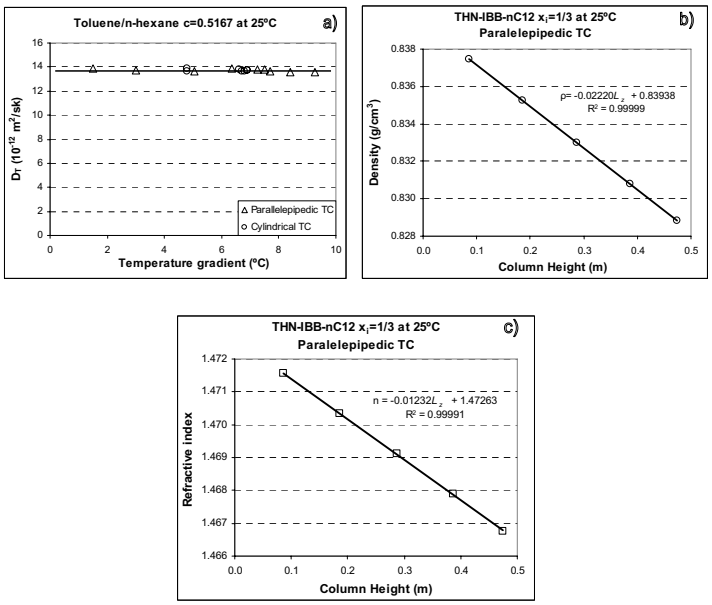

Fig. 2: *a) Thermodiffusion coefficient D_T in function of the temperature gradient applied between the two vertical walls. Mixture toluene/n-hexane with toluene mass fraction c=0.5167 at 25ºC. Comparison between both TCs: cylindrical and parallelepipedic. b) density ρ of the ternary mixture THN-IBB-nC12 with molar fraction $x_i = 1/3$ at 25ºC in function of the height of the parallelepipedic TC. c) refractive index n of the ternary mixture THN-IBB-nC12 with molar fraction $x_i = 1/3$ at 25ºC in function of the height of the parallelepipedic TC.*

3.2 Thermal Diffusion of ternary mixtures

As happens in binary mixtures the density gradient with elevation in the TCs is also linear for ternary mixtures (see as an example Fig.2b). The refractive index has also a linear behaviour (see as an example Fig.2c).

Table II shows the thermal diffusion coefficients D_T^i obtained with both TCs and the thermophysical properties of the ternary mixture with mass fraction $c_i = 1/3$ compared to published values [3,4]. The differences in D_T^i between the results of both TCs (parallelepipiedic and cylindrical) are of 2-4%, although the differences with previously published values are of 20-25%.

Mixture	α (10^{-4} K^{-1})		μ (10^{-3} Pas)		D_T^{THN} (10^{-12} m^2/sK)			D_T^{nC12} (10^{-12} m^2/sK)		
	This work	Refs. [3,4]	This work	Refs. [3,4]	Paral. TC	Cyl. TC	Refs. [3,4]	Paral. TC	Cyl. TC	Refs. [3,4]
$c_i = 1/3$	9.142	9.344	1.289	1.370	1.087	1.110	0.874	-1.251	-1.202	-1.02
$x_i = 1/3$	9.188	-	1.274	-	1.094	1.083	-	-1.244	-1.214	-

Table II: *Comparison between experimental data of parallelepipedic and cylindrical TCs and published values [3,4] for the ternary mixture THN-IBB-nC12 with mass fraction* $c_i = 1/3$ *and molar fraction* $x_i = 1/3$ *at 25ºC. We present the thermophysical parameters like thermal expansion* α *and dynamic viscosity* μ.

In table II we also specify the thermal diffusion coefficients D_T^i of the ternary mixture with molar fraction $x_i = 1/3$ found with both TCs. The differences between both TCs are less than 3%. Regarding the results of both ternary mixtures (mass and molar fraction $c_i = x_i = 1/3$) the thermal diffusion coefficients D_T^i of each component hardly do not change due to the small differences in mass concentrations between both ternarys. This is also reflected in the viscosity and thermal expansion coefficients. For the third component of the mixture (IBB) we can not determine with accuracy its thermal diffusion coefficient because of its small separation throughout the TCs as can be observed in Fig. 3. THN moves towards the cold wall of the TC, *n*C12 moves towards the warm wall and IBB has a small tendency to go to the cold wall, but it is so small that we can not measure accurately its mass separation (less than 1%) between the two ends of the TC, at least with this analysis method. The error accumulation in the determination of mass concentration of IBB ($c_{IBB} = 1 - c_{THN} - c_{nC12}$) and the small separation of this component in the ternary mixture prevent the determination of its thermal diffusion coefficient with reliability.

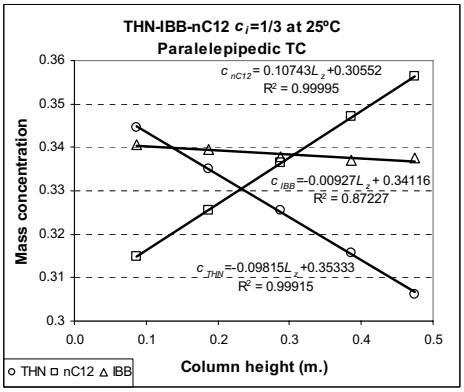

Fig. 3: *Mass separation throughtout the parallelepipedic TC of the three components of the ternary mixture THN-IBB-nC12 with mass fraction* $c_i = 1/3$.

4 Conclusions

This is the first study in ternary mixtures where the experimental results of two installations with different configurations of TCs are compared. The agreement between both TCs, parallelepipedic and cylindrical configurations, is excellent. The thermodiffusion coefficients D_T^i of the components in the ternary mixtures with mass and molar fractions $c_i = x_i = 1/3$ are quite similar due to the small difference in mass concentration of the components between both mixtures.

It can not be determined accurately the thermodiffusion coefficient of the IBB because of its small mass separation between the two ends of the TC. Therefore, the D_T^i of the mixture THN-IBB-*n*C12 that we consider significant by means of this analysis method are the corresponding ones to the components THN and *n*C12 (D_T^{THN} and D_T^{nC12}).

Acknowledgment

This paper presents results partly obtained in the framework of the following projects, GOVSORET (PI2008-14) and the grant (BFI05.449) of the Basque Government, and TESBLUR (CTQ2005/09389/C02/01/PPQ) of the Spanish Government.

References

[1] Platten J., Bou-Ali M., Costesèque P., Dutrieux J., Köhler W., Leppla C., Wiegand S. and G.Wittko G., Philosophical Magazine, **83**, 1965 (2003).

[2] Blanco P., Polyakov P., Bou-Ali M.M., Wiegand S., 8th Internacional Meeting on Thermodiffusion IMT8. Poster SFL-01 (2008).

[3] Bou-Ali M.M. and Platten J.K., J Non-Equilibrium Thermod. **30**, 385 (2005).

[4] Leahy-Dios A., Bou-Ali M.M., Platten J.K. and Firoozabadi A., J. Chem. Physics **122** 234502-1 (2005).

[5] Blanco P., Bou-Ali M., Platten J.K., Alonso de Mezquia D., Urteaga P., 8th Internacional Meeting on Thermodiffusion IMT8. Poster CPX-02 (2008).

[6] Georis P., Montel F., Van Vaerenbergh S., Decroly Y. and Legros J., Proceedings of the European Petroleum Conference, **1**, 57 (1998).

[7] Van Vaerenbergh S., Shapiro A., Galliero G., Montel F., Legros J., Caltagirone J., Daridon J. and Saghir Z., European Space Agency, (Special Publication) ESA SP **1290**, 202 (2005).

[8] Firoozabadi A., Ghorayeb K. and Shukla K., AIChE **46**, 892 (2000).

[9] Khawaja M., Jiang C.G., Van Vaerenbergh S. and Saghir M., Journal of non-equilibrium Thermodynamics, **30**, 359 (2005).

[10] Larre J.P., Platten J.K., G. Chavepeyer, J. Heat Mass Transfer **40**, 545 (1997)

[11] Urteaga P., Bou-Ali M.M., Madariaga J., Santamaría C., Blanco P., and Platten J., in Thermodiffusion: Basics and Applications, edited by M.M. Bou-Ali and J.K. Platten, (Mondragon Unibertsitateko Zerbitzu Editoriala, Spain, 2006), p.449.

[12] Blanco P., Bou-Ali M.M., Platten J.K., Madariaga J., Urteaga P., and Santamaría C., J. Non-Equilib. Thermodyn. **32**, 309 (2007).

[13] Platten J. K., Bou-Ali M. M., Blanco P., Madariaga J. A., Santamaría C., J. Phys. Chem. B, **111**, 11524-11530 (2007).

[14] Bou-Ali, M.; Ecenarro, O.; Madariaga, J.; Santamar¡a, C. & Valencia, J., Entropie **218**, 5 (1999).

[15] Leahy-Dios, A. and Firoozabadi, A, In M.M. Bou-Ali, J.K. Platten (Ed in Thermodiffusion: Basics and Applications, edited by M.M. Bou-Ali and J.K. Platten, (Mondragon Unibertsitateko Zerbitzu Editoriala, Spain, 2006), p.419.

[16] Kolodner, P.; Williams, H. & Moe, C., J. Chem. Phys. **88**, 6512 (1988).

[17] Köhler, W. & Muller, B., J. Chem. Phys. **103**, 4367 (1995).

[18] Bou-Ali, M.; Ecenarro, O.; Madariaga, J.; Santamar¡a, C. & Valencia, J., Journal of Physics: Condensed Matter, **10**, 3321-3331 (1998).

[19] Zhang, K.; Briggs, M.; Gammon, R. & Sengers, J., J. Chem. Phys. **104**, 6881 (1996).

Remarks on the analysis method for determining the mass fractions in ternary mixtures of alkanes

P. Blanco, M. M. Bou-Ali, J. K. Platten, D. Alonso de Mezquia and P. Urteaga

MGEP Mondragon Goi Eskola Politeknikoa, Manufacturing Department. Loramendi 4, Apdo. 23, 20500 Mondragon, Spain

E-mail: pblanco@eps.mondragon.edu

Abstract

Until now, in the few experimental works on ternary mixtures the analysis method of each component's concentration consists of measuring the density and refractive index of the mixture. Knowing these two properties of the mixtures one can determine the mass concentration of each component after the thermodiffusion process in a thermogravitational column and therefore establish the thermal diffusion coefficient of each component in the ternary mixture [1,2]. The experimental study carried out in this work shows that the analysis method used in previous works on ternary mixtures is inappropriate when working with ternary liquid mixtures of n-alkanes because of the linear dependence between the density and the refractive index of the mixtures.

1 Introduction

Up to now only a few experimental works exist where the thermodiffusion coefficients D_T^i in multicomponent mixtures of more than two components have been determined [1,2]. Bou-Ali and Platten [1] have presented a determination of the thermodiffusion coefficients D_T^i of the components of the ternary mixture *n*C12-THN-IBB together with a possible empirical correlation suggested a few years before [3] using the corresponding binary thermodiffusion coefficients obtained in the benchmark of Fontainebleau [4]. In a second work [2], Alana *et al*. have also presented the thermodiffusion coefficients of the components for the ternary mixture *n*C8-*n*C10-MN, as well as the molecular diffusion coefficients D_{ij}. To carry out these experiments the thermogravitational technique (for D_T^i) and the open ended tube technique (for D_{ij}) have been used, showing experimentally their potentiality to determine the transport properties of multicomponent mixtures.

The methodology used in both works to analyse compositions (i.e., to determine the two independent mass fractions c_1 and c_2) of removed samples necessary to access the transport properties (D_T^i and D_{ij}) is the same: measurements of the density ρ_{mix} and the refractive index n_{mix} of the mixture, and comparison with prior calibration curves $\rho_{mix}(c_1, c_2)$ and $n_{mix}(c_1, c_2)$. For more details about the methodology, see [1,2].

The n-alkane ternary mixtures selected in this work are n-hexane/n-dodecane/n-octadecane (*n*C6-*n*C12-*n*C18), n-octane/n-dodecane/n-hexadecane (*n*C8-*n*C12-*n*C16) and n-heptane/n-nonane/n-hexadecane (*n*C7-*n*C9-*n*C16) with mass fraction c_i=1/3 or a mass ratio of 1:1:1 and at 25ºC. In all these mixtures, the density and the refractive index are linearly dependent and therefore the calibration curves $\rho_{mix}(c_1, c_2)$ and $n_{mix}(c_1, c_2)$ have the same behaviour with the mixture's changes of concentration. Due to this fact, and in contradistinction with the n-alkane–aromatic systems, it is not possible to experimentally determine the mass fractions c_1 and c_2 in mixtures of n-alkanes only using the measured values of $\rho_{mix}(c_1, c_2)$ and $n_{mix}(c_1, c_2)$.

2 Experimental

2.1 Materials and Equipment

The liquids used in this work are normal alkanes and were purchased from Merck with a purity of over 99%. An Anton Paar DMA 5000 vibrating quartz U-tube densimeter having a repeatability of $1 \cdot 10^{-6}$ g/cm^3 and an Anton Paar RXA 156 refractometer with a repeatability of $2 \cdot 10^{-5}$ nD have been used to determine the density and refractive index of the studied mixtures. The mixtures have been prepared using a 310 g capacity scale with an accuracy of 0.0001 g.

2.2 Analysis method of mass concentration

In the thermogravitational technique, to determine the thermal diffusion coefficients it is indispensable to reveal the mass concentration of each component in the mixture. In binary mixtures $c_j = 1 - c_i$ and therefore, to determine the mass concentrations, a previous calibration is done from the measurements of a mixture property like density $\rho(c_i)$ [5] or refractive index $n(c_i)$ [6]. However, in ternary mixtures the knowledge of two mass fractions is needed ($c_k = 1 - c_i - c_j$), and consequently for the previous calibration two mixture properties are required, typically the density $\rho(c_i, c_j)$ and the refractive index $n(c_i, c_j)$. As we are working with small variations of concentration we can suppose the density and refractive index as linear with the mass concentration of the components. We can express the density and the refractive index as:

$$\rho = a + b \cdot c_i + d \cdot c_j \tag{1}$$

$$n = a' + b' \cdot c_i + d' \cdot c_j \tag{2}$$

being a, b and d the constant parameters of the plane formed with the density as a function of the mass concentrations of the components i and j in the ternary mixture (i+j+k) (see for an example the figure 1a). a', b' and d' are the constant parameters of the plane formed with the refractive index as a function of the mass concentrations of the components i and j in the ternary mixture (i+j+k) (see for an example the figure 1b). These two equations must be independent to be able to determine the three mass concentrations from the density and refractive index measurements.

We established two calibration planes (eqs. 1 and 2) for each one of the three ternary mixtures studied in this work. It consists of preparing up to 25 samples of known mass concentration around the mass fraction of interest c=1/3. In every preparation, first we introduce the less volatile component (the n-alkane with greater molecular weight), then the second component and finally the most volatile one. We would like to point out that one of the components used in this work, the n-octadecane, is solid at room temperature, therefore we heated it in a water bath until it became liquid.

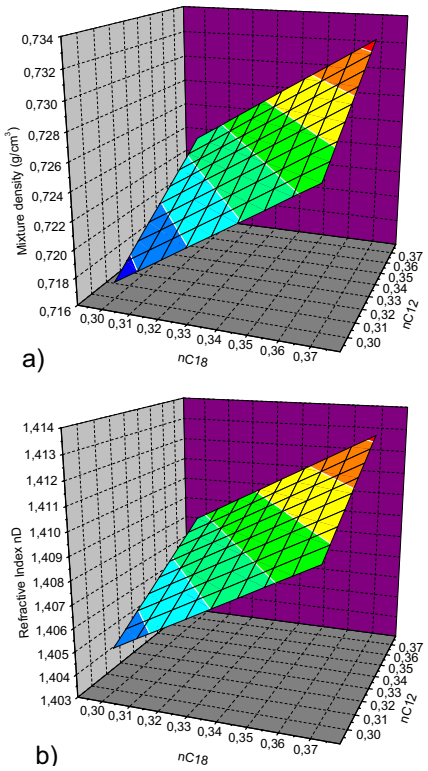

Fig. 1: *Calibration planes of density and refractive index for the mixture nC6-nC12-nC18 around the mass concentration of c_i=1/3.*

3 Results and Discussion

In this work we chose different ternary mixtures because we wanted to study the influence of the chain length of the components in the thermodiffusion coefficients of normal alkane ternary mixtures. The first ternary mixture studied in this work has been *n*C6-*n*C12-*n*C18. There is six carbon atoms difference between the smaller, medium and greater components. The second mixture has been *n*C8-*n*C12-*n*C16. In this case, the difference is of four carbon atoms. In both cases, the plot (fig. 2a and fig. 2b) of refractive index as a function of the mixture's density shows a linear dependency which indicates that both properties behave the same according to the changes of the mixture's concentration. We thought that the effect of having the same carbon atom difference between the compounds could be the reason for this conduct. Therefore, we prepared another ternary mixture in which the carbon atoms difference between the compounds does not follow any proportion. We have chosen the ternary mixture *n*C7-*n*C9-*n*C16. In this last case, the

behaviour of the mixture's density with the refractive index is the same as in previous two mixtures (see fig. 2c).

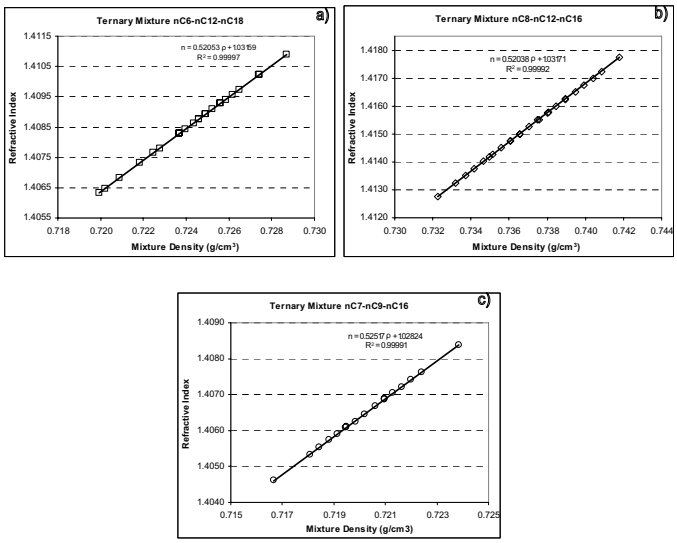

Fig. 2: *Mixture density in function of the refractive index of the mixtures nC6-nC12-nC18, nC8-nC12-nC16 and nC7-nC9-nC16 at 25ºC.*

Therefore, taking into account equations 1 and 2 we can not determine the three independent mass concentrations only measuring the density and the refractive index of a n-alkane ternary mixture. Looking at these results, and due to the variety of ternary mixtures tested in this work, we can expect that this relationship between density and refractive index would be the same in any ternary mixture of n-alkanes. We would need another accurately measurable physical property to be able to determine the mass concentration of the components of a mixture. At the same time this property can not behave in the same way as the density or refractive index does dependent on mass concentration changes. Let us think that it would be even more difficult to use the deflection of different laser beams with different wavelengths as is proposed in [7].

4 Conclusions

In all the n-alkane ternary mixtures studied in this work the density and the refractive index are linearly dependent and therefore one can not determine the mass fractions of each component in the mixture with the analysis method used in the few experimental works up to now [1,2]. Consequently, we find it difficult to determine both the thermodiffusion coefficients and the cross and main diffusion coefficients of n-alkane

ternary mixtures if we can not reveal the mass concentrations of the components in a ternary mixture after the thermodiffusion and diffusion processes. More work should be done to understand this unexpected behaviour between apparently independent physical properties such as density and refractive index.

Acknowledgment

This paper presents results partly obtained in the framework of the following projects, GOVSORET (PI2008-14) and the grant (BFI05.449) of the Basque Government, and TESBLUR (CTQ2005/09389/C02/01/PPQ) of the Spanish Government.

References

[1] Bou-Ali M.M. and Platten J.K., J Non-Equilibrium Thermod. **30**, 385 (2005).

[2] Leahy-Dios A., Bou-Ali M.M., Platten J.K. and Firoozabadi A., J. Chem. Physics **122,** 234502-1 (2005).

[3] Larre J.P., Platten J.K., G. Chavepeyer, J. Heat Mass Transfer **40**, 545 (1997)

[4] Platten J., Bou-Ali M., Costesèque P., Dutrieux J., Köhler W., Leppla C., Wiegand S. and G.Wittko G., Philosophical Magazine, **83**, 1965 (2003).

[5] Bou-Ali M. M., Ecenarro O., Madariaga J. A., Santamaria C. M., and Valencia J. J., J. Phys.:Condens. Matter **10**, 3321 (1998).

[6] Dutrieux J. F., Platten J. K., Chavepeyer G., and Bou-Ali M. M., J. Phys. Chem. B **106**, 6104 (2002).

[7] Kjetil B. Haugen, Firoozabadi A., J. Phys. Chem. B **110,** 17678 (2006).

Soret effect of nonionic surfactants in water studied by different transient grating setups

S.Datta[1], H.Ning[2], T.Sottmann[1], S.Wiegand[2]

[1] Institut für Physikalische Chemie,
Universität zu Köln, Luxemburger Str. 116, D-50939 Köln, Germany
[2] IFF, Forschungszentrum Jülich, Germany

Contact: sascha.datta@uni-koeln.de

Abstract

We studied the thermal diffusion behavior of the nonionic surfactant solution $C_{12}E_6$/water at different concentrations and temperatures using Thermal Diffusion Forced Rayleigh Scattering (TDFRS). Two different types of TDFRS setups have been applied. In the classical TDFRS, we use an Argon laser to write the optical grating into the sample by using a small amount of ionic dye to convert the optical grating into a temperature grating. In the other setup, called IR-TDFRS, we use an infrared laser as the writing beam, which utilizes the water absorption band to convert the optical grating into a temperature grating. The measurements by IR-TDFRS show a one-mode signal for all concentrations and temperatures, while the signal in the classical TDFRS consists of two modes for higher temperatures and lower surfactant concentrations [H. Ning *et al*., J. Phys. Chem. B., 110, 10746(2006)]. We find good agreement between the Soret coefficients determined in the IR-TDFRS and the ones derived from the first fast mode in the previous studies. The Soret coefficient of the nonionic solutions is positive and enhanced at the critical point. In general, the Soret coefficient of the micelles tends to increase with temperature. We found that the presence of the second mode observed in the classical TDFRS is related to the addition of the ionic dye, but even with the ionic dye it is not possible to observe a second mode in the IR-TDFRS. The origin of the second mode is discussed in terms of charged micelles and an inhomogenous dye distribution in the temperature gradient.

1 Introduction

Surfactant molecules, which show amphiphilic properties due to their hydrophilic and hydrophobic part, form micelles in water, when the concentration of the monomer is beyond a critical micelle concentration (*cmc*). The size, shape and structure of the micelles depend on concentration and temperature. Surfactant solutions are of great interest due to their ample phase behavior, rich physical properties, and their extensive applications in industry, agriculture, biology and daily life [1–3]. The study of the thermal diffusion process in complex fluids is an interesting topic with numerous applications, which is still not understood on a microscopic level. Several experimental techniques have been used to study the thermal diffusion behavior of surfactant systems. Using a beam deflection and thermal lens setup, Piazza *et al.* investigated an ionic surfactant, sodium dodecyl sulphate (SDS), in water [4,5]. The Soret coefficient of SDS shows an exponential dependence on the temperature and $1/S_{\mathrm{T}}$ scales linearly with the concentration. For a mixture of SDS and a nonionic surfactant β-dodecyl-maltoside (DM) a sign change of the Soret coefficient was observed with increasing temperature [5]. Ning *et al.* studied a series of nonionic surfactants in water in a wide temperature and concentration range using thermal diffusion forced Rayleigh scattering (TDFRS) [6, 7]. For their measurements a small amount of the ionic dye basantol yellow is added in order to create a sufficient temperature gradient. At higher temperatures and lower concentrations the concentration part of the signal consists of two modes. Although it turned out that the two-mode signal can be suppressed by the addition of a simple salt, such as sodium chloride (NaCl), the origin of the second mode is still an open question.
The objective of this work is to get a better understanding of the origin of the second concentration mode. Therefore we study the thermal diffusion behavior of $C_{12}E_6$ in water using an IR-TDFRS setup, which avoids the addition of the dye.

2 IR-TDFRS experiment

A detailed description of the IR-TDFRS setup and the sample preparation can be found in [8] and [9]. Two intersecting laser beams at λ = 980 nm create an optical grating into the sample. Due to the weak absorption maximum of the water molecules at λ = 975 nm the optical intensity grating is converted into a temperature grating, which results in a refractive index grating. This grating is probed by the diffraction of a He-Ne laser beam, operating at λ = 633 nm. In contrast to the classical TDFRS setup the experiment is simplyfied because the dye, which influences the phase behavior of nonionic surfactants in water, is not needed.

3 Results

Fig.1 shows the phase diagram of the aqeous surfactant system. All our measurements are performed in the isotropic L_1 phase. The System $C_{12}E_6$/water shows a two phase region (denoted as L_1'+L_1") at high temperatures. Here, L_1' represents the more dilute surfactant phase and L_1" the more concentrated one. Using the $C_{12}E_6$ ordered from SIGMA-ALDRICH we found a critical concentration of $w_{\mathrm{c}} = 0.021 \pm 0.001$ at a critical temperature of $T_{\mathrm{c}} = 51.53 \pm 0.02$ °C, which slightly differs from literature [11]. It is

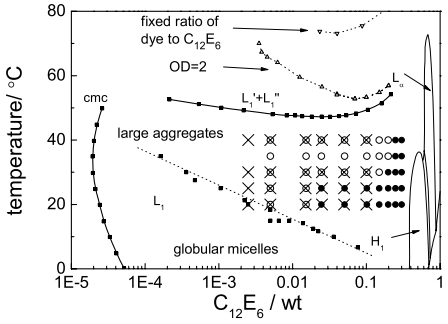

Fig. 1: *The phase diagram of $C_{12}E_6$ in water (taken from [10]) and influence of the ionic dye basantol yellow. Measurements by IR-TDFRS ($\times$) and by classical TDFRS, which shows one-mode signal (●) and two-mode signal (◯), respectively. The different phases in the phase diagram are indicated as follows: diluted surfactant phase (L_1'), concentrated surfactant phase (L_1"), hexagonal (H_1), lamellar (L_α) and isotropic sponge phase (L_3). Also shown is the critical micellar concentration (cmc). Lines in the figures are guides to the eye.*

known that $C_{12}E_6$ forms small spherical micelles in the L_1 phase at low surfactant concentrations and low temperatures, while with increasing concentration and temperature large cylindrical micelles are found [12]. In Fig.1 we can also see that the addition of the dye shifts the two phase boundary towards higher temperatures. If the dye content is kept constant (OD = 2, $\triangle$), the shift of the two-phase boundary to higher temperatures is more pronounced in the low surfactant region. On the other hand if we fix the ratio of the weight fraction of the dye in the mixture of dye and surfactant to δ = 0.0444 ($\bigtriangledown$) (implying that the dye acts as a co-surfactant), the two phase boundary shifts parallel by $\triangle T$ = 25 °C. The temperature shift of the two phase boundary in the presence of basantol yellow is probably caused by the electrostatic repulsion between the micelles, which get charged by the incorporation of the ionic dye molecules in the micelles.

With the classical TDFRS we performed systematic measurements of $C_{12}E_6$ in water using a small amount of dye necessary to reach an optical density between 1.5-2 cm^{-1} at λ = 488 nm. As indicated in the phase diagramm a second mode occurred for the measurements at lower surfactant concentrations and higher temperatures. We found, that an increase of the dye content leads to a second mode, which becomes stronger if the dye content is further increased [9]. Furthermore, we found in our previous work that the addition of salt suppresses the second mode [7] and at the same time leads to a decrease of the two phase boundary to its original position in the pure $C_{12}E_6$/water system. In the IR-TDFRS experiment we obtain only one mode signals, even if we add the ionic dye. This shows, that it is not only the presence of the ionic dye which causes the second mode.

The Soret coefficients of $C_{12}E_6$ measured by the IR-TDFRS setup are displayed in Fig.2. All Soret coefficients are positive, which means that the micelles migrate to the cold

side. For the system $C_{12}E_6$ at 40 °C, the Soret coefficient S_T reaches a maximum close to the critical concentration w_c = 0.021, which is a consequence of the critical slowing down [13]. For the lower temperatures at 25 °C and 20 °C, we observe an ambiguous minimum around surfactant concentrations 0.005 and 0.025, respectively, while at higher surfactant concentrations S_T increases monotonically, which might be related with the increasing viscosity. The variations at lower concentrations is probably a consequence of structural changes in the surfactant solution, as can be seen in Fig.1 the transition boundary between globular and large cylindrical micelles falls in the same region [12]. Also many other experimental and theoretical studies show that the Soret coefficient of colloids and microemulsions depends on the particle size [14–16].

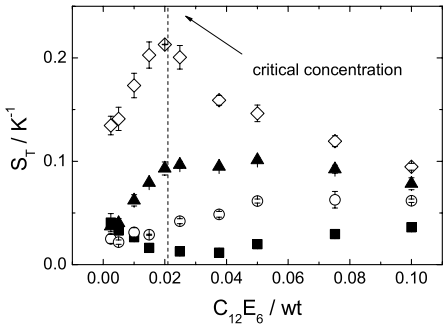

Fig. 2: *The dependence of the Soret coefficient of $C_{12}E_6$ in water on the surfactant content at different temperatures T = 20 °C (■), 25 °C (◯), 30 °C (▲) and 40 °C (◊) measured by IR-TDFRS.*

4 Discussion

We assume, that the inhomogeneous distribution of the dye molecules in the interference grating plays an important role for the formation of the second mode. In the experiment with the dye exists certainly a dynamic equilibrium between *dye-infected* micelles and ordinary micelles + dye molecules in solution. The IR-TDFRS measurements show that the ordinary micelles move to the cold site. An open question is whether the *dye-infected* micelles migrate also to the cold side or to the warm side. The two possible scenarios are sketched in Fig.3.

In model A we assume both typs of micelles move to the cold side, while in model B *dye-infected* micelles move to the warm side. This assumption might be justified, because we previously observed [9] that the addition of the SDS and basantol yellow decreases the Soret coefficient, which means that charged micelles are more thermophilic. In model A due to absorption of the blue light by basantol yellow a temperature grating is formed and then both kinds of micelles move to the cold side (Fig.3A). Due to the enrichment

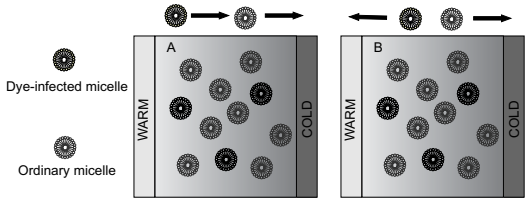

Fig. 3: *Ordinary and* dye-infected *micelles move in a temperature gradient. (A) Both micelles move to the cold side. (B) Ordinary micelles move to the cold side, while* dye-infected *micelles move to the warm side.*

of the dye in the cold region, the temperature gradient is weakened, which results in a weakening of the concentration gradient, and a backward motion of part of the micelles starts. This can cause a second mode.

In modell B (Fig.3B) the *dye-infected* micelles move to the warm side. After equilibration of the temperature grating the ordinary micelles move to the cold side, while at the same time the *dye-infected* micelles migrate to the warm side. This movement is reflected in the first mode. Due to the enrichment of the dye in the warm regions of the grating, the temperature gradient is strengthened and again a feedback mechanism starts, and more *dye-infected* micelles will move to the warm side, which would lead to the negative second mode.

5 Conclusions

In this work, we present the thermal diffusion behavior of $C_{12}E_6$ measured by the recently developed IR-TDFRS setup [8]. The temperature gradient is achieved due to a weak absoprtion band of water in the near-infrared and not as in the classical TDFRS experiment through the absorpion of blue light by the dye basantol yellow [7]. While in the classical TDFRS experiment the addition of the dye can lead to a second mode, this second mode is not observed in the IR-TDFRS experiment, even if the dye is added. The nonionic surfactant $C_{12}E_6$ shows positive Soret coefficients in water, which indicates that the micelles move to the cold side. The occurrence of a second mode in the classical TDFRS and the absence of this mode in the IR-TDFRS can be explained by some sort of feedback mechanism, which leads to a modulation of the grating in the case of the blue writing laser.

Acknowledgment

The authors thank Reinhard Strey for his constant interest in this work and his support. We also appreciate the technical support of Hartmut Kriegs. This work was partially supported by the Deutsche Forschungsgemeinschaft grants So 913 and Wi 1684.

References

[1] L. Quintero. *J. Disper. Sci. Technol.*, 23:393, 2002.

[2] M. Knoche *Weed Res.*, 34:221, 1994

[3] S. Ezrahia, E. Tuvala, and A. Aserinb. *Adv. Colloid Interfac.*, 128-130:77, 2006.

[4] R. Piazza, and A. Guarino. *Phys. Rev. Lett.*, 88:208302, 2002.

[5] S. Iacopini, R. Rusconi, and R. Piazza. *Eur. Phys. J. E*, 19:59, 2006.

[6] H. Ning, R. Kita, and S. Wiegand. *Progr. Colloid Polym. Sci.*, 133:111, 2006

[7] H. Ning, R. Kita, H. Kriegs, J. Luettmer-Strathmann, and S. Wiegand. *J. Phys. Chem. B.*, 110:10746, 2006

[8] S. Wiegand, H. Ning, and H. Kriegs. *J. Phys. Chem. B.*, 111:14169-14174, 2007.

[9] H. Ning, S. Datta, T. Sottmann, and S. Wiegand. *J. Phys Chem.*, Submitted, 2008.

[10] R. Strey, and A. Pakusch. in *Proceedings of the 5th International Symposium on Surfactant in Solution*, edited by K. Mittal and P. Bothorel. (Plenum, New York), 1986, pp. 465–472.

[11] K.-V. Schubert, R. Strey, and M. Kahlweit. *J. Colloid Interf. Sci.*, 141:21, 1991.

[12] R. Strey. *Ber. Bunsenges. Phys. Chem.*, 100:182, 1996.

[13] J. P.Wilcoxon, D. W. Schaefer, E. W. Kaler. *J. Chem. Phys.*, 90:1909, 1989.

[14] S. Duhr, and D. Brauna. *Phys. Rev. Lett.*, 96:168301, 2006.

[15] D. Vigolo, G. Brambilla, and R. Piazza. *Phys. Rev. E*, 75:040401, 2007.

[16] S. Duhr, and D. Braun. *P. Natl. Acad. Sci.*, 103:19678, 2006.

Soret-driven concentration fluctuations in a chemically reacting liquid mixture

José M. Ortiz de Zárate[1], Jan V. Sengers[2], Dick Bedeaux[3], and Signe Kjelstrup[3]

[1]Departamento de Física Aplicada I, Universidad Complutense, 28040 Madrid, Spain
[2]Institute for Physical Science and Technology, University of Maryland, College Park, Md 20742-8510, USA
[3]Department of Chemistry, Norwegian University of Science and Technology, Trondheim 7491, Norway

Contact: jmortizz@fis.ucm.es

Abstract

In a liquid mixture subjected to a stationary temperature gradient, concentration fluctuations exhibit a strong long-ranged nonequilibrium enhancement, arising because the temperature gradient induces a concentration gradient through the Soret effect. Theory and experiments have shown that the intensity of such nonequilibrium concentration fluctuations varies as q^{-4} with the wave number q of the fluctuations. In this paper we investigate how a chemical reaction affects concentration fluctuations in a liquid mixture. If the reaction-diffusion system is in thermal equilibrium, the decay rate of the concentration fluctuations is affected by the chemical reaction, but the intensity is not. If a temperature gradient is present, the induced concentration profile is characterized by a penetration depth d. For diffusion-controlled chemical reactions the penetration depth is large, whereas for reaction-controlled processes the penetration depth is small. The intensity of the nonequilibrium concentration fluctuations depends on whether the wavelength of the fluctuations is smaller or larger than the penetration depth d. When the wavelength is smaller than d, the intensity still varies as q^{-4} with the wave number q, just as in the absence of the chemical reaction. When the wavelength is larger than d, the intensity will vary as q^{-2}. Hence, observing the crossover of the intensity from a q^{-4} to a q^{-2} dependence by light scattering or shadowgraphy may in principle provide a method for determining the penetration depth d of a chemical reaction.

1 Introduction

In a non-isothermal fluid mixture concentration fluctuations are induced by the Soret effect [1]. In this paper we investigate how such nonequilibrium concentration fluctuations are affected by the presence of a chemical reaction. We first briefly review the hydrodynamic equations describing such a system. In Sec. 2, we discuss in detail the temperature and concentration profiles in the steady state. Then, in Sec. 3, we present our main results by analyzing concentration fluctuations around the steady-state solution described in Sec. 2.

A detailed treatment of non-equilibrium thermodynamics of chemically reacting fluid mixtures can be found in the monograph (Section XI.8) of de Groot and Mazur [2] and we basically follow the same approach [3]. We present here just the relevant hydrodynamic equations, while briefly discussing the approximations and phenomenological relationships upon which they are based. The balance laws applicable to our problem are balance of mass, balance of momentum and balance of energy [1–3]. In terms of barycentric fluid velocity $\mathbf{v}$, mass density ρ, concentration of first species $c_1 \equiv c$ and temperature T, one obtains the following set of hydrodynamic equations for a binary mixture [3]:

$$\begin{aligned}
\rho\left[\frac{\partial \mathbf{v}}{\partial t} + (\mathbf{v}\cdot\boldsymbol{\nabla})\mathbf{v}\right] &= -\boldsymbol{\nabla} p + \eta\nabla^2\mathbf{v}, \\
\rho\left[\frac{\partial c}{\partial t} + \mathbf{v}\cdot\boldsymbol{\nabla} c\right] &= -L_{QJ}\,\nabla^2\left(\frac{1}{T}\right) + L_{JJ}\,\nabla^2\left(\frac{\Delta g}{T}\right) - \frac{L_{\mathrm{r}}}{T}\Delta g, \\
\rho c_p\left[\frac{\partial T}{\partial t} + \mathbf{v}\cdot\boldsymbol{\nabla} T\right] + \rho\Delta h\left[\frac{\partial c}{\partial t} + \mathbf{v}\cdot\boldsymbol{\nabla} c\right] &= -L_{QQ}\,\nabla^2\left(\frac{1}{T}\right) + L_{JQ}\,\nabla^2\left(\frac{\Delta g}{T}\right),
\end{aligned} \tag{1}$$

which have to be combined with the equation of state $\Delta g = \Delta g(p, T, c)$ and the divergence-free flow condition ($\boldsymbol{\nabla}\cdot\mathbf{v} = 0$), which is the main assumption included in the derivation of (1). In the hydrodynamic equations (1), p is the pressure, η the viscosity, c_p the isobaric specific heat capacity, and

$$\Delta h = \mu_1 - T\left(\frac{\partial \mu_1}{\partial T}\right)_{p,c} - \mu_2 + T\left(\frac{\partial \mu_2}{\partial T}\right)_{p,c} = \Delta g - T\left(\frac{\partial \Delta g}{\partial T}\right)_{p,c} \tag{2}$$

is the difference in specific enthalpy between the two components of the mixture, with $\Delta g = \mu_1 - \mu_2$ being the difference in specific Gibbs energy (or minus the affinity). It is implicit that a chemical reaction exists between the two components of the mixture, so that a mass ξ of species 1 is created by unit volume and unit time [3]. In Eqs. (1), the dissipative fluxes are related to the physical gradients in the system by linear phenomenological laws:

$$\mathbf{Q} = -L_{QQ}\,\frac{\boldsymbol{\nabla} T}{T^2} - L_{QJ}\,\boldsymbol{\nabla}\left(\frac{\Delta g}{T}\right), \tag{3a}$$

$$\mathbf{J} = -L_{JQ}\,\frac{\boldsymbol{\nabla} T}{T^2} - L_{JJ}\,\boldsymbol{\nabla}\left(\frac{\Delta g}{T}\right), \tag{3b}$$

$$\xi = -L_{\mathrm{r}}\,\frac{\Delta g}{T}. \tag{3c}$$

Because of their different tensorial character there is no coupling between the chemical-reaction rate ξ and the heat $\mathbf{Q}$ and mass diffusion $\mathbf{J}$ fluxes [2]. The phenomenological laws (3a)-(3c) are written in terms of Onsager coefficients L_{QQ}, L_{JJ}, L_{QJ}, L_{JQ} and $L_{\rm r}$, with $L_{QJ} = L_{JQ}$. It is convenient to relate these Onsager coefficients to the transport coefficients: the thermal conductivity λ, the diffusion coefficient D, and the dimensionless thermal diffusion ratio k_T [3]:

$$D = \frac{L_{JJ}}{\rho T}\left(\frac{\partial \Delta g}{\partial c}\right)_{p,T}, \quad \lambda = \frac{1}{T^2}\left[L_{QQ} - \frac{L_{QJ}^2}{L_{JJ}}\right], \quad \rho D T k_T = L_{QJ} - L_{JJ}\Delta h, \quad (4)$$

Notice that we neglect barodiffusion, implying that $\Delta g = \Delta g(T, c)$ only.
It is worth mentioning that the linear phenomenological law (3c) for ξ is only valid for small deviations from chemical equilibrium [2]. In this respect we mention that recent developments [4] have shown that by introducing an internal *mesoscopic* variable to describe the advancement of a chemical reaction, a linear phenomenological law similar to (3c) can be formulated in terms of that *mesoscopic* variable, thereby extending the validity of linear non-equilibrium thermodynamics (and its associated theory of fluctuating hydrodynamics) beyond the classical limits. Extension of the fluctuation theory on the basis of mesoscopic nonequilibrium thermodynamics will be considered in a future publication.

2 Steady-state solution

Due to the presence of a chemical reaction, even a linear version of nonequilibrium thermodynamics gives nonlinear steady concentration profiles [2]. We assume a temperature profile $T_{\rm s}(x)$ in the x-direction, such that at $x = 0$ the temperature $T_{\rm s}(0) = T_1$ and at $x = L$ the temperature $T_{\rm s}(L) = T_2$. We consider the stationary solution with $\mathbf{v} = 0$ and uniform pressure, and with $\mathbf{J} = 0$ at the boundaries $x = 0$ and $x = L$. The stationary temperature profile $T_{\rm s}(x)$ and the stationary reaction Gibbs-energy profile $\Delta g_{\rm s}(x)$ are then obtained by equating the LHS of Eqs. (1) to zero:

$$0 = -L_{QJ}\frac{d^2}{dx^2}\left(\frac{1}{T_{\rm s}}\right) + L_{JJ}\frac{d^2}{dx^2}\left(\frac{\Delta g_{\rm s}}{T_{\rm s}}\right) - L_r\frac{\Delta g_{\rm s}}{T_{\rm s}}, \quad (5a)$$

$$0 = -L_{QQ}\frac{d^2}{dx^2}\left(\frac{1}{T_{\rm s}}\right) + L_{JQ}\frac{d^2}{dx^2}\left(\frac{\Delta g_{\rm s}}{T_{\rm s}}\right). \quad (5b)$$

Here we include the Soret effect in the evaluation of the steady state, unlike a recent publication on the subject [5]. For simplicity and following refs. [2, 5], we assume that all Onsager coefficients are constants, independent of position. In the chemical literature, the temperature dependence of the rate $L_{\rm r}$ is usually not neglected, and an Arrhenius dependence [6], or other more complicated nonlinear kinetic expressions are assumed for $L_{\rm r}(T)$. These approaches lead to a system of nonlinear coupled differential equations for the temperature and activity profiles, that can be solved only numerically. However, it turns out that the non-equilibrium fluctuations around the stationary solution of (5) depend only slightly on whether the linear or nonlinear approach is used. For simplicity, we consider here the linear version of (5), extensively reviewed elsewhere [2]. Then, the

steady temperature profile solution of (5) is:

$$\frac{T_1T_2}{T_{\rm s}(x)} = \bar{T} + \frac{\Delta T}{\tilde{Z}L}\left\{\cosh\left(\frac{L}{2d}\right)\left(x-\frac{L}{2}\right) + \left(\frac{L^2}{d\phi^2}-d\right)\sinh\left[\frac{1}{d}\left(x-\frac{L}{2}\right)\right]\right\}, \quad (6)$$

where $\bar{T} = (T_1+T_2)/2$ and $\Delta T = T_2 - T_1$. Furthermore,

$$\tilde{Z} = 2\left(\frac{L}{d\phi^2}-\frac{d}{L}\right)\sinh\left(\frac{L}{2d}\right) + \cosh\left(\frac{L}{2d}\right), \quad (7)$$

$$\frac{1}{d^2} = \frac{L_rL_{QQ}}{L_{JJ}L_{QQ}-L_{JQ}^2} = \frac{\phi^2}{L^2}\left\{1+\frac{\epsilon_{\rm D}}{Le}\left[1+\frac{k_T\Delta\tilde{h}}{\epsilon_{\rm D}}\right]^2\right\}, \quad \frac{\phi^2}{L^2} = \frac{L_{\rm r}}{\rho DT}\left(\frac{\partial\Delta g}{\partial c}\right)_T, \quad (8)$$

with the Lewis number $Le = \lambda/\rho c_p D$ and

$$\epsilon_{\rm D} = \frac{k_T^2}{c_pT}\left(\frac{\partial\Delta g}{\partial c}\right)_{p,T}, \qquad \Delta\tilde{h} = \frac{\Delta h}{c_pT}, \quad (9)$$

being the dimensionless Dufour effect ratio and the dimensionless specific enthalpy of reaction, respectively. Here we have slightly changed the definition of $\tilde{Z}$ as compared to our previous publication on the subject [3].

The temperature profile (6) is expressed in terms of the boundary conditions and two parameters: ϕ and d. The parameter d has units of length and is commonly referred to as the "penetration depth" of the chemical reaction [2, 6]. For simplicity we consider here the limit $Le \to \infty$. In this limit we have $\phi = L/d$ exactly and, hence, only one parameter (ϕ) is independent. As can be easily verified by substituting $\phi = L/d$ in Eq. (7) for $\tilde{Z}$ and then in Eq. (6), it turns out that in the large Le limit the temperature profile is always linear, regardless of the value of ϕ. In spite of this, the concentration profile induced by the temperature gradient depends on ϕ even for large Le. This is shown in Fig. 1, for concentration profiles obtained from Eq. (6), and the corresponding expression for $\Delta g_{\rm s}(x)$. Profiles displayed in Fig. 1 are for large Lewis number ($\phi = L/d$), and for $k_T\Delta\tilde{h}/\epsilon_{\rm D} = -0.1$. The data are divided by $L/2$ times the concentration gradient $\nabla c_0 = -k_T\Delta T/\bar{T}$ that would be present when $L_{\rm r} = 0$.

For a so-called "diffusion-controlled" process $d \gg L$, corresponding to small values of ϕ. Conversely, if $d \ll L$ we have a "reaction-controlled" process (also referred to as "activation-controlled" or activated processes), implying large values of ϕ. The limit $\phi \to 0$ corresponds to no chemical reaction present ($L_{\rm r} = 0$), the system is extremely diffusive and the concentration profile becomes fully linear. The limit $\phi \to \infty$ corresponds to a extremely reaction-controlled process and the concentration profile is mostly determined by the enthalpy of reaction, except in two small boundary layers.

3 Nonequilibrium fluctuations

We have evaluated the concentration fluctuations around the steady-state profiles described in the previous section [3] by applying a standard version of fluctuating hydrodynamics [1], including fluctuating parts in the dissipative fluxes. To simplify the set of

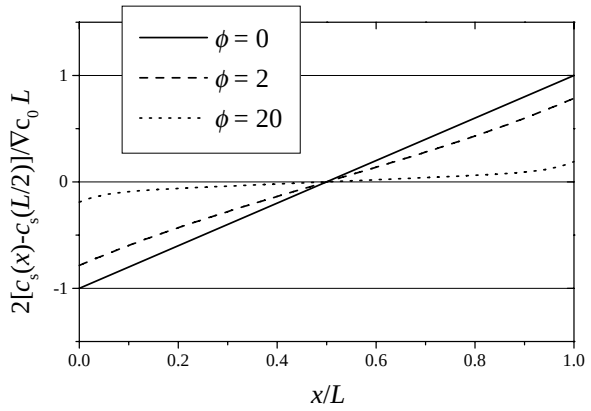

Fig. 1: *Concentration profile for $Le \to \infty$ and three values of ϕ. The limit $\phi = 0$ corresponds to no chemical reaction present. Large values of ϕ correspond to a reaction-controlled process.*

governing equations we employed a large Lewis-number approximation, as in previous work for nonreacting mixtures [7]. In this limit temperature fluctuations can be neglected and only the coupling between velocity and concentration fluctuations needs to be considered.

One further simplification is that we identify the stationary concentration gradient that, initially, is a position-dependent magnitude with its value at the center of the cell. This approximation is consistent with having neglected the position dependence of all thermophysical properties of the mixture. With this approximation, the non-equilibrium structure factor depends only on the value $\nabla c_\mathrm{s}|_{L/2}$ of the concentration gradient at $L/2$, and not on the detailed $c_\mathrm{s}(x)$. Hence, our final result will be only slightly sensitive to whether a linear or a nonlinear (numerical) approach is used to obtain the stationary solution of (6). Furthermore, we do not consider boundary conditions for the fluctuating fields in the present work. In general, boundary conditions are not needed to reproduce the proper asymptotic behavior of the non-equilibrium hydrodynamic fluctuations at small wave lengths (but still large enough to be in the hydrodynamic regime) [1, 7]. Due to confinement, deviations from our solution are expected for larger wavelengths.

After the chain of approximations summarized above, the intensity of nonequilibrium concentration fluctuations in terms of a dimensionless wave number $\tilde{q} = qL$ is given by [3]:

$$S_{cc}(\mathbf{q}) = S_{cc}^{(\mathrm{E})} \left\{ 1 + \tilde{S}_{cc}^{(\mathrm{NE},0)} \, \frac{\tilde{q}_\parallel^2}{\tilde{q}^4 \, [\tilde{q}^2 + \phi^2]} \right\}, \tag{10}$$

where $S_{cc}^{(\mathrm{E})}$ is the equilibrium intensity of concentration fluctuations [3], which is unaffected by the presence of a chemical reaction [8], and $\tilde{S}_{cc}^{(\mathrm{NE},0)}$ represents a normalized non-equilibrium enhancement of the concentration fluctuations:

$$\tilde{S}_{cc}^{(\mathrm{NE},0)} = \frac{\left(\nabla c_\mathrm{s}|_{L/2} \right)^2}{\nu D L^4} \left(\frac{\partial \Delta g}{\partial c} \right)_T . \tag{11}$$

Equation (10) exhibits the typical structure of non-equilibrium fluctuations, containing a non-equilibrium enhancement which explicitly depends on the wave number q, so that the equal-time non-equilibrium concentration fluctuations are spatially long ranged. The non-equilibrium enhancement exhibits a crossover from the well-known q^{-4} dependence observed in nonreacting liquid mixtures [1] to a q^{-2} dependence for smaller wave numbers. The q^{-2} behavior is the one typically found when studying long-range nonequilibrium fluctuations in isothermal reacting mixtures [1, 8, 9]. The crossover from a q^{-4} (nonisothermal nonreacting) to a q^{-2} (nonequilibrium but isothermally reacting) behavior occurs at wave numbers of the order $\tilde{q}_{\rm CO} \simeq \phi$, which (in the large Le limit) is the inverse of the penetration depth of the stationary solution, Fig. 1. Penetration depths in reacting liquid mixtures typically vary from 0.01 to 1 cm [2], so that for a layer with $L \simeq 1$ mm dimensionless ϕ values range between 0.1 and 10.

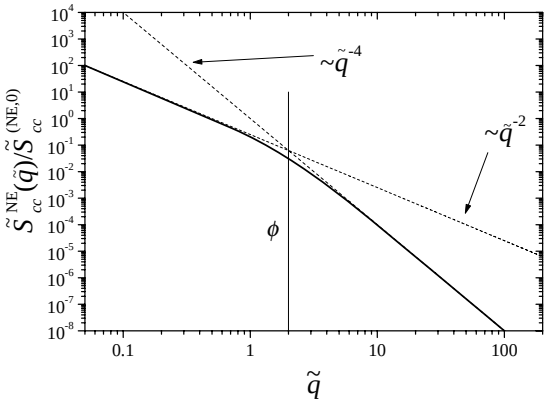

Fig. 2: *Dimensionless enhancement of non-equilibrium concentration fluctuations as a function of dimensionless wave number, $\tilde{q} = qL$, for $\phi = 2$. The crossover from the asymptotic q^{-4} dependence to a q^{-2} dependence at smaller wave numbers is evident.*

As an illustration of our results we present in Fig. 2 a plot of the dimensionless nonequilibrium enhancement of the concentration fluctuations as a function of the dimensionless wave number. The plot is for $\phi = 2$, which is an intermediate value. Figure 2 shows a clear crossover from the asymptotic q^{-4} dependence at larger wave numbers (unaffected by the chemical reaction) to a q^{-2} dependence for smaller wave numbers. When the process is diffusion controlled ϕ is small, the concentration profile is almost linear and nonequilibrium fluctuations show a $\tilde{q}^{-4}$ dependence in most of the range. Conversely, for reaction-controlled processes ϕ is large and the $\tilde{q}^{-2}$ dependence dominates plots like Fig. 2.

References

[1] J. M. Ortiz de Zárate and J. V. Sengers, *Hydrodynamic Fluctuations in Fluids and Fluid Mixtures* (Elsevier, Amsterdam, 2006).

[2] S. R. de Groot and P. Mazur, *Non-Equilibrium Thermodynamics* (North-Holland, Amsterdam, 1962), Dover edition, 1984.

[3] J. M. Ortiz de Zárate, J. V. Sengers, D. Bedeaux, and S. Kjelstrup, J. Chem. Phys. **127**, 034501 (2007).

[4] I. Pagonabarraga, A. Pérez-Madrid, and J. M. Rubí, Physica A **237**, 205 (1997).

[5] J. Xu, S. Kjelstrup, D. Bedeaux, and J. M. Simon, Phys. Chem. Chem. Phys. **9**, 969 (2007).

[6] Y. Demirel, Chem. Eng. Sci. **61**, 3379 (2006).

[7] J. M. Ortiz de Zárate, J. A. Fornés, and J. V. Sengers, Phys. Rev. E **74**, 046305 (2006).

[8] C. W. Gardiner, *Handbook of Stochastic Methods*, 2nd ed. (Springer, Berlin, 1985).

[9] G. Nicolis, A. Amellal, G. Dupont, and M. Mareschal, J. Mol. Liq. **41**, 5 (1989).

Convection and confinement

Localized steady states in binary fluid convection

Oriol Batiste[1], Isabel Mercader[1], Arantxa Alonso[1] and Edgar Knobloch[2]

[1] Departament de Física Aplicada, Universitat Politècnica de Catalunya, Barcelona, Spain
[2] Department of Physics, University of California, Berkeley, CA 94720, USA

Contact: oriol@fa.upc.es

Abstract

Numerical simulations of convection in binary mixtures in 2-dimensional containers have shown the existence of confined states that consist of regions of developed steady convection surrounded by quiescent fluid [1]. These localized states or *convectons*, in an infinite domain can contain an arbitrary number of convection rolls [10].
The confined states are organized into a pair of branches that snake towards the spatially periodic SOC state in the parameter space [6]. As this occurs the *convectons* add rolls in a pairwise fashion, thereby becoming broader and broader until the entire cell is filled. We also show that the snaking branches originate in an Eckhaus bifurcation from the uniform steady state and that the width of the snaking region depends on the separation ratio of the system. The existence of these states in 3-dimensional containers is also demonstrated.

1 Formulation of the problem

Binary mixtures are characterized by cross-diffusion quantified by the separation ratio S. When $S < 0$ the heavier component (of concentration C) migrates up the temperature gradient. Thus in a layer heated from below the destabilizing temperature gradient competes with a stabilizing concentration gradient that develops in response to the heating. The system is described by the dimensionless equations

$$\mathbf{u}_t + (\mathbf{u}\cdot\nabla)\mathbf{u} = -\nabla P + \sigma R[(1+S)\theta - S\eta]\hat{\mathbf{z}} + \sigma\nabla^2\mathbf{u}, \quad (1)$$

$$\theta_t + (\mathbf{u}\cdot\nabla)\theta = w + \nabla^2\theta, \quad (2)$$

$$\eta_t + (\mathbf{u}\cdot\nabla)\eta = \tau\nabla^2\eta + \nabla^2\theta, \quad (3)$$

together with the incompressibility condition

$$\nabla\cdot\mathbf{u} = 0. \quad (4)$$

Here $\mathbf{u} \equiv (u, w)$ is the velocity field in (x, z) coordinates, P is the pressure, and θ denotes the departure of the temperature from its conduction profile, in units of the imposed temperature difference $\Delta T = T_1 - T_0 > 0$ across the layer. The variable η is defined such that its gradient represents the dimensionless convective mass flux. Thus $\eta \equiv \theta - \Sigma$, where $C = 1 - z + \Sigma$ is the concentration of the heavier component in units of the concentration difference that develops across the layer as a result of cross-diffusion. The system is specified by four dimensionless parameters: the Rayleigh number R providing a dimensionless measure of the imposed temperature difference ΔT, the separation ratio S that measures the resulting concentration contribution to the buoyancy force due to cross-diffusion, and the Prandtl and Lewis numbers σ, τ, in addition to the aspect ratio Γ. We adopt no-slip, fixed temperature and no mass flux boundary conditions at the horizontal plates, and periodic boundary conditions in the horizontal direction, with period Γ.
Equations (1)-(4) are solved in two dimensions using a spectral code, with a Fourier expansion in the horizontal and a Chebyshev collocation method in the vertical. For the time evolution a second order time-splitting algorithm proposed in [2] is used. Below we describe our results for water-ethanol mixtures with parameter values used in different

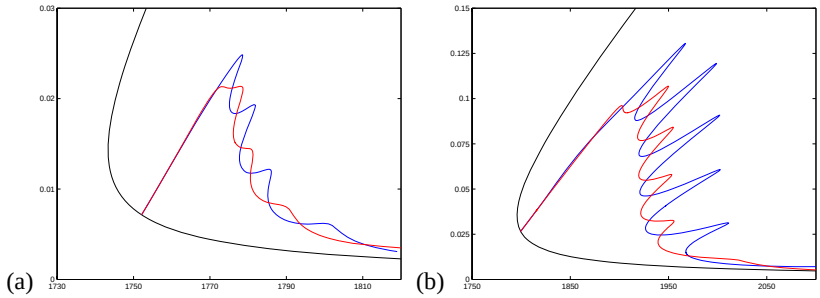

Fig. 1: *Branches of odd and even confined steady states for a mixture with* $\sigma = 6.22$, $\tau = 0.009$ *and (a)* $S = -0.021$, *(b)* $S = -0.127$, *both in a* $\Gamma = 14$ *domain.*

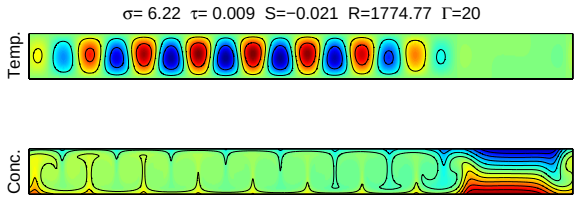

Fig. 2: *Temperature θ and concentration C in a large convecton almost filling the domain (top of the snaking region).*

experiments [3, 4]. In addition, to calculate steady solutions in an efficient manner we have adapted a pseudo-spectral first-order time-stepping formulation to carry out Newton's method [5], and implemented a continuation code to follow branches of stationary solutions.

2 Branches of snaking solutions

We have seen that the convectons are organized into a pair of branches that snake towards the spatially periodic SOC state [6]. As this occurs the convectons add rolls in a pairwise fashion, thereby becoming broader and broader. We have attributed this behavior to the presence of a pinning interval in the Rayleigh number characterized by fronts separating the conduction and convection states, which are locked to the latter [7]. Although we have not studied the stability of these states in detail we have confirmed the existence of multiple coexisting stable convectons within the pinning region in sufficiently long domains.

In figure 1(a) we show a pair of snaking branches for a mixture with $S = -0.021$ in a $\Gamma = 14$ domain. Both solutions bifurcate from the SOC branch at $R = 1752.10$ below the saddle-node. This bifurcation point corresponds to an Eckhaus instability of the SOC state with n rolls to perturbations that break its invariance under the translations $T_{\Gamma/n}$. We have independently calculated the location of this bifurcation using spatial Floquet analysis with $d = 1/n$ [8], and found a perfect agreement with the steady state branch calculation. Thus we can predict the existence of different snaking branches using linear

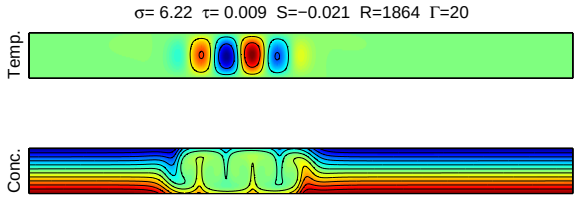

Fig. 3: *Temperature θ and concentration C in a small convecton at the bottom of the snaking region.*

stability analysis, and compute these branches by adding a small perturbation to the SOC state and following the branches into the snaking regime.
Figure 1(b) shows that the width of the snaking region depends on the separation ratio of the system: the existence region of confined solutions is substantially wider when $S = -0.127$ than for $S = -0.021$. This is a consequence of a larger interval of subcriticality of the SOC state when $S = -0.127$. Note that the amplitudes of the snaking in the odd and even branches differ, with the even branch snaking with a much larger amplitude. Nonetheless both branches are born simultaneously in an Eckhaus bifurcation that takes place at $R = 1799.5$.

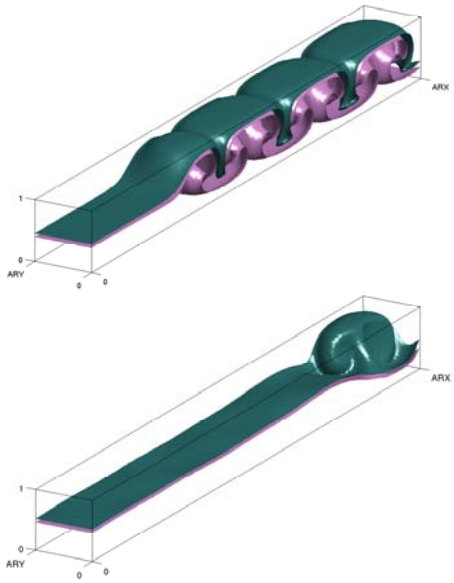

Fig. 4: *Three-dimensional convecton in a He^3-He^4 mixture. Confined steady steate (left) and snapshot of a confined oscillatory steate (right).*

3 3D states

All the solutions presented thus far assume that the dynamics are two-dimensional, i.e., that the rolls are invariant under translation along the roll axes, and that there are no instabilities breaking this invariance. In experiments in narrow annular domains transverse instabilities are suppressed, but the influence of the walls transverse to the rolls remains. In previous work [9] we have analyzed how the stability of the basic state is modified in the fully 3D case, and found significant differences from the 2D case. We show here, via direct numerical simulation for He^3-He^4 parameters, that convectons persist in a narrow 3D cell. For these parameters 2D convectons are known to be present in a broad interval of Rayleigh numbers [10]. We use a rectangular box of aspect ratio $\Gamma_x = 10$, $\Gamma_y = 1$,

with a $200 \times 30 \times 20$ grid. Preliminary results show that convectons are indeed present and stable in this system, and exhibit the same properties as their 2D counterparts, i.e., coexistence of stable convectons with an arbitrary number of rolls, suggesting a snaking structure. Surprisingly we have also found a completely 3-dimensional confined oscillatory state that consists in a single cell attached to an end-wall.

4 Conclusions

We have shown the existence of confined steady states in binary fluid convection, and explained some of their observed properties in the framework of the snaking fenomena they display. We have also demonstrated the existence of these states using 3-dimensional numerical simulations in a closed container with realistic boundary conditions. Unexpectedly we have also obtained a new kind of confined oscillatory state that have a completely 3-dimensional character.

Acknowledgment

This work is supported by DGICYT under grant FIS2006-08954 and by AGAUR under grant 2005SGR-0024.

References

[1] Batiste, O. & Knobloch, E. 2005 Simulations of localized states of stationary convection in ^{3}He-^{4}He mixtures. *Phys. Rev. Lett.* **95**, 244501.

[2] Hugues, S. & Randriamampianina, A. 1998 An improved projection scheme applied to pseudospectral method for the incompressible Navier-Stokes equations. *Int. J. Numer. Methods Fluids* **28**, 501–521.

[3] Kolodner, P., Glazier, J. A. & Williams, H. 1990 Dispersive chaos in one-dimensional traveling-wave convection. *Phys. Rev. Lett.* **65**, 1579–1582.

[4] Kolodner, P. 1992 Observations of the Eckhaus instability in one-dimensional traveling-wave convection. *Phys. Rev. A* **46**, 1739–1742.

[5] Mamum, C. K. & Tuckerman, L. S. 1995 Asymmetry and Hopf bifurcation in spherical Couette flow. *Phys. Fluids* **7**, 80–91.

[6] Batiste, O., Knobloch, E., Mercader, I. & Alonso, A. 2006 Spatially localized binary fluid convection. *J. Fluid Mech.* **560**, 149–158.

[7] Burke, J.& Knobloch, E. 2006 Localized states in the generalized Swift-Hohenberg equation. *Phys. Rev. E*, **73**, 056211.

[8] Prat, J., Mercader, I. & Knobloch, E. 1998 Resonant mode interactions in Rayleigh-Bénard convection. *Phys. Rev. E* **58**, 3145–3156.

[9] Alonso A., Batiste O. 2004 Onset of oscillatory binary fluid convection in three-dimensional cells, *Theor. Comp. Fluid Dyn.* **18**, 221–229.

[10] Batiste, O. & Knobloch, E. 2005 Simulations of localized states of stationary convection in ^{3}He-^{4}He mixtures. *Phys. Rev. Lett.* **95**, 244501.

Thermoosmotic transfer of ferrocolloids through a capillary porous layer in the presence of transversal magnetic field

Elmars Blums, Gunars Kronkalns and Michail Maiorov

Institute of Physics, University of Latvia, Latvia

E-mail: eblums@sal.lv

Abstract

The paper is devoted to studying the ferroparticle transfer in non-isothermal capillary porous layer in the presence of a steady uniform magnetic field. The examined two-component ferrofluid consists of magnetite nanoparticles coated with oleic acid and suspended in tetradecane. The measured thermoosmotic pressure difference is directed toward the temperature gradient. The unsteady pressure curve primarily grows and after reaching a maximum starts to decrease exponentially. Homogeneous magnetic field B, directed normally to the membrane, causes a growth of the pressure difference. The measurement results are interpreted in frame of linear theory of irreversible thermodynamics. Three fluxes j_i (the flow of solvent j_1, the particle flux j_2 and the heat flux j_3) contain three summands proportional to thermodynamic driving forces $\nabla\varphi_i$ (gradients of pressure p, particle chemical potential φ_c and temperature T). Approximate solution of simplified filtration equations allows evaluating from measured pressure curves the filtration coefficient, the coefficients of solutal osmosis and thermoosmosis as well as (employing the Onsager relations) the coefficient of particle convective transfer. External magnetic field induces an additional pressure difference across the porous layer and evokes an increase in the chemical potential of particles. Due to dependence of fluid magnetization on both the particle concentration and the temperature, the field effects manifest themselves as an increase in thermoosmotic pressure and some reduction of solutal osmosis. The separation curves calculated in frame of such model employing the evaluated transport coefficients agree well with experiments performed in the presence of a uniform magnetic field oriented normally to the membrane.

1 Introduction

Magnetic nanoparticles and ferrocolloids have interesting medical application possibilities. One the most popular novel idea is magnetic hyperthermia of tissues, particularly for cancer treatment. Unsteady magnetic field of relatively low amplitude and of median frequency may cause intensive energy dissipation in colloidal particles. The heating induces remarkable temperature gradients in surrounding medium and may cause a particle thermophoretic or thermoosmotic transfer. Since the heating intensity depends on particle concentration, it is important to investigate the dynamics of particle transfer in tissues. Besides, the nanoparticle transfer in porous media is an important problem also for technical applications. Preliminary experiments indicate significant changes in particle separation in non-isothermal porous layers [1] and strong intensification of particle thermal transfer through a grid in the presence of a magnetic field [2]. The present paper is devoted to studying the ferroparticle transfer in non-isothermal capillary porous layer in the presence of a steady uniform magnetic field.

2 Experimental

The mass transfer experiments are performed employing two equal cylindrical volumes (V_0 = 2.65 cm^3) kept at different temperatures (lower temperature below) by water-flow thermostats and divided by chemically stable wide-pore capillary layer of thickness δ = 0.78 mm formed by five separate filter sheets. The porosity of the filter ε = 0.8, the average pore diameter 1 μm. The cross-sectional area of the filter S = 1.8 cm^2. The volumes are connected to differential hydrostatic manometer. The manometer tubes of cross sectional area s = 5.7 mm^2 are located outside the thermo-stated regions and have equal temperatures. Thermoosmotic pressure (difference of fluid level in tubes h) is measured by a web camera and processed by PC. The examined two-component ferrofluid consists of magnetite nanoparticles coated with oleic acid and suspended in tetradecane. Special efforts are made to remove any excess of surfactant (its part not chemically bounded with nanoparticles). The volumetric concentration of magnetic phase in colloid φ_2 = 0.05, the mean "magnetic" radius of colloidal particles r = 4.1 nm. The measured thermoosmotic pressure is directed toward the temperature gradient. Unsteady pressure difference primarily grows but after reaching a maximum starts decreasing exponentially. A homogeneous magnetic field **B**, directed normally to the membrane, causes a growth of the pressure difference.

3 Results and Discussion

3.1 Phenomenological model and dynamics of thermoosmosis

The measurement results are interpreted in frame of linear theory of irreversible thermodynamics [3]. Three fluxes $\mathbf{j}_i$ (the flow of solvent $\mathbf{j}_1$, the particle flux $\mathbf{j}_2$ and the heat flux $\mathbf{j}_3$) contain three summands proportional to thermodynamic driving forces $\nabla\mu_i$

(gradients of chemical potentials of solvent μ_1 and solute μ_2 and gradient of temperature T). The potential μ_1 is proportional to molar volume of solvent V_1 and pressure p ($\mu_1 = V_1\nabla p$), but μ_2 depends on ratio between volume fractions of solutes φ_2 and of solvents $\varphi_1 = 1\text{-}\varphi_2$: $\mu_2 = RT\cdot\ln(\varphi_2/(1\text{-}\varphi_2))$. In colloids of low particle concentration ($\varphi_1 = 1$, $\varphi_2 = \varphi << 1$) the mass fluxes of solvent and solutes can be written in the following form (V_2 is molar volume of solute):

$$\mathbf{j}_1 = \mathbf{u}_1 = -\alpha_{11}V_1^2\nabla p + \alpha_{12}V_1RT\frac{\nabla\varphi}{\varphi} + \alpha_{13}V_1\frac{\nabla T}{T} \tag{1}$$

$$\mathbf{j}_2 = \mathbf{u}_2\varphi = -\alpha_{21}V_1V_2\nabla p + \alpha_{22}V_2RT\frac{\nabla\varphi}{\varphi} + \alpha_{23}V_2\frac{\nabla T}{T} \tag{2}$$

The phenomenologic coefficients α_{ik} are related to transport coefficients which can be detected experimentally by following dependencies: filtration $a = \alpha_{11}V_1^2\rho g\delta$, osmosis $d = \alpha_{12}V_1RT$, thermoosmosis $d_T = \alpha_{13}V_1/T$, reverse osmosis $A = \alpha_{21}V_1V_2\rho g\delta/\varphi$, mass diffusion $D = -\alpha_{22}V_2/\varphi$ and thermodiffusion $D_T = -\alpha_{23}V_2/(\varphi T)$. Then the equations (1) and (2) obey the following form:

$$\mathbf{u}_1 = -a\frac{\nabla p}{\rho g\delta} + d\frac{\nabla\varphi}{\varphi} + d_T\nabla T \tag{3}$$

$$\mathbf{u}_2\varphi = -A\varphi\frac{\nabla p}{\rho g\delta} - D\nabla\varphi - D_T\varphi\nabla T \tag{4}$$

Solvent flux (3) causes a development of liquid volume difference in both chambers which results in appearing a liquid level difference h in tubes subjected to both volumes for osmotic pressure measurement. Both the mass flux (4) and the solvent flux (3) cause development of particle concentration difference in both chambers. As a result the mass conservation equations for solvent and for solute are interrelated. To simplify the problem, the present analysis is preformed assuming that osmotic processes relax significantly faster than phoretic ones. Besides, a relatively slow relaxation of pressure curves allows considering steadiness of the concentration gradients in filter layer. Under such simplifications the solution of mass conservation equations with the account of (3) and (4) give:

$$\frac{h}{\delta} = \frac{\gamma}{\beta-\alpha}[\exp(-\beta t) - \exp(-\alpha t)] + \frac{c}{\alpha}[1 - \exp(-\alpha t)] \tag{5}$$

where $\alpha = \frac{2Sa}{s\delta^2}$, $\beta = \frac{Sm}{V_0\delta}$, $\gamma = \frac{2ndS}{ms\delta^2}$, $c = \frac{2S}{\delta^2 s}\left(d_T\Delta T - \frac{nd}{m}\right)$, $m = 2d + 2D_e + Ah + D_{Te}\Delta T$ and $n = 2(d_T\Delta T + D_{Te}\Delta T + ah - Ah)$.

Mass transfer through the layer is influenced not only by hydrostatic pressure but also by magnetic field H. If φ or temperature at both sites of the layer is different, even uniform transversal field induces a magnetic pressure difference across the layer [4]:

$$\Delta p = p_h - p_c + \frac{\mu_0}{2}(M_c^2 - M_h^2) \tag{6}$$

The chemical potential of magnetic solute also is field dependent. For colloids of Langevin type magnetization ((v_p is particle volume, M_s – saturation magnetization of its material)

$$M = \varphi_2 M_s L(\xi) = \varphi_2 M_s (\coth \xi - \frac{1}{\xi}) \qquad \xi = \frac{\mu_0 v_p M_s H}{kT} \tag{7}$$

the molar chemical potential μ_2 (for one particle) is [5]:

$$\mu_2 = kT[\ln(\varphi/(1-\varphi) - \ln\frac{\sinh\xi}{\xi}] \tag{8}$$

The fluid magnetization M and the internal magnetic field H (since ∇H=-∇M at B=const) depend on particle concentration and on temperature. As a result the magnetic field effects determined by (6) and (7) manifest themselves as an increase in thermoosmotic pressure, changes of solutal osmosis and, possible, as a magnetodifffusion and a magnetic Soret effect.

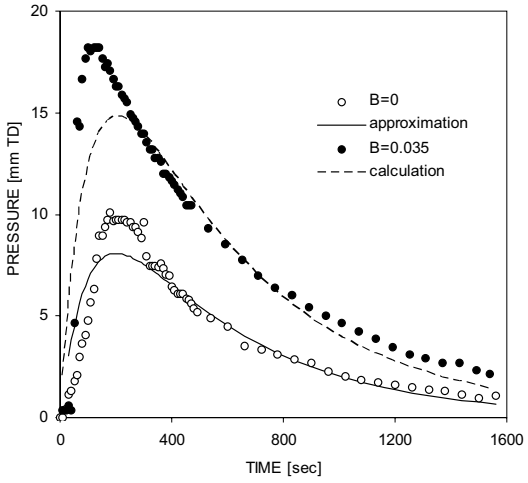

Fig. 1: *Dynamics of thermoosmotic pressure. Fitting parameters found for curve with B = 0 are used to calculate the curve with B = 0.035 T.*

3.2 Comparison with experiments

Experimental curves of osmotic pressure dynamics presented in Fig. 1 agree well with the expression (5). Under long time the unsteady pressure difference relaxes to a zero ($c = 0$). This concedes an assuming that the mass transfer through the layer is influenced mostly by osmotic processes whereas the particle transport (convective, diffusion and thermodiffusion) is small (only first summands of m and n should be taken into account).

The fitting constants γ, α and β, found from the zero-field experiment, correspond to the following values of transport coefficients: $d = 1.1 \cdot 10^{-8}$ m^2/s, $d_T = 2.9 \cdot 10^{-11}$ m^2/s, $a = 9.4 \cdot 10^{-11}$ m^2/s. Additionally, the Onsager relation $\alpha_{12} = \alpha_{21}$ allows calculating the coefficient $A = 1.1 \cdot 10^{-11}$ m^2/s. The diffusion coefficient of nanoparticles $D = kT/6\pi\eta r = 1.2 \cdot 10^{-11}$ m^2/s. Since the Soret coefficient $S_T \approx 0.12$ 1/T [2], the thermodiffusion coefficient also is small $D_T \approx 1.4 \cdot 10^{-12}$ m^2/s·K. Since the filtration velocity of solvent in pores is very slow, the coefficient a may be calculated directly employing Darcy law according to which $a = K\rho g\delta/\eta$ with K being the filter permeability [6]:

$$K = \frac{d_c^2 \sigma^3}{150(1-\sigma)^2} \tag{9}$$

Such calculations give slightly higher value $a = 1.3 \cdot 10^{-10}$ m^2/s.
The obtained coefficients d and $d_T \Delta T$ (experiments are performed at temperature difference $\Delta T = 50$ K) are significantly higher than the other transport coefficients. This means that the simplifications, mentioned in previous sections, mostly are well grounded and the solution (5) reflects the physical problem correctly. Nevertheless, there are some problematic moments: an uncertainty of initial thermal conditions (relaxation of temperature in chambers lasts approximately 40 - 60 s) and unsteadiness of concentration gradient in initial stage (relaxation of concentration inside the layer $t_d = \delta^2/d$ lasts 20 – 30 s). Besides, partial influence of filtration and reverse osmosis might also be a reason why the curves in initial regime disagree with the exponential law (5) (terms with h in m and n may not be neglected).
The dashed curve of Fig. 1 is calculated employing the above given values of a, d and d_T and introducing in equations (3) and (4) the magnetic summands of pressure and chemical potential. It is assumed that the fluid magnetization obeys Langevin law (7) and the pyromangetic coefficient of particles is detected experimentally from measurements of saturation magnetization of the colloid. The presented in Fig. 1 results show relatively good agreement between the calculation and the experiment.

4 Conclusions

The mass transfer of hydrocarbon based ferrocolloids in nonisothermal wide-pore membrane is determined mostly by osmotic and thermoosmotic forces. Magnetophoretic

force and surface pressure cause increase of osmotic flux and of thermoosmosis, whereas the opposite effects (magnetic Soret effect and magnetodiffusion of particles) are small.

Acknowledgment

The work is supported by Latvian Science Foundation (Project 05.0026) and European Regional Development Foundation, ERAF Latvia,
(ERAF/CFLA/05/APK/2.5.1/000002/002).

References

[1] E. Blums, G. Kronkalns, M.M. Maiorov, A. Mezulis, J. Magn. Magn. Materials, **289** (March, 2005), 275-277.

[2] E. Blums, The European Physical Journal E - Soft Matter, **15,** (November 2004) No. 3, 271-276.

[3] N. V. Churaev. *Physical Chemistry of Heat and Mass Transfer Processes in Porous Media* (Himiya, Moscow, 1990).

[4] E. Blums, Yu. A. Mikhailov and R. Ozols. *Heat and Mass Transfer in MHD Flows* (World Scientific, Singapore, 1987).

[5] E. Blums, A. Cebers and M. M. Maiorov. *Magnetic Fluids* (Walter de Gryuter & Co., Berlin - New-York, 1997).

[6] A. V. Lykov, *Heat and Mass Transfer Handbook*, (Energia, Moscow, 1972).

Quasiperiodic gravitational modulation of convection in magnetic fluid

T. Boulal[1], S. Aniss[1], M. Belhaq[1]

[1]University Hassan II Aïn Chock, Laboratory of Mechanics, Faculty of Sciences, BP 5366 Maârif, Casablanca, Morocco

E-mail: tboulal@yhoo.fr, s.aniss@fsac.ac.ma, m.belhaq@fsac.ac.ma

ABSTRACT

Thermal instability in a horizontal Newtonian magnetic liquid layer with non-magnetic rigid boundaries is investigated in the presence of a vertical magnetic field and a quasiperiodic forcing. The analysis is restricted to static and linear law of magnetization. Performing a Galerkin projection truncated to the first order, the governing linear system corresponding to the onset of convection is reduced to a damped quasiperiodic Mathieu equation. The threshold of convection corresponding to quasiperiodic solutions is determined in the case of a heating from below. We show that a modulation with two incommensurate frequencies has a stabilizing or a destabilizing effect depending on the frequencies ratio. The effect of the Prandtl number is also examined for different frequency ratios.

1 FORMULATION

Consider a magnetic fluid layer bounded between two non magnetic horizontal plates, having respectively constant temperatures, T_o at $z = -d/2$ and T_1 at $z = d/2$ ($T_o \succ T_1$). Assume that the fluid layer is submitted to vertical quasiperiodic motion according to the law of displacement, $z = b_1 \cos(\omega_1 t) + b_2 \cos(\omega_2 t)$, in the presence of the external vertical magnetic field, $\mathbf{H}^{ext} = H_o \mathbf{k}$. The dimensional frequencies, ω_1 and ω_2, are incommensurate. The parameters b_1 and b_2 are the amplitudes of motion, H_o is a constant magnetic field and **k** is the unit vector upward. By means of a Galerkin projection truncated to the first order and trial functions used in [1-2], the governing linear system corresponding to the onset of convection is reduced to the following damped quasiperiodic Mathieu equation

$$\frac{d^2 g}{d\tau^2} + 2\mu_1 \frac{dg}{d\tau} + \left[\delta + \varepsilon\left(cos(\tau) + cos(\omega\tau)\right)\right] g = 0 \tag{1}$$

Here $g(\tau)$ is the amplitude of temperature, $\tau = \Omega_1 t$, $\mu_1 = \frac{c_1}{\Omega_1}$, $\delta = \frac{c_2\left(R_o - Rg - c_3\, Rm\right)}{\Omega_1^2}$, $\varepsilon = -c_2\, Fr_1\, Rg$ and $\omega = \frac{\Omega_2}{\Omega_1}$ in which $2c_1 = \left(\frac{306}{31} + q^2\right) + Pr\left(\frac{504 + 24q^2 + q^4}{12 + q^2}\right)$, $c_2 = \frac{121\, q^2}{124\left(12 + q^2\right)}$ and $c_3 = 1 - \frac{42}{55\left(1 + \frac{q^2}{12} + \frac{q}{2\left(1 + \chi_o^2\right)}\right)}$. Note that Ω_1 and Ω_2 are the dimensionless frequencies of ω_1 and ω_2, respectively.

The parameters q, Pr, χ_o and Fr_1 denote the wave number, the Prandtl number, the magnetic susceptibility and the Froude number, respectively. In this case, the gravitational and magnetic Rayleigh numbers are

$$Rg = \frac{\beta\, g\,(T_o - T_1)\, d^3}{\nu\,\kappa}, \quad Rm = \frac{\mu_o\, \gamma_a^2\,(T_1 - T_o)^2\, d^2\, H_o^2}{\mu\,\kappa\,(1 + \chi_o)^3} \tag{2}$$

where $\gamma_a = \frac{\chi_o}{T_a}$ (T_a is the average temperature), μ_o the magnetic permeability, ν the kinematics viscosity, μ the dynamic viscosity, κ the thermal diffusivity and β the coefficient of thermal expansion. The quantity $R_o = \frac{4\left(504 + 24q^2 + q^4\right)\left(306 + 31q^2\right)}{121\, q^2}$ corresponds to the Rayleigh number of the marginal stability curve for the classical Rayleigh-Bénard problem.

2 RESULTS AND DISCUSSION

2.1 Stationary Onset of Convection of the Unmodulated case

The stationary convective instability of a horizontal magnetic liquid layer heated from below in the presence of an uniform vertical magnetic field was predicted by Finlayson [3]. Here, we obtain, from equation (1), the stationary marginal stability curve given by $\delta = 0$ and then $R_o - Rg - c_3\, Rm = 0$.

2.2 Quasiperiodic Parametric Convective Instability

To produce quasiperiodic parametric resonance in equation (1), we introduce the change of variables inspired from the work by Gresho and Sani [4]

$$Rmo - Rg = Ra \qquad Rm = f_m \Omega^2 Ra$$

where Ra is a positive number and f_m is an arbitrary positive constant. The ratio of the magnetic and gravitational forces is now defined by

$$M_2 = \frac{R_m}{Rg} = \frac{f_m\, \Omega_1^2}{f_m\, \Omega_1^2 - 1} \tag{3}$$

Following [5], we use the harmonic balance method to determine the marginal stability curves by means of expansion

$$g(t) = \sum_{n=0}^{\infty} \sum_{m=-\infty}^{\infty} \left[A_{nm}\, cos\left(\frac{n + m\omega}{2} \tau \right) + B_{nm}\, sin\left(\frac{n + m\omega}{2} \tau \right) \right] \tag{4}$$

in which we may set, without loss of generality, $A_{-n,-m} = A_{n,m}$ and $B_{-n,-m} = -B_{n,m}$. Approximate results are obtained by a truncation of the infinite sums in Equation (4) and then replaced by sums from 0 to N for n and from $-N$ to N for m, respectively. Equations (1) and (4) allow us to obtain two homogenous algebraic systems in A_{nm} and B_{nm} which can be combined to obtain one homogenous system in A_{nm}. This system will have a nontrivial solution only if its determinant vanishes. For each N, the dimension of this system is $2N^2 + 2N + 1$. For the case $N = 4$ considered in the current paper, the corresponding system dimension is 41. Nevertheless, the analysis is facilitated by putting the system in upper triangular form. In this analysis, the vanishing determinant can be given formally in the form $F(Rm, q, fm, \chi_0, Pr, Fr_1, \Omega_1, \omega) = 0$ in which all parameters of the physical problem are taken into account. The marginal stability curves $Rm(q)$ are determined numerically by fixing the arbitrary positive constant fm, the magnetic

susceptibility χ_0, the dimensionless frequency Ω_1, the frequency ratio ω, the Prandtl number Pr and the Froude number Fr_1. Hereafter, we focus attention on the curves corresponding to the critical magnetic Rayleigh number Rm_c and wave number q_c versus the dimensionless frequency Ω_1.

Figure 1 illustrates the evolution of the critical magnetic Rayleigh number as a function of Ω_1 ($100 \le \Omega_1 \le 300$) for different values of the frequencies ratio, $\omega = \frac{1}{\sqrt{37}}$, $\omega = \sqrt{2}$ and $\omega = \sqrt{37}$. Note that the value $Rm_c = 2542$ corresponds to the unmodulated case. These results show that the modulation with two incommensurate frequencies has a stabilizing or a destabilizing effect depending on the ratio of the frequencies. This finding is an extension of a previous study in which only a periodic modulation was considered [2].

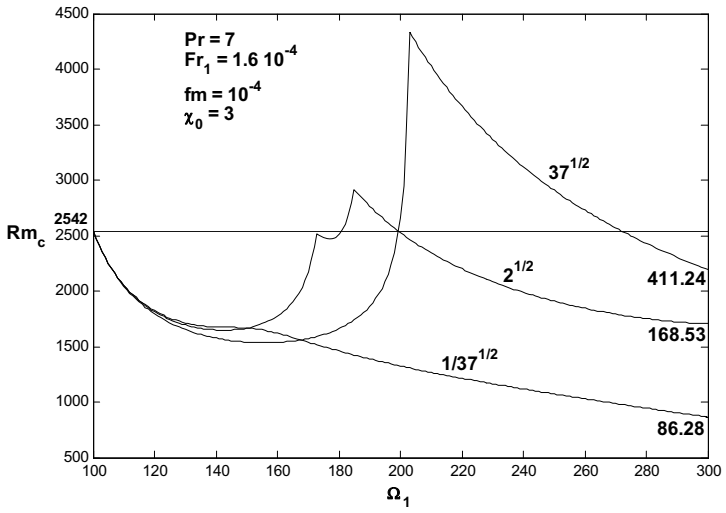

Fig. 1: *Heating from below - Evolution of the critical magnetic Rayleigh number Rm_c vs dimensionless frequency Ω_1 for different values of the irrational frequencies ratio ω.*

We illustrate in Figure 2 the dependence of the critical magnetic Rayleigh number, Rm_c, on the Prandtl number, Pr, for $\Omega_1 = 120$, $Fr_1 = 1.6\,10^{-4}$ and for different values of the irrational frequencies ratio. It can be seen from figure 2 that the largest critical magnetic Rayleigh number, corresponding to the maximum of stabilization, increases with decreasing ω and then the stabilizing effect decreases with the frequency ratio. However, for high values of Prandtl number, the critical magnetic Rayleigh number for all the profiles tends, as expected, to the value of the unmodulated case.

3 CONCLUSIONS

In this work we have studied the effect of vertical quasiperiodic oscillations on the onset of convection in an infinite horizontal magnetic liquid layer with rigid boundaries. The linear equations of convection are reduced to a damped quasiperiodic Mathieu equation where the quasiperiodic solutions characterize the onset of convection. Furthermore, the effect of the frequencies ratio on the convection threshold has been observed. This ratio plays an important role in controlling the onset of convection.

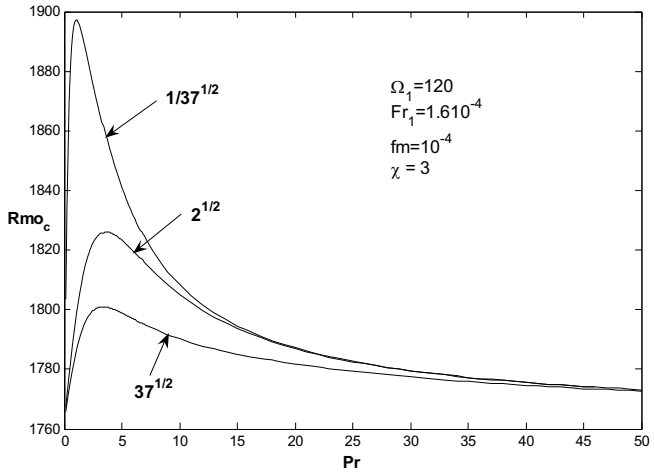

Fig. 2: *Heating from below - Evolution of the critical magnetic Rayleigh number Rm_c vs Prandtl number Pr for different values of the irrational frequencies ratio ω.*

References

[1] G. Z. Gershuni, and E. M. Zhukhovitskii, *Convective Instability of Incompressible Fluid* (Keter Publisher, Jerusalem, 1976)

[2] S. Aniss, M. Belhaq and M. Souhar, ASME J. Heat Transfer **123**, 428, (2001)

[3] B. A. Finlayson, J. Fluid Mech., Vol. 40, part 4, 753, (1970)

[4] P. M. Gresho and R. L. Sani, J. Fluid Mech., Vol. 40, 783, (1970)

[5] T. Boulal, S. Aniss, M. Belhaq and R. Rand, Physical Review E 76:056320, (2007)

Theoretical determination of effective thermodiffusion coefficients, application to the description of mass transfer in porous media

H. Davarzani, J. Chastanet, M. Marcoux and M. Quintard

IMFT, Groupe d'Etude sur les Milieux Poreux, Toulouse, France

E-mail: marcoux@imft.fr

Abstract

The presence of a temperature gradient in porous media may generate mass fluxes associated to Soret effect. This can modify species concentrations of the fluids flowing through the porous media and lead to local accumulations. In this study, we determine the effective Darcy-scale, coefficients for heat and mass transfer in porous media using a volume averaging technique. Especially, we study the influence of the Péclet number and the conductivity ratio on the effective thermodiffusion coefficients. The closure problems related to the pore-scale physics are solved over periodic unit cells representative of the porous structure. The results show that, for low Péclet number, the effective Soret number in porous media is the same as the one in the free fluid and that it does not depend on the conductivity ratio. On the opposite, in convective regimes, the effective Soret number decreases. In this case a change of conductivity ratio will change the effective thermodiffusion coefficient as well as the effective thermal conductivity coefficient. The macroscopic model obtained by this method is validated by comparison with direct numerical simulations at the pore-scale. A good agreement is observed between theoretical predictions coming from the resolution of the macro-scale problem and numerical simulations at the pore-scale. This demonstrates the validity of the proposed theoretical model.

1 Introduction

Modeling and description of mass transport in porous media is still a basic challenging problem in many applications: reservoir engineering, chemical engineering, environmental hydrology, etc. Several studies have been devoted to the description of two-phase flow [2], reactive media [4] and multi-component mixtures [1]. In the meantime, the considered media can also be subjected to thermal gradients coming from natural origin (geothermal gradients, intrusions, …) or from anthropic anomalies (waste storages, …). This can dramatically modify the concentrations of the fluids flowing through the porous medium [3].

The aim of this study is to characterize the modifications induced by thermodiffusion on mass transport in porous media. The main objective is the determination of the effective thermodiffusion coefficient using a volume averaging technique.

2 Upscaling and macroscopic equation

We consider in this study a binary mixture flowing through the porous medium subjected to a thermal gradient. It is well known from irreversible thermodynamics that the mass and heat fluxes are affected by Soret and Dufour effects respectively. In this study, we neglect the Dufour effect, which is a correct approximation for liquids. Furthermore, we assume that the physical properties of the fluid and solid are constant. Stokes's equation is used for describing the flow motion at the pore-scale. The pore-scale mass conservation is described by the following equation and boundary conditions for the fluid phase (β-phase)

$$\frac{\partial c_\beta}{\partial t} + \nabla.\left(c_\beta \mathbf{v}_\beta\right) = \frac{1}{ReSc}\nabla.\left(\nabla c_\beta + \Psi \nabla T_\beta\right), \text{ in the } \beta\text{-phase} \tag{1}$$

$$\text{BC1: } \mathbf{n}_{\beta\sigma}.\left(\nabla c_\beta + \Psi \nabla T_\beta\right) = 0, \text{ at } \mathcal{A}_{\beta\sigma} \tag{2}$$

where c_β , T_β are the concentration and temperature fields, and the dimensionless numbers Ψ, Re and Sc are separation factor, Reynolds and Schmidt numbers respectively.

Because the direct solution of the convection-diffusion equation is in general impossible due to the complex geometry of the porous medium, equations describing average concentrations and velocities must be developed [4]. After performing the volume averaging on the original boundary value problem and solving the associated closure problem in a representative unit cell, the final form of the transport equations contains local averages, rather than micro-scale point values. Thus, the microscopic equations that hold for a point in space are developed into the appropriate macroscopic equations, which hold at a given point for some volume in space.

The equations of conservation of mass at the Darcy-scale have been obtained, in dimensionless form as

$$\frac{\partial\left\langle \varepsilon_\beta c_\beta \right\rangle^\beta}{\partial t} + \nabla.\left(\varepsilon_\beta \left\langle \mathbf{v}_\beta \right\rangle^\beta \left\langle c_\beta \right\rangle^\beta \right) = \frac{1}{ReSc} \nabla.\left(\frac{\mathbf{D}^*_\beta}{D_\beta}.\nabla\left\langle c_\beta \right\rangle^\beta + \frac{\Psi \mathbf{D}^*_{\mathbf{T}\beta}}{D_{T\beta}}.\nabla\left\langle T \right\rangle \right) \quad (3)$$

where $\mathbf{D}^*_\beta$ and $\mathbf{D}^*_{\mathbf{T}\beta}$ are effective diffusion and thermodiffusion tensors. $\langle T \rangle$, $\left\langle c_\beta \right\rangle^\beta$ and $\left\langle \mathbf{v}_\beta \right\rangle^\beta$ are the macroscopic temperature [2], the intrinsic average concentration and the interstitial average velocity, which obeys Darcy's law.

3 Results and Discussion

3.1 Effective tensors

From the upscaling procedure, the effective coefficients in the Darcy-scale equations may be obtained by solving so-called pore-scale "closure problems" on periodic unit cells representative of the porous structure. These closure problems were solved for different Péclet numbers and thermal conductivity ratios. Results for the effective Soret number ($S_T = D_{T\beta}/D_\beta$) are illustrated in Fig. 1, where Pe is the cell Péclet number.

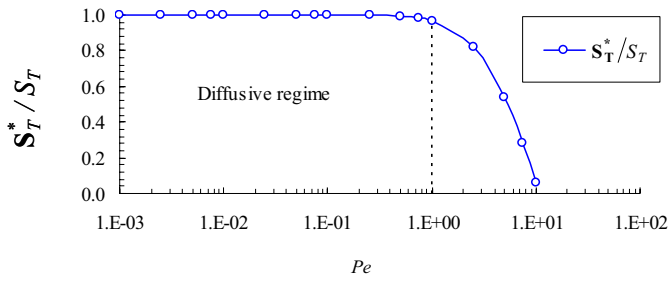

Fig. 1: *Effective Soret number as a function of Péclet number* ($k_\sigma \approx 0$)

This figure shows that, for the diffusive regime, one can use the same Soret number at the Darcy-scale as the one in the free fluid ($\mathbf{S}^*_\mathbf{T}/S_T = \mathbf{1}$). Beyond $Pe \approx 1$ the Soret effect decreases with increasing convection. Thermal properties of the fluid and even the solid matrix have also to be taken into account in the thermodiffusion process, as shown in Fig. 2. This figure shows that increasing the solid thermal conductivity increases the value of

the effective thermodiffusion coefficient for convective regimes but it has not influence on thermodiffusion for diffusive regimes.

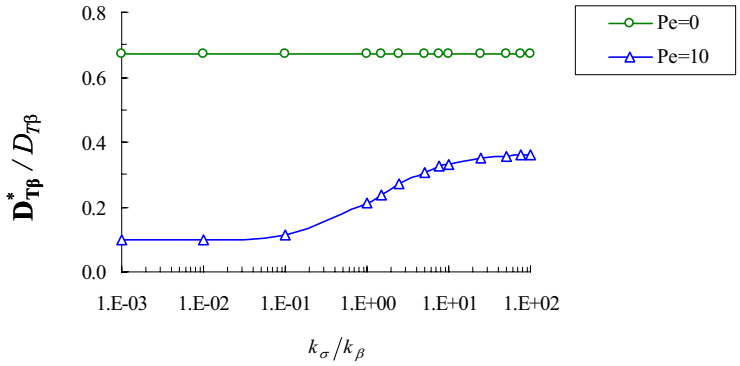

Fig. 2: *The influence of conductivity ratio (k_σ / k_β) on effective thermodiffusion coefficients*

3.2 Macroscopic simulation and validation

In order to validate the theory developed by the up-scaling technique in the previous section, we have compared the results obtained by prediction from the one-dimensional macro-scale equations with the results obtained from direct simulations performed on a porous medium made of a 2D array of cylinders (Fig. 3). In the macro-scale problem the effective coefficients have been obtained from the solution of the closure problems.

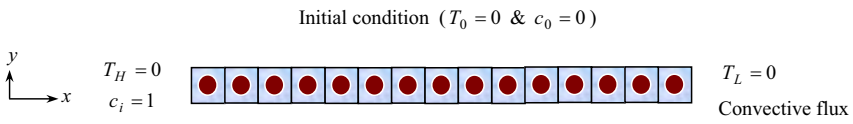

Fig. 3: *Schematic of spatially periodic porous media (T_H : High Temperature and: T_L Low Temperature).*

Calculations have been carried out in the case of a binary mixture whose physico-chemical properties are general. Here we have fixed these properties to be $Sc = 1$, $Pr = 1$ and $\Psi = 1$. Microscopic scale simulations, as well as the resolution for the macroscopic problem, have been performed using COMSOL Multiphysics finite elements code.

Fig. 4 shows the spatial distribution of concentration at different times for a ratio of conductivity equal to 10 ($Pe = 0$). The micro-scale values are cell averages obtained from the micro-scale fields. One observes a very good agreement between the micro-scale simulation and the macro-scale predictions.

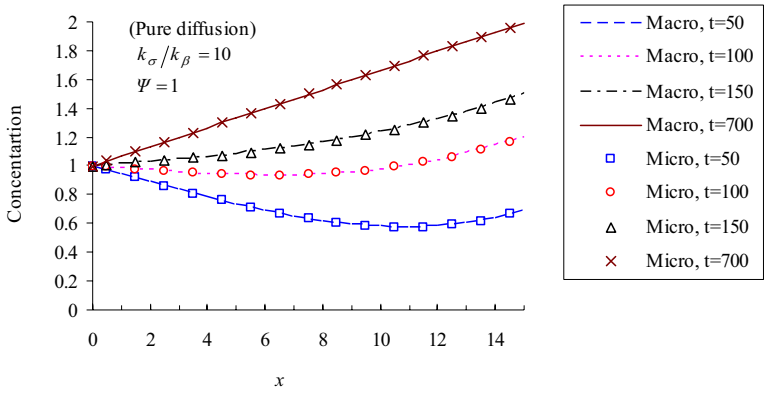

Fig. 4: *Comparison between macro and micro scale concentration ($k_\sigma / k_\beta = 10$).*

In Fig. 5 the steady-state distribution of the concentration is plotted for different Péclet numbers. One can see clearly that the concentration profile changes with the Péclet number. For example, for $Pe = 0.75$, because the medium has been homogenized thermally by advection in most of the porous domain, the concentration profile is almost the same as in the isothermal case (without thermodiffusion). Near the exit boundary, there is a temperature gradient which generates a considerable change in the concentration profile.

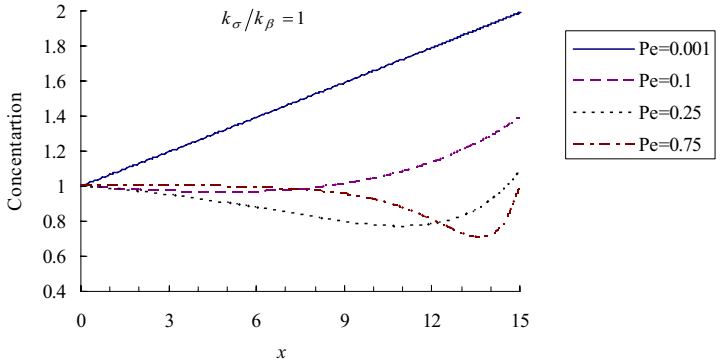

Fig. 5: *Influence of Péclet number on thermodiffusion ($k_\sigma / k_\beta = 1$)*

4 Conclusions

In this study, we showed that the effective thermodiffusion coefficient may depart from the micro-scale value because of advection effects. For these convective regimes, it is shown that the effective thermodiffusion coefficient depends in a complex manner of the pore-scale properties (geometry, conductivity ratio, …). This may be of a great importance when evaluating the concentration in applications like reservoir engineering, waste storage, and soil contamination.

It was found a good agreement between the macro-scale resolution and micro-scale, direct simulation, which validates the proposed theoretical model.

References

[1] M. Quintard, L. Bletzaker, D. Chenu, and S. Whitaker, Chemical Engineering Science **61**, 2643, (2006)

[2] M. Quintard, M. Kaviany, and S. Whitaker, Advances in Water Resources **20**, 77, (1997)

[3] P. Costeseque, T. Pollak, J. K. Platten, and M. Marcoux, European Physical Journal E **15**, 249, (2004)

[4] S. Whitaker, *The method of Volume Averaging* (Kluwer Academic Publishers, Dordrecht, The Netherlands, 1999)

Thermal convection of binary mixes in thin channels

V.A. Demin and A.F. Glukhov

Theoretical Physics Department, Perm State University, Russia

E-mail: demin@psu.ru

Abstract

The mechanisms of flow's excitation and specific overcritical regimes of thermal convection in Hele-Shaw cell have been investigated experimentally and theoretically for binary mixes with well-known thermodiffusive properties. The influence of oscillatory regimes near the boundary of stability on dopant distribution has been studied. It is found for a binary mix with normal thermal diffusion that specific oscillatory flows take place near the threshold of convection in Hele-Shaw cell, similarly to connecting channels.

1 Introduction

In the case of normal Sore effect thermal convection of binary mix in a horizontal fluid layer heated from below develops as a result of instability with respect to monotonous disturbances. The same instability situation is observed for cavities of different forms that have wide horizontal boundaries. In similar cavities heated from below there is thermodiffusive division of mix components along vertical axis. So there is the opinion that the oscillatory convection in binary mix near the boundary of stability exists for only anomalous thermal diffusion when there is the competition of thermal gravitational mechanism of convection excitation and thermal diffusive one.

Our experimental and theoretical results show that the oscillatory convection in binary mix is possible to be observed near the boundary of stability for normal thermodiffusion in specific conditions. According to the basic assumption explaining experiments the complex oscillatory regimes in binary mixes for positive Sore coefficient are determined by thermodiffusive division of mix components in horizontal plane when the fluid moves predominantly along vertical heat-conducting boundaries [1-3]. Thin Hele-Shaw cell and convective loop elongated in vertical direction (connected channels) are examples of the cavities in which the same flows could be observed.

2 Experimental technique

The laboratory model has been made to study convective flows in the Hele-Shaw cell experimentally (Fig. 1). The working cavity (height h = 32 mm, length l = 17 mm, and thickness $2d$ = 1.5 mm) is bounded from above and from below by heat exchangers. There are channels drilled in the heat exchangers to organize opposing flows of the thermostatting fluid. These conditions ensure uniform temperature along the upper and lower boundaries of the cavity. On the one side, the cavity is bounded by a plexiglass array 16 mm thick which made it possible to observe the flow. The large size of the arrays almost eliminates all external thermal effects.

The temperature difference between heat exchangers and temperature distribution inside the cavity are measured by differential copper–Constantan thermocouples (the length of junctions inside the cavity is equal to 0.75 mm). Thermocouple data, taken by voltmeter V7-54/3 are processed by the personal computer. As a measure of the flow rate the non-dimensional parameter $\Theta = |\zeta|/\Delta T$ has been used, where ζ is the thermocouple reading and ΔT is the vertical temperature difference between the heat exchangers.

The mixtures of CCl_4 in decane $C_{11}H_{22}$ and Na_2SO_4 in water had been used as the working fluids. The coefficients of concentration density of these mixtures are high. Therefore even small concentration gradients create fairly strong non-uniformities of density which cause the onset of convection. The mixtures were prepared in a glass flask and, before being poured into the cell, were thoroughly mixed for 10 – 15 min by intense shaking.

In pure fluids (water, decane and CCl_4) heated from below, convection develops in accordance with the known theoretical and experimental results on the convective instability of one-component Newtonian fluids.

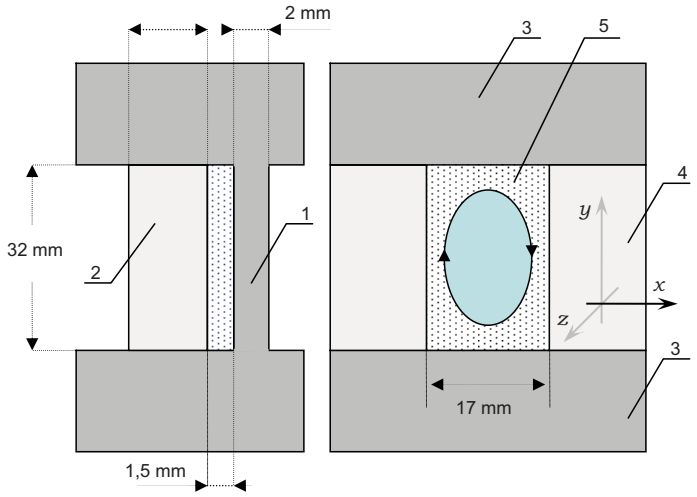

Fig. 1: *Experimental setup; 1 – aluminum plate, 2, 4 – plexiglass plates, 3 – aluminum heat exchangers, 5 – working cavity.*

For small vertical temperature differences, these fluids are in stable mechanical equilibrium. In this case the non-dimensional parameter Θ is equal to zero. When the critical temperature difference is attained, a monotonous convective circulation flow branches softly from the equilibrium. The flow rate increases with the growth of temperature gradient. The thermal Rayleigh number has been determined in terms of the temperature gradient $\Delta T/H$ as follows:

$$\mathrm{Ra_t} = \frac{g\beta_t d^4}{\nu\chi}\nabla T,$$

where g is the gravity acceleration; β_t, ν, χ are thermal-expansion coefficient, kinematic viscosity and thermal diffusivity. Sometimes, instead of the Rayleigh number it was more convenient to use the supercriticality parameter $\mu_t = \mathrm{Ra_t}/\mathrm{Ra_{tc}}$. Within the limits of experimental error, the curve $\Theta = \Theta(\mu_t)$ was reproduced on both paths for increase and decrease of μ_t. In the experiments, two flow directions occurred with the same probability: one with positive and other with negative value of thermocouple signal.

When the Hele-Shaw cell is occupied by a mixture of the working fluids, the results change qualitatively. The oscillatory growth of disturbances begins in the cell when the

critical Rayleigh number is attained and, depending on the supercriticality and the initial conditions, ends in either a stationary circulation or in oscillating flow with alternation of the mixture circulation direction. Experimental points of stationary and oscillating regimes for mixtures with different concentrations $\Theta = \Theta(\mu_t)$ and theoretical amplitude curves are presented in Fig. 2.

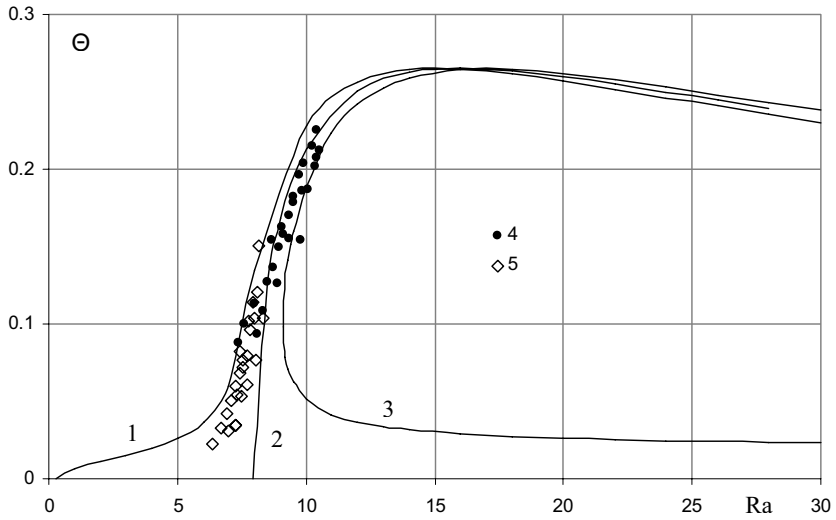

Fig. 2: *Amplitude curves for binary-mixture flows in the Hele-Shaw cell: stationary flows for $\varepsilon = 0.36$ (1), $\varepsilon = 0$ (2) and $\varepsilon = -0.2$ (3); experimental data (4,5) as a functions of the supercriticality $\mu(t)$; 4 – oscillatory regimes, 5 – steady-state flow.*

Theoretical graph $\Theta = \Theta(\mu_t)$ has a characteristic maximum with $\Theta_{max} \approx 0.25$ that agrees with the experiments and theory for connected channels. In the case $\mu_t > 1$ the process of transition from equilibrium ended in oscillations which were accompanied by a periodic change in the direction of one-vortex flow in the cell. These oscillations with constant amplitude were realized in the right-hand neighborhood of the critical point Ra_{tc} within a very narrow region ($\mu_t \approx 1 - 1.2$).

Non-linear oscillations have been characterized by non-zero average value of thermocouple signal, see Fig. 3. Thus, in experiment convective instability of equilibrium in binary liquid mixtures is related with the oscillatory growth of the initial disturbances and is accompanied by hysteresis with respect to the Rayleigh number. Thus it is necessary to use the theory of thermoconcentration convection to explain these effects.

3 Theoretical investigation

3.1 Equations system and non-dimensional parameters

The Hele-Shaw cell has rigid, heat conducting boundaries. Coordinate system with the y-axis oriented along the vertical has been presented in Fig. 1*b*. In this coordinate system a unit vector $\boldsymbol{\gamma}(0, 1, 0)$ is directed vertically upward. The cell is heated from below so that, on the vertical boundaries, a linear temperature distribution is maintained. It will be shown below that, for this temperature distribution, the binary liquid can be in a state of mechanical equilibrium.

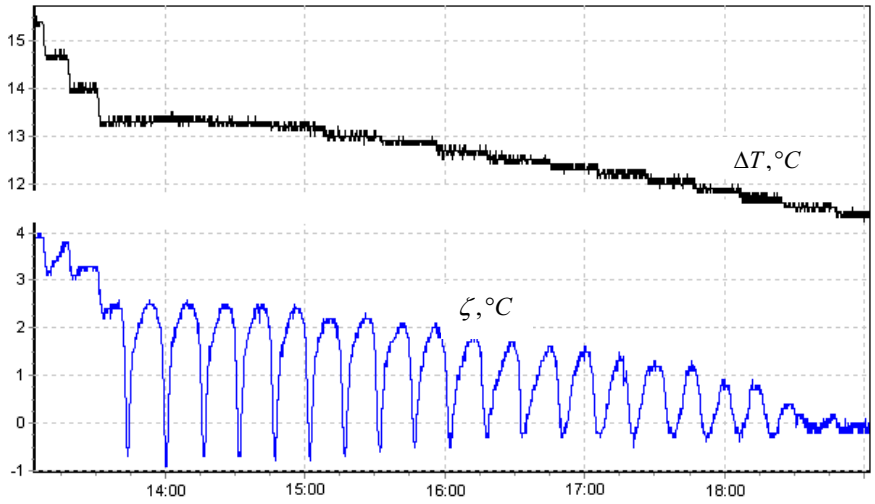

Fig. 3: *Thermocouple data in dependence on time when the temperature difference between heat exchangers decreases.*

For modeling the convective flows of a binary mixture, we use the equations for an incompressible fluid obtained on the basis of the hydrodynamic equations in the Boussinesq approximation [4]:

$$\frac{\partial \boldsymbol{v}}{\partial t} + (\boldsymbol{v}\nabla)\boldsymbol{v} = -\nabla p + \Delta \boldsymbol{v} + \frac{\mathrm{Ra}H}{\mathrm{Pr}}(T - C)\boldsymbol{\gamma}, \quad \operatorname{div} \boldsymbol{v} = 0 \tag{1}$$

$$\frac{\partial T}{\partial t} + (\boldsymbol{v}\nabla)T = \frac{1}{\mathrm{Pr}}\Delta T, \quad \frac{\partial C}{\partial t} + (\boldsymbol{v}\nabla)C = \frac{1}{\mathrm{Sc}}(\Delta C + \varepsilon \Delta T) \tag{2}$$

where $\boldsymbol{v}$, T, p, C are the velocity, temperature, pressure, and heavy-admixture concentration fields. The scales used for non-dimensional variables in equations (1), (2) are: the cell's half-width [d] for distance, [d^2/ν] for time, [Θ] for temperature, [$\Theta\beta_t/\beta_c$] for concentration, and [$\rho\nu^2/d^2$] for pressure. Here ρ is the mean density of the fluid; Θ is vertical temperature difference between the heat exchangers. Equations (1), (2) contain four non-dimensional parameters, namely:

$$\mathrm{Pr} = \frac{\nu}{\chi}, \quad \mathrm{Sc} = \frac{\nu}{D}, \quad \mathrm{Ra} = \frac{g\beta_t \Theta d^3}{\nu\chi}, \quad \varepsilon = \frac{\alpha\beta_c}{\beta_t}.$$

Three parameters are the Prandtl, Schmidt, and Rayleigh numbers, respectively. Additional non-dimensional parameter in the problem ε characterizes the thermal diffusion in the mixture ($\alpha = k_T/T$, where k_T is the thermodiffusion ratio). The coefficient β_c describes the density dependence on concentration. In the case considered, $\beta_c < 0$ because CCl_4 in decane and Na_2SO_4 in water are heavy admixtures. The effects associated with the presence of an admixture are also characterized by the diffusion D and thermodiffusion α coefficients. In the approximation (1), (2), it is assumed that the diffusion and heat fluxes are related with the concentration and temperature gradients by the formulas $\boldsymbol{J} = -\rho D\left(\nabla C + \alpha\nabla T\right)$, $\boldsymbol{q} = -\kappa\nabla T$, where κ is the thermal conductivity.

In the calculations, on vertical boundaries of the cell the no-slip condition $\boldsymbol{v} = 0$ is imposed. The cell's walls were assumed to be perfectly heat-conducting. Accordingly, on the vertical wide boundaries of the calculation domain the temperature disturbances were zero. Moreover, on the impermeable rigid walls the normal component of the diffusion flux density J_n vanishes. The boundary condition for non-dimensional diffusion flux density has the form:

$$\frac{\partial C}{\partial \boldsymbol{n}} + \varepsilon\frac{\partial T}{\partial \boldsymbol{n}} = 0 \tag{3}$$

3.2 Mechanical equilibrium state

At a certain value of the temperature gradient, mechanical equilibrium state exists that is characterized by the absence of fluid motion (zero velocity):

$$\frac{\partial}{\partial t} = 0, \quad \boldsymbol{v} = 0, \quad p = p_0, \quad T = T_0, \quad C = C_0.$$

Here T_0, p_0, and C_0 are the equilibrium temperature, pressure, and admixture concentration. Applying the **curl** operator to equation (1) for momentum, we obtain the system of equations for a binary mixture in the state of mechanical equilibrium

$$\left[\nabla T_0 \times \boldsymbol{\gamma}\right] - \left[\nabla C_0 \times \boldsymbol{\gamma}\right] = 0, \quad \Delta T_0 = 0, \quad \Delta C_0 = 0, \tag{4}$$

In what follows, the specific case of constant temperature gradient has been analyzed that corresponds to the linear temperature distribution $T_0 = -z/H$ and heating from below. In this case, the Laplace equation for the temperature is satisfied identically. The other equations of system (4) make it possible to find the equilibrium admixture distribution in the channels formed as a result of thermal diffusion. With account for boundary condition (3) on the upper and lower channel boundaries, the linear vertical heavy-admixture concentration distribution has been received $C_0 = \varepsilon z/H$.

3.3 Method of solution

The height and length of the Hele-Shaw cell are greater than the width one $H >> d$ in experiments. This make it possible to use the plane-trajectory approximation $\boldsymbol{v}(v_x, v_y, 0)$ and to introduce stream function in the calculations $v_x = \partial\psi/\partial y, \quad v_y = -\partial\psi/\partial x$.

The fields of temperature deviation and stream function for one-vortex flow are approximated by trigonometric functions. Also it is convenient to introduce the new variable $F = C + \varepsilon T$. Taking into account the structure of the equations, the expansion of the field $F(x,y,z,t)$ can be represented with the help of special combinations of trigonometric functions. Substituting the expansions for ψ, T and F in the original equations (1), (2), after application of the Galerkin procedure the system of amplitude equations for ψ_{11}, t_{02}, t_{11}, f_{02}, f_{11} take place which is solved numerically using a standard integration Mathlab-7 procedure. The calculations were performed using the time-relaxation method. Also analytical solution of the problem has been received in stationary case.

4 Results and Discussion

In accordance with the experiments, the calculations were performed for Hele-Shaw cell with non-dimensional height $H = 42$ and length $L = 22$. In a homogeneous liquid $\varepsilon = 0$, as the critical Rayleigh number is exceeded, convection takes place “softly” (Fig. 2, curve *2*). Depending on the initial disturbance, one-vortex flows with both directions of circulation may develop in the cell. The situation changes radically if an admixture is present in the liquid. It follows from Fig. 2 that, development of intensive convection is “hard” for anomalous thermodiffusion, with the threshold being determined by an increase in the oscillatory disturbances. In the experiments for the mix Na_2SO_4 in water the Schmidt number was much greater than the Prandtl number, thus realistic values of parameters were taken as $\mathrm{Pr} = 7$, $\mathrm{Sc} = 2100$, $\varepsilon = 0.36$ in the calculations that corresponds to this admixture with normal thermodiffusion. For a small supercriticality, a disturbance introduced into the fluid grows and then the stationary flow with small amplitude is established. In the calculations, non-linear oscillating regimes are observed for moderate values of supercriticality (Fig. 4) which are similar to experimental oscillations (Fig. 3).

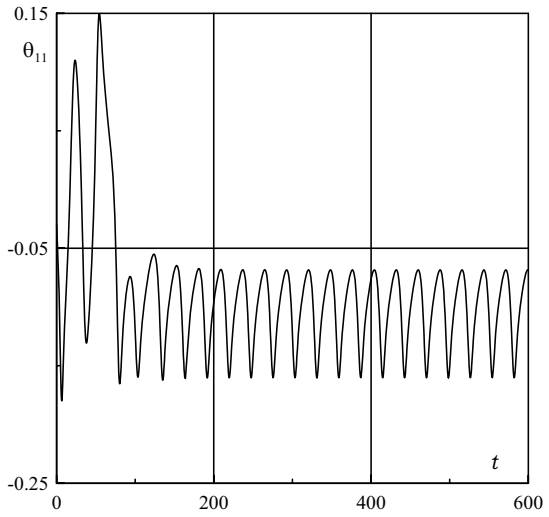

Fig. 4: *Thermocouple data in dependence on time when the temperature difference between heat exchangers decreases.*

The calculations performed for positive and negative values of the coefficient ε satisfactorily describe the experimental results. The mechanism responsible for the effects observed is mainly attributable to the thermodiffusion separation of the mixture which is due to the horizontal temperature gradients $\nabla_x T$, $\nabla_y T \sim \Theta/d$ = 10 K/cm rather than to the weak vertical gradients $\nabla_z T = \Delta T/h \sim 2$ K/cm with a characteristic component separation time $h^2/D \sim 500$ hours. The horizontal gradients occur only in the circulating fluid. The separation time across the channel is $d^2/D \sim 15$ min, which coincides in order of magnitude with the time of circulation of the fluid in the cell, i.e. a liquid particle is able to change its composition during the motion in the cell. For a fairly slow circulation, there is a feedback effect of the concentration non-uniformities generated by thermal diffusion on the convective flow. It should be emphasized that the same behaviour of a binary mix had been observed in connected channels [1-3].

5 Conclusions

The mix effect on thermal convection in Hele-Shaw cell has been studied experimentally and theoretically over a wide range of variation of the governing parameters. Depending on the supercriticality both stationary and oscillatory convective regimes are possible in binary mixtures. The model proposed makes it possible theoretically to describe the nonlinear oscillations, whose presence at small supercriticalities demonstrates the fairly complex behavior of the hydrodynamic system. Special emphasis was placed on

calculating the admixture concentration distribution across the cell. It was confirmed that the oscillatory character of the convection near the threshold is attributable precisely to the thermodiffusion effect.

Acknowledgment

The research described in this publication was made possible in part by Award *N* PE-009-0 of the U.S. Civilian Research & Development Foundation for the Independent States of the Former Soviet Union (CRDF) and Russian Foundation of Basic Researches (grant Ural-2007 *N* 07-08-96035).

References

[1] A.F. Glukhov, V.A. Demin, G.F. Putin, J. Fluid Dynamics. Vol. 42, No. 2 (2007)

[2] V.A. Demin, A.F. Glukhov, J. Bulletin of Perm State University. Physics, Vol. 1/6 (2007)

[3] V.A. Demin, A.F. Glukhov, J. Bulletin of Perm State University. Physics, Vol. 1/17 (2008)

[4] G.Z. Gershuni, E.M. Zhukhovitsky, *Convective instability of incompressible fluid* (Keter, Jerusalem, 1976)

Linear stability analysis of the Soret-driven monocellular flow in a horizontal porous layer subjected to vertical vibrations

B. Elhajjar[1], A. Mojtabi[1] and M. C. Charrier-Mojtabi[2]

[1] IMFT, UMR CNRS INP/UPS 5502, Université Paul Sabatier, Toulouse III, France
[2] PHASE, EA 3028, Université Paul Sabatier, Toulouse III, France

E-mail: mojtabi@imft.fr, elhajjar@imft.fr

Abstract

The Soret-driven convection in a horizontal porous layer with a large aspect ratio saturated by a binary fluid and subjected to vertical high frequency vibrations was studied. The influence of vertical vibrations on the stability of the monocellular flow obtained for particular ranges of the physical parameters of the problem was investigated. We considered the case of high frequency, small amplitude vibrations so that a formulation using time averaged equations could be used. The monocellular flow obtained for $\psi > \psi_{mono}$ function of Le, where ψ is the separation ratio and Le the Lewis number, leads to a migration of the species towards the two vertical boundaries of the cell. 2D direct numerical simulations of the averaged governing equations were performed using both a finite element code (Comsol) and a spectral collocation method. The numerical results and linear stability analysis showed that the vertical vibrations delay the transition from monocellular flow to multicellular flow making it possible to separate the species for a high value of the Rayleigh number.

1 Introduction

The problem under consideration concerns the interaction between two phenomena: Soret-driven convection and thermo-vibrational convection in a porous medium.
Thermogravitational diffusion is the combination of two phenomena: convection and thermodiffusion. The coupling of these two phenomena leads to species separation. In 1938, Clusius and Dickel [1] successfully carried out the separation of gas mixtures in a vertical cavity (TGC). Furry, Jones and Onsager [2], (FJO theory) developed the theory of thermodiffusion to interpret the experimental processes of isotope separation. Subsequently, many works appeared, aimed at justifying the assumptions or extending the results of the theory of FJO to the case of binary liquids [3]. Other works were related to the improvement of the experimental devices to increase separation. Lorenz and Emery [4] proposed the introduction of a porous medium into the cavity. Platten et al. [5] inclined the cavity to increase separation. Elhajjar et al. [6] used a horizontal cavity with temperature gradients imposed on the horizontal walls to improve the separation process with the use of two control parameters. Many works have been devoted to thermo-vibrational convection in porous media. Charrier Mojtabi et al. [7] investigated the influence of vibrations on Soret driven convection in a horizontal porous cell heated from below or from above. They showed that the vertical vibrations had a stabilizing effect while the horizontal vibrations had a destabilizing effect. In the present paper, we use the same formulation as the one used by Charrier Mojtabi et al. [7], and we verify that it is possible to carry out the species separation of a binary mixture in this geometrical configuration, and that the vibrations can be used to delay the loss of stability of the monocellular flow, which allows separation at a higher Rayleigh number. We consider the case of high frequency, small amplitude vibrations, so that a formulation using time averaged equations can be used. The results of the linear stability analysis of the monocellular flow in an infinite porous layer heated from below, in the case of a separation ratio $\psi > 0$, are corroborated by the direct numerical simulations.

2 Mathematical formulation

We considered a rectangular cavity with aspect ratio $A = L / H$, where H is the height of the cavity along the vertical axis and L is the width along the horizontal axis. The aspect ratio was assumed infinite in the stability analysis. The cavity was filled with a porous medium saturated by a binary fluid for which the Soret effect was taken into account. The impermeable horizontal walls were kept at different, uniform temperatures. The vertical walls were impermeable and adiabatic. All the boundaries were assumed rigid. The cavity was subjected to linear harmonic oscillations in the vertical direction (amplitude b and dimensional pulsation ω). For the governing equations, we adopted the Boussinesq approximation and Darcy equation for which the non-stationary term was taken into account. When we consider the referential related to the oscillating system, the gravitational field $\mathbf{g}$ is replaced by: $\mathbf{g} + b\varpi^2 \sin(\varpi t')\mathbf{e}_z$ where $\mathbf{e}_z$ is the unit vector along the vertical axis (vibration axis) and t' the dimensional time. In the limiting case of high frequency and small amplitude vibrations, the averaging method can be applied to

study thermal vibrational convection [8]. According to this method, each field is subdivided into two parts: the first part varies slowly with time (i.e. the characteristic time is large with respect to the period of the vibrations) and the second one varies quickly with time (i.e. the characteristic time is of the order of magnitude of the vibrational period).
Thus the averaged flow equations are:

$$\begin{aligned}
&\nabla.\mathbf{V} = 0 \\
&B\frac{\partial \mathbf{V}}{\partial t} + \mathbf{V} = -\nabla P + Ra(T + \psi C)\mathbf{e_z} + Rv[\mathbf{W}.(\nabla T + \frac{\psi}{\varepsilon}\nabla C)]\ \mathbf{e_z} \\
&\frac{\partial T}{\partial t} + \mathbf{V}.\nabla T = \nabla^2 T \\
&\varepsilon\frac{\partial C}{\partial t} + \mathbf{V}.\nabla C = \frac{1}{Le}(\nabla^2 C - \nabla^2 T) \\
&(T + \psi\,\mathbf{C})\mathbf{e_z} = \mathbf{W} + \nabla\xi\ ;\ \nabla.\mathbf{W} = 0
\end{aligned} \tag{1}$$

Here, $\mathbf{V}, P, T, C$ are the averaged fields (i.e. the mean value of the field calculated over the period $\tau = 2\pi/\omega$) and $\mathbf{W}$ a field introduced for mathematical reasons. $B = Da(\rho c)_f /[(\rho c)^* \varepsilon Pr]$, where Pr is the Prandtl number, $(\rho c)_f$ the volumetric heat capacity of the fluid, and $(\rho c)^*$ the equivalent heat capacity of the fluid and the porous medium. Rv characterizes the intensity of the vibrations. $Da = K/H^2$ is the Darcy number and K the permeability of the porous medium. $Ra = K\,g\,\beta_T\,H\,\Delta T\,(\rho c)_f /(\lambda^* \upsilon)$ is the thermal Rayleigh number, where β_T is the coefficient of thermal expansion, ΔT the temperature difference between the horizontal walls, λ^* the equivalent conductivity of the fluid and the porous medium, and ν the kinematic viscosity of the mixture. $\psi = -(\beta_T/\beta_c)(D_T{}^*/D^*)C_i(1-C_i)$ the separation ratio, where β_c is the coefficient of mass expansion, $Le = a/D^*$ the Lewis number, where a is the coefficient of thermal diffusivity. $\varepsilon = \varepsilon^*(\rho c)_f /(\rho c)^*$ the normalized porosity (where ε^* is the porosity).
The dimensionless boundary conditions are:

$$\begin{aligned}
&T = 1\ for\ z = 0\ ;\ T = 0\ for\ z = 1\ ;\ \frac{\partial T}{\partial x} = \frac{\partial C}{\partial x} = 0\ for\ x = 0, A\ ; \\
&\nabla C.\mathbf{n} = \nabla T.\mathbf{n}\ for\ z = 0,1\ ;\ \mathbf{V}.\mathbf{n} = 0\ and\ \mathbf{W}.\mathbf{n} = 0\ \forall M \in \partial\Omega
\end{aligned} \tag{2}$$

In the momentum equation the term $B\partial\mathbf{V}/\partial t$ is usually neglected since B is of order 10^{-6}. However, in our problem, high frequency vibrations cause very large accelerations, making it necessary to consider this non-stationary term [9]. Sovran et al. [10] showed that at the onset of convection $Ra_{cs} = 12/\psi Le$ and k_{cs}=0, $\forall$ Rv, for $\psi > \psi_{mono} = 1/(40Le/51 - 1)$.

3 Linear stability analysis of the monocellular flow

In the case of a shallow cavity $A >> 1$, we considered the parallel flow approximation used by Cormack et al. [11]. We obtain the velocity, temperature and concentration fields:

$$\begin{cases} T_0 = 1 - z, U_0 = Ra\, m\psi\,(1/2 - z) \\ C_0 = m\,x + (m^2\, Ra\, Le\psi(3z^2 - 2z^3))/12 - z - (m^2\, Ra\, Le\psi)/24 + (1 - mA)/2 \\ m = \pm\sqrt{(10\, Le\, Ra\psi - 120)}/(LeRa\psi) \end{cases} \quad (3)$$

Separation, $S = mA$, is defined as the difference in mass fraction of the denser component in the vicinity of the left and the right vertical walls of the cell. Then the maximum separation is obtained for $Ra = 24/(Le\psi)$. We studied the stability of the monocellular solution in order to confirm that the species separation could occur in a horizontal porous cell heated from below. For this study, we write the governing equations using the perturbations of the different fields. The second order terms are neglected; we obtain the linear equations where the unknown functions are the perturbations. The perturbations are developed in normal modes. The resulting linear problem is solved using the 4th order Galerkin method. The critical values of the Rayleigh number and the wave number were obtained for a stationary and a non-stationary bifurcation. For the values of ψ and Le studied, the critical Rayleigh number leading to stationary bifurcation is always higher than the one leading to Hopf bifurcation. So, in this study, we focus on the values of the critical wave number k_{c2} and the critical Rayleigh number Ra_{c2}. The results of linear stability analysis for $Le = 20$ and $\psi = 0.1$ are presented in tables I. It can be observed, in this table, that the vibrations have a stabilizing effect and lead to an increase in the critical value of the thermal Rayleigh number. So the vibrations can be used to maintain the monocellular flow and then allow the separation of the binary mixture components over a wide range of thermal Rayleigh number. It should be mentioned that vibrations reduce the critical wave number k_{c2}. This means that vibrations can also be used to decrease the number of convective cells at the transition from monocellular flow to the multicellular flow.

Rv	**0**	**10**	**20**	**30**	**40**	**50**	**60**	**70**	**80**	**90**	**100**
Ra_{c2}	32.79	37.95	42.49	46.60	50.83	53.83	57.08	60.14	63.03	65.78	68.41
k_{c2}	2.80	2.59	2.42	2.28	2.16	2.07	1.99	1.91	1.85	1.80	1.75

Table 1 *Effect of vibrations on the critical values of Rayleigh number* Ra_{c2} *and wave number* k_{c2} *associated with transition from monocellular to multicellular flow for* $Le = 20$, $\varepsilon = 0.5$, $\psi = 0.1$, *and* $B = 10^{-6}$ *(Galerkin method of order 4).*

4 Numerical simulations

In the results presented below, the values of B and ε were fixed at 10^{-6} and 0.5 respectively. The results for $Le = 20$ are presented. For $Le = 20$ and $\psi = 0.1$, the stability analysis shows that, without vibrations, the monocellular flow loses its stability, via a Hopf bifurcation, for the critical parameters $Ra_{c2} = 32.79$. For the same mixture ($\psi = 0.1$) under vibrations characterized by a Rayleigh number $Rv = 50$, the monocellular flow loses its stability for $Ra_{c2} = 53.83$. These results were confirmed by the direct numerical simulations, using a finite element method (Comsol industrial code) and a spectral collocation method.

Fig. 1 shows the streamlines for $Ra = 33$ corresponding to the transition from monocellular flow to multicellular flow without vibrations ($Rv = 0$). Fig. 2 shows the isoconcentrations and the streamlines for the same mixture with the same parameters but with vibrations ($Rv = 50$).

It was noted that, with vibrations, the monocellular flow could be maintained for a higher value of the Rayleigh number leading to the separation of the species between the left and the right vertical walls of the horizontal cell. This monocellular flow remains stable up to $Ra = 54$. Fig. 3 shows the streamlines at the transition from monocellular flow to multicellular flow ($Ra = 54$) for $Rv = 50$.

Fig. 1: *Streamlines for $Le = 20$, $\psi = 0.1$, and $Ra = 33$ without vibrations ($Rv = 0$).*

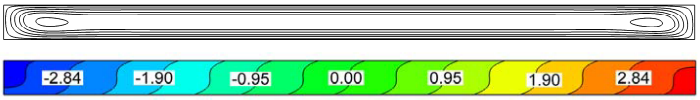

Fig. 2: *Isoconcentrations and streamlines for $Le = 20$, $\psi = 0.1$, $Ra = 33$, and $Rv = 50$.*

Fig. 3: *Streamlines for $Le = 20$, $\psi = 0.1$, $Ra = 54$, and $Rv = 50$.*

5 Conclusion

Analytical and numerical techniques were used to study the stability of the mono-cellular flow obtained, for given values of $\psi > 0$, when the equilibrium solution lost its stability in a large aspect ratio horizontal porous layer saturated by a binary fluid and subjected to vertical high frequency vibrations. The direct nonlinear numerical simulations performed using a finite element method and a spectral collocation method corroborate the results of the linear stability analysis and allow the study of the flow structures which appear after the bifurcation. It was highlighted that the monocellular flow associated with a stratified concentration field led to a horizontal separation of the binary mixture components. It was

observed that vibrations had a stabilizing effect leading to an increase in the critical value of the Rayleigh number corresponding to the transition between monocellular and multicellular flow. Thus vertical vibrations allow species separation over a wider range of Rayleigh numbers.

References

[1] K. Clusius, G. Dickel, Naturwisse **6**, 546, (1938)
[2] W. H. Furry, R. Clark Jones, L. Onsager, Physical Review **55**, 1083, (1939)
[3] S. R. De Groot, Physica **9**, 8, 801, (1942)
[4] M. Lorenz, A. H. Emery, Chemical Engineering Science **11**, 1, 16, (1959)
[5] J. K. Platten, M. M. Bou-Ali, and J. F. Dutrieux, Journal of Physical Chemistry **B 107**, 42, 11763, (2003)
[6] B. Elhajjar, A. Mojtabi, M. Marcoux, M. C. Charrier-Mojtabi, Comptes Rendus Mécanique **334**, 10, 621, (2006)
[7] M. C. Charrier Mojtabi, Y. P. Razi, K. Maliwan, A. Mojtabi, Numerical Heat Transfer Part A-Applications **46,** 10, 981, (2004)
[8] G.Z. Gershuni, D.V. Lyubimov, Thermal Vibrational Convection (Wiley, Chichester, 1998)
[9] G. Bardan, A. Mojtabi, Physics of. Fluids **12**, 11, 1, (2000)
[10] O. Sovran, M.C. Charrier-Mojtabi, M. Azaiez and A. Mojtabi, IHTC12, Grenoble, 2002
[11] D. E. Cormack, L. G. Leal, J. Imberger, Journal of fluid Mechanics **65**, 2, 209 (1974)

Diffusive mass transport under vibrations

Yu. Gaponenko[1,2], V. Shevtsova [1]

[1] Microgravity Research Center, Universite Libre de Bruxelles, Bruxelles, Belgium
[2] Institute of Computational Modelling SB RAS, Krasnoyarsk, Russia

Contact: ygaponen@ulb.ac.be, vshev@ulb.ac.be

Abstract

We report on a numerical study of the mixing of two miscible fluids in gravitationally stable configuration. In the absence of external forces the diffusion process leads to the mixing of species. The aim of this study is to analyze the physical mechanism by which vibrations affect the mixing characteristic of two stratified miscible fluids. The translational periodic vibrations of a rigid cell filled with different mixtures of water-isopropanol ($Sc = 1120$) are imposed. The vibrations with a constant frequency and amplitude are directed along the interface. Our results highlight the strong interplay between gravity and vibrational impact, the relative weight of each effect is determined by ratio vibrational Ra_{vib} and classical Rayleigh numbers, Ra. When the vibrational effect is relatively stronger, the Kelvin-Helmholtz instability develops along the vertical solid walls. Later in time this instability undergoes transition to Rayleigh-Taylor instability. With increasing of gravity level the following dynamic transitions are observed: the life-time of Kelvin-Helmholtz instability is decreasing; only Rayleigh-Taylor instability is observed and, finally, the mixing is controlled by diffusion mechanism. The critical value of characteristic parameters for the onset of these instabilities are identified.

1 Introduction

Two miscible liquids when brought into contact inside a container will mix i.e. become homogeneous via molecular mass diffusion. Depending on the volume of liquids, spatial homogenization by random molecular motion occurs over a long time scale. However added periodical translational vibration of vessel generates an inertial force which acts like a gravity. In that case, if the density depends on the concentration and the direction of vibrations does not coincide everywhere with the direction of the density (concentration) gradient, a solutovibrational (concentration-vibrational) convection is observed.
Vibrations, acting on density difference may essentially influence on the fluid dynamics and mass transport [1]. Siddavaram & Homsy [2] has analyzed the mixing of fluids when the stationary contribution of gravity was omitted and the fluids were initially separated by vertical "interface". The mixing of liquids with simultaneous lateral heating was studied by Chang& Alexander [3]. The main objective of the current study is to investigate the effects of high-frequency vibrations on the mixing characteristics, mass transfer, flow organization, and hydrodynamic instabilities.

2 Formulation of the problem

The cubic cell of $L = 10\,mm$ length is filled with two miscible liquids: both liquids consist of the same components, water and isopropanol, in different proportions. The layer of heavier/denser liquid (51% of water) is at the bottom and lighter (5% of water) is on the top (gravitationally stable configuration). The system is kept at constant temperature. The vibrations are imposed along the horizontal interface, see Fig 1. An interface is assumed to be sharp, and the width of the region over which the initial concentration changes from 1 to 0 is assumed to be $0.03\,L$. This system is subjected to periodical oscillations of the

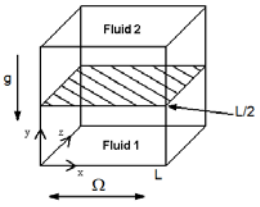

Fig. 1: *Geometry of the system.*

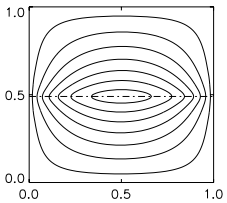

Fig. 2: *Snapshot of the full flow;*

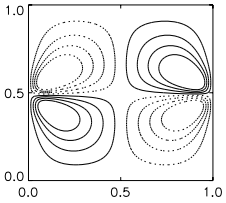

Fig. 3: *Mean flow at the very beginning,* $t = 1$

vessel along the x-axis according to the law $f = Acos(\Omega\, t)$. The imposed excitations induce the oscillatory acceleration that is directed along the x-axis, its the maximal value is $a_{os} = A\Omega^2$. Hereafter we will consider high frequency vibrations, i.e. period of oscillations τ_{os} is smaller than viscous ($\tau_{vis} = L^2/\nu$) and diffusion ($\tau_D = L^2/D$) times and the amplitude A is finite.

$$\tau_{os} = \frac{2\pi}{\Omega} \ll \tau_{vis} = \frac{L^2}{\nu} \;\rightarrow\; \Omega \gg \nu/L^2 \quad \text{and for amplitude} \quad \frac{A\beta_c \Delta c}{L} \ll 1 \qquad (1)$$

Then all physical quantities may be presented as the superposition of a mean (slow) and pulsational (fast) parts [1], [4].

$$\hat{\mathbf{F}} = \mathbf{F}_{mean} + \mathbf{F}_f, \tag{2}$$

where $\mathbf{F}_{mean}$ represents the slow components and $\mathbf{F}_f$ stands for the fast components, that depend on (x, y, t) and (x, y, t, τ) respectively, and $\tau = \Omega t$ is the fast time.
It is known that for aqueous solutions of alcohols, the viscosity and the diffusion coefficient are strongly depending on composition. Therefore the viscosity and the diffusion coefficients are considered as function of concentration. We will restrict our study by 2D calculations and converse the problem into stream-function vorticity formulation. For the mean fields a stream function, ψ, such that $v_x = \partial\psi/\partial y,\ v_y = -\partial\psi/\partial x$ and a vorticity, $\omega = \partial v_y/\partial x - \partial v_x/\partial y$ are introduced. The governing equations in the Boussinesq approximation can be written as

$$\begin{aligned}
&\frac{\partial\omega}{\partial t} + \mathbf{v}\cdot\nabla\omega = \nabla\left(\frac{\nu(c)}{\nu_0}\nabla\omega\right) - \mathrm{Gr}\frac{\partial c}{\partial x} + \frac{\mathrm{Ra_{vib}}}{\mathrm{Sc}}\left(\frac{\partial c}{\partial y}\frac{\partial^2\Phi}{\partial x^2} - \frac{\partial c}{\partial x}\frac{\partial^2\Phi}{\partial x\partial y}\right), \\
&\frac{\partial c}{\partial t} + \mathbf{v}\cdot\nabla c = \nabla\left(\frac{D(c)}{\nu_0}\nabla c\right), \\
&\nabla^2\psi = -\omega,\ \ \nabla^2\Phi = -\nabla c\,\mathbf{s}.
\end{aligned} \tag{3}$$

Here $\omega, \psi, \mathbf{v}, c$ describe dimensionless quantities of the mean flow. Hereafter the subscript "mean" is dropped. Φ is the amplitude of fast pressure, which is periodically for τ [4].

$$P_f = -\beta_c A\Omega^2\Phi(x, y, t)cos(\tau),$$

The scales of length, time, velocity, pressure, and concentration are L, L^2/ν_0, ν_0/L, $\rho_0\nu_0^2/L^2$ and Δc, respectively. The boundary conditions are the following:

$$\begin{aligned}
&x = 0, 1 : \psi = \partial_x\psi = 0,\ w_x = 0,\ \ \partial_x c = 0,\ \partial_x\Phi = -c; \\
&y = 0, 1 : \psi = \partial_y\psi = 0,\ w_y = 0,\ \ \partial_y c = 0,\ \partial_y\Phi = 0
\end{aligned}$$

Initially fluids are at rest, then $\psi = 0$, $w = 0$, $C = 1$, for $0 \le y < 0.5$ and $C = 0$ for $0.5 \le y < 1.0$.
A finite-difference method in both directions is utilized. The Poisson equation for the stream function ψ and for the amplitude Φ of fast pressure were solved by introducing an artificial iterative term, analogous to the time-derivative one. ADI method is used to solve the time-dependent problem for vorticity, the concentration, the pulsatory pressure amplitude and the stream function. More detail about numerical procedure one may find in [5].
All reference values, noted by subscript "0" are taken at the equilibrium conditions, i.e. the mean values for two mixtures at the initial state. The problem is governed by three parameters: vibrational Raleigh number, $\mathrm{Ra_{vib}}$, the Schmidt number, Sc, the Grashof number, Gr or its analog, the Raleigh number, $Ra = Gr \cdot Sc$

$$\mathrm{Ra_{vib}} = \frac{(A\tilde{\omega}\beta_c\,\Delta c\,L)^2}{2\nu_0 D_0},\ \mathrm{Sc} = \frac{\nu_0}{D_0},\ \mathrm{Gr} = \frac{g_0\beta_c\Delta c L^3}{\nu_0^2}. \tag{4}$$

Two of these parameters are fixed, $Sc = 1.12 \cdot 10^4$, $Ra_{vib} = 5.597 \cdot 10^7$. The third parameter, Gr or Ra, is changing. The gravity level, expressed via the Grashof number, is varied from $g = 0$ until $g = 0.165\,g_0$.

3 Results and Discussion

Different flow regimes were observed depending on the ratio of Gr and Ra_{vib}. Vibrations act on the non-uniformity of density and generate an oscillatory convection, which starts at the cross-section of the interface with solid walls. The net flow, see Eqs. 2 consists of one vortex, which occupies the entire cell and half of the period rotates to the one side and another half of the period to the opposite side, see Fig 2. For relatively strong external excitations (see Eqs. 1) due to inertia the fluid cannot immediately return to its initial position and convective mean flow is created. The vibrations cause mean flow in such a way, that heavy/denser liquid moves up along the both solid walls, $x = 0$ and $x = 1$ and less dense moves down. Two weak vortexes with the opposite direction of the circulation are formed in each fluid, see Fig 3. Further development of the mass transfer is strongly depends on the ratio gravity level and vibrational stimuli.

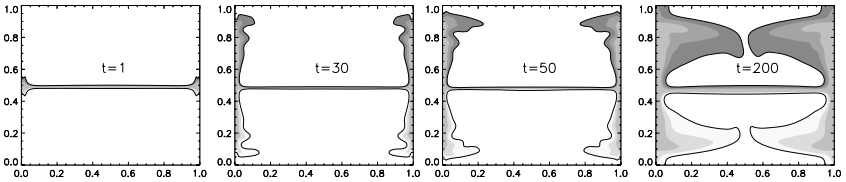

Fig. 4: *Evolution of the concentration front; Gr=0*

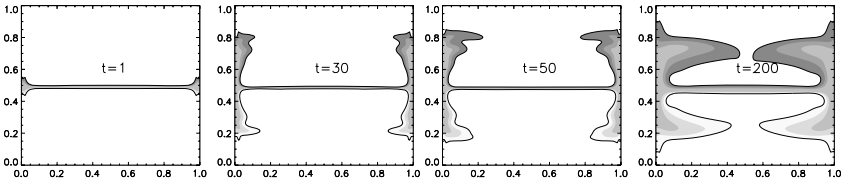

Fig. 5: *Evolution of the concentration front; Gr=1500*

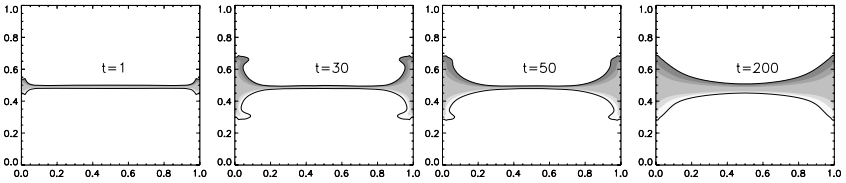

Fig. 6: *Evolution of the concentration front; Gr=5000*

Here we will discuss the fluid behavior in the upper liquid until it is not stated otherwise. In the Figs 4-6 the leading profiles are $c = 0.3$ and $c = 0.7$ at upper and lower liquid correspondingly for different Grashof numbers. Non-shadowed space corresponds to the concentration close to zero (one) in upper (lower) fluid. From the very beginning the concentration front is running along the solid walls, creating a head in the case of $Gr = 0$ and $Gr = 1500$, compare figures at $(t = 1 \div 30)$. The leading zone (we consider isolines $c = 0.3$) expands and rolls up, and denser liquid is intruded into a less dense, see $(t = 50)$. The flow for $Gr = 0$ is similar to Kelvin-Helmholtz instability which is observed in free

shear layers and gravity currents. The observed Kelvin-Helmholtz instability appears almost immediately with the imposing vibrations and exists during certain time interval. The horizontal solid wall impose constrain on the approaching the concentration front and it turns inside the cell, creating another flow organization, when the denser liquid is on top of the less dense, Fig. 4-5 $(t = 50 \div 200)$. This scenario is a kind of the Rayleigh-Taylor instability, which is observed in ground conditions (when heavy liquid is on the top). Further the denser liquid starts to descend, being expanding, and it splits the region of low concentration in two zone, $(t = 200)$. Thus, two additional vortexes appear near the horizontal wall, and it leads to the oscillatory regime. For this set of parameters the amplitudes of the velocity and of the concentration oscillations slowly decay with time. The gravity reduce the speed of rolling up velocity and at $Gr \geq 1500$ Kelvin-Helmholtz instability did not observed. For $Gr \geq 5000$ the gravity force is so strong that heavier liquid slightly rolls up and then diffusive process dominates.

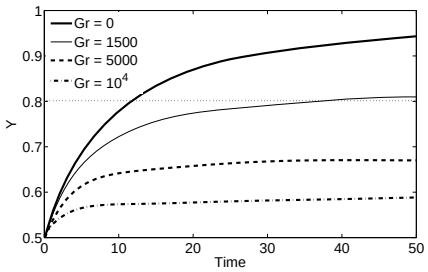

Fig. 7: *Mixture's front propagation.*

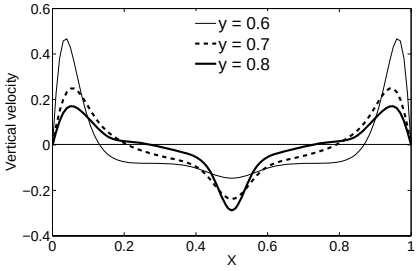

Fig. 8: *Vertical velocity for* $Gr = 0$

The propagation of the leading front $c = 0.3$ with time is shown in Fig. 7, where for the parameters above the horizontal line $y \approx 0.8$ the Kelvin-Helmholtz instability is observed. The distribution of vertical velocity Fig. 8 shows the strong flow near the vertical walls.

4 Conclusions

The effect of external vibrations on the flow organization in two immiscible fluids was investigated, when $Ra_{vib} = 5.597 \cdot 10^7$ and $Sc = 1120$. For $Gr \leq 1500$ the Kelvin-Helmholtz and Rayleigh-Taylor instabilities were observed. In the interval $1500 \leq Gr \leq 5000$ only Rayleigh-Taylor instabilities was observed. For $Gr \geq 5000$ mixing is controlled by diffusion.

Acknowledgment

This work is supported by the Belgian Federal Science Policy Office.

References

[1] Gershuni G.Z., Lyubimov D.V., Thermal vibrational convection, Wiley, England, 1998

[2] Siddavaram V.K., Homsy G.M.,J. Fluid Mech.,**562**, pp.445-475 (2006).

[3] Chang Q., Alexander J.I., C.R. Mecanique, **335**, pp.304-314 (2007)

[4] Zenkovskaya S.M., Simonenko I.B., Izv. AN SSSR, Ser. Mekhan. Zhidk. i Gaza. 1965, N. 5, P. 51-55.

[5] Gaponenko Yu.A., Pojman J.A., Volpert V.A., Zenkovskaja S.M., J. of Appl. Mech. and Tech. Physics. **47**, pp.49-59 (2006). (http://www.springerlink.com/content/1573-8620/)

Numerical modeling of two-dimensional natural convection

K. Gueraoui[1,2], M. Taibi[1], N. Dahmani[1], A. Mrabti[1],
Y. M. Haddad[2] and G. Zeggwagh[3]

[1] *Équipe de modélisation numérique et théorique en mécanique des fluides et en environnement, LPT, Faculté des Sciences, Rabat, Maroc.*

[2] *Département de Génie Mécanique, Université d'Ottawa, Ottawa, Canada, K1N 6N5*

[3] *Laboratoire de Mathématiques Appliquées, Faculté des Sciences Rabat-Agdal, B.P. 1014, Rabat, Maroc*

E-mail: kgueraoui@yahoo.fr

Abstract

This study is a numerical application devoted to the validation of a numerical procedure based on the finite differences and developed for two-dimensional natural convection problems in confined surrounding. One is interested in the effects of the number of Rayleigh and the influence of the slope of the cavity compared to the horizontal on the flow structure and the heat transfer.

1 Introduction

Charlson and Sani [1] report that by approximating an infinite layer by a finite layer of fluid confined inside rectangular or cylindrical walls. Since, the two-dimensional natural convection in confined surrounding did not cease causing the interest of the scientists, and this for at least two reasons. First is related to the diversity of the problems frequently encountered in technology and where the phenomena of natural convection are motive fluids or disturbing flows and heat transfers; such as: continuous casting of a metal, moulding of castings, engines thermonuclear, storage of energy by latent heat or the crystalline growth. The second reason linked with the complexity (coupling, non-linearity) of the systems governing such phenomena of convection and which, in fact, offer an experimental plot very appreciated for the development of new analytical methods of analysis as well as numerical [2-3]. The structure of the flow changes substantially with the number of Rayleigh, the ratio of aspect and the thermal boundary conditions with the side wall. It is thus the effect of these three parameters which we will present in this work.

2 Formulation

2.1 Equations

The equations are those deduced from the laws of conservation of the mass and the momentum and the energy. The physical properties are considered constant except for the density supposed to vary with the temperature but only in the term of gravity forces according to the approximation of Boussinesq.

Equation of continuity

$$\nabla.\mathbf{V} = 0 \tag{1}$$

Equation of conservation of momentum

$$\frac{D\mathbf{V}}{Dt} = -\frac{1}{\rho_0}\nabla p + \nu\nabla^2 + \left[1 - \beta\left(T - T_0\right)\right]\mathbf{g} \tag{2}$$

Equation of transport of energy

$$\frac{DT}{Dt} = \kappa\nabla^2 T \tag{3}$$

For the two-dimensional flows it proves to be convenient to replace the primitive variables, pressure and velocity, by the stream function, ψ and the no null component, Ω of the rotational vector of the velocity.

The equation of continuity makes it possible to define the stream function by:

$$U = \frac{1}{r^n}\frac{\partial \psi}{\partial z} \; ; \; W = -\frac{1}{r^n}\frac{\partial \psi}{\partial r} \tag{4}$$

And the scalar equations are then:

$$\frac{\partial \Omega}{\partial t} + \frac{1}{r^n}\frac{\partial \left(r^n U \Omega\right)}{\partial r} + \frac{\partial (W\Omega)}{\partial z} - n\frac{U}{r}\Omega = \nu\left(\frac{\partial^2 \Omega}{\partial r^2} + \frac{n}{r}\frac{\partial \Omega}{\partial r} + \frac{\partial^2 \Omega}{\partial z^2} - n\frac{\Omega}{r^2}\right) \tag{5}$$

$$-g_0\beta\left(\frac{\partial T}{\partial r}\cos\gamma - \frac{\partial T}{\partial z}\sin\gamma\right)$$

$$\frac{\partial T}{\partial t} + \frac{1}{r^n}\frac{\partial \left(r^n UT\right)}{\partial r} + \frac{\partial (WT)}{\partial z} = \kappa\left(\frac{\partial^2 T}{\partial r^2} + \frac{n}{r}\frac{\partial T}{\partial r} + \frac{\partial^2 T}{\partial z^2}\right) \tag{6}$$

$$\Omega = \frac{1}{r^n}\left(\frac{\partial^2 \psi}{\partial r^2} - \frac{n}{r}\frac{\partial \psi}{\partial r} + \frac{\partial^2 \psi}{\partial z^2}\right) \tag{7}$$

n is worth zero for the rectangular geometry and one for the cylindrical geometry.
In the case of a horizontal cavity$(\gamma = 0)$, the equation of the transport of the vorticity highlights well the role of the horizontal gradient of the temperature$\frac{\partial \Theta}{\partial r}$, in the activation of the mechanism of the natural convection. This gradient causes to initiate the flow by creating a mechanical imbalance in the fluid mass initially at rest.

2.2 Boundary conditions

The condition of no slip to the rigid walls is translated for the stream function by:

$$\psi = \frac{\partial \psi}{\partial r} = \frac{\partial \psi}{\partial z} = 0 \quad \text{for} \quad z = 0 \quad et \quad z = H \tag{8}$$

$$\psi = \frac{\partial \psi}{\partial r} = \frac{\partial \psi}{\partial z} = 0 \quad \text{for} \quad r = 0 \quad et \quad r = L \tag{9}$$

The thermal boundary conditions are:

$$T = T_C \quad \text{for} \quad z = 0 \tag{10}$$

$$T = T_F \quad \text{for} \quad z = H \tag{11}$$

$$\frac{\partial T}{\partial r} = 0 \quad \text{for} \quad r = 0 \quad et \quad r = L \tag{12}$$

3 Adimensionnalisation

The adimensionnalisation of the equations is carried out by means of the reference variables $\mathrm{R}, \kappa / R$, ΔT_0 $(= T_C - T_F)$, R^2 / κ for the length, the velocity, the temperature and time, respectively. The non dimensional equations are written:

$$U = \frac{1}{r^n}\frac{\partial \psi}{\partial z} \; ; W = -\frac{1}{r^n}\frac{\partial \psi}{\partial r} \tag{13}$$

$$\frac{\partial \Omega}{\partial t} + \frac{1}{r^n}\frac{\partial \left(r^n U\Omega\right)}{\partial r} + \frac{\partial (W\Omega)}{\partial z} - n\frac{U}{r}\Omega = \mathrm{Pr}\left(\frac{\partial^2 \Omega}{\partial r^2} + \frac{n}{r}\frac{\partial \Omega}{\partial r} + \frac{\partial^2 \Omega}{\partial z^2} - n\frac{\Omega}{r^2}\right) \tag{14}$$

$$- \mathrm{Ra}\,\mathrm{Pr}\left(\frac{\partial \Theta}{\partial r}\cos\gamma - \frac{\partial \Theta}{\partial z}\sin\gamma\right)$$

$$\frac{\partial \Theta}{\partial t} + \frac{1}{r^n}\frac{\partial \left(r^n U\Theta\right)}{\partial r} + \frac{\partial (W\Theta)}{\partial z} = \frac{\partial^2 \Theta}{\partial r^2} + \frac{n}{r}\frac{\partial \Theta}{\partial r} + \frac{\partial^2 \Theta}{\partial z^2} \tag{15}$$

$$\Omega = \frac{1}{r^n}\left(\frac{\partial^2 \psi}{\partial r^2} - \frac{n}{r}\frac{\partial \psi}{\partial r} + \frac{\partial^2 \psi}{\partial z^2}\right) \tag{16}$$

Θ being a reduced temperature defined by: $\Theta = \dfrac{T - T_F}{\Delta T_0}$ and always lies between 0 and 1.

4 Numerical methods

The space discretization of the transport equations of the vorticity and energy will be done using the precise differences centered with the order two (as well for the convectif terms as for the diffusion). The equation giving the stream function will be discretized using a precise Hirsh diagram to the order four and whose relations are developed in this reference [4].

5 Results and interpretations

One considers an enclosure of an aspect ratio AF equal to one and a fluid of a number of Prandtl of 0.71. The number of Rayleigh is 2.10^4. At the beginning the dynamic fields and the temperature are calculated in a horizontal cavity$(\gamma = 0°)$. These results are then used as initial condition for the solution of the following case of slope, and so on until$\gamma = 90°$. The fluid near of the lower hot surface is then heated and tends to reach the cold upper surface. In spite of the slowing down effect of viscosity near the wall, it is near this wall that the upswing is most intense (Fig 1). Until an angle of inclination of 10° the flow almost does not change a structure but loses in intensity, A$\gamma = 15°$, the flow regains in intensity without changing structure. For an angle of inclination of 30°, the direction of rotation of the cells was reversed (Fig 2), but the transfer of heat and the dynamic variables continued to grow. With 45° the dynamic variables drop but the number of Nusselt continuous to grow until an angle of 60°. Beyond that, the flow loses in intensity until an angle of 90°.

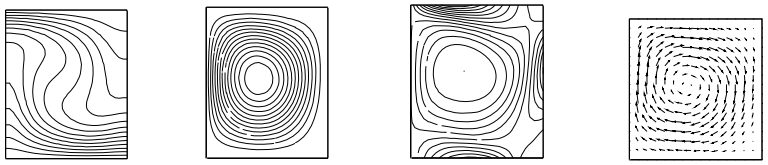

Fig 1: *Isotherms, curves of stream, Iso-swirls and field of velocities for AF=1, Ra = 2. 10^4, Pr = 0.71, side walls perfectly adiabatic and a null slope.*

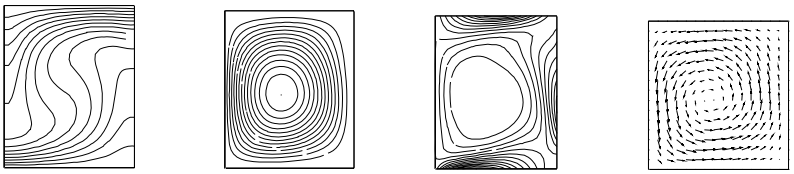

Fig 2: *Isotherms, curves of stream, Iso-swirls and field of velocities for AF=1, Ra = 2. 10^4, Pr = 0.71, side walls perfectly adiabatic and a slope of 30°.*

6 Conclusion

In conclusion, this study allowed the validation of a code based on the finite differences and devoted to the natural convection in confined surrounding. This validation, made on a

rectangular geometry, showed a good agreement with results published by other authors [4].

It will be noticed in particular that the number of Nusselt falls with the increase in the slope from 0° to 10° then this number increases with the increase in the angle of inclination until $\gamma = 50°$ where it reaches the absolute maximum. Beyond that, the number of Nusselt fall until reaching its minimum at $\gamma = 90°$.

References

[1] G.S.CHARLSON, R.L. SANI, Thermoconvective Instability in a Bounded Cylindrical Fluid Layer, Int. J. Heat Mass Transfert, Vol. 13, pp. 1479-1496, (1970).

[2] C.Y.SOONG, P.Y.TZENG, D.C.CHIANG, T.S. SHEU, Numerical Study on Mode-Transition Of Natural Convection In Differencially Heated Inclined Enclosures, Int. J. Heat Mass Transfer, Vol. 39, N° 14, pp. 1869-1882, (1996).

[3] D.MUKOTMONI, K.T. YANG, Thermal Convection In Small Enclosures: An Atypical Bifurcation Sequence, Int. J. Heat Mass Transfer, Vol. 38, N° 1, pp. 113-126, (1995).

[4] O. TERHMINA, A. MOJTABI, B. ROUX, A Numerical Procedure for Three-Dimensional Mixed Convection Developing Flows in an Axisymmetric Geometry, Eur. J. Mech., B/Fluids, Vol., 11, No. 1, pp. 21-38, (1992).

Theoretical and numerical model for the lowest layers of the atmosphere

K. Gueraoui[1,2], M. Taibi[1], I. Aberdane[1], A. Dhiri[1],
Y. M. Haddad[2] and G. Zeggwagh[3]

[1] *Équipe de modélisation numérique et théorique en mécanique des fluides et en environnement, LPT, Faculté des Sciences, Rabat, Maroc.*

[2] *Département de Génie Mécanique, Université d'Ottawa, Ottawa, Canada, K1N 6N5*

[3] *Laboratoire de Mathématiques Appliquées, Faculté des Sciences Rabat-Agdal, B.P. 1014, Rabat, Maroc*

E-mail: kgueraoui@yahoo.fr

Abstract

The main objective of the present paper is a two-dimensional theoretical and numerical modeling of the atmospheric pollution by considering the advection-diffusion-reaction process in a turbulent flow (kε model) of a Newtonian fluid.

A finite volume method is used to solve the equations and to determine the temperature, T, the fluid velocities, u, w, respectively in Cartesian coordinates ($\vec{e}_x$, $\vec{e}_z$), the pressure, P and the pollutant concentration profile, c.

This study, considered as an important step in modelling atmospheric pollution, may also be fit to other industrial applications.

1 Introduction

The air pollution, resulting from the industrial development, represents a serious threat for the human, animal and vegetable life.
In order to understand and better manage the transport of the gas traces and the pollutants existing in the air, several models of the quality of air were developed. These models are used to simulate the changes which can emerge in the chemical composition of the atmospheric air, with an aim of establishing an effective strategy to meet the requirements of the quality of the air. The theoretical model of transport and chemical reactions in the atmospheric air is described by a system of non stationary equations with partial derivatives. The equations which describe such phenomena, in general, are solved numerically by using approximate methods such as the finite differences, the finite volumes, the finite elements or the spectral methods [1].
The originality of this work is a two-dimensional numerical and theoretical modeling of the atmospheric pollution by holding account simultaneously; in the equations of the transfer of energy, transport of the pollutants; the turbulent and non stationary character of the flow, the compressible character of the fluid and phenomena of diffusion, advection and chemical reactions.

2 Theoretical model

The theoretical modeling of the phenomenon of the air pollution is based on three fundamental processes coupled between them; namely the flow of the fluid, the transfer of energy and the transport of the pollutants.

2.1 Equations of flow of the fluid and the transfer of energy

2.1.1 Equations of flow of the fluid

The turbulent flow of the fluid is controlled by the conservation equations of the mass and the momentum of a Newtonian, compressible fluid in the gravitational field [2].

$$\frac{\partial \rho^*}{\partial t} + div \rho^* \vec{u}^* = 0 \tag{1}$$

$$\frac{\partial \rho^* u^*}{\partial t} + div\left(\rho^* u^* \vec{u}^*\right) = -\frac{\partial p^*}{\partial x} + \eta \, div \overrightarrow{grad}\, u^* \tag{2}$$

$$\frac{\partial \rho^* w^*}{\partial t} + div\left(\rho^* w^* \vec{u}^*\right) = -\frac{\partial p^*}{\partial z} + \eta \, div \overrightarrow{grad}\, w^* - \rho^* g \tag{3}$$

With: $\vec{u} = u^*(x,z)\vec{e}_x + w^*(x,z)\vec{e}_z$
Where $\vec{u}^*$ is the field speed of the fluid, $(\vec{e}_x, \vec{e}_z)$ the unit vectors associated to the Cartesian coordinates, g the acceleration of gravity, ρ^* the bulk mass of the fluid, u^* and

w^* the velocity components of the fluid respectively in the directions $\vec{e}_x$ and $\vec{e}_z$, η the viscosity of the fluid and p^* its pressure.

In order to study the effect of the fluctuations, it is supposed that the variables u^*, w^*, p^* and ρ^* can be written in the form of the sum of an average component and a disturbing term such as:

$$u^* = u + \tilde{u} \tag{4}$$

$$w^* = w + \tilde{w} \tag{5}$$

$$p^* = p + \tilde{p} \tag{6}$$

$$\rho^* = \rho + \tilde{\rho} \tag{7}$$

By introducing the equations (4-7) into the equations (1-3) and by admitting the assumption that the disturbing term of the bulk mass, $\tilde{\rho}$, is negligible in front of the average component, ρ [3], the equations (1-3) become:

$$\frac{\partial \rho}{\partial t} + div\,\rho\vec{u} = 0 \tag{8}$$

$$\frac{\partial \rho u}{\partial t} + div\left(\rho u \vec{u}\right) = -\frac{\partial p}{\partial x} + \eta\, div\,\overrightarrow{grad}\,u + \left[-\frac{\partial \rho \overline{\tilde{u}^2}}{\partial x} - \frac{\partial \rho \overline{\tilde{u}\tilde{w}}}{\partial z}\right] \tag{9}$$

$$\frac{\partial \rho w}{\partial t} + div\left(\rho w \vec{u}\right) = -\frac{\partial p}{\partial z} + \eta\, div\,\overrightarrow{grad}\,w + \left[-\frac{\partial \rho \overline{\tilde{u}\tilde{w}}}{\partial x} - \frac{\partial \rho \overline{\tilde{w}^2}}{\partial z}\right] - g\rho \tag{10}$$

It is introduced into the equations (9) and (10) three new variables:

Normal stress of Reynolds: $-\rho\,\overline{\tilde{u}^2}$ and $-\rho\,\overline{\tilde{w}^2}$, and

the shear stress of Reynolds: $-\rho\,\overline{\tilde{u}\tilde{w}}$

2.1.2 Equation of the transfer of energy

The transfer of energy in the atmosphere is described by the following equation:

$$\frac{\partial \rho^* i^*}{\partial t} + div\,\rho^* i^* \vec{u}^* = -p^*\, div\vec{u}^* + div\left(K\,\overrightarrow{grad}\,T^*\right) + \phi + S \tag{11}$$

Where i^* is the internal energy of the fluid, K the thermal tensor of conductivity, T^* the temperature of the fluid, ϕ the quantity of heat generated per unit of volume and time as result of viscous dissipation and S the quantity of heat generated by any source in the fluid.
By admitting that the fluid behaves as a perfect gas [2], we will have:

$$i^* = C_V T^* \tag{12}$$

$$p^* = \rho^* \frac{R T^*}{M_a} \tag{13}$$

Where: R is the constant of perfect gases, C_V the specific heat at constant volume, and M_a the molar mass of air.
While introducing the equation (12) into the equation (11), it comes:

$$\frac{\partial(\rho^* C_V T^*)}{\partial t} + div(\rho^* C_V T^* \vec{u}^*) = -p^* div\vec{u}^* + div\left(K \overrightarrow{grad}\, T^*\right) + \phi + S \tag{14}$$

This equation is also written in form:

$$\frac{\partial(\rho C_V T)}{\partial t} + div(\rho C_V T \vec{u}) = -p\, div\vec{u} + div\left(K \overrightarrow{grad}\, T\right) + \phi + S + \left[-\frac{\partial\left(\rho C_V \overline{\tilde{u}\tilde{T}}\right)}{\partial x} - \frac{\partial\left(\rho C_V \overline{\tilde{w}\tilde{T}}\right)}{\partial z}\right] \tag{15}$$

2.1.3 Model of turbulence

The model of turbulence is a computing process to close the system made up of the equations of the flow (8-10) and the equation of transfer of the energy (15). In the present study, we chose the model suggested by Boussinesq [4].
There will be then the five following expressions:

$$-\rho \overline{\tilde{u}}^2 = 2\eta_t \frac{\partial u}{\partial x},\quad -\rho \overline{\tilde{w}}^2 = 2\eta_t \frac{\partial w}{\partial z},\quad -\rho \overline{\tilde{u}\tilde{w}} = \eta_t\left(\frac{\partial u}{\partial z} + \frac{\partial w}{\partial x}\right),\quad -\rho \overline{\tilde{u}\tilde{T}} = K_t \frac{\partial T}{\partial x},$$
$$-\rho \overline{\tilde{w}\tilde{T}} = K_t \frac{\partial T}{\partial z}$$

Where: η_t is the turbulent viscosity and K_t the turbulent thermal diffusivity. These two terms define the turbulent number of Prandtl/Schmidt:

$$\sigma_t = \frac{\eta_t}{K_t} \tag{16}$$

With:

$$\eta_t = \rho\, l_m^2 \left|\frac{\partial u}{\partial z}\right|$$

Where: l_m is the scale length.
Using these quantities the equations of flow of the fluid and transfer of energy become:

$$\frac{\partial \rho}{\partial t} + \frac{\partial \rho u}{\partial x} + \frac{\partial \rho w}{\partial z} = 0 \tag{17}$$

$$\frac{\partial\, \rho\, u}{\partial\, t} + \frac{\partial\, \rho\, uu}{\partial\, x} + \frac{\partial\, \rho\, u\, w}{\partial\, z} = -\frac{\partial\, p}{\partial\, x} + \eta \left[\frac{\partial^2 u}{\partial\, x^2} + \frac{\partial^2 u}{\partial\, z^2}\right] \tag{18}$$

$$+2\frac{\partial}{\partial x}\left(\rho l_m^2 \frac{\partial u}{\partial x}\left|\frac{\partial u}{\partial z}\right|\right) + \frac{\partial}{\partial z}\left(\rho l_m^2 \left(\frac{\partial u}{\partial z} + \frac{\partial w}{\partial x}\right)\left|\frac{\partial u}{\partial z}\right|\right) \tag{19}$$

$$\frac{\partial\, \rho\, w}{\partial\, t} + \frac{\partial\, \rho\quad wu}{\partial\, x} + \frac{\partial\, \rho\quad ww}{\partial\, z} = -\frac{\partial\, p}{\partial\, z} + \eta \left[\frac{\partial^2 w}{\partial\, x^2} + \frac{\partial^2 w}{\partial\, z^2}\right]$$

$$+\frac{\partial}{\partial x}\left(\rho l_m^2 \left(\frac{\partial u}{\partial z} + \frac{\partial w}{\partial x}\right)\left|\frac{\partial u}{\partial z}\right|\right) + 2\frac{\partial}{\partial z}\left(\rho l_m^2 \frac{\partial w}{\partial z}\left|\frac{\partial u}{\partial z}\right|\right) - \rho g \tag{20}$$

$$\frac{\partial(\rho C_V T)}{\partial t} + \frac{\partial(\rho C_V T u)}{\partial x} + \frac{\partial(\rho C_V T w)}{\partial z} = -p\frac{\partial u}{\partial x} - p\frac{\partial w}{\partial z}$$

$$+\frac{\partial}{\partial x}\left(K_{xx}\frac{\partial T}{\partial x} + K_{xz}\frac{\partial T}{\partial z}\right) + \frac{\partial}{\partial z}\left(K_{xz}\frac{\partial T}{\partial x} + K_{zz}\frac{\partial T}{\partial z}\right)$$

$$+\phi + S + \frac{\partial}{\partial x}\left(\rho\frac{C_V}{\sigma_t} l_m^2 \frac{\partial T}{\partial x}\left|\frac{\partial u}{\partial z}\right|\right) + \frac{\partial}{\partial z}\left(\rho\frac{C_V}{\sigma_t} l_m^2 \frac{\partial T}{\partial z}\left|\frac{\partial u}{\partial z}\right|\right)$$

2.2 Equation of the transport of aqueous solution

In the present study, we will treat the case of N species of concentration C_i^* in the fluid. The concentration C_i^* of each species i, at every moment, obeys the following transport equation:

$$\frac{\partial C_i}{\partial t} + u_j \frac{\partial C_i}{\partial x_j} + C_i \frac{\partial u_j}{\partial x_j} = \frac{\partial}{\partial x_k}\left(D^i_{kj} \frac{\partial C_i}{\partial x_j} + M_{kj} \frac{\partial C_i}{\partial x_j} \right) \tag{21}$$

$$+ S_i(x, z, t) + R_i(C_1, C_2, \ldots, C_N, T)$$

Where: R_i is the rate of generation of species i by the chemical reactions and S_i the rate of addition of species i at the moment t.
We consider in this study the chemical reactions hereafter and which are at the base of any modeling of the air pollution [5]:

$$NO_2 + h\nu \xrightarrow{k_1} NO + O(P^3)$$
$$O(P^3) + O_2 \xrightarrow{k_2} O_3$$
$$NO + O_3 \xrightarrow{k_3} O_2 + NO_2$$

k_1, k_2 and k3 are the coefficients, known, of the chemical reactions.

3 Method and process of resolution

3.1 Method of resolution

In this work, we chose the use of the finite Volumes Method [6].

3.2 Computing processes

Calculations are started with the values of velocities *u* and *w* exit of the initial profile. The solution of the equation (17) allows the determination of the bulk mass, ρ.
The knowledge of this value and the solution of the equations (18-19) allow the determination of the velocities *u* and *w*.
The temperature is then given starting from the solution of the equation (20). Using the law of perfect gases, we determine the pressure. The concentrations C_i are given using the solution of the equation (21).
The sizes *u* and *w* are then reappraised; their corrected values make it possible to reiterate and this until convergence of the solution.

4 Results

On figure 1, we present the variation of the pressure according to the height. We note that the pressure decreases with the height, this is in a perfect agreement with the results obtained by other authors [2].

The temperature Variation according to height is illustrated on figure 2. We notice on this figure that the temperature, also, decreases with the height. This can be explained by the fact that the atmosphere behave as a perfect gas and since the volume remains constant then, according to the law of perfect gas, the temperature must also decrease with height.

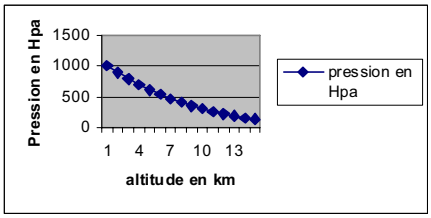

Fig 1: *Variation of the pressure according to the height*

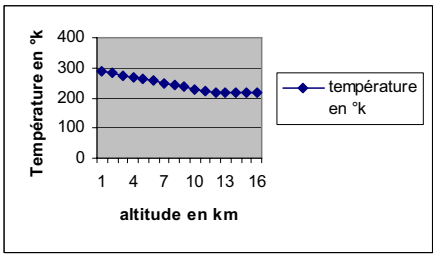

Fig 2: *Variation in the Temperature according to the height*

References

[1] Mac Rae G. J., Goodin W. R. et Seinfeld J. H., Numerical Solution Of Atmospheric Diffusion Equation For Chemically Reacting Flows, J. Comput. Phys., 45, pp. 1-42, (1982).

[2] Seinfeld J.M. et Pandis S.N., Atmospheric chemistry and physics from air pollution to climate change, Wiley, New-York, (1998).

[3] Anderson D. A., Tannehill J. C. et Pletcher R. H., 1984, Computational Fluid Mechanics And Heat Transfer, Hemisphere Publishing Corporation, Taylor & Francis Group, New York, (1984).

[4] Versteeg H. K. et Malalasekera W., An Introduction To Computational Fluid Dynamics. The Finite Volume Method, Longman Group Ltd., England, (1995).

[5] Verwer J.G., Hundsdorfer W. H. et Blom J. G., Numerical Time Integration For Air Pollution Models. Report MAS-R9825, (1998).

[6] Patankar S. V., Numerical Heat Transfer And Fluid Flow, Hemisphere Publishing Corporation, Taylor et Francis Group, New York, (1980).

Gain of Soret separation in binary mixture due to vibrations

D. E. Melnikov, V.M. Shevtsova

MRC, CP-165/62, Université Libre de Bruxelles (ULB)
50, Av. F.D. Roosevelt, B-1050 Brussels, Belgium.

Contact: dmelniko@ulb.ac.be

Abstract

Three-dimensional double-diffusive convection with Soret effect in a cubic cell filled with a binary mixture with positive Soret coefficient is considered under static and vibrational accelerations. The liquid is heated from above and is subjected to high frequency vibrations (the vibration period is much smaller than any characteristic time) perpendicular to the imposed temperature gradient. Two extreme situations are considered: weightlessness ($0g$) and Earth gravity ($1g$). Due to the Soret effect the lighter liquid is accumulated on the top of the heavier one and thus creating stable density stratification in the system.
The problem is investigated numerically by solving three-dimensional Navier-Stokes, energy, and concentration equations. Component separation due to the Soret effect is analyzed. While evolution of the constituents separation is a monotonously growing function of time regardless the static gravity, its saturation values are different. Compared to the value of the Soret separation achieved under conditions of absence of any flow in the liquid, vibrations alone decrease it via generating an mean thermo-vibrational convective flow, which mixes the liquid. Imposing vibrations under $1g$ enhances the separation, because the convection increases the imposed temperature gradient across the cell without mixing the liquid.

1 Introduction

A temperature gradient ∇T maintained through a multi-component liquid causes a diffusion phenomenon called the Ludwig Soret effect, resulting in separation of the constituents. The separation is counteracted by molecular diffusion, which in turn leads to mixing. Finally, a stable state will be attained in the system when a concentration profile is established in the domain. In ideal case of absence of any fluid motions, the established concentration profile is linear in the direction of the temperature gradient resulting in separation

$$\Delta\tilde{C} = -S_T C_0(1 - C_0)\Delta T, \tag{1}$$

where S_T and C_0 are the Soret coefficient and mass fraction of the considered component, ΔT is the imposed temperature difference. In our study we analyze a parameter called Soret separation

$$S_R = (C_{cold} - C_{hot})/\Delta\tilde{C}, \tag{2}$$

which is the difference of the mean concentrations at the cold and hot walls, scaled by $\Delta\tilde{C}$. It is believed that any convective liquids motion decreases the separation ($S_R < 1$). Shevtsova et al. [1] numerically investigated the effect of static gravity g perpendicular to ∇T in a wide range of gravity $0 < g/g_0 < 10^{-1}$, $g_0 = 9.81m/s^2$ is the earth gravity. They obtained that increasing gravity decreases the components separation. Coupling the static gravity with co-directed low frequency vibrations resulted in further decreasing the Soret separation. Heating the binary mixture with negative S_T from above leads to instability because the heavier component gets accumulated above the lighter one. As a result it triggers convection, and the components separation decreases [2]. When heated from above, the instability never occurs in a solution with positive S_T but external vibrations can influence S_R.

Vibrational convection refers to the specific flows that appear when a fluid with density gradient is subjected to external vibrations [3]. It is called thermo-vibrational convection in case of temperature non-homogeneity. It is shown that the flow can be represented as a superposition of a quick part, which oscillates with the frequency of vibration, and of a slow timeaverage part (mean flow). The mean flow shows how the liquid particles are drifting. And this is through the resulting mean flow that vibrations influence both temperature and concentration fields.

In this paper we will show that thermo-vibrational convection may favourize the thermodiffusion, and the Soret separation obtains values higher unity, i.e. $S_R > 1$.

2 Governing equations and boundary conditions

The following dimensionless nonlinear time-dependent momentum, energy, mass and continuity equations governing the evolution of the system are solved:

$$\frac{\partial \mathbf{v}}{\partial t} + \mathbf{v}\nabla\mathbf{v} = -\nabla p + \nabla^2\mathbf{v} - \frac{Ra_{st}\mathbf{e_z} + Ra_{os}cos(\omega t)\mathbf{e_x}}{Pr}\left(\Theta + \psi c\right), \tag{3}$$

$$\frac{\partial \Theta}{\partial t} + \mathbf{v}\nabla\Theta = \frac{1}{Pr}\nabla^2\Theta, \tag{4}$$

$$\frac{\partial c}{\partial t} + \mathbf{v}\nabla c = \frac{Le}{Pr}\left(\nabla^2 c - \nabla^2\Theta\right) \tag{5}$$

$$\nabla \cdot \mathbf{v} = 0. \tag{6}$$

here ψ is the separation ratio, $\mathbf{e_z}$ is the unit vector directed upwards. The system is heated from above under either weightlessness ($0g$) or g_0. The velocity, time, pressure and temperature scales are respectively $V_{ch} = \nu/L$, $t_{ch} = L^2/\nu$, $P_{ch} = \rho_0 V_{ch}^2$, $\Delta T = T_{hot} - T_{cold}$ (Fig. 1). The size of the cell $L = 0.01m$ is used as a length scale, ν is the liquid kinematic viscosity and ρ_0 stands for the liquid density at T_{cold}. The mass fraction is scaled by $C_{ch} = \Delta\tilde{C}$ (see eq. (1)).
The *stationary* Rayleigh number $Ra_{st} = (g\beta_T L^3 \Delta T)/(\nu a) < 0$, β_T is the thermal expansion coefficient, a is the thermal diffusivity. $Ra_{os} = Ra_{st}(A\omega^2)/g$ is *oscillatory* Rayleigh number due to vibrations. Imposed vibrations are perpendicular to the density gradient with displacement amplitude of $A = 2.5cm$ and of frequency f either 1 or $2Hz$, yielding $Ra_{os} = 23\,300$ and $93\,300$ respectively and $\omega = 2\pi f t_{ch}$ to be either 165.37 or 330.74. Ra gets values according to the static gravity, i.e. either 0 or $233\,600$. The Prandtl and Lewis numbers are defined as $Pr = \nu/a$ and $Le = D/a$, D is the diffusion coefficient.

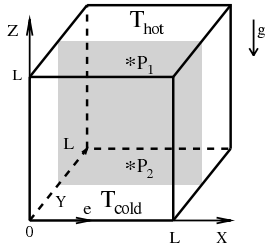

Fig. 1: *Geometry of the problem*

The simulations were performed in a cubic cell (Fig. 1) with $Pr = 44.7$ and $\psi = 0.44$, which correspond to 50% water - isopropanol solution. Lewis number in eq.(5) equals $Le = 0.01$. Initially the mixture is homogeneous with the mass fraction of the heavier component (water) $C_0 = 0.5$. Due to the Soret effect the lighter liquid is accumulated on the top of the heavier one and thus creating stable density stratification.
Boundary conditions include: zero velocity at the rigid walls $\mathbf{v} = 0$; constant temperatures at the top and bottom $\Theta(z = 0) = 0, \quad \Theta(z = 1) = 1$; thermally insulated lateral walls: $\partial_y \Theta(y = 0, 1) = \partial_x \Theta(x = 0, 1) = 0$. Absence of mass flux at the impermeable rigid walls gives: $\partial_n(c - \Theta) = 0$.

3 Results and Discussion

Response of the Soret separation S_R to imposed vibrations depends on the stationary gravity level. Figure 2 shows steady value of S_R obtained after long computations as a function of the frequency f of vibrations. Increasing f makes S_R to deviate more from unity (dotted line). In absence of gravity the separation is diminishing, while under Earth gravity S_R is increasing. However, the increase is not as strong as the decrease (only 14% versus 47% respectively).
We discovered that these different behaviors are due to different mean thermo-vibrational flow structures. Analysis of the mean flow and of the concentration distribution is performed at the end of the calculations when the Soret separations attains steady value. The

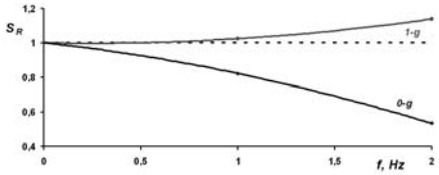

Fig. 2: *Soret separation as function of frequency of imposed vibrations. Dotted line shows unity, the value of S_R obtained in absence of any liquid flow.*

mean flow, concentration and temperature are calculated via a common procedure of averaging the appropriate variable over time within one vibrational period $1/f$. The mean flow in case of $f = 2Hz$, as visualized by arrows, is presented on Figs. 3(a) and 4(a).

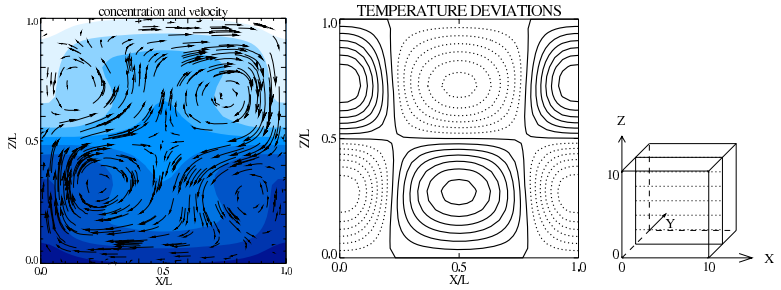

(a) (b)

Fig. 3: $0g$, $2Hz$*: (a) - mean flow (arrows) and concentration (colors); (b) - deviations of mean temperature from linear profile, dotted and solid lines show negative and positive values.*

In line with the theoretical findings of [3], a four vortices mean flow is observed under $0g$. However, under $1g$ the mean flow has a one vortex structure (compare Figs. 3(a) and 4(a)). The two flows, while having close values of maximum velocity ($6.1 \cdot 10^{-6} m/s$ under $0g$ and $4.8 \cdot 10^{-6} m/s$ under $1g$), differ by direction of displacement of the liquid along z axis. In the central part, the four-vortices motion brings colder liquid towards the hot wall the warmer one towards the cold wall. Near the lateral walls, a reversed liquid's displacement takes place. As a result, the temperature gradient across the cell is decreased in the center (Fig. 3(b)) and is increased in the adjacent to the lateral walls regions, but the net temperature gradient's variation is zero. At the same time, because of the absence of gravity the four vortices mean flow mixes the liquid and thus deacreases concentration near the cold and hot walls. Finally, $(C_{cold} - C_{hot})$ becomes smaller than $\Delta\tilde{C}$ (defined in eq. (1)), and $S_R \sim (C_{cold} - C_{hot})$ gets smaller than unity.
The one vortex flow in turn increases the imposed temperature gradient across the cell (see Fig. 4(b)) and thus helps the separation due to the thermodiffusion. The convective mass transport is however zero. The flow tries to displace colder and heavier liquid upwards along the $x = 1$ wall and the warmer and lighter one downwards along the opposite wall,

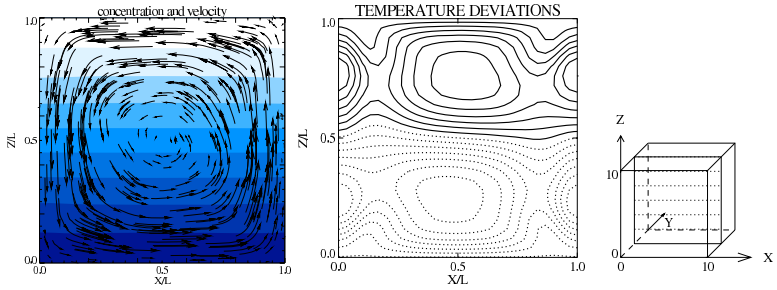

(a) (b)

Fig. 4: $1g, 2Hz$*: (a) - mean flow (arrows) and concentration (colors); (b) - deviations of mean temperature from linear profile, dotted and solid lines show negative and positive values.*

but this initiative meets an immediate counteraction of buoyancy. The concentration field stays unperturbed (Fig. 4(a)).
In can be concluded that the two cases have different mechanisms influencing the separation. Mixing due to convection (Fig. 3(a)) resulting in mass transport, which decreases S_R under $0g$. Under $1g$, it is the increased temperature gradient inside the liquid due to the convection (Fig. 4(b)) that is intensifying the thermodiffusion, which increases S_R. One can suggest that if the imposed vibrations generate a flow strong enough for overpowering the buoyancy, the Soret separation will be decreased even under non-zero gravity.

4 Conclusions

Separation of the constituents due to the Soret effect in a cubic cell filled with a binary mixture is numerically investigated. We found that the thermo-vibrational convection due to imposed vibrations decreases the separation of the components in weightlessness. However, it helps the separation under $1g$ making it stronger than in absence of liquid flow. Increasing the vibrational stimuli helps the constituents to separate even more.

Acknowledgment

This work is supported the PRODEX Programme managed by the European Space Agency in collaboration with the Belgian Federal Science Policy Office.

References

[1] V. M. Shevtsova, D. E. Melnikov, J. C. Legros, Y. Yan, Z. Saghir, T. Lyubimova, G. Sedelnikov, B. Roux, Physics of Fluids **19**, 017111 (2007)

[2] D. E. Melnikov, A. Mialdun, V. M. Shevtsova, J. Nonequilibrium Thermodynamics, **32**, 1 (2007)

[3] G. Z. Gershuni, and D. V. Lyubimov, *Thermal Vibration Convection*, (John Wiley & Sons Ltd., 1998)

Spatio-temporal dynamics near the onset of convection for binary mixtures in cylindrical containers

Isabel Mercader[1], Arantxa Alonso[1] and Oriol Batiste[1]

[1] Dep. Física Aplicada, Univ. Politècnica de Catalunya, Barcelona, Spain

Contact: isabel@fa.upc.edu, arantxa@fa.upc.edu, oriol@fa.upc.edu

Abstract

Pattern selection near the onset of convection in a cylindrical container heated from below is investigated numerically for a water-ethanol mixture considering parameter values and boundary conditions relevant to experiments.The onset of convection occurs via a subcritical Hopf bifurcation in which the critical mode is strongly influenced by small variations of the aspect ratio of the cell. Simulations for subcritical and supercritical Rayleigh numbers reveal differences in the dynamics. Very close to the critical value, convection is erratic and focuses along one or more diameters of the cell; growths and collapses of the convection amplitude take place, but convection eventually dies away for subcritical values and persists for slightly supercritical values. For larger supercritical values convection grows progressively in amplitude, expanding slowly until a large-amplitude state is reached. Depending on the reduced Rayleigh number the final state can be a non-steady state filling the cell or a disordered confined state.

1 Introduction

Convection in vertically heated binary-liquid mixtures is an excellent system for the study of pattern formation, especially for negative separation ratio mixtures, $S < 0$. In such mixtures, the primary bifurcation is subcritical and gives rise to a state of oscillatory convection. With the aim of analyzing the dynamics in truly three-dimensional geometries, several experiments on cylindrical cells have been done [1–3]. The results of these experimental works indicate that new behavior prevails. Waves that travel in the radial direction are present, and traveling-wave convection patterns typically consist of several competing domains of traveling waves propagating in different directions. Transient localized pulses of traveling-wave convection similar to the states found in annular cells were observed, but these pulses either decayed back to pure conduction or grew to fill the cell. The numerical work on this system is scarce [4], since these types of three-dimensional computations are very costly. The high performance achieved by present computers makes it possible nowadays to address fully three-dimensional computations. In a recent paper [5], we have simulated the Boussinesq 3D equations for binary fluid convection for cylinders of aspect ratio $\Gamma = 11$ and $\Gamma = 10.5$ ($\Gamma \equiv R/d$, where R is the radius of the cell and d its height). The main results and achievements of this work are summarized in these proceedings.

2 Results and Discussion

We present numerical 3D simulations of convection in binary fluids with a negative separation ratio confined to a vertical cylinder in the neighborhood of the initial oscillatory instability. We consider a S=-0.09 water-ethanol mixture (Prandtl number $\sigma = 24$) in cells of aspect ratio $\Gamma = 11$ and $\Gamma = 10.5$. The choice of parameters in this paper is motivated by the experiments performed by Lerman et al. [1–3] on $S \approx -0.08$ mixtures in cylindrical cells of aspect ratio $\Gamma = 10.91, 11.53$.

To perform the simulations, we have developed a highly efficient time-evolution spectral code that solves the full convection equations in primitive variables and cylindrical coordinates [6, 7]. Despite this, and the increasing power of present computers, it is worth emphasizing that 3D computations on binary mixtures in moderate/large aspect ratio cells, such as the ones we consider, remain extremely costly.

The linear evolution is strongly influenced by the aspect ratio of the cell: while odd azimuthal Fourier modes dominate the dynamics in the $\Gamma = 11$ cell, even modes control the early stages of evolution in the $\Gamma = 10.5$ case. However, modes with wave-number higher than the critical one tend to grow at much faster rates and dominate the nonlinear regime, as observed in the experiments [3]. During the nonlinear evolution, after the earlier stages of convection, the system goes through a variety of states (see 1). Although the primary bifurcation is known to be subcritical, for subcritical values of the Rayleigh number, R, convection dies away after some bursting episodes ($R = 1916, \Gamma = 11$). For slightly supercritical Rayleigh numbers, the system can exhibit small amplitude bursting behavior ($R = 1918, \Gamma = 11$) for a long time (growths and collapses of convection amplitude take place), in a way that bears a strong resemblance to the dispersive chaotic states observed in large aspect ratio annular containers for small negative values of the separation ratio [8, 9]. For supercritical values, the system evolves to form large amplitude

localized states, which can combine stationary, traveling wave and quiescent regions. The Nusselt number, a mesure of the heat transport, increases progressively while blobs of disordered convection form around the cell center convection.On some occasions, these blobs evolve filling slowly the whole cell with domains of large amplitude nearly stationary rolls.($R = 1934, \Gamma = 11$). On other occasions, when the cell is almost filled, quiescent regions grow again and the system evolve, decreasing the Nusselt number, toward a confined structure ($R = 1925, \Gamma = 10.5$) .

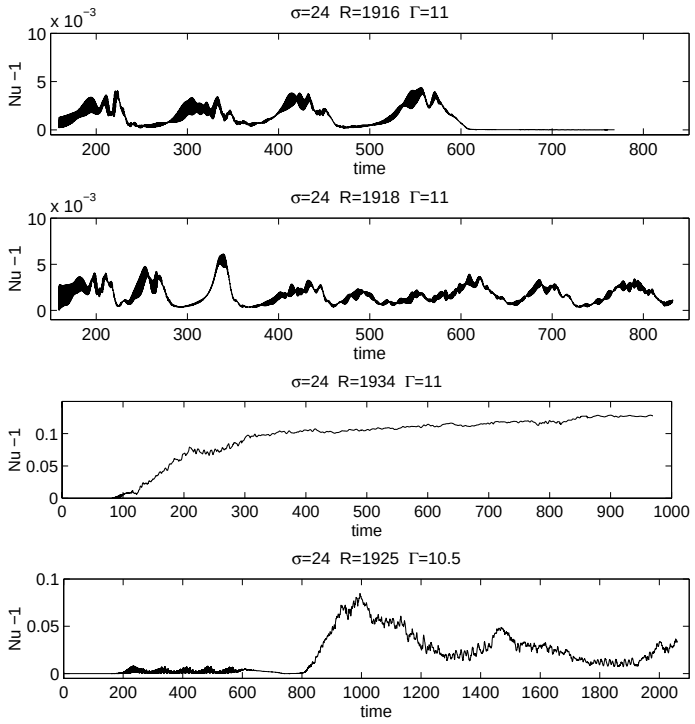

Fig. 1: *Times series (Nusselt number versus time) showing the amplitude of convection for different solutions during the nonlinear evolution. a)* $R = 1916, \Gamma = 11$*, b)* $R = 1918, \Gamma = 11$*, c)* $R = 1934, \Gamma = 11$ *and d)* $R = 1925, \Gamma = 10.5$*.*

In contrast to pure fluid convection, cylindrical binary fluid convection exhibits a clear tendency to form localized and highly confined structures embedded in a background of quiescent fluid. The diversity of confined patterns is startling. On one hand, small amplitude states consisting of stripes of convection aligned along one or more cell diameters or radii, are observed during the early transients for subcritical and slightly supercritical values of the control parameter. Also in this regime, when the system exhibits bursting behavior, convection can take the form of tiny highly localized pulses that are surrounded by a conductive state (see Fig. 2).
On the other hand, for larger values of the Rayleigh number, transitory localized pat-

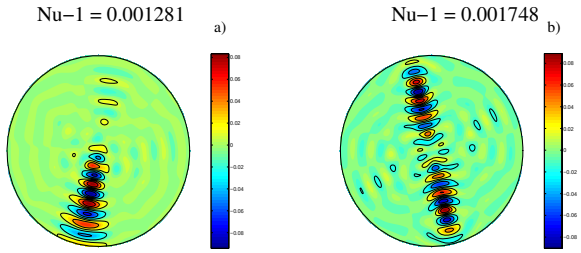

Fig. 2: *(Color on line) Contour plots of temperature at mid height, for two states in the small amplitude bursting behaviour, showing the azimuthal focusing along one radius and a diameter of the cell. The value of the Rayleigh number is in a) slightly supercritical (*$R = 1919, \Gamma = 10.5$*), and in b) slightly subcritical, (* $R = 1914, \Gamma = 11$*).*

terns can consist of oscillatory regions of squares, disordered blobs of oscillatory convection and competing domains of traveling waves and steady convection. However, states of confined convection could be persistent as suggested by our simulations for $R = 1925, \varepsilon = 3.974 \times 10^{-3}$ in a $\Gamma = 10.5$ cylinder, (see Fig. 3a). These states are wall attached, extremely nonlinear and appear after the collapse of an almost cell-filling state. Finally, for slightly greater Rayleigh numbers the system evolves slowly to a cell-filling state of convection rolls (see Fig. 3b). Although the time scale of our simulations is bigger than the experimental one, we have not reached a completely stationary state.

3 Conclusions

The dynamics observed within a narrow range of Rayleigh numbers around the onset of convection is of unquestionable complexity, but general agreement between the reported experimental observations and our numerical results is obtained, although some differences have also been found. The differences are probably due to non-Boussinesq effects, which can be important in experiments [2], but are not taken into account in our simu-

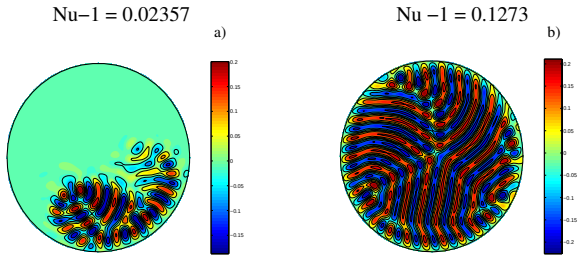

Fig. 3: *(Color on line) Contour plots of temperature at mid height, for two states of large amplitude in the supercritical regime. a) Persistent localized state for* $R = 1924, \Gamma = 10.5$*, and b) non-steady cell-filling state for* $R = 1934, \Gamma = 11$.

lations. The most interesting result is the tendency to form localized structures. Such patterns are continuously evolving and combine domains of traveling waves and quasi-steady convection. The highly nonlinear localized states can be persistent in time, as suggested by our simulations for $R = 1925$ in a $\Gamma = 10.5$ cylinder, and $R = 1924$ in $\Gamma = 11$ (not shown here), contrary to what has been observed experimentally.

Acknowledgment

This work is supported by DGICYT under grant FIS2006-08954 and by AGAUR under grant 2005SGR-0024.

References

[1] Lerman K., Bodenschatz E., Cannell D.S., and Ahlers G., Phys. Rev. Lett. **70(23)**, p 3572 (1993).
[2] Lerman K., Ahlers G., and Cannell D. S., Phys. Rev.E **53(3)**, R2041 (1996).
[3] Lerman K., Cannell D.S., and Ahlers G., Phys. Rev. E **59(3)**, 2975 (1999).
[4] Ch. Jung, and B. Huke and M. Lücke, Phys. Rev. Lett **81**, 3651(1998).
[5] Mercader I., Alonso A., and Batiste O., Phys. Rev. E **77**, 036313 (2008).
[6] Marqués F., Mercader I., Batiste O., and López J., J. Fluid Mech. **580**, 303 (2007).
[7] López J., Marqués F., Mercader I., and Batiste O., J. Fluid Mech. **590**, 187 (2007).
[8] Kolodner P., Slimani S., Aubry N., and Lima R., Physica D **85**, 165 (1995).
[9] Alonso A., Batiste O., Meseguer A., and Mercader I., Phys. Rev. E **75**, 026310 (2007).

Marangoni convection in binary and nano-fluids in the presence of the Soret effect

Alla Podolny[1], Alex Nepomnyashchy[1 2] and Alex Oron[3]

[1]Department of Mathematics, Technion, Haifa 32000, Israel
[2]Minerva Center for Nonlinear Physics of Complex Systems, Technion, Israel
[3]Department of Mechanical Engineering, Technion, Haifa 32000, Israel.

Contact: asspekto@tx.technion.ac.il

Abstract

Investigation of the Marangoni convection in binary fluids in the framework of linear stability theory was started several decades ago. One of the most promising applications of the Marangoni flow in binary solutions is the use of these working fluids in heat pipes under reduced gravity conditions. Recently a new class of fluids, nanofluids, has been successfully applied in heat transfer devices. We consider a relatively thick fluid layer under terrestrial gravity conditions subjected to a transverse temperature gradient. A concentration gradient is induced due to the Soret effect. Therefore, in such layers a combined Rayleigh-Marangoni convection takes place, while the deformation of free surface is irrelevant. We show that the correct model for the description of the hydrodynamics and heat transfer in nanofluids is identical to the system of equations for binary mixture with the Soret effect in the limit of asymptotically small Lewis numbers L. We study the case of the long-wave instability of the system with poorly conducting boundaries in the limit of asymptotically small Lewis numbers. The behavior of the critical Marangoni and Rayleigh numbers depends on the relationship between the small parameters of the problem. We consider L as a basic small parameter, while the smallness of wave number k and Biot number Bi with respect to L can be different. Our approach is novel and it potentially unfolds the entire picture for small- L fluids. Consideration of the nanofluids, even in the framework of the binary-fluid model, calls for solution of new non-trivial mathematical problems. In the framework of the new approach, a typical behavior of monotonic and oscillatory instability boundaries is investigated in various limits of parameters.

Investigation of the Marangoni convection in binary fluids in the framework of a linear stability theory was started several decades ago [1]. Recently, a new class of fluids, nanofluids, has been successfully applied in heat transfer devices. Nanofluids are suspensions of nanoparticles (e.g. carbon, metals and metal oxides) in the size range of about 10 to 50 nm in a carrier fluid (e.g. water, ethylene glycol and lubricants). From the point of view of dynamics and heat/mass transfer, a typical nanofluid behaves as a Newtonian binary fluid with an extremely small Lewis number ($L \leq 10^{-4}$) and high Soret coefficient [2-4]. While a significant progress has been made on the buoyancy convection in nanofluids [2-8], including binary nanofluids [9-12], the Marangoni convection in nanofluids is still hardly investigated, though an essential influence of nanoparticles on surface tension has been revealed in some experiments [13-15]. The latter phenomenon can be significant for applications of nanofluids in boiling devices [13], including those used in microgravity conditions.

In order to develop a realistic two-component model for transport phenomena in nanofluids it is important to understand the mechanisms by which the nanoparticles move relatively to the carrier fluid. According to the estimations in the paper of [16] Brownian diffusion and thermophoresis may become important as a slip mechanisms while gravity settling is negligible. Thus, the diffusion mass flux for the nanoparticles can be written as the sum of the two components: the first one is proportional to the concentration gradient, referred to as "diffusion", while the second one is proportional to the temperature gradient, referred here as to "Soret effect".

$$\vec{j}_p = \vec{j}_{p,B} + \vec{j}_{p,T} = -\rho_p D_B \nabla c - \rho_p D_T \frac{\nabla \vartheta}{\vartheta}. \tag{1}$$

Here $D_B = \dfrac{k_B\,\vartheta}{3\,\pi\,\mu\,d_p}$ is Brownian diffusion coefficient that ranges from 4×10^{-10} to $4 \times 10^{-12}\ m^2/s$, k_B is the Boltzmann's constant, ϑ is temperature, μ is dynamic viscosity of the fluid ($\mu \sim 1\ mPa\ s$), d_p is a nanoparticle diameter $d_p < 100\ nm$, ρ_p is the mass density of the nanoparticles ($\rho_p \sim 4\ g/cm^3$), c is nanoparticle volumetric fraction, $D_T = \delta \dfrac{\mu}{\rho}\, c$, is "thermal diffusion coefficient", $\delta = \delta(k_{th}, k_{th}^{(p)})$ is the dimensionless parameter depending on thermal conductivities of the fluid k_{th} and particle material $k_{th}^{(p)}$. For alumina nanoparticles, in water $\delta \sim 0.006$.

We consider a fluid layer in terrestrial gravity conditions subjected to a transverse temperature gradient. Concentration gradient is induced due to the Soret effect. The layer is exposed to the ambient gas phase at its nondeformable free surface.

The system of governing equations consists of continuity equation, Navier-Stocks equation, energy equation and convection-diffusion equation, respectively

$$\nabla \cdot \vec{v} = 0, \tag{2}$$

$$\vec{v}_t + (\vec{v} \cdot \nabla)\vec{v} = -\rho_0^{-1} \nabla\, p + \nu\, \nabla^2 \vec{v} \tag{3}$$

$$\vartheta_t + \vec{v} \cdot \nabla \vartheta = \kappa \nabla^2\, \vartheta + \frac{\rho_p\, \eta_p}{\rho\, \eta} \left\{ D_B \nabla c \cdot \nabla \vartheta + D_T \frac{\nabla \vartheta \cdot \nabla \vartheta}{\vartheta} \right\} \tag{4}$$

$$c_t + \vec{v} \cdot \nabla c = \nabla \left\{ D_B\, \nabla c + D_T \frac{\nabla \vartheta}{\vartheta} \right\}. \tag{5}$$

Here, $\vec{v}$, ϑ, c are, respectively, the velocity, temperature and concentration fields in the fluid, ν is kinematic viscosity, κ - thermal diffusivity, ρ is fluid density ($\rho \sim 1\, g/cm^3$), η is nanofluid specific heat, η_p is nanoparticle specific heat. The equation (4) states that heat can be transported in nanofluids by convection (second term on the left-hand side), conduction (first term on right-hand side) and also by nanoparticle diffusion (second, third terms on right-hand side). It should be noted that two last terms on the right-hand side in the nanofluid energy equation (4) account for the additional contribution associated with the nanoparticle motion relative to the base fluid. The equation (5) states that nanoparticles can move homogeneusly with the fluid (second term on left-hand side), but they also possess a slip velocity relatively to the fluid due to Brownian diffusion and thermophoresis.

In the framework of our theory we consider two convection mechanisms. First, surface tension is assumed to depend on both temperature and particle concentration, so both thermo- and soluto -capillary effects are taking into account.

$$\sigma(\vartheta, c) = \sigma_0 - \sigma_t(\vartheta - \vartheta_0) + \sigma_c(c - c_0), \tag{6}$$

where $\sigma_0 = \sigma(\vartheta_0, c_0)$ is reference value of surface tension, $\sigma_t = -\partial\sigma/\partial\vartheta, \quad \sigma_c = \partial\sigma/\partial c$. Second, the liquid density ρ is assumed to depend on both the temperature ϑ and particle concentration c,

$$\rho = \rho_0[1 - \widetilde{\beta}(\vartheta - \vartheta_0) - \widetilde{\gamma}(c - c_0)], \tag{7}$$

where ρ_0, ϑ_0, c_0 are, respectively, reference values of density, temperature and solute concentration, $\widetilde{\beta} = -\dfrac{1}{\rho_0}\left(\dfrac{\partial\rho}{\partial\vartheta}\right)_p$, $\widetilde{\gamma} = -\dfrac{1}{\rho_0}\left(\dfrac{\partial\rho}{\partial c}\right)_p$. Thus, the effect of buoyancy is also included in the analysis. Therefore, a combination of Rayleigh and Marangoni convection takes place here.

To estimate the relative importance of the various transport mechanisms in nanofluids, it is useful to make the governing equations non-dimensional. For this purpose, we use the following scaling.

$$\begin{gathered} t \to \frac{h_0^2}{D}t,\ (x,z) \to h_0(x,z),\ (u,w) \to \frac{D}{h_0}(u,w), \\ \vartheta \to \vartheta_\infty + ah_0T,\ ah_0 = \Delta\vartheta,\ c \to \alpha a h_0 C,\ p \to \frac{\mu D}{h_0^2}p. \end{gathered} \tag{8}$$

Equations (2-5) take form

$$\begin{gathered} \nabla\cdot\vec{v} = 0, \\ P^{-1}L[\vec{v}_t + (\vec{v}\cdot\nabla)\vec{v}] = -\nabla p + \nabla^2\vec{v}, \\ T_t + \vec{v}\cdot\nabla T = L^{-1}\nabla^2 T + K_C\nabla C\cdot\nabla T + K_T\nabla T\cdot\nabla T, \\ C_t + \vec{v}\cdot\nabla C = \nabla^2 C + F_T\nabla^2 T. \end{gathered} \tag{9}$$

Let us carry out order-of-magnitude estimations of the contribution of each term in the right-hand side of non-dimensional nanofluid energy equation:

$$K_C = \frac{\rho_p\,\eta_p}{\rho\,\eta}\cdot\frac{D_T}{D}\cdot\alpha\,\Delta\vartheta \sim 10,\ K_T = \frac{\rho_p\,\eta_p}{\rho\,\eta}\cdot\frac{D_T}{D}\cdot\frac{\Delta\vartheta}{\vartheta_\infty} \sim 10,\ K_C,\ K_T \ll L^{-1} \sim 10^7. \tag{10}$$

One can see that heat transfer associated with nanoparticle dispersion is negligible, as compared with heat conduction and convection. Note, that the Soret effect can not be neglected:

$$F_T = \frac{D_T}{D} \cdot \frac{1}{\vartheta_\infty} \cdot \frac{1}{\alpha} \sim 1. \tag{11}$$

Here we used the values of parameters shown above and temperature difference $\Delta\vartheta = 10\,K$, while the temperature of the ambient gas phase is $\vartheta_\infty = 300\,K$. Therefore, the correct model for the description of the hydrodynamics and heat and mass transfer in nanofluids is identical to the system of equations for a binary mixture with the Soret effect:

$$\begin{gathered} \nabla \cdot \vec{v} = 0, \\ P^{-1}L[\vec{v}_t + (\vec{v}\cdot\nabla)\vec{v}] = -\nabla p + \nabla^2\vec{v} + R_{th}\,(T-\overline{T})\cdot\vec{e}_z + R_c\,(C-\overline{C})\cdot\vec{e}_z, \\ L(T_t + \vec{v}\cdot\nabla T) = \nabla^2 T, \\ C_t + \vec{v}\cdot\nabla C = \nabla^2 C + \nabla^2 T. \end{gathered} \tag{12}$$

Here buoyancy effect is also incorporated. The boundary conditions at the bottom rigid surface $z = 0$ reflect the no-slip condition for the velocities, a specified heat flux and mass impermeability.

$$z = 0: \quad \vec{v} = 0, \quad T_z = -1, \quad C_z = 1, \tag{13}$$

At the free non-deformable liquid-gas interface, the boundary conditions are, respectively, the kinematic boundary condition, heat and mass flux balance, and balance of tangential stresses.

$$\begin{gathered} z = 1: \quad \vec{v}\cdot\vec{e}_z = 0, \quad T_z + Bi\,T = 0, \quad C_z - Bi\,T = 0, \\ \partial_z u = M_c C_x - M_{th} T_x. \end{gathered} \tag{14}$$

The dimensionless parameters of the problem are given as $P = \dfrac{\nu}{\kappa}$ - Prandtl number, $L = \dfrac{D}{\kappa}$ - Lewis number, $Bi = \dfrac{qh_0}{k_{th}}$ - Biot number, $M_{th} = \dfrac{\sigma_t a h_0^2}{\mu D}$ -thermal Marangoni number, $M_c = \dfrac{\alpha\sigma_c a h_0^2}{\mu D}$ - concentration Marangoni number, $\chi = \dfrac{M_c}{M_{th}} = \dfrac{\alpha\sigma_c}{\sigma_t}$ - Soret number, $R_{th} = \dfrac{g\widetilde{\beta} a h_0^4}{D\nu}$ - thermal Rayleigh number, $R_c = \dfrac{g\widetilde{\gamma}\alpha a h_0^4}{D\nu}$ - concentration Rayleigh number, $\varphi = \dfrac{R_c}{R_{th}} = \dfrac{\alpha\widetilde{\gamma}}{\widetilde{\beta}}$ - buoyancy separation number, $\Sigma = \dfrac{\sigma h_0}{\mu\kappa}$ - inverse capillary number.

We consider linear stability analysis of the base state given by

$$\begin{gathered} \vec{v}_0 = 0, \;\; T_0 = -z + \frac{1+Bi}{Bi}, \\ C_0 = z, \;\; p_0 = (R_c - R_{th})\frac{z^2}{2} + const\cdot z + const. \end{gathered} \tag{15}$$

We introduce stream function ψ, so that $u = \psi_z, \quad w = -\psi_x$.

A two-dimensional linear problem for a non-deformable interface is solved using normal modes for perturbation functions.

$$(u, w, p, T, C, \psi) = (\widetilde{u}(z), \widetilde{w}(z), \widetilde{p}(z), \widetilde{T}(z), \widetilde{C}(z), \widetilde{\psi}(z))e^{ikx+\omega t}, \tag{16}$$

where k and ω are wave number and growth rate of the disturbances, respectively.
As a result, we obtain the following linear problem for perturbation functions

$$\begin{gathered}\omega\, P^{-1}\, L(\widetilde{\psi}'' - k^2\widetilde{\psi}) = \widetilde{\psi}'''' - 2k^2\widetilde{\psi}'' + k^4\widetilde{\psi} - i\,k\,R_{th}\,\widetilde{T} - i\,k\,R_c\,\widetilde{CT}, \\ L\,[\omega\widetilde{T} + ik\widetilde{\psi}] = -k^2\widetilde{T} + \widetilde{T}'', \\ \omega\widetilde{C} - ik\widetilde{\psi} = -k^2\widetilde{C} + \widetilde{C}'' + \chi(-k^2\widetilde{T} + \widetilde{T}''),\end{gathered} \tag{17}$$

with boundary conditions at $z = 0$:

$$\widetilde{\psi} = \widetilde{\psi}' = 0, \quad \widetilde{T}' = \widetilde{C}' = 0, \tag{18}$$

and at $z = 1$:

$$\begin{gathered}\widetilde{\psi} = \widetilde{\psi}' = 0, \quad \widetilde{T}_z + Bi\,\widetilde{T} = 0, \quad \widetilde{C}_z - Bi\,\widetilde{T} = 0, \\ \widetilde{\psi}'' = ik\,(M_c\widetilde{C} - M_{th}\widetilde{T}),\end{gathered} \tag{19}$$

We study the case of long-wavelength Marangoni+Rayleigh convection of the system with poorly conducting boundaries in the limit of asymptotically small Lewis numbers. The behavior of the critical Marangoni number is determined by the relationships between the Biot, Lewis and wave numbers. In order to obtain the full neutral curve we consider several distinguished limits. First we consider long-wave monotonic instability threshold in the case when $Bi \sim L$. In this limit two subcases are considered: $k^2 \sim L$ and $k^4 \sim L$. In the leading order of approximation, we obtain the following expression for the monotonic instability threshold for both limits

$$1 - \frac{\chi\, M_0}{48} + \frac{\varphi\, R_0}{320} = 0, \tag{20}$$

Introducing the Bond number $B = R_{th}/M_{th}$ we obtain

$$M_0 = \frac{960}{-3\,B\,\varphi + 20\,\chi}. \tag{21}$$

A second order correction in the subcase $k^4 \sim L$, i.e., $k = \varepsilon\, K,\ L = \varepsilon^4\, l,\ Bi = \varepsilon^4\,\beta$ is given by

$$M_2 = \frac{-640\,K^2\ (261\,B^2\,\varphi^2 - 3608\,B\,\varphi\,\chi + 9240\,\chi^2)}{231\,(3\,B\,\varphi - 20\,\chi)^3}. \tag{22}$$

Therefore, long-wave monotonic instability with $k_c = 0$ sets when $B\,\varphi/\chi < 3.3945$ and when $B\,\varphi/\chi > 10.4292$. In the other subcase $k = \varepsilon\, K,\ L = \varepsilon^2\, l,\ Bi = \varepsilon^2\,\beta$, the second order correction to the monotonic instability threshold is written as

$$M_2 = A\,K^2\left[1 - \frac{F}{K^2 + \beta}\right], \tag{23}$$

where

$$A = \frac{M_2|_{K^4 \sim L}}{K^2}, \quad F = \frac{693\, l\, (3\, B\, \varphi - 20\, \chi)(3\, B(\varphi - 1) - 20\, (1 + \chi))}{522\, B^2\, \varphi^2 - 7216\, B\, \varphi\, \chi + 18480\, \chi^2} \tag{24}$$

Our analysis shows that in this limit in the regions of parameters $B\,\varphi/\chi < 3.3945$ and $B\,\varphi/\chi > 10.4292$ the monotonic neutral curve has minimum of the absolute value in the long-wave region either at finite $K_c^{(\beta)} = \sqrt{\sqrt{F^{(\beta)}} - 1}$ for $F^{(\beta)} > 1$ or the minimum is attained at $K_c^{(\beta)} = 0$ for $F^{(\beta)} \leq 1$, here $K_c^{(\beta)} = K/\sqrt{\beta},\ F^{(\beta)} = F/\sqrt{\beta}$. It should be noted that the previous limit is particular case of the latter one for when K tends to infinity.

The onset of long-wave oscillatory instability in the framework of linear stability theory is further investigated and the domains of the parameters, where destabilization of the neutral curve takes place with the growth of the wave number K are determined in terms of Soret number, separation ratio and Rayleigh number.

A typical behavior of monotonic and oscillatory instability thresholds is investigated in the all distinguished limits of parameters. Finally, investigation of Marangoni convection is considered in the case of sufficiently thin films, when buoyancy is neglected. Comparison of the obtained results shows drastic changes of the instability criteria in the case of combined Marangoni+Rayleigh convection.

References

[1] J.L.Castillo , M.G.Velarde, Phys. Lett. A 66, 489, (1978).

[2] M.I.Shliomis, M.Souhar, Europhys. Lett., 49 (1), 55-61 (2000).

[3] S.Mazzoni, R.Cerbino, D.Brogioli, A.Vailati, M.Giglio, Eur. Phys. J. E 15, 305-309, (2004).

[4] M.C.Kim, J.S.Hong, C.K.Choi, AIChE Jornal, 52, (7), 2333-2339, (2006)

[5] Y.Xuan, Q.Li, Int. J. Heat Fluid Flow, 21, 58 (2000).

[6] Y.Xuan, W.Roetzel, Int. J. Heat Mass Transfer 43, 3701 (2000).

[7] K.Khanafer, K.Vafai, M.Lightstone, Int. J. Heat Mass Transfer, 46, 3639-53 (2003).

[8] J.Kim, Y.T.Kang, C.K. Choi, Phys.Fluids, 16, 2395-401 (2004).

[9] A.Ryskin, H.W.Muller, H.Pleiner, Phys.Rev.E 67, 46302 (2003).

[10] J.Kim, Y.T.Kang, C.K. Choi, J. Nanoscale Microscale Therm. Eng. 10(1), 29-39 (2005).

[11] J.Kim, J.Y.Jung, Y.T.Kang, Int.J.Refrigeration 30, 50-57 (2007).

[12] J.Kim, J.Y.Jung, C.K.Choi, Int. J. Refrigeration 30, 323-328 (2007).

[13] H.S.Xue, J.R.Fan, Y.C.Hu, R.H.Hong and K.F.Cen, J. Appl. Phys. 100, 104909, (2006).

[14] L.Dong, D.Johnson, Langmuir, 19, 10205-10209, (2003).

[15] L.Dong, D.Johnson, Adv. Space Res., 32 (2), 149-153, (2003).

[16] J.Buongiorno, Journal of Heat Transfer, 128, 240-250, (2006).

Anomalous diffusion in porous media

J. Prehl[1], K. H. Hoffmann[1], M. Hofmann[2], G. Rünger[2], S. Tarafdar[3]

[1] Department of Physics, Chemnitz University of Technology, Germany
[2] Department of Computer Science, Chemnitz University of Technology, Germany
[3] Condensed Matter Physics Research Centre, Jadapur University, India

Contact: {janett.prehl, hoffmann}@physik.tu-chemnitz.de

Abstract

We studied anomalous diffusion under the influence of an external force on finite regular Sierpinski carpets. In order to investigate the time development of the probability density $p(r,t)$ we utilize the master equation approach. Thus, we are able to determine important quantities depending on their space direction $e \in \{x,y\}$, like the mean drift velocities $\langle v_{\mathrm{dr}_e}\rangle$, the mean square displacements $\langle e^2\rangle$ and the random walk dimensions d_{w_e}. Applying different force strengths in x-direction we find a maximum $\langle v_{\mathrm{dr}_x}\rangle$ for small to medium force strengths in x. According to $\langle x^2\rangle \sim t^{\frac{2}{d_{\mathrm{w}_x}}}$, we determine that $d_{\mathrm{w}_x} < 2$ along the external force. So, diffusion seems to be superdiffusive, although diffusion is hindered by structure and delayed be waiting times. Finally, this seems to be the result of two competing effects. First, the particles get accelerated due to the external force. However, they get also trapped according to the complex structure which takes more time to escape caused by the external force. Thus, the distribution spreads faster with than without an external force and $d_{\mathrm{w}_x} < 2$.

1 Introduction

In technology and science we can observe many anomalous diffusion processes influenced by external forces. Examples are the impedance spectroscopy measurements as for polymer electrolytes [1], hopping electron conduction in doped semiconductors in strong electric fields [2], or diffusion of particles in gels under high gravity or centrifugal force as in chromatographic columns [3].
The external force causes diffusing particles to move preferred in direction of the external force direction. Besides, also the complex structure of real materials [4], like self-similarities of certain length scales, play an important role. We apply regular Sierpinski carpets (SC), a special kind of fractals, to model these complicate structures. SCs are defined by a generator, which is a square divided in $n \times n$ subsquares (see Fig. 1). There are m subsquares labeled black and the rest are white that means they are removed. In order to construct a SC we start with a generator and in each iteration step we replace every black subsquare by a scaled down version of the generator. If this is repeated ad infinitum, the limit object is a SC, where we define its fractal dimension d_f as $d_\mathrm{f} = \frac{\log m}{\log n}$.
As real materials have a smallest length scale of self-similarity, we stop the iteration process after l times and we obtain an iterator of depth l. Furthermore, we combine copies of the iterator to one carpet. Thus, we model the effect that disordered media are rather homogeneous at large length scales [5].
It is known that such complex structures lead to anomalous subdiffusion [6]. So the mean square displacement $\langle r^2(t)\rangle$ of diffusing particles increases not linear in time t, as for normal diffusion, but

$$\langle r^2(t)\rangle \sim t^{\frac{2}{d_\mathrm{w}}}, \tag{1}$$

where $d_\mathrm{w} > 2$ is the random walk dimension [7].
In the next section we will introduce our simulation model and the chosen parameters. Afterwards, we present our results and we will discuss them. Finally a short conclusion is given.

2 Diffusion model in disordered media

We model the diffusion on SCs with the master equation approach. With this approach we are able to calculate the time evolution of the probability density $p(r,t)$ of many particles or random walks on SCs. Analyzing the resulting $p(r,t)$ we can determine many important quantities depending on their space direction $e \in \{x, y\}$, as the mean drift velocities $\langle v_{\mathrm{dr}_e}\rangle$, the mean square displacements $\langle e^2\rangle$ and thus, the random walk dimensions d_{w_e}, and many more.
The probability density $p(r_i,t)$ describes the probability p of a walker to be at time t at a certain position $r_i = (x, y)$. The new $p(r, t+1)$ can be calculated as

$$p(r_i, t+1) = \Gamma_{ii} p(r_i, t) + \sum_{j \in \langle i\rangle} \Gamma_{ij} p(r_j, t), \tag{2}$$

where $j \in \langle i\rangle$ represents all neighboring black squares r_j of r_i, Γ_{ij} is the transition probability for a walker to move from square r_j to r_i and Γ_{ii} is the probability to stay. We choose our transition probabilities according to the blind ant model [8]. That means every

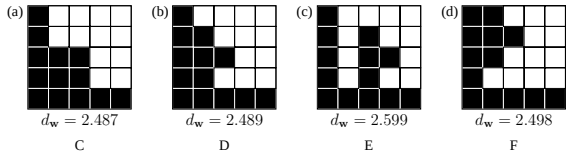

Fig. 1: *Four different generator patterns with same* $d_f = 1.59$

neighboring square is chosen with a probability of $1/4$. If there is a neighboring black square, Γ_{ji} is set to $\Gamma_{ji} = 1/4$. The walker stays on its current position with a probability $\Gamma_{ii} = 1 - \sum_{j \in \langle i \rangle} \Gamma_{ji}$, if there is white square.
We modified the transition probabilities according to the external force, we want to apply [9]. Thus, we defined a vector $\underline{b} = (b_x, b_y)$ with $b_x, b_y \in [0 : 1]$ for the external force strength. So our new transition probabilities to neighboring black squares are

$$\Gamma_{ij} = \frac{1}{2d} \left(1 + \underline{e}_{ji} \underline{b}\right), \tag{3}$$

with d as space dimension and $\underline{e}_{ji}$ as unit vector pointing to the four neighboring squares r_j.
Implementing the master equation approach requires an efficient processing of large data sets. In every time step we need to calculate the probabilities $p(r_i, t+1)$ for all squares r_i using the probabilities of the previous time step and the neighboring information of the SCs. The irregular carpet structure requires appropriate data structures and efficient algorithms for querying, calculating and storing all necessary data. Because of the high computational workload and the memory requirements, a parallel implementation based on the Task Pool Teams concept [10] was used to solve the master equation on regular and randomized SCs .

3 Results and discussion

We applied four different generator patterns, shown in Fig. 1, with same fractal dimension d_{f} but different random walk dimension d_{w}, in order to analyze effects of structures like dead ends to the diffusion influenced by an external force, like temperature difference, magnetic or electric fields. The external force is chosen to be along the positive x-axis. We investigated two important quantities for different iteration depths $l = 1, 2, 4$. But, we will present all results for $l = 2$, and in first order for generator E, as time scales and structure elements are appropriate to show and to discuss all necessary phenomena, however they appear in all iteration depths. We calculated the drift velocities $\langle v_{\mathrm{dr}_e} \rangle$ and the second central mean square displacements $\langle D^2(X_e) \rangle = \langle e \rangle^2 - \langle e^2 \rangle$, both in x- and y-direction, and depending on the external force.
First, we present our results of the drift velocity $\langle v_{\mathrm{dr}_e} \rangle$ over the external force strength b_x for the generators C, D, E, and F (see Fig. 2). We know that for homogeneous media we find a monotonic increasing $\langle v_{\mathrm{dr}_x} \rangle$ for increasing b_x. However, in Fig. 2(a), we see a non-monotonic response of $\langle v_{\mathrm{dr}_x} \rangle$ for increasing b_x [9,11]. We observe a maximum $\langle v_{\mathrm{dr}_x} \rangle$ for small to medium amplitudes. Perpendicular to the force, in y-direction (Fig. 2(b)), we

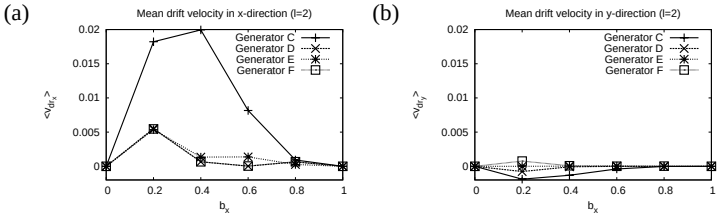

Fig. 2: *Here the mean drift velocities $\langle v_{dr_e} \rangle$ in x- and y-direction for different force strengths b_x are shown for all generators (see Fig. 1).*

find such a non-monotonic behavior for $\langle v_{\mathrm{dr}_y} \rangle$ at smaller order of magnitudes. But, this small drift is caused by the fractal structure of the medium, where diffusion takes place.
Then we analyze the time development of the mean square displacement $\langle D^2(X_e) \rangle$, which can be seen in Fig. 3 for generator E. The vertical lines in the graph represent the average number of time steps $t_1 = 4298$ and $t_2 = 281753$ to cross the linear size of an iterator of depth $l = 1$ and 2. Furthermore, we also introduce a reference graph for normal diffusion ($d_{\mathrm{w}} = 2$).
In Fig. 3(a), we observed that along the external force and within the fractals regime ($t < t_2$) the slopes of $\langle D^2(X_x) \rangle$ are steeper than normal diffusion, thus $d_{\mathrm{w}_x} < 2$. This corresponds to superdiffusion. On the other hand, we find that without an external force ($b_x = 0$) and perpendicular to the force (see Fig. 3(b)) the slopes are flatter than normal diffusion, so $d_{\mathrm{w}_y} > 2$ and subdiffusive behavior can be seen. In all cases we recognize that diffusion crosses over to normal diffusion for long time scales ($t > t_2$).
Although diffusion is hindered by structure and particles get trapped in dead ends we observe a superdiffusive behavior along the external force. In order to analyze that phenomena we determine the marginal distribution $\tilde{p}(x,t) = \sum_y p((x,y),t)$ of $p(r,t)$. We plotted $\tilde{p}(x,t)$ over x (Fig. 4) for generator E at time $t = 489$ for $b_x = 0$ and $b_x = 0.4$. The vertical line represents the mean value $\langle x \rangle$ of $p(r,t)$.
For $b_x = 0$, we see that $\langle x \rangle$ is close to the maximum peak of $\tilde{p}(x,t)$ at the position $x = 0.79$. Moreover, the distribution is fast decaying to both sides similarly. However, applying an external force $\langle x \rangle$ and the main peak of $\tilde{p}(x,t)$ are not at the same position. Furthermore, we do not observe only one major peak, but three and the whole distribution

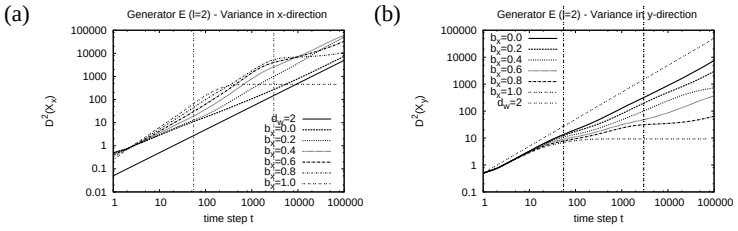

Fig. 3: *It is presented the central mean square displacement $D^2(X_e)$ in x- and y-direction over time t for an iterator of depth $l = 2$ of generator E (see Fig. 1(c)).*

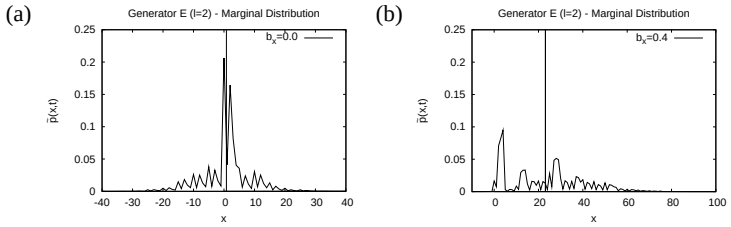

Fig. 4: *The marginal distribution $\tilde{p}(x,t)$ over x is shown for generator E ($l = 2$) (see Fig. 1(c)) for $b_x = 0.0$ and $b_x = 0.4$.*

is flatter for $b_x = 0.4$ than for $b_x = 0$.
That means, particles follow two competing effects. First they move preferred and thus faster along the external force. But they still get trapped according to the structure. If the traps lay along the force direction, it takes more time to escape. The distribution flattens down much faster and $d_{w_x} < 2$. So, we see an overlapping of subdiffusion, trapping and ballistic motion.

4 Conclusions

We studied anomalous diffusion on regular SC structures under the influence of an external force. Therefore, we investigated four different generator pattern with six different external force strengths applied at iteration depth $l = 2$.
We determined the probability distribution $p(r,t)$ and thus, the mean value $\langle x \rangle$, mean drift velocities $\langle v_{\mathrm{dr}_e} \rangle$ and central mean square displacements $\langle D^2(X_e) \rangle$ in x- and y-direction ($e \in \{x, y\}$). We found a non-linear response of $\langle v_{\mathrm{dr}_x} \rangle$ with increasing force strength in x-direction and we obtained maximum $\langle v_{\mathrm{dr}_x} \rangle$ for small and medium forces. Moreover, we observed $d_{w_x} < 2$ along the external force. That implies a superdiffusive process, although diffusion is hindered by dead ends and waiting times.
An explanation gave us the analysis of the corresponding marginal distributions $\tilde{p}(x,t)$. We observed that particles undergo two competing effects, the acceleration due to the external force and a stopping and waiting corresponding to the trapping in dead ends along the external field. Thus, the distribution spreads and flattens much faster. So, d_{w_x} is larger than the 'normal' subdiffusional process on fractals and even larger than normal diffusion.

References

[1] M. Maitra, et al., Physica A, **346**, 199 (2004)
[2] H. Böttger, et al., Phil. Mag. B, **42**, 297 (1980)
[3] L. Fischer, *An introduction to gel chromatography* (North-Holland Publishing Company, Amsterdam, 1971)
[4] B. B. Mandelbrot, *The fractal Geometry of Nature* (W. H. Freeman and Company, New York, 1983)

[5] S. Tarafdar, et al., Physica A, **292**, 1 (2001)
[6] S. Havlin, et al., Adv. Phys., **36**, 695 (1987)
[7] A. Franz, et al., Fractals, **8**, 155 (2000)
[8] P. G. de Gennes, La Recherche, **7**, 919 (1976)
[9] J. Balg, *Diffusion on Fractals*, (http://archiv.tu-chemnitz.de/2007/0103/, Chemnitz, 2006)
[10] K. H. Hoffmann, et al., in W. E. Nagel, et al., eds., *Euro Par 2006, Parallel Processing* (Springer, Berlin, 2006)
[11] H. Böttger, et al., phys. stat. sol. (b), **113**, 9 (1982)

Stability of multicomponent convection in vertical layer with thermal diffusion

I. Ryzhkov[1,2], V. Shevtsova[1]

[1] Microgravity Research Center, Universite Libre de Bruxelles, Belgium
[2] Institute of Computational Modelling SB RAS, Krasnoyarsk, Russia

Contact: iryzhkov@ulb.ac.be

Abstract

The linear stability of convection in a vertical layer of multicomponent fluid is investigated. The basic state is a plane–parallel return flow, where a linear temperature profile in the cross–section induces linear profiles of concentrations due to the Soret effect. The limit of long–wave perturbations is investigated analytically. It is found that long–wave instability is caused by the interplay between the basic flow and concentration waves with long scale in vertical direction. The instability regions in the space of control parameters (separation ratios) are constructed and critical Grashof numbers are plotted for ternary mixtures. It is shown that the instability region becomes larger with increasing the difference between diffusive properties of components. The analysis of characteristic decrements behavior with increasing the Grashof number reveales different instability scenarios depending on the values of control parameters: monotonic/oscillatory onset, stabilization after the onset, and even repeated destabilization. To investigate the case of finite wave–numbers, calculations are performed by the method of direct integration with orthogonalization combined with the shooting procedure. They confirm that the most dangerous monotonic mode corresponds to zero wave number in the instability regions discovered by the long–wave analysis. However, the oscillatory onset is found to occur at finite wave numbers.

1 Introduction

Multicomponent mixtures can show a variety of convective phenomena due to a complex interplay between heat and mass transfer processes, such as cross–diffusion and the Soret and Dufour effects. Convective instabilities in binary fluids have been extensively investigated (see [1] and references therein), but for ternary and higher mixtures the number of studies is rather limited. Among other reasons, the importance of such studies relates to the fact that transport coefficient measurement methods employing convection are being extended to multicomponent fluids [2].

This work deals with linear stability of convective flow in a side–heated vertical slot with a multicomponent mixture in the presence of Soret effect. The limit of long–wave perturbations is investigated analytically and numerically. The instability zones and critical Grashof numbers are plotted for ternary mixture and instability mechanism is discussed.

2 Governing equations and basic state

Consider a mixture with n components, which is placed in a long vertical layer of width $2L$ (Fig. 1). A temperature difference $2\Delta T$ is applied between no–slip and impermeable lateral walls. The density is assumed linear in temperature and concentration of components: $\rho = \rho_0\big[1 - \beta_T T - \beta_1 C_1 - \cdots - \beta_{n-1} C_{n-1}\big]$, where T and C_i are the deviations from the mean values. We take the scales of length L, time L^2/ν, velocity $\mathrm{g}\beta_T \Delta T L^2/\nu$, temperature ΔT, and concentration of i^{th} component $\beta_T \Delta T/\beta_i$. Here ν is the viscosity and g is the gravity acceleration. The dimensionless equations of multicomponent convection in Boussinesq approximation have the form [4]

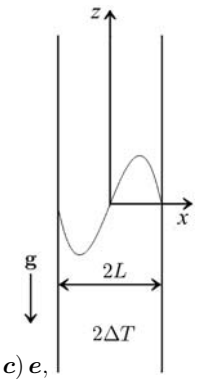

Fig. 1: *Vertical layer.*

$$
\begin{aligned}
&\partial_t \boldsymbol{u} + \mathrm{Gr}\,(\boldsymbol{u}\cdot\nabla)\,\boldsymbol{u} = -\nabla p + \nabla^2 \boldsymbol{u} + (\Theta + \boldsymbol{I}\cdot\boldsymbol{c})\,\boldsymbol{e},\\
&\partial_t \Theta + \mathrm{Gr}\,(\boldsymbol{u}\cdot\nabla)\,\Theta = \mathrm{Pr}^{-1}\,\nabla^2\Theta,\\
&\partial_t \boldsymbol{c} + \mathrm{Gr}\,(\boldsymbol{u}\cdot\nabla)\,\boldsymbol{c} = \mathcal{SC}\,(\nabla^2\boldsymbol{c} - \boldsymbol{\psi}\nabla^2\Theta),\\
&\nabla\cdot\boldsymbol{u} = 0,
\end{aligned}
\tag{1}
$$

where $\boldsymbol{c} = (c_1, \ldots, c_{n-1})$ is the vector of concentrations. The system includes the Prandtl number $\mathrm{Pr} = \nu/\chi$, the Grashof number $\mathrm{Gr} = \mathrm{g}\beta_T \Delta T L^3/\nu^2$, the square matrix $\mathcal{SC} = \nu^{-1} B D B^{-1}$ (D is the diffusion matrix and $B = \mathrm{diag}\{\beta_i\}$). The separation ratios $\boldsymbol{\psi} = (\psi_1, \ldots, \psi_{n-1}) = -\beta_T B D^{-1} \boldsymbol{D_T}$ characterize the Soret effect ($\boldsymbol{D_T}$ is the vector of thermal diffusion coefficients). In addition, $\boldsymbol{e} = (0, 0, 1)$ and $\boldsymbol{I} = (1, \ldots, 1)$ is $(n-1)$ dimensional vector.

The basic state is a plane–parallel return flow $\boldsymbol{u} = (0, w(x))$, $\Theta(x)$, $\boldsymbol{c}(x)$, which satisfies the conditions

$$
x = \pm 1: \quad w = 0, \quad \Theta = \pm 1, \quad \frac{\partial \boldsymbol{c}}{\partial x} - \boldsymbol{\psi}\frac{\partial \Theta}{\partial x} = 0; \qquad \int_{-1}^{1} w\,dx = 0, \quad \int_{-1}^{1} \boldsymbol{c}\,dx = 0.
$$

and has the form

$$w_0 = \frac{\Psi+1}{6}(x-x^3), \qquad \Theta_0 = x, \qquad \boldsymbol{c} = \boldsymbol{\psi} x. \tag{2}$$

Here $\Psi = \psi_1 + \cdots + \psi_{n-1}$ is the net separation ratio. In the basic state, the applied temperature difference induces separation of components due to the Soret effect. The sign of ψ_i determines the direction of component segregation (to the hot or cold wall). The horizontal density variation results in convective flow driven by buoyancy force. The flow (2) can be observed in thermogravitational column at the transient state [5].

3 Stability problem

We analyze linear stability of basic state (2) with respect to two–dimensional perturbations of the form $\big(\varphi(x),\, \theta(x),\, \boldsymbol{\xi}(x)\big)\, \exp(-\lambda t + ikz)$ for stream function, temperature, and composition, respectively. The stability problem is written as ($\Delta = \partial_{xx} - k^2$ and the prime stands for ∂_x):

$$\begin{aligned}
&\Delta^2\varphi + ik\,\mathrm{Gr}\,(w_s''\,\varphi - w_s\,\Delta\varphi) + \theta' + \boldsymbol{I}\cdot\boldsymbol{\xi}' = -\lambda\Delta\varphi,\\
&\mathrm{Pr}^{-1}\Delta\theta + ik\,\mathrm{Gr}\,(\Theta_s'\,\varphi - w_s\,\theta) = -\lambda\,\theta,\\
&\mathcal{SC}\,(\Delta\boldsymbol{\xi} - \boldsymbol{\psi}\Delta\theta) + ik\,\mathrm{Gr}\,(\boldsymbol{c}_s'\,\varphi - w_s\,\boldsymbol{\xi}) = -\lambda\,\boldsymbol{\xi},\\
&x = \pm 1: \qquad \varphi = \varphi' = 0, \qquad \theta = 0, \qquad \boldsymbol{\xi}' - \boldsymbol{\psi}\,\theta' = 0.
\end{aligned} \tag{3}$$

In this work, we study the limit of long–wave perturbations. The solution is expanded in series with respect to the wave number k, which is assumed to be small:

$$(\varphi,\, \theta,\, \boldsymbol{\xi},\, \lambda) = \sum_{m=0}^{\infty} (\varphi_m,\, \theta_m,\, \boldsymbol{\xi}_m,\, \lambda_m)\, k^m. \tag{4}$$

Substituting the expansions into (3) and equating the terms with the same order of k, we obtain the equations for coefficients. Solving zero and first order system gives the approximations $\lambda_0 = \lambda_1 = 0$ to the decrement λ. From the second order system, we derive the equation for λ_2:

$$\det\left[\frac{2\mathrm{Gr}^2(\Psi+1)}{2835}\Big(\Upsilon + (\Psi+1)E\Big)\,\mathcal{SC}^{-1} + \mathcal{SC} - \lambda_2 E\right] = 0, \tag{5}$$

where E is the unity matrix and Υ is a matrix, every column of which coincides with the vector $\boldsymbol{\psi}$. Equation (5) is a polynomial of degree $n-1$ with respect to λ_2. So, there exist $n-1$ modes for n–component mixture in the limit of long–wave approximation with $\lambda \approx \lambda_2 k^2$. Note that when $\Psi = -1$, the basic state of mechanical equilibrium (see (2)) is stable with respect to the long–wave perturbations (since the eigenvalues of diffusion matrix are always real and positive).

The analysis of perturbation structure (eigenfunctions of (3) in the form (4)) allows one to understand the long–wave instability mechanism. We found that in an isothermal fluid layer, only damping density disturbances caused by long–scale concentration waves in vertical direction exist. When heating is applied, the basic flow (see Fig. 1) shifts these waves upwards and downwards producing density variations, which result in the

velocity disturbance in the form of convection cells. The growth/decay of perturbations is connected with the horizontal stratification in temperature and composition in the basic state (2). Indeed, a horizontal shift of a small fluid element leads to the density difference between this element and the surrounding fluid. The resulting buoyancy force induces motion in vertical direction, which may lead to the development of instability. With time, the homogenization of temperature and composition between the fluid element and its surroundings occurs. During this process, the density difference, and, consequently, the buoyancy force acting on the element may increase or decrease since the relaxation times for diffusion of heat and different components of the mixture can significantly differ. So, a complex instability behavior can be expected in multicomponent mixtures.

4 Instability in ternary mixture

Let us consider the case of ternary fluid. The diffusion matrix is assumed diagonal, i.e. $\mathcal{SC} = \mathrm{diag}\,\{\,\mathrm{Sc}_{11}^{-1},\,\mathrm{Sc}_{22}^{-1}\,\}$, where $\mathrm{Sc}_{ii} = \nu/D_{ii}$ are the Schmidt numbers. All results can be extended to non–diagonal case by the technique described in [6]. Let us introduce the ratio $s = \mathrm{Sc}_{11}/\mathrm{Sc}_{22}$, which satisfies the inequality $0 < s \leqslant 1$ (otherwise, we change the order of components). Eliminating the parameters related to the second component by using $\psi_2 = \Psi - \psi_1$ and $\mathrm{Sc}_{22} = \mathrm{Sc}_{11}/s$, from (5) we obtain a quadratic equation with the roots $\lambda_2^{\pm}$ for the decrement λ_2. To find the threshold of monotonic instability, we put $\lambda_2 = 0$ and find two roots

$$\big(\mathrm{Gr}_m^{\pm}\big)^2 = \frac{2835}{4\mathrm{Sc}_{11}^2(\Psi+1)^2\,(2\Psi+1)}\left[-\big(\psi_1(s^2-1)+\Psi(s^2+2)+s^2+1\big)\pm\right. \tag{6}$$
$$\left.\pm\sqrt{\big(\psi_1(s^2-1)+\Psi(s^2+2)+s^2+1\big)^2-4s^2(\Psi+1)(2\Psi+1)}\right].$$

For $\Psi = -1$, there is no solution and for $\Psi = -1/2$ we have multiple root $\big(\mathrm{Gr}_m^*\big)^2 = 5670\,s^2/\mathrm{Sc}_{11}^2/(2\psi_1(1-s^2)-s^2)$. The threshold of oscillatory instability is obtained by setting $\lambda_2 = i\omega$. The critical Grashof number is given by

$$\big(\mathrm{Gr}_o\big)^2 = -\frac{2835\,s(s+1)}{2\mathrm{Sc}_{11}^2(\Psi+1)\big(\psi_1(s-1)+\Psi(s+2)+s+1\big)} \tag{7}$$

and the critical frequency is

$$\omega^2 = \frac{s(s+1)^2(\Psi+1)(2\Psi+1)}{\mathrm{Sc}_{11}^2\big(\psi_1(s-1)+\Psi(s+2)+s+1\big)^2} - \frac{\psi_1(s^3-1)+\Psi(s^3+2)+s^3+1}{\mathrm{Sc}_{11}^2\big(\psi_1(s-1)+\Psi(s+2)+s+1\big)}. \tag{8}$$

To find the instability regions in the parameter space (Ψ, ψ_1, s), we require that the right–hand sides of formulae (6)–(8) and the expression under the square root in (6) must be positive. The analysis shows that instability exists for $-1 < \Psi < -1/2$ with the monotonic onset at Gr_m^-. It is the only unstable region for $s = 1$ (here components have the same diffusive properties and the mixture behaves like a binary one [3]). When $0 < s < 1$, additional instability regions

appear. In Fig. 2, they are shown by the shaded area for $s = 0.5$. Sectors 2 and 3 with the monotonic onset at Gr_m^- and Gr_m^+, respectively, are limited by the curves

$$\psi_m^{\pm} = \frac{\Psi(s^2+2)+s^2+1}{1-s^2} \pm \frac{2s\sqrt{(\Psi+1)(2\Psi+1)}}{1-s^2}.$$

It can be shown that when s is changing from 1 to 0, the boundaries of sectors 2 and 3 monotonically approach the line $\psi_1 = 2\Psi + 1$ (the direction is shown by arrows). In addition, sector 4 with the oscillatory onset at Gr_o appears. We conclude that the difference in diffusive properties leads to the enlargement of instability region. This fact is consistent with the reasoning in Section 3.

It was found that when diffusive properties of components are close ($s \to 1$), the critical Grashof number is mainly determined by the net separation ratio and weakly depends on ψ_1. With decreasing s, the latter dependence becomes very pronounced. It is illustrated by Fig. 3, where the dependence of Gr_m^- on ψ_1 is shown for $\Psi = -0.75$ and $\mathrm{Sc}_{11} = 500$. At the point $\psi_1 = \Psi$, there is no Soret separation of component 2 ($\psi_2 = 0$), which explains the crossing of the curves.

We also analyzed the behavior of decrements $\lambda_2^{\pm}$ with increasing the Grashof number and found different instability scenarios depending on Ψ, ψ_1, s: monotonic/oscillatory onset, stabilization after the onset, and even repeated destabilization. The case of finite wave numbers was investigated numerically by the method of integration with orthogonalization. It confirmed that the most dangerous monotonic mode corresponds to $k = 0$, but showed that the oscillatory instability sets in at finite k. An example of complex instability scenario is shown in Fig. 4: a long–wave monotonic onset is followed by stabilization and then oscillatory onset at finite k.

5 Conclusions

Long–wave instability in a vertical multicomponent fluid layer with Soret effect have been investigated analytically and numerically. The instability zones in the parameters space and critical Grashof numbers are plotted for ternary mixture. It was shown that instability region becomes larger with increasing the difference between diffusive properties

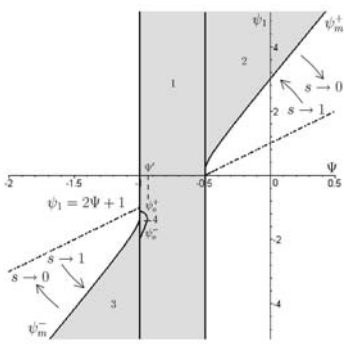

Fig. 2: *Long–wave instability zones for ternary mixture on the plane* (Ψ, ψ_1).

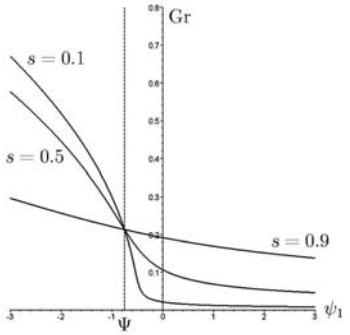

Fig. 3: *Critical Grashof numbers,* $\Psi = -0.75$.

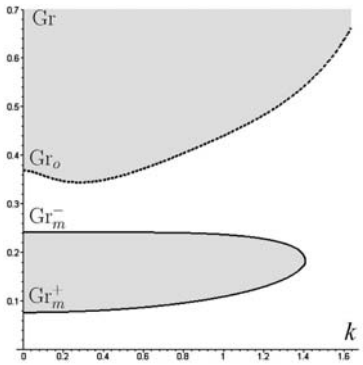

Fig. 4: *Monotonic and oscillatory neutral curves,* $\Psi = -1.25$, $\psi_1 = -3.5$, $s = 0.5$, $Sc_{11} = 500$.

of components. A variety of instability scenarios with increasing the Grashof number is found.

Acknowledgment

The work is supported by the INTAS YS Project 06–1000014–6257 and the Russian Foundation for Basic Research Project 08-01-00762-a.

References

[1] M.C. Cross and P.C. Hohenberg. Rev. Mod. Phys. **65**, 851 (1993).

[2] K. Haugen and A. Firoozabadi. J. Chem. Phys. **122**, 014516 (2005).

[3] G.Z. Gershuni, E.M. Zhukhovitskii, L.E. Sorokin. J. Appl. Math. Mech. **46** (1), 66 (1982).

[4] I. Ryzhkov and V. Shevtsova. Phys. Fluids **19**, 027101 (2007).

[5] J.F. Dutrieux, J.K. Platten, G. Chavepeyer, M.M. Bou-Ali. J. Phys. Chem. B **106**, 6104 (2002).

[6] I. Ryzhkov and V. Shevtsova. On the cross–diffusion and Soret effect in multicomponent mixtures, Microgravity Science and Techn., accepted, in press.

Colloids

Single-particle thermal diffusion of charged colloids: Double-layer theory in a temperature gradient

J.K.G. Dhont[1], W.J. Briels[2]

[1] IFF, Forschungszentrum Jülich, Germany
[2] University of Twente, The Netherlands

Contact: j.k.g.dhont@fz-juelich.de, w.j.briels@utwente.nl

Abstract

The force on a charged colloid due to a temperature gradient is calculated, from which the Soret coefficient is obtained. The thermophoretic force consists of two types of contributions : (i) a force due to the temperature dependence of the internal energy of the double layer and (ii) forces related to the temperature-induced deformation of the double layer. To leading order in temperature gradients, the force (i) can be obtained from irreversible thermodynamics considerations where temperature-gradient induced deformation of the double layer can not be accounted for, while the forces (ii) must be obtained from a detailed analysis of the temperature-gradient induced deformation of the double layer. The present calculation is based on an Debye-Hückel theory for the double-layer structure in a small temperature gradient, including solvent friction forces that arise from electro-osmotic flow that is induced within the deformed double layer [1].

The thermal diffusion coefficient of colloidal particles consists, to a good approximation, of additive contributions from single-particle properties and contributions stemming from interactions between colloids. Single-particle contributions relate to the response of the solvation layer, the structure of the solid core material and the electric double-layer to a temperature gradient. As far as the electric double layer is concerned, there are three forces acting on a colloidal sphere. The origin of these forces is schematically depicted in Fig.1.

First of all, the temperature dependence of the internal electrostatic energy W of the double layer and surface charges gives rise to a force $\mathbf{F}_W$, which is referred to here as the *internal force* and is equal to $-\nabla W = -\nabla T\, dW/dT$ (with T the temperature). The internal energy can be calculated as the work necessary to reversibly charge the colloidal sphere. To leading order in temperature gradients this leads to,

$$\mathbf{F}_W \;=\; -\frac{\nabla T(z)}{T}\,\frac{Q^2}{16\,\pi\,\epsilon\,R}\,\frac{\kappa R}{(\,1+\kappa R\,)^2}\,\left\{\,1-\frac{d\ln\epsilon}{d\ln T}\,\left(\,1+\frac{2}{\kappa R}\,\right)\right\}\,, \qquad (1)$$

where Q is the total free surface charge, ϵ is the dielectric constant of the solvent, R is the radius of the sphere and κ is the inverse Debye length. Note that, to leading in temperature-gradients, the internal force can be calculated without having to consider the temperature-gradient induced deformation of the double layer. The result (1) can therefore also be obtained from irreversible-thermodynamics considerations [2].

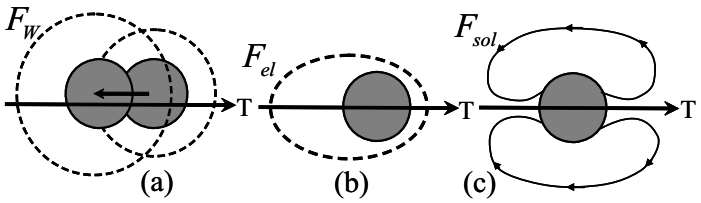

Fig. 1: *The three forces acting on a charged colloidal sphere, fixed at the origin, in a temperature gradient. (a) The internal force* $\mathbf{F}_W$ *due to the change of the double-layer structure on displacement of the sphere. The dashed lines indicate the extent of the unperturbed double-layer at the ambient temperature. (b) The electric force* $\mathbf{F}_{el}$ *that is due to the non-spherically symmetric double-layer structure. The dashed line indicates the asymmetry of the double layer. (c) The solvent-friction force* $\mathbf{F}_{sol}$ *is due to the solvent flow that is induced by electric body forces arising from the asymmetry of the double-layer structure. Here, the lines indicate solvent flow lines. Figure is taken from ref. [1].*

There are two additional forces which are the result of temperature-gradient induced deformation of the double layer.

The temperature gradient will induce an asymmetry in the double-layer charge distribution. This is, roughly speaking, due to the temperature dependence of the double-layer thickness. On the colder side of a colloidal sphere in water, the Debye screening length is larger as compared to the warmer side. As a result, the center-of-charge of the double layer does no longer coincide with the center-of-charge of the surface-charge distribution of the colloidal sphere. This results in an *electric force* $\mathbf{F}_{el}$ of the double layer on the

surface charges of the sphere (see Fig.1b),

$$\mathbf{F}_{el} \;=\; \frac{1}{2}\oint_{\partial V} dS\;\sigma_t(\mathbf{r})\;\left[\,\mathbf{E}^{+}(\mathbf{r})+\mathbf{E}^{-}(\mathbf{r})\,\right]\;, \tag{2}$$

where $\mathbf{E}^{+}$ and $\mathbf{E}^{-}$ are the electric field strengths on approach of the surface of the spherical colloid from the outside and inside of the core, respectively, and σ_t is the total surface charge density, including both free surface charges and charges due to dielectric polarization.
Due to the asymmetry of the charge distribution, electric body forces will set the solvent in motion. This solvent flow acts with a *solvent-friction force* $\mathbf{F}_{sol}$ on the surface of the sphere (see Fig.1c),

$$\mathbf{F}_{sol} \;=\; -\oint_{\partial V} dS\;\mathbf{f}(\mathbf{r})\;, \tag{3}$$

where $\mathbf{f}$ is the force per unit area that a surface element of the core of the colloids exerts on the solvent.

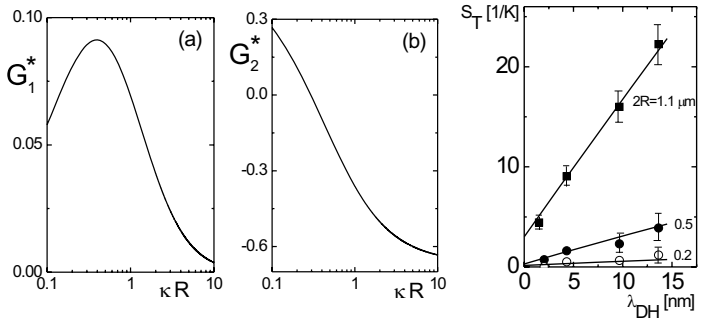

Fig. 2: *The functions (a) $G_2^{\star}(x) \equiv x\,G_1(x)/(1+x)^2$ and (b) $G_2^{\star}(x) \equiv x\,G_2(x)/(1+x)^2$ that determine the contributions to the Soret coefficient in eq.(4) due to the temperature-induced deformation of the double layer. Most right figure : experimental Soret coefficients as a function of the Debye length $\lambda_{DH} = \kappa^{-1}$ for colloidal polystyrene spheres of various radii [3]. The solid lines correspond to the force in eq.(1).*

The total thermophoretic force $\mathbf{F}_T = \mathbf{F}_W + \mathbf{F}_{el} + \mathbf{F}_{sol}$ will set the sphere in motion, leading to thermodiffusion. What is neglected here is the flow-induced deformation of the charge distribution, which is known from electrophoresis to contribute to the velocity of the order of a few percent. In order to explicitly evaluate the forces (2,3), the temperature-gradient induced asymmetry of the double layer needs to be quantified. We therefore extended the Debye-Hückel theory to include a small temperature gradient, which then enables the calculation of the electric force and the solvent friction force [1]. The resulting expression for the Soret coefficient reads,

$$T\,S_T \;=\; T\,S_T^W \;+\; \frac{\epsilon_0}{\epsilon}\,\frac{\beta\,Q^2}{16\,\pi\,\epsilon\,R}\,\frac{\kappa\,R}{(1+\kappa\,R)^2}\,\left[\;\chi\;G_1(\kappa\,R) - \frac{d\ln\epsilon}{d\ln T}\;G_2(\kappa\,R)\;\right]\;, \tag{4}$$

where ϵ and ϵ_0 are the dielectric constants of the solvent and vacuum, respectively. The functions G_1 and G_2 in eq.(4) describe the contribution to the Soret coefficient due to the temperature-induced deformation of the double layer. These functions take the relatively simple form,

$$\begin{aligned} G_1(x) &= -E(x)+1\,, \\ G_2(x) &= E(x)-\frac{2}{3}\,x-2+\frac{1}{2}\,x^{-1}\,, \end{aligned} \tag{5}$$

where E is defined as,

$$E(x) \;=\; 2\,x\,\exp\{2x\}\int_x^\infty dz\,\frac{\exp\{-2\,z\}}{z}\,. \tag{6}$$

The functions $G_j^\star \equiv x\,G_j/(1+x)^2$ are plotted in Fig.2. Furthermore, S_T^W is the contribution to the Soret coefficient corresponding to the internal force (1), that is, due to the temperature dependence of the internal energy W of the double layer,

$$T\;S_T^W \;=\; \frac{\beta\,Q^2}{16\,\pi\,\epsilon\,R}\;\frac{\kappa\,R}{(1+\kappa\,R)^2}\left[1-\frac{d\ln\epsilon}{d\ln T}\left(1+\frac{2}{\kappa\,R}\right)\right]\,. \tag{7}$$

This contribution to the Soret coefficient can also be found from irreversible thermodynamics considerations [2], where temperature-gradient induced deformation of the double layer is not accounted for.

Two things are to be noticed. First of all, the forces due to temperature-gradient induced deformation of the double layer are dielectrically screened, so that these forces are typically a factor ϵ_0/ϵ smaller than the internal force. Experimental results, like those in the most right figure in Fig.2, can therefore be explained on the basis of irreversible thermodynamics only. The effects of the temperature-gradient induced asymmetry of the double layer are relevant in less polar solvents. Experiments on such systems have not yet been performed. It would also be interesting to probe the solvent flow around a charged colloidal sphere in a temperature gradient. Secondly, the contribution of these two forces to the Soret coefficient do not vanish for very thin double layers. This is due to the temperature dependence of the dielectric constant of the solvent, giving rise to an asymmetric screening of surface charges.

References

[1] J.K.G. Dhont, W.J. Briels, Eur. Phys. J. E **25**, 61 (2008).

[2] J.K.G. Dhont, S. Wiegand, S. Duhr, D. Braun, Langmuir **23**, 1674 (2007).

[3] S. Duhr, D. Braun, Proc. Natl. Acad. Sci. U.S.A. **103**, 19678 (2006).

What Soret can learn from Seebeck

E. Bringuier

Matériaux et Phénomènes Quantiques, CNRS UMR 7612, Université Denis-Diderot (Paris 7), case 7021, 10 rue A. Domon et L. Duquet, 75205 Paris Cedex 13, France

E-mail: erb@ccr.jussieu.fr

Abstract

Particle transport in a temperature gradient is known as the Ludwig-Soret effect in a binary fluid mixture and as the Seebeck effect in an electric conductor. In this paper, both effects are described within the same framework. Energetic interpretations of the effects ensue. It is shown how the modeling of the Seebeck effect can shed light on the Soret effect, especially the existence of two signs of the Soret coefficient.

1 Steady-state thermodynamics of the Lorentz model

The Lorentz model considers mobile particles in a passive medium unperturbed by the flow of the particles. At constant pressure, if two subsystems 1 and 2 of the medium exchange particles and energy, the entropy change is [1]

$$\mathrm{d}S = \left(\frac{1}{T_1} - \frac{1}{T_2}\right)\mathrm{d}U_1 - \left(\frac{\tilde{\mu}_1}{T_1} - \frac{\tilde{\mu}_2}{T_2}\right)\mathrm{d}N_1 \tag{1}$$

where T is the absolute temperature and $\tilde{\mu}$ is the chemical potential of the particles. In Eq. (1), account has been taken of the conservativity of energy U and particle number N. In a continuous medium where T and $\tilde{\mu}$ are functions of position, Eq. (1) becomes

$$\dot{\Sigma} = \boldsymbol{\nabla}\left(\frac{1}{T}\right)\cdot\mathbf{j}_\mathrm{U} + \boldsymbol{\nabla}\left(-\frac{\tilde{\mu}}{T}\right)\cdot\mathbf{j}_\mathrm{N}, \tag{2}$$

where $\dot{\Sigma}$ (in $\mathrm{J\cdot K^{-1}\cdot m^{-3}\cdot s^{-1}}$) is the rate of entropy production, and $\mathbf{j}_\mathrm{U}$ (resp. $\mathbf{j}_\mathrm{N}$) is the energy (resp. particle) current density, in $\mathrm{J\cdot m^{-2}\cdot s^{-1}}$ (resp. $\mathrm{m^{-2}\cdot s^{-1}}$). For small enough disequilibria $\boldsymbol{\nabla}(1/T)$ et $\boldsymbol{\nabla}(-\tilde{\mu}/T)$, the steady-state response to the disequilibria is taken to be linear, namely

$$\mathbf{j}_\mathrm{N} = L_\mathrm{NN}\boldsymbol{\nabla}\left(-\frac{\tilde{\mu}}{T}\right) + L_\mathrm{NU}\boldsymbol{\nabla}\left(\frac{1}{T}\right), \tag{3}$$

$$\mathbf{j}_\mathrm{U} = L_\mathrm{UN}\boldsymbol{\nabla}\left(-\frac{\tilde{\mu}}{T}\right) + L_\mathrm{UU}\boldsymbol{\nabla}\left(\frac{1}{T}\right) \tag{4}$$

The second law of thermodynamics demands the positivity of $(L_{ij})_{i,j\,=\,U,N}$, namely $L_\mathrm{NN} > 0$, $L_\mathrm{UU} > 0$ and $L_\mathrm{UU}L_\mathrm{NN} - L_\mathrm{UN}L_\mathrm{NU} > 0$.

Let us write $\mathbf{j}_\mathrm{U}$ as $\mathbf{j}_\mathrm{F} + \underline{U}\mathbf{j}_\mathrm{N}$ so that, in the absence of a particle flow, we have an ordinary (Fourier) heat flow $\mathbf{j}_\mathrm{F}$, and $\mathbf{j}_\mathrm{N}$ adds a contribution to $\mathbf{j}_\mathrm{U}$. This is achieved by letting

$$\mathbf{j}_\mathrm{F} = \frac{L_\mathrm{UU}L_\mathrm{NN} - L_\mathrm{UN}L_\mathrm{NU}}{L_\mathrm{NN}}\boldsymbol{\nabla}\left(\frac{1}{T}\right) \text{ and } \underline{U} = \frac{L_\mathrm{UN}}{L_\mathrm{NN}} \tag{5}$$

Identifying the prefactor of $\boldsymbol{\nabla}(1/T)$ to κT^2 yields the thermal conductivity κ of Fourier's law: it is checked that $\kappa > 0$. The quantity $\underline{U}$ has the meaning of an energy transported by each particle in the absence of $\boldsymbol{\nabla}T$, as is apparent in the so-called energy-transport models [2,3].

Introducing the heat current $\mathbf{j}_\mathrm{Q} = \mathbf{j}_\mathrm{U} - \tilde{\mu}\mathbf{j}_\mathrm{N}$, defined by removing the local binding energy $\tilde{\mu}$ of particles, it is possible to rewrite Eqs. (3) and (4) as

$$\mathbf{j}_N = \frac{L_{NN}}{T}\left[-\nabla\tilde{\mu} - \left(\frac{L_{NU}}{L_{NN}} - \tilde{\mu}\right)\frac{\nabla T}{T}\right], \tag{6}$$

$$\mathbf{j}_Q = \mathbf{j}_F + \left(\frac{L_{UN}}{L_{NN}} - \tilde{\mu}\right)\mathbf{j}_N. \tag{7}$$

2 Application to the thermoelectric effects in solids

In an electrically conducting solid, the charge current density **J** is given by the following phenomenological law [4-6]

$$\mathbf{J} = \sigma(\mathbf{E}' - S\nabla T), \tag{8}$$

where the electromotive field $\mathbf{E}' = -\nabla(\tilde{\mu}_e/q)$ involves the electrochemical potential $\tilde{\mu}_e = \tilde{\mu}_c + qV$ of carriers henceforth assumed to be of a single type, of charge q, and V is the electrical potential. The law (8) uses an electrical conductivity σ and a Seebeck coefficient S (in V/K, not to be confused with entropy). Equivalently, the carrier current density is

$$\mathbf{j}_N = \frac{\sigma}{q^2}\left(-\nabla\tilde{\mu}_e - qS\nabla T\right) \tag{9}$$

Take $\nabla T = 0$. When $\tilde{\mu}_e$ reduces to qV, Ohm's law is recovered; when $\tilde{\mu}_e$ reduces to $\tilde{\mu}_c$, we have Fick's law, with diffusivity $D = (\sigma/q^2)(\partial\tilde{\mu}_c/\partial n)_T$. Since the chemical potential should include qV, the law (9) can be cast on the pattern (6), with

$$L_{NN} = \sigma T/q^2 \quad \text{and} \quad L_{NU}/L_{NN} = \tilde{\mu}_e + qST \tag{10}$$

The second phenomenological law of thermoelectricity is [4-6]

$$\mathbf{j}_Q = -\kappa\nabla T + \Pi\mathbf{J}, \tag{11}$$

where Π is the Peltier coefficient. Writing $\mathbf{j}_Q = -\kappa\nabla T + q\Pi\mathbf{j}_N$ yields $\underline{U} = \tilde{\mu}_e + q\Pi$. Experiment shows that $\Pi = TS$, which is tantamount to $L_{NU} = L_{UN}$. The latter symmetry relation is a manifestation of microscopic reversibility [1,4]. Since

$$qS = (\underline{U} - \tilde{\mu}_e)/T \tag{12}$$

the Seebeck coefficient is seen to be proportional to the difference between the energy of transport $\underline{U}$ and the binding energy $\tilde{\mu}_e$, also called Fermi level in solid-state physics. Relation (12) provides an energetic interpretation for S.

3 Steady-state thermodynamics of a binary mixture

In a binary fluid mixture A-B, the disequilibria are $\nabla(1/T)$, $\nabla(-\tilde{\mu}_A/T)$ and $\nabla(-\tilde{\mu}_B/T)$, and the rate of production of entropy is [7]

$$\dot{\Sigma} = \nabla\left(\frac{1}{T}\right)\cdot\mathbf{j}_U + \nabla\left(-\frac{\tilde{\mu}_A}{T}\right)\cdot\mathbf{j}_A + \nabla\left(-\frac{\tilde{\mu}_B}{T}\right)\cdot\mathbf{j}_B \tag{13}$$

discarding the contribution from viscosity effects. Consider now the convection ($n\mathbf{u}$), interdiffusion of B into A ($\mathbf{j}$), and interdiffusion-related energy ($\mathbf{j}_E$) current densities:

$$\mathbf{j}_B = nc\mathbf{u} + \mathbf{j} \quad \text{and} \quad \mathbf{j}_A = n(1-c)\mathbf{u} - \mathbf{j} \tag{14}$$

$$\mathbf{j}_U = nh\mathbf{u} + \mathbf{j}_E \tag{15}$$

In these definitions, n is the total particle density (of A and B), c is the mole fraction of B, $\mathbf{u} = (1-c)\mathbf{u}_A + c\mathbf{u}_B$ is the average velocity of the mixture, and $h = (1-c)h_A + ch_B$ is the enthalpy per particle (h_A and h_B are the partial molecular enthalpies of A and B).

Using the new currents and the Gibbs-Duhem and Gibbs-Helmholtz relations yields [7]

$$\dot{\Sigma} = \nabla\left(\frac{1}{T}\right)\cdot\mathbf{j}_E + \nabla\left(-\frac{\tilde{\mu}_{BA}}{T}\right)\cdot\mathbf{j} \tag{16}$$

where $\tilde{\mu}_{BA} = \tilde{\mu}_B - \tilde{\mu}_A$ is an exchange chemical potential. One can see that the over-all quantities $n\mathbf{u}$ and $nh\mathbf{u}$ do not contribute to $\dot{\Sigma}$. Convection is reversible, interdiffusion is not.

It is possible to apply the formalism of § 1 with $\mathbf{j}_N \to \mathbf{j}$, $\mathbf{j}_U \to \mathbf{j}_E$, and $\tilde{\mu} \to \tilde{\mu}_{BA}$. However, the phenomenological law of the Ludwig-Soret effect, defining the Soret coefficient S_T,

$$\mathbf{j} = ncD\left(-\frac{\nabla c}{c} - S_T\nabla T\right) \tag{17}$$

uses $\nabla c/c$ instead of $\nabla\tilde{\mu}_{BA}$. Reexpressing Eq. (3), we get

$$\mathbf{j} = -\frac{L_{NN}}{T}\left(\frac{\partial\tilde{\mu}_{BA}}{\partial c}\right)_{p,T}\nabla c - \frac{1}{T^2}(L_{NU} - h_{BA}L_{NN})\nabla T \tag{18}$$

where $h_{BA} = h_B - h_A$ stems from the Gibbs-Helmholtz relation. Identification yields

$$nD = \frac{L_{\mathrm{NN}}}{T}\left(\frac{\partial \tilde{\mu}_{\mathrm{BA}}}{\partial c}\right)_{p,T} \tag{19}$$

$$TS_{\mathrm{T}} = \frac{1}{c\left(\frac{\partial \tilde{\mu}_{\mathrm{BA}}}{\partial c}\right)_{p,T}}\left(\frac{L_{\mathrm{NU}}}{L_{\mathrm{NN}}} - h_{\mathrm{BA}}\right) \tag{20}$$

Microscopic reversibility entails $L_{\mathrm{NU}} = L_{\mathrm{UN}}$, so that the thermal-diffusion factor is given by

$$TS_{\mathrm{T}} = \frac{\underline{U} - h_{\mathrm{BA}}}{c\left(\frac{\partial \tilde{\mu}_{\mathrm{BA}}}{\partial c}\right)_{p,T}} \tag{21}$$

That expression allows for an energetic interpretation of thermal diffusion: it is due to the difference between the transported energy $\underline{U}$ (at fixed p and T) and the difference h_{BA} between the partial molecular enthalpies of the components.

The transported energy $\underline{U}$ is defined through $\mathbf{j}_{\mathrm{E}}$ according to Eq. (7), namely

$$\mathbf{j}_{\mathrm{E}} = -\kappa \boldsymbol{\nabla} T + (\underline{U} - \tilde{\mu}_{\mathrm{BA}})\mathbf{j} \tag{22}$$

The contribution to $\mathbf{j}_{\mathrm{E}}$ other than the Fourier current gives rise to the so-called Dufour effect. The prefactor of $\mathbf{j}$ can equivalently be written as

$$c\left(\frac{\partial \tilde{\mu}_{\mathrm{BA}}}{\partial c}\right)_{p,T} TS_{\mathrm{T}} + h_{\mathrm{BA}} - \tilde{\mu}_{\mathrm{BA}} = c\left(\frac{\partial \tilde{\mu}_{\mathrm{BA}}}{\partial c}\right)_{p,T} TS_{\mathrm{T}} - T\left(\frac{\partial \tilde{\mu}_{\mathrm{BA}}}{\partial T}\right)_{p,c} \tag{23}$$

The next section examines how models of the Peltier effect can give insight into $\underline{U}$.

4 Specific models of the Seebeck effect

We have previously shown that the Seebeck and Soret effets are expressible in terms of an isothermal transported energy $\underline{U}$. In the former effect, $\underline{U}$ is referenced to the chemical potential $\tilde{\mu}_{\mathrm{e}}$ of the mobile particles, whereas in the latter it is referenced to the exchange molecular enthalpy h_{BA}. From Eq. (21) one understands why S_{T} is usually positive. Exchanging B with A has an energetic cost usually exceeding the mere interchange of B and A, depending on the energy barrier to be overcome in between. If $S_{\mathrm{T}} < 0$ is measured, then the process is energetically assisted by some mechanism [8,9] or coupled to the diffusion of other species [10]. To better understand the Soret effect, it is insightful to turn to the Seebeck effect, many models of which have been devised. Actually, the Peltier

effect is easier to model as it is isothermal. In what follows, we restrict ourselves to purely electronic mechanisms of isothermal heat transport not involving lattice vibrations, to which electrons are coupled.

Generally speaking, within the Lorentz framework it is found that [6,11-13]

$$\underline{U} = \langle\langle E\rangle\rangle + E_{\mathrm{D}} \tag{24}$$

where $E_{\mathrm{D}} = \langle D(E)\rangle/\langle\mu(E)\rangle$ involves the diffusivity $D(E)$ and mechanical mobility $\mu(E)$ as functions of the carrier energy E, and $\langle\ \rangle$ denotes an equilibrium statistical average. In semiconductors, where carrier statistics is non-degenerate, $E_{\mathrm{D}} = kT$. In metals, where carrier statistics is degenerate, E_{D} is of the order of the Fermi energy $E_{\mathrm{F}} = \tilde{\mu}_{\mathrm{e}} - E_{\mathrm{c}}$ at $T = 0\mathrm{K}$, where E_{c} is the bottom of the conduction band. As for $\langle\langle E\rangle\rangle$, it is a transport average of E, distinct from the equilibrium average $\langle E\rangle$ whose derivative $\mathrm{d}\langle E\rangle/\mathrm{d}T$ is the heat capacity of the carrier gas. If the momentum-relaxation rate varies as $(E - E_{\mathrm{c}})^{-r}$, one obtains, in the case of nearly-free conduction electrons (characterized by an effective mass) [6,11,13],

$$\langle\langle E\rangle\rangle = E_{\mathrm{c}} + \left(\tfrac{3}{2} + r\right)kT \tag{25}$$

In the Drude model where the rate is independent of E (i.e. $r = 0$), $\underline{U} = \langle E\rangle + kT$ in a semiconductor looks like a function of the thermodynamic state. In general, however, $\underline{U}$ depends on the kinetics of the carrier gas through the energy dependence r of the momentum-relaxation rate. That is why, contrary to W. Thomson's assumption, $q\Pi = \underline{U} - \tilde{\mu}_{\mathrm{e}}$ is not an equilibrium property of the carrier gas.

Whether conduction electrons or holes are considered, it is found that $q\Pi > 0$. Thus, nearly-free charge carriers transport a positive heat $\underline{U} - \tilde{\mu}_{\mathrm{e}}$. In metals, conduction electrons cannot be considered as nearly-free particles as the band structure is not parabolic far from E_{c}. Using Sommerfeld's expansion, one finds (with $q = -e < 0$) [11,13,14]

$$q\Pi = \frac{(\pi kT)^2}{3}\frac{\mu(E_{\mathrm{c}} + E_{\mathrm{F}})}{D(E_{\mathrm{c}} + E_{\mathrm{F}})} \tag{26}$$

Now between energy-dependent mobility and diffusivity, there exists a general relation independent of statistics, namely [15]

$$N(E)\,\mu(E) = \frac{\mathrm{d}}{\mathrm{d}E}[N(E)\,D(E)] \tag{27}$$

where $N(E)$ is the energy density of conduction states. Depending on the band structure of the metal, $N(E)$ is an increasing or decreasing function of E. The same is true of $D(E)$, which is a microcanonical average involving two functions of momentum, namely the group velocity and the vector mean free path or momentum-relaxation rate [12,15]. Again, we find that $q\Pi$ is not an equilibrium property of the carrier gas. From Eq. (27), within a purely electronic model of the Peltier effect we expect $q\Pi$ to be either positive or negative. This is indeed confirmed by experimental measurements: $q\Pi > 0$ in Na and $q\Pi < 0$ in Cu in the 10-400 K range [16]. In the latter material, Eq. (27) implies $\mu(E_c + E_F) < 0$. It means that conduction electrons at the Fermi level lose energy under the influence of an electric force, wherefore isothermal energy transport occurs contrariwise to particle transport. This is akin to the unusual (negative) sign of the Soret coefficient, although relation (23) between $\underline{U} - \tilde{\mu}_{BA}$ and S_T is less straightforward than relation (12) between $\underline{U} - \tilde{\mu}_e$ and S.

5 Conclusions

Using steady-state thermodynamics to describe both the Soret and Seebeck effects is not new [17] but does not appear so far to have been used to compare and connect their microscopic modelings. The analogue of the chemical potential of a mobile charge in a conductor is the exchange chemical potential in a binary mixture.

However, the Soret and Seebeck coefficients are not defined by means of analogous variables. In both effects, the particle-transport coefficient is related to an isothermal transport energy which is conceptually easier to handle. In metals, the Peltier energy is found to exhibit both signs in purely electronic models, depending on the dispersion relation and relaxation kinetics of the conduction electrons. This finding should foster the development of new models of the Soret and Dufour effect.

References

[1] R. Balian, *From Microphysics to Macrophysics*, vol. II (Springer, Berlin, 1992).

[2] N. Ben Abdallah, P. Degond and S. Genieys, J. Stat. Phys. **84**, 205 (1996).

[3] T. Grasser, T.-W. Tang, H. Kosina and S. Selberherr, Proc. IEEE **91**, 251 (2003).

[4] C. Kittel, *Elementary Statistical Physics* (Wiley, New York, 1958).

[5] W. Jones and N. H. March, *Theoretical Solid-State Physics* (Wiley-Interscience, London, 1973), vol. 2 chapter 6.

[6] P. N. Butcher, in *Crystalline Semiconducting Materials and Devices*, edited by P. N. Butcher, N. H. March and M. P. Tosi (Plenum, New York, 1986), pp. 131-194.

[7] [7] N. Pottier, *Physique statistique hors d'équilibre: Phénomènes irréversibles linéaires* (CNRS Editions, Paris, 2007).

[8] R. G. Mortimer and H. Eyring, Proc. Nat. Acad. Sci. USA **77**, 1728 (1980).

[9] M. E. Schimpf, in *Thermal Nonequilibrium Phenomena in Fluid Mixtures*, edited by W. Köhler and S. Wiegand (Springer, Berlin, 2002), pp. 285-309.

[10] M. P. Santos, S. L. Gómez, E. Bringuier and A. M. Figueiredo Neto, Phys. Rev. E **77**, 011403 (2008).

[11] A. Haug, *Theoretische Festkörperphysik* (F. Deuticke, Wien, 1964).

[12] E. Bringuier, Phys. Rev. E **61**, 6351 (2000).

[13] E. Bringuier, *Electrocinétique: Transport de l'électricité dans les milieux matériels* (CNRS Editions, Paris, 2005).

[14] J. M. Ziman, *Principles of the Theory of Solids*, 2nd edition (Cambridge U. P., 1972).

[15] E. Bringuier, Philos. Mag. B **77**, 959 (1998).

[16] J. S. Dugdale, *The Electrical Properties of Metals and Alloys* (Edward Arnold, London, 1977).

[17] L. D. Landau and E. M. Lifshitz, *Fluid Mechanics* (Pergamon, Oxford, 1959) and *Electrodynamics of Continuous Media* (Pergamon, Oxford, 1963).

The Dynamics for the Soret Motion of a Charged Spherical Colloid

S. N. Rasuli[1], R. Golestanian[2]

[1] School of the Physics, IPM(Institute for Theoretical Physics and Mathematics), P.O.Box 19395-5531, Tehran, Iran
[2] Department of Physics and Astronomy, University of Sheffield, Sheffield S3 7RH, UK

Contact: rasuli@mail.ipm.ir, r.golestanian@sheffield.ac.uk

Abstract

The Soret effect for a single charged colloidal particle, has been studied by different experimental groups in recent years [1, 2] and still seems a challenging topic. We know two distinct theoretical approaches to this phenomenon. The First, motivated with Ruckenstein in 1981 [3], is based on solving hydrodynamics equations for the charged fluid around colloid. This approach was restricted to colloids with thin double-layer around them [3–5], and was verified with Piazza and Guarino in 2002 [1]. The second approach however uses Gibbs enthalpy [2, 6] to predict the density profile of a colloid in a temperature field. It is seemed that this approach has been tested successfully for Polystyrene beads by Duhr and Braun [2]. Recently, Astumian [7] suggested that, we can interpret the Ruckenstein's approach as the deterministic motion of a charged colloid in a temperature field, while attribute the second approach to its stochastic Langevin motion in the temperature field [7]. Accepting his suggestion, two mentioned approaches, may come together in a unified theory which addresses both kinds of motion simultaneously.
Here, we extend the Ruckenstein's hydrodynamics approach to a colloid with arbitrary double-layer around it. We consider the dielectrophoretic force in our formalism, and since the Boltzmann weight is hardly reliable in the presence of a temperature gradient, we solve the diffusion equation to find ions densities. We consider both the convective and ions Soret motion in ions current densities [8].
For a weakly charged colloid, our equations are explicitly solved. The result has the Ruckenstein's formula, as its proper limiting case. For a colloid with high surface potential also, we solve the equations numerically. We confront the results with existing experimental data [1, 2] and possible agreements and/or disagreements are discussed [8, 9].

1 Introduction

Consider a charged spherical colloid, in a solution of water with added salt. The solution is subjected to a spatially varying temperature profile and our aim is to find its Soret coefficient. It is usually assumed that the Soret coefficient closely relates to particle drift velocity, due to the temperature gradient, (*i.e.* $\vec{V}_{drift} = -DS_T\vec{\nabla}T$) [3, 5]. This assumption however, is not completely justified, since the random motion of a colloid in the presence of a temperature gradient may also cause its non homogenous concentration [7]. However, this does not violates the existence of a propulsion mechanism, which cause particle deterministic motion (here called as Soret motion) toward hotter or colder side. Here trying to probe such a deterministic motion, we begin with equations, which govern the dynamics of fluid motion, ions densities, and electric potential, in the presence of a temperature gradient. We look for a steady answer of these coupled equations [8, 9].
For a weakly charged colloid, we use the Debye-Hückel approximation, and find an analytic answer for its Soret motion. Then, to find the Soret motion of a particle with arbitrary surface potential, we manipulate numerical calculations. Our results, however, seems insufficient to completely describe existing experimental observations [1, 2]. We hope that considering the fluctuation induced motions, will improve our results to find acceptable consistency with the experimental data.

2 Dynamical Equations

Dipolar water molecules and salt ions, around colloidal particle, are interacting with each other and with the colloid trough electric potential/field. To find the electric potential/field, we solve the Poisson equation $-\vec{\nabla}\cdot\varepsilon\vec{\nabla}\phi = 4\pi\sum_i q_i C_i$. Here q_i and C_i are the charge and concentration of the ith type of ions in solution, and ε is the electric permittivity of medium. Due to its dependence on local temperature, ε is spatially varying. The fluid velocity field (*i.e.* $\vec{V}(\vec{r},t)$) is governed with the Navier-Stocks equation. But as we are dealing with an incompressible fluid (*i.e.* $\vec{\nabla}\cdot\vec{V} = 0$), and in the low Reynolds number limit, the Navier-Stocks equation simplifies to

$$\frac{\partial}{\partial t}\vec{V} = \eta\nabla^2\vec{V} - \vec{\nabla}P + \vec{F} \tag{1}$$

where t is the time, η fluid viscosity, P fluid pressure, and $\vec{F}$ the body force fluid feels. The fluid is a solution of charged ions and water dipolar molecules. It feels a net force of $\vec{f}_{ion} = -\vec{\nabla}\phi\sum_i q_i C_i$, due to electric force on ions. Each of water molecules also, has a dipolar moment of $\vec{p}$. The spatial variation of electric field causes a net force of $(\vec{p}.\vec{\nabla})\vec{E}(\vec{r})$ on each molecule. This leads to a body dielectrophoretic force of [10]:

$$\vec{f}_{water} = \vec{\nabla}\left(\frac{\varepsilon-1}{8\pi}|\vec{E}|^2\right) - \left(\frac{1}{8\pi}|\vec{E}|^2\right)\vec{\nabla}\varepsilon \tag{2}$$

on fluid. Therefore, $\vec{F}$ will be $\vec{f}_{ion} + \vec{f}_{water}$.
Considering the Soret motion, we are expecting a permanent and steady motion which eventually creates a time independent concentration profile. Therefore, we look for a steady time independent phenomenon, in the colloid framework. So we simplify Eq.(1)

to the steady Stocks equation:

$$-\eta\nabla^2\vec{V} = -\vec{\nabla}\left(P - \frac{\varepsilon-1}{8\pi}|\vec{E}|^2\right) - \vec{\nabla}\phi\sum_i q_i C_i - \left(\frac{1}{8\pi}|\vec{E}|^2\right)\vec{\nabla}\varepsilon \tag{3}$$

Here, $P - \frac{\varepsilon-1}{8\pi}|\vec{E}|^2$ behaves like pressure and eliminates if we focus on the fluid velocity field [9].
At last, to find ions densities, C_i, we define a mean current density:

$$\vec{J_i} = -D_i\vec{\nabla}C_i - \mu_i C_i q_i\vec{\nabla}\phi + \vec{V}C_i - D_i C_i S_T^{\text{ion}}\vec{\nabla}T \tag{4}$$

Here D_i and μ_i are the diffusion coefficient and mobility of ith species respectively (they are relating together with Einstein formula: $D_i(\vec{r}) = \mu_i K_B T(\vec{r})$). S_T^{ion} also, is ions Soret coefficient. The conventional term, $-D_i C_i S_T^{\text{ion}}\vec{\nabla}T$, is added to generalize Fick's equation to non-isothermal condition. We restrict ourself to $1:1$ salts, so expect equal Soret coefficient for both types of co-ions and counter-ions [12]. Then, to find ions densities in colloid framework, we solve the steady conservation equation: $\vec{\nabla}\cdot\vec{J_i} = 0$.

3 Analytic solution

For a weakly charged colloid, we use the Debye-Hückel approximation to solve our equations. The colloid drift velocity will be found as:

$$\vec{V_D} = \frac{-\varepsilon\phi_S^2}{48\pi}\frac{\vec{\nabla}T}{\eta T_0}\left[(1-\alpha+T_0 S_T^{\text{ion}})F(\kappa a) + 2\alpha - G(\kappa a)\right] \tag{5}$$

Here $\phi_S = Zq/\varepsilon a(1+\kappa a)$ is the (zeta) potential of the surface of the colloid, a is colloid radius, and $\kappa = \sqrt{8\pi q^2 C_0/\varepsilon k_{\text{B}} T_0}$ is the inverse Debye length. In addition $F(x) = 2x - 4x^2 e^{2x} E_1(2x)$ and $G(x) = \frac{x}{6}[x(1+x)(12-x^2)e^x E_1(x) + 8 - 11x + x^3 - 24xe^{2x}E_1(2x)]$, with $E_1(x) = \int_x^\infty e^{-s}ds/s$. As shown in Fig.1, they have asymptotic limits of $F(x) = 1$ and $G(x) = 0$ for $x \to \infty$ and $F(x) \simeq 2x$ and $G(x) \simeq 4x/3$ for $x \ll 1$.

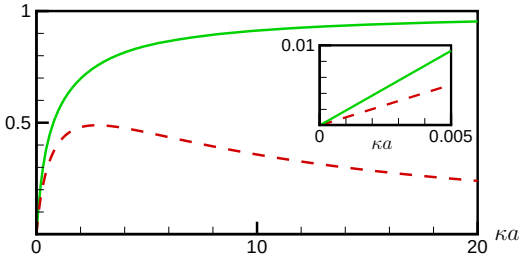

Fig. 1: *$F(\kappa a)$ (solid green line) and $G(\kappa a)$ (dashed red line) versus κa. Inset: showing the small κa behavior.*

It is interesting to look at Eq.(5) in two limits of an infinitely thin and infinitely thick double-layer. For a thin double-layer (*i.e.* $\kappa a \gg 1$) Eq.(5) simplifies to:

$$\vec{V}_D = \frac{-\varepsilon\phi_S^2}{48\pi}\frac{\vec{\nabla}T}{\eta T_0}\left[1+\alpha+T_0 S_T^{\rm ion}\right] \qquad (6)$$

This confirms older Ruckenstein result $(-\varepsilon\phi_S^2/48\pi)(\vec{\nabla}T/\eta T_0)$ [3], if we note note that he neglected both the dielectrophoretic force (*i.e.* $\alpha = 0$) and ions Soret motion (*i.e.*$S_T^{\rm ion} = 0$).
The other limit of an infinitely thick double-layer (*i.e.* $\kappa a \ll 1$) corresponds to zero salt density in solution (*i.e.* $C_0 = 0$). The colloid drift velocity will be found as $2\alpha(-\varepsilon\phi_S^2/48\pi)(\vec{\nabla}T/\eta T_0)$. It means that in the absence of ions, the phenomenon is totally governed by dielectrophoretic force, or the force which dipolar water molecules feels.
Finally, we compare our analytic results with Duhr *et.al.* data for Polystyrene beads [2]. The beads are weakly charged and inside the Debye-Hückel regime. Sadly, our results are considerably (*e.g.* 60 times) smaller than Duhr *et.al.* observations. To compare our results with other experimental data, we manipulate numerical calculations.

4 Numerical Solution

Piazza and Guarino have measured the Soret coefficient of Sodium Dodecyl Sulfate (SDS) micelles [1]. A SDS micelle however, is a highly charged colloid [13], and we should manipulate numerical calculations to find its Soret drift velocity. Here, we use the model, suggested by Srinivasan *et.al* [9, 13], to estimate its radius, aggregate number and charge. We consider a spherical colloid of radius $a = 2.5$nm, mean aggregate number of $N \simeq 120$, and charge of $Z = 50 - 60$e (the charge depends on ionic strength of solution). We lift our data by a constant value, which refers to possible non-electrostatic effects

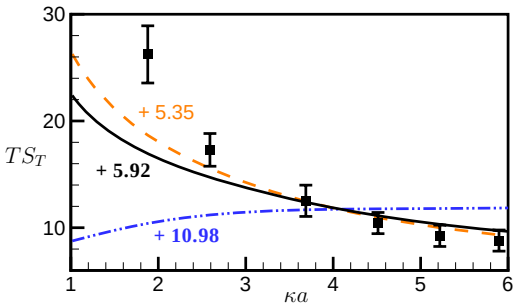

Fig. 2: *Comparison of our theory and Piazza* et.al. *data: The solid (black) curve is result of our full calculation. For the dashed-dotted (blue) curve, we have turned off the dielectrophoretic force in our formalism, and for the dashed (orange) curve, we have neglected the effect of convective motion on ions densities. The number beside each curve, shows the constant we added to obtain the best fit.*

in Soret motion, and use the dimensionless variable of TS_T to compare our results with experimental data. The results come in Fig.(2). The Solid (black curve) shows our full result. There is an acceptable harmony for $\kappa a > 3$, but it is lost as we go to smaller κas, and further amendments of this theory have not given us better agrement yet [9].
To find a deeper understanding, we track the contributions of convective motion and dielectrophoretic force in our result. The dashed-dotted (blue) curve in Fig.(2) shows our results with dielectrophoretic force turned off. Even the trend of the curve is changed. It shows that, like analytic regime, the dielectrophoretic force is non negligible. The dashed (orange) curve in Fig.(2) also, shows our results when the correction due to the convective motion on ions densities is turned off. TS_T seems to be intensified and yields a better agrement. Maybe it means that fluid motion is washing ions away from their positions, and weakening the colloid Soret motion.

5 Conclusions

In conclusion, this hydrodynamics theory seems insufficient to explain existing experimental observations. Considering the Piazza *et.al.* experiment, it has non negligible predictions. Therefore, we can not forget about the hydrodynamics based theories in Soret effect. But to obtain better agreements further extensions are required. Maybe an important extension will be the consideration of the fluctuation induced motions.

Acknowledgment

We are grateful to E. Bringuier, R. Ejtehadi, F. Miri, and P. Pincus for helpful discussions, A. Naji for his assistance.

References

[1] R. Piazza and A. Guarino, Phys. Rev. Lett. **88**, 208302 (2002)
[2] S. Duhr and D. Braun, Proc. Natl. Acad. Sci. U.S.A. **103** 19678 (2006); S. Duhr and D. Braun, Phys. Rev. Lett. **96**, 168301 (2006)
[3] E. Ruckenstein, J. Colloid. Interface. Sci. **83**, 77 (1981)
[4] B V Derjaguin, N V Churaev and V M Muller, *Surface Forces* (Consultants Bureau (Plenum), New York, 1987).
[5] K.I. Morozov, JETP. **88**, 944 (1999)
[6] J. K. G. Dhont *et al.*, Langmuir **23**, 1674-83 (2007)
[7] R.D. Astumian, Proc. Nat. Acad. Sci. USA **104**, 3 (2007)
[8] S.N. Rasuli and R. Golestanian, submitted to PRL (see also: ArXiv 0708.0090v1)
[9] S.N. Rasuli and R. Golestanian, unpublished
[10] L.D. Landau and E.M. Lifshitz, *Electrodynamics of Continuous Media* (Butterworth-Heinenmann, Oxford, 1984)
[11] *C.R.C. Handbook* (Jhon Wiley and Sons, NewYork, 1995)
[12] D.R. Caldwell, J. Phys. Chem. **77**, 2004 (1973); F.S. Gaets *et al.*, J. Phys. Chem **86**, 2967 (1982); P.N. Snowdon *et al.*, Trans. Faraday. Soc. **56**, 1812 (1960)
[13] V. Srinivasan *et.al*, Langmuir **19**, 9932 (2003)

[14] D. Stigter, J. Phys. Chem. **68**, 3603 (1964)
[15] C. Debuschewitz and W. Köhler, Phys. Rev. Lett. **87**, 055901 (2001); S. Wiegand, J. Phys.: Condens. Matter **16**, R357 (2004)

Simulations

New theoretical model for thermal diffusion: Prigogine's approach revisited!

P.-A. Artola[1], B. Rousseau[1], G. Galliéro[2]

[1]Laboratoire de Chimie Physique, UMR 8000
Université de Paris Sud 11
91405 Orsay Cedex - France
[2]Laboratoire des Fluides Complexes, UMR 5150
Université de Pau et des Pays de l'Adour
BP 1155
64013 Pau Cedex - France

Contact: bernard.rousseau@lcp.u-psud.fr

Abstract

We present a new model for thermal diffusion and we compare its results to both simple and realistic systems. This model is derived from a kinetic approach with explicit mass and chemical contributions. It involves self-diffusion activation free energies, following Prigogine's original approach. We performed furthermore both equilibrium and non equilibrium molecular dynamics in order to compute respectively the self diffusion activation free enthalpies and the Soret coefficient when no experimental data were available. Our model is in very good agreement with simulation data on Lennard-Jones mixtures, and a good behavior is noted for the water ethanol mixture where the composition dependence at which the Soret coefficient changes its sign is predicted very accurately. We lastly propose a new water ethanol experiment at higher temperature in order to check the validity of our model.

1 Introduction

Thermal diffusion, or Soret effect, occurs when a mixture is subjected to a thermal gradient. Molar fraction gradients appear as a response [1]. The transport coefficient associated is the Soret coefficient. Its sign indicates if the related species goes preferentially to the hot or the cold, its value gives the amplitude of the separation. Usually small for simple fluids, its value can be three or four orders of magnitude higher in complex fluids than in alkanes mixtures for instance [1]. Experiments became really accurate a few decades ago (see for instance [2]). Köhler showed that the Soret coefficient can be split into three additive terms, a mass, a moment of inertia and a "chemical" contribution [3]. At that point, several theoretical attempts based on variational approaches were proposed but they seem inaccurate (see for instance a review of these models in [4]) even on the simplest mixtures [5].
Firoozabadi [6] and later Saghir [7] proposed an Onsager's like approach to the Soret effect. Using a thermodynamic approximation to estimate thermal energy transported [8], their approach reproduces accurately the chemical part of the Soret coefficient [5]. Another "theoretical" problem is that these last approaches depend on adjustable parameters. As it has been shown several times, these approaches are very similar to activated processes (see for instance [9]), like Prigogine used in his model [10], and all these theories are self consistent. The remaining problem is that the mass effect of thermal diffusion is not taken into account in all these descriptions [11].
In this work, we show, using basics in Transition State Theory, how to modify Prigogine's equations to input this mass effect inside the derivation [11]. We propose a way to estimate the activation energies, following Drickamer's idea, and show that it clearly is compatible with Firoozabady and Saghir's estimations. The new formula derived with this method reproduces results on simple Lennard-Jones systems with high accuracy.

2 A new derivation following Prigogine's model of thermal diffusion

2.1 Classical Prigogine model

Prigogine proposed a model for thermal diffusion that is a simple "swap" between two particles 1 and 2. His approach follows an activated model for diffusion [10]. We consider that the thermal gradient is along the z direction. Particle 1 is on the "left" (cold) side, and particle 2 on the "right" (hot) side. What has to be noted is that the coordinate reaction is the local temperature. So forth, particles 1 and 2 are not exactly at the same temperature. Prigogine showed that the swap flux can be written as :

$$J^+ \propto x_1(z - dz/2)x_2(z + dz/2) \exp\left(-\frac{\Delta G_1^\#}{R(T - dT/2)}\right) \exp\left(-\frac{\Delta G_2^\#}{R(T + dT/2)}\right)$$

where x_i is the local molar fraction of species i, $\Delta G_i^\#$ are the diffusion activation free enthalpies, simply defined as:

$$D_i = D_i^0 e^{-\beta \Delta G_i^\#}$$

Using equilibrium molecular dynamics, we determined these diffusion activation free enthalpies as the slope of the logarithm of the diffusion coefficients versus the temperature for Lennard-Jones systems. We used two energetic parameters, a cross interaction parameter k_{12} and a direct interaction parameter ψ_ε (see [5]). For each molar fraction, we computed at the equilibrium the self diffusion coefficients of each species using the mean square displacement correlation for 5 temperatures, the mean temperature T_0 and then for four others at $T_0 \pm 3\,K$, $T_0 \pm 6\,K$. Given the flux expression, we can easily write the equivalent flux in the other direction. At the stationnary state, the total flux cancels. This gives the simple expression for the Soret coefficient :

$$S_{T,1}^P = \frac{\Delta G_2^\# - \Delta G_1^\#}{RT^2}$$

2.2 Mass effect

As was shown many times, the Soret coefficient is mass dependent (see for instance [3]). In our systems, we firstly considered same mass particles. We then decided to change the mass of one of the two species with a ratio: $\psi_M = M_2/M_1 = 2.0$
We decided to apply Prigogine's model for this system. Figure 1 presents the results we had using Prigogine's model. As can be noted, Prigogine's model is mass independent. This can be understood as follows: in Transition State Theory, mass interferes on the reaction coordinate. Physically, it means that the position of the transition state depends on the masses (see for instance the revue from Truhlar [12], or [13]). For Prigogine's thermal diffusion model, this coordinate is the local temperature. It is then needed to "rescale" this reaction coordinate with the masses of the particles. This gives a new expression for the mass flux that is :

$$J^+ \propto x_1(z - dz/2)x_2(z + dz/2) \exp\left(-\frac{\Delta G_1^\#}{R(T - \xi_1 dT)}\right) \exp\left(-\frac{\Delta G_2^\#}{R(T + \xi_2 dT)}\right)$$

where ξ_i defines barycentricly the transition state as:

$$\xi_1 = \frac{M_2}{M_1 + M_2} \quad \xi_2 = \frac{M_1}{M_1 + M_2}$$

The derivation is then exactly the same than Prigogine's one and one will find (defining the mass ratio as $\psi_M = M_2/M_1$):

$$S_{T,1} = 2\frac{\Delta G_2^\# - \psi_M \Delta G_1^\#}{(1 + \psi_M)RT^2}$$

This equation can be expressed in the form of different contributions, as introduced by Köhler:

$$S_{T,1} = \frac{\Delta G_2^\# - \Delta G_1^\#}{RT^2} + \frac{1 - \psi_M}{1 + \psi_M}\frac{\Delta G_2^\# + \Delta G_1^\#}{RT^2}$$

Figure 1 shows the results of our new "revisited Prigogine's model" for thermal diffusion. As we can see, it is accurate for our Lennard-Jones systems.
Some remarks about our model has to be precised:

- In our new formula, the moment of inertia term does not appear. We are not able at this stage to propose a formula. Some work about this problem has already be done and suggests a not so simple picture of independence of the mass and the moment of inertia terms [15].
- For low density, we are no longer in an activated regime, so forth the usual Chapman Enskog [14] term has to be added to our formula.
- For isotopic effects, our formula seems composition independent, instead of what has already been seen for high isotopic effect on Lennard-Jones mixtures. This feature is not taken into account yet [16].

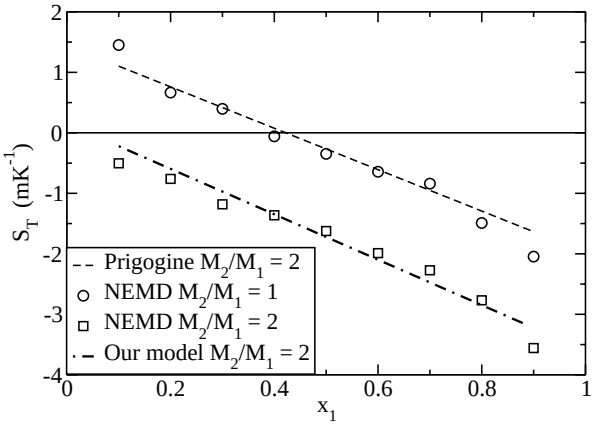

Fig. 1: *Soret coefficients computed from NEMD simulations compared to our new kinetic model including the mass effect. Parameters are:* $k_{12} = 1.75$ *and* $\psi_\varepsilon = 1.4$

3 Conclusion

We introduce a new model of thermal diffusion following the historical model written by Prigogine. As we show, this new model is accurate for Lennard-Jones systems, even for different masses. We reproduce Köhler's picture of different additive contributions. In our presentation, we will present results on the water ethanol mixture and the results of our model on this more "realistic" model.

References

[1] S. Wiegand, *Thermal diffusion in liquid mixtures and polymer solution*, Journal of Physics: Cond. Mat., **16**, R357-R379 (2004)

[2] J. K. Platten and M. M. Bou-Ali and P. Costesèque and J. F. Dutrieux and W. Köhler and C. Leppla and S. Wiegand and G. Wittko, *Benchmark values for the Soret, thermal diffusion and diffusion coefficients of three binary organic liquid mixtures*, Phil. Mag., **83** (17-18), 1965-1971 (2003)

[3] C. Debuschewitz and W. Köhler, Phys. Rev. Lett. **87**, 055901 (2001)

[4] L.J.T.M. Kempers, *A comprehensive thermodynamic theory of the Soret effect in a multicomponent gas, liquid, or solid*, J. Chem. Phys., **115** (14), 6330-6341 (2001)

[5] Pierre-Arnaud Artola and Bernard Rousseau, *Microscopic Interpretation of a Pure Chemical Contribution to the Soret Effect*, Phys. Rev. Lett., **98** (12), 125901 (2007)

[6] K. Shukla and A. Firoozabadi, *A New Model of Thermal Diffusion Coefficients in Binary Hydrocarbon Mixtures* Ind. Eng. Chem. Res., **37**, 3331-3342 (1998)

[7] C.G. Jiang and M.Z. Saghir and S. Derawi and M. Kawaji, *Accuracy of the theoretical calculation of the Soret coefficient for water-ethanol mixtures in comparison with experimental data*, Journal of Non-Equilibrium Thermodynamics, **30**, 337-358 (2005)

[8] G. Glasstone, K. J. Laider, H. Eyring, *Theory of Rate Processes*, Mc Graw-Hill Book Company, Inc, New York, 1941

[9] Stanislaw Sieniutycz, *Thermodynamic Structure of Nonlinear Macrokinetics in Reaction-Diffusion Systems*, Open Systems & Information Dynamics **11** (2), 185-202 (2004)

[10] I. Prigogine and L. De Brouckère and R. Amand, *Recherche sur la thermodiffusion en phase liquide (2ème communication)*, (11-12), 851-860 (1950)

[11] Pierre-Arnaud Artola, Bernard Rousseau and Guillaume Galliero, Unpublished yet

[12] Antonio Fernàndez-Ramoz, James A. Miller, Stephen J. Klippenstein and Donald G. Truhlar, *Modeling the Kinetics of Biomolecular Reactions*, Chemical Revue, **106**, 4518-4584, (2006)

[13] Jeffrey I. Steinfeld, Joseph S. Francisco, William L. Hase, *Chemical Kinetics And Dynamics*, Pretence Hall, Englewood Cliffs, New Jersey 1989

[14] S. Chapman and T.G. Cowling, *The Mathematical Theory Of Non-Uniform Gases*, Cambridge University Press, 1939

[15] Guillaume Galliéro, Bernard Duguay, Jean-Paul Caltagirone and Franois Montel, *Thermal Diffusion Sensitivity to the Molecular Parameters of a Binary Equimolar Mixture, a Non-Equilibrium Molecular Dynamics Approach*, Fluid Phase Equilibria, **208**, 171188, (2003)

[16] Guillaume Galliéro, Mathilde Bugel, Bernard Duguay and Francois Montel, *Mass Effect on Thermodiffusion using Molecular Dynamics*, J. Non-Equilib. Thermodyn. **32**, 251258 (2007)

Molecular description: influence on thermodiffusion in non-polar simple mixtures

Guillaume Galliero

Laboratoire des Fluides Complexes (UMR-5150), Université de Pau et des Pays de l'Adour, BP 1155, F-64013 PAU Cedex, France.

E-mail: guillaume.galliero@univ-pau.fr

Abstract

Using NonEquilibirum Molecular Dynamics on model systems, new insights on the influence of the molecular description on thermodiffusion in non polar mixtures is provided. First, is studied the influence of the interaction potential shape (between Lennard-Jones and two definitions of an "equivalent" Exponential-6 potential). Quite surprisingly, it appears that, even in very dense systems, the amplitude of thermodiffusion in binary equimolar "isotopic" mixture is nearly independent of the choice of the potential when temperature and density are used as inputs. Then, it is shown, on diatomic Lennard-Jones mixtures of varying bond lengths that the usual mass and momentum inertia contribution decomposition seems suitable but is not perfectly respected. In addition, the momentum inertia contribution to thermodiffusion is found to be of the same sign than the pure mass effect one. Finally, using ternary and "equivalent" binary mixtures defined through a one-fluid approximation, it is shown that the usual mixing rule on mass induces non negligible deviations on thermodiffusion. An alternative mixing rule is proposed which allows a correct estimation of what occurs in ternary mixtures by using "equivalent" binary ones.

1 Introduction

Thermodiffusion is believed to be the transport property which is the most sensitive to the molecular description [1]. Hence, when accurate experimental results exist, this property may be a severe test for molecular models and/or theories that rely on molecular concepts. Evolved kinetic theories have shown that the nature of the interaction potential and molecular description [1] may affect strongly thermodiffusion in low density mixtures. More recently, using molecular dynamics (MD) simulations on Lennard-Jones dense mixtures, the influence of molecular parameters on thermodiffusion has been analyzed [2-3] and clearly shows that, in binary mixtures, the heaviest, smallest, most "energetic" species tends to migrate toward the cold area relatively to the other species. In addition, using lattice and MD simulations, it has been shown that the cross interaction parameters may affect the amplitude and the sign of thermodiffusion in model mixtures [4-6]. Elsewhere, experiments on mixtures with an isotopic substitution have shown that, it is possible to decompose the Soret coefficient in one part due to the mass of the species (proportional to $\Delta m/\Sigma m$), one to the inertia momentum (proportional to $\Delta I/\Sigma I$) and one to everything else (the so called "chemical" part) [7]. It should be noted that such an assumption implies that no couplings occurs between the dynamic and the static (thermodynamic) contributions to the thermodiffusion, which is questionable [8].

In this work, using NonEquilibirum Molecular Dynamics on model systems, is provided further information on the influence on thermodiffusion of the molecular description in non polar mixtures. In particular, are studied the influence of the interaction potential shape (between Lennard-Jones and Exponential-6 potentials), the possibility to separate additively mass and moment inertia contributions and the limitations of a one-fluid approximation to reduce a ternary mixture to an "equivalent" binary one.

2 Theory and Modelling

2.1 Interaction potentials

In this work, two different kinds of effective truncated potentials have been used to describe interactions between particles, the Lennard-Jones 12-6 (LJ) and the Exponential-6 (Exp-6) potentials, that can be written respectively as:

$$U_{LJ} = \varepsilon\left[\left(\frac{r_m}{r}\right)^{12} - 2\left(\frac{r_m}{r}\right)^{6}\right] \tag{1}$$

$$U_{Exp-6} = \varepsilon\left[\left(\frac{6}{n-6}\right)e^{-\alpha\left(\frac{r}{r_m}-1\right)} - \left(\frac{n}{n-6}\right)\left(\frac{r_m}{r}\right)^{6}\right] \tag{2}$$

where ε is the potential strength, r_m the distance at which the potential is minimum, α the stiffness of the repulsive slope and r the intermolecular separation. In order to define reduced variables, has been used, σ, the "atomic diameter", which is the distance at which the potential is null. To define the Exp-6 "equivalent" to the LJ, two alternatives derived analytically [9] have been used that lead to n=13.772 (Exp1) and n =14.338 (Exp2).

When Lennard-Jones chains are involved, a harmonic spring with a stiffness constant equal to $30000\varepsilon/\sigma^2$ has been used to define intramolecular interactions.

2.2 Simulations details

Simulations have been performed on systems composed of 1500 particles in cubic boxes with full periodic conditions. Berendsen Thermostat and Barostat have been used. The Non-Equilibrium scheme proposed by Hafskjold et al. has been used to generate a biperiodical thermal gradient [10]. After discarding the transient state, thermal diffusion factors, α_T, have been estimated using data collected for 5 to 10.10^6 timesteps in order to ensure a sufficient statistic. The cutoff radius, r_c, has been taken equal to 2.5σ except for the study of the influence of the potential shape (where r_c=3.5σ).

3 Results and Discussion

3.1 Influence of the potential shape

To quantify the thermodiffusion sensibility to the potential shape in various dense states, MD simulations have been performed on equimolar "isotopic" mixtures (r_m and ε are equal for both compounds and m_2=10m_1) for the LJ, Exp1 and Exp2.

ρ*	T*	α_T LJ	α_T Exp1	α_T Exp2
0.3	1.5	0.801±121	0.797±150	0.778±145
0.3	2.5	0.909±101	0.909±89	0.927±104
0.7	2.5	2.067±128	2.038±185	2.014±127
0.8	1	2.362±144	2.485±157	2.402±290
0.8	2.5	2.322±178	2.287±198	2.33±147
0.9	1	2.339±287	2.261±298	2.346±306
0.9	2.5	2.479±151	2.437±138	2.359±128

Table 1: *Thermal diffusion factors, α_T, of LJ, Exp1 and Exp2 in "isotopic" equimolar mixtures (m_2/m_1=10) for various thermodynamic states.*

Quite surprisingly, see Table 1, taking into account intrinsic uncertainties on the values (≈10 %), it appears that both Exp1 and Exp2 potentials were able to provide α_T values very close to those obtained using the LJ potential, (Average Absolute Deviation is equal to 2.3 % when using Exp1 and 1.9 % when using Exp2). In addition, the deviations do not exhibit any trend with the thermodynamic state and do not particularly increases for the densest states.

Thus, the behavior noted on α_T is interesting as it unambiguously shows that, for a given set of T^* and ρ^*, thermal diffusion in "isotopic" mixtures is not largely affected by the choice of the potential shape (at least between Exp-6 and LJ) in moderate to high densities systems. Therefore, with the precision accessible by MD simulations at that time, contrary to what occurs in more complex mixtures, thermal diffusion cannot always serve to discriminate between potential shapes as commonly believed.

3.2 Momentum Inertia contribution

Mixtures of LJ diatomic chains described by the same molecular parameters (volume, energy, bond length) except the mass (m_2/m_1=10) have been studied (mixtures are so "ideal" in the thermodynamic sense and hence the thermal diffusion factor should be only dependent to the mass and the inertia momentum of both species). Keeping T^* and P^* constant, we have changed the bond length, L^* ($=L/\sigma$), and performed the simulation in dense equimolar binary mixture (T^*=2, P^*=5.3). In such systems, if the decomposition proposed in [7] is correct, thermodiffusion should be constant whatever the bond length (because for that precise case $\Delta I/\Sigma I$ reduces to $\Delta m/\Sigma m$)..

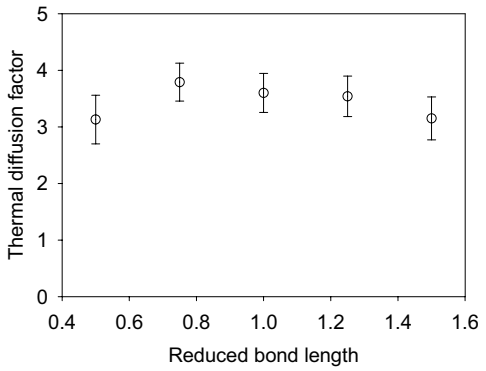

Fig. 1: *Thermal diffusion factor in binary equimolar mixtures of Lennard-Jones chains with two segments and m_2/m_1=10 for different bond length at T^*=2 and P^*=5.3.*

From the results provided on Fig. 1, it appears that the thermal diffusion factor is slightly dependent to the bond length, which means that the decomposition proposed in [7] makes sense for this situation but is not perfectly respected. In addition, in all cases the thermal diffusion factor is larger than the one due to the mass effect only, equal to 2.35±0.15. This indicates that the momentum inertia contribution is always positive (but smaller than that of mass effect alone), which is consistent with experiment findings [7].

3.3 One-fluid approximation

Most of the fluids of interest (especially in the petroleum industry) are multicomponent by nature. Usually a lumping scheme is used to reduce the number of compounds involved. At the microscopic scale this consists in defining pseudo-compounds "equivalent" to a mixture of real ones through a one-fluid approximation. As a first test of such one-fluid approximation on mass for thermodiffusion, two ternary mixtures for four different thermodynamic states have been simulated. The two ternary mixtures are the following:

-First mixture: $\sigma_i=\sigma_j$, $\varepsilon_i=\varepsilon_j$, $x_1=0.5$, $x_2=x_3=0.25$ and $m_1=1$, $m_2=5$ and $m_3=15$.

-Second mixture: $\sigma_i=\sigma_j$, $\varepsilon_i=\varepsilon_j$, $x_1=0.5$, $x_2=x_3=0.25$, $m_1=1$, $m_2=20/11$ and $m_3=200/11$.

The two binary "equivalent" mixtures (through a one-fluid approximation) have been defined so that components 2 and 3 are gathered to form a unqiue "equivalent" pseudocompound. The way this pseudocompound is defined depends on the choice of the mixing rule on mass. The first rule used is the usual linear law (weighted by the molar fractions) and the second one writes as:

$$m_x^{1/2} = \sum_i \sum_j x_i x_j \left(\frac{2 m_i m_j}{m_i + m_j} \right)^{1/2} \tag{3}$$

	$T^*=1.5$, $\rho^*=0.3$	$T^*=2.5$, $\rho^*=0.3$	$T^*=1$, $\rho^*=0.7$	$T^*=2.5$, $\rho^*=0.7$
Mix. 1, linear law	12.9	10.7	1.8	1.0
Mix. 2, linear law	25.4	24.0	17.5	28.2
Mix. 1, eq. (3)	5.7	2.4	-1.8	-1.0
Mix. 2, eq. (3)	3.2	-1.3	2.1	8.0

Table 2: *Deviations (in percentage) between thermal diffusion ratios, k_T, of the first compound in the ternary mixtures and the binary "equivalent" ones using the linear law on mass and the law defined by eq. (3).*

Table 2 clearly shows that the usual linear law on mass, despites a reasonable estimation, induces non negligible deviations that are larger in low density systems and for the mixtures for which component 2 and 3 have a large mass ratio. In fact, using the linear mixing rules, eq. (18), the "equivalent" mass of component 2 and 3 is overestimated. In addition, results provided in Table 2 clearly confirm that the mixing rule on mass defined by eq. (3) seems to be more efficient that the usual linear one, deviations being lower than 10 % for the systems studied.
It should be mentioned that the extension of such a scheme to multicomponent mixtures is straightforward. Nevertheless, the choice of the reference compound is important as long as the scheme does not ensure that the sum of all k_T is equal to zero.

4 Conclusions

In this work, using non-equilibrium Molecular Dynamics simulations, have been analysed various aspects of the influence of the molecular description on thermodiffusion in simple non polar fluid mixtures for various thermodynamic states.

In a first part is studied the influence of the shape of the potential (between LJ and Exp-6 ones) on the amplitude of thermodiffusion in binary equimolar "isotopic" mixtures. From the simulation results, quite surprisingly, it appears that, for such mixtures, thermodiffusion is nearly independent of the potential shape even in very dense states.

In a second section, by varying the bond length in diatomic equimolar mixtures, is analysed the momentum inertia contribution to thermodiffusion. It appears that, in all cases the momentum inertia contribution is positive (of the same sign than the pure mass effect) but is not perfectly independent of the bond length. This implies that a simple addition between momentum inertia and mass effects makes senses but does not hold perfectly in such systems with high mass ratios.

In a last part, is quantified the effect of a one-fluid approximation when trying to reduce a ternary mixture to a simple binary one in "isotopic" mixtures. It is shown that the usual mixing rule on mass is inadequate. Nevertheless, if an appropriate law is used (eq. 3), it appears that such lumping scheme may be a seducing approach.

Acknowledgment

A part of this work, has been supported by the Diffusion and Soret Coefficient project (ESA).We gratefully acknowledge computational facilities provided by TREFLE laboratory.

References

[1] S. Chapman and T.G. Cowling, *The Mathematical theory of non-uniform gases*, Cambridge Mathematical Library, 1970.

[2] P. Bordat, D. Reith and F. Müller-Plathe, J. Chem. Phys. **115**, 8978 (2001).

[3] G. Galliero, Fluid Phase Equi. **224,** 13 (2004).

[4] G. Galliero, B. Duguay, J.P. Caltagirone and F. Montel, Fluid Phase Equi. **208**, 171 (2003).

[5] P.A. Artola and B. Rousseau, Phys. Rev. Lett. **98**, 125901 (2007).

[6] J. Luettmer-Strathmann, Int. J. of Thermophys. **26**, 1693 (2005).

[7] C. Debuschewitz and W. Köhler, Phys. Rev. Lett. **87**, 055901 (2001).

[8] G. Galliero, M. Bugel and B. Duguay, J. of NonEqui. Thermo. **32**, 251 (2007).

[9] G. Galliero, C. Boned, Submitted to J. Chem. Phys.

[10] B. Hafskjold, T. Ikeshoji and S.K. Ratkje, Mol. Phys. **80**, 1389 (1993).

Non-isothermal gravitational segregation by molecular dynamics simulations

Guillaume Galliero[1], François Montel[2]

[1]*Laboratoire des Fluides Complexes (UMR-5150), Université de Pau et des Pays de l'Adour, BP 1155, F-64013 PAU Cedex, France.*
[2]*TOTAL SA Avenue Larribau, F-64018 PAU Cedex, France.*

E-mail: guillaume.galliero@univ-pau.fr

Abstract

In this work, for the first time ever to the best of our knowledge, a molecular dynamics scheme is proposed to study gravitational segregation of isothermal and non-isothermal fluid mixtures in convection free configuration. The simulations (in a dense supercritical state) have been performed on equimolar binary Lennard-Jones "isotopic" mixtures (M_2/M_1=10) for various amplitudes of gravity and thermal field that are both oriented vertically. First, in an isothermal situation, as expected, the lightest component is shown to enrich at the top and these simulations have confirmed the fact that the segregation characteristic time is related to the mass-diffusion one even if the precise dynamics should be further studied. Then, it is demonstrated that, in all cases, the molecular dynamics equilibrium concentration profiles are consistent with what can be estimated from the macroscopic theory of such process taking into account correctly the thermodiffusion contribution. In addition, it is shown that, under huge thermal gradients, when heated from below, the thermodiffusion may even reverse the concentration profile so that the heaviest species becomes enriched at the top of the cell.

1 Introduction

A precise knowledge of the initial state of a petroleum reservoir is crucial in order to optimize its development plan. Such knowledge relies on the ability of describing correctly the distribution of the hydrocarbons in the reservoir which is mainly modeled by the gravity field through the gravitational segregation [1]. In fact, just by adding the gravity contribution to the chemical potential (described by an *ad hoc* thermodynamic model) it is possible to estimate the composition of the fluid column from the one at a reference depth. Nevertheless, in many fields, the compositional profile computed so differs from the actual one. So, one had to introduce other external forces such as the thermal field (through the thermodiffusion), external fluxes, chemical reactions … But a complete picture is hard to achieve, especially in formulating the dynamic of the evolution of the compositional profile, even if some recent improvement has been performed [1-2].

One system of interest to improve the species distribution estimation in a reservoir is the one where only gravitational and geothermal (through thermodiffusion) forces modify the composition profile in a convection free configuration. In such situation, generally, these two forces induce opposite effects on the distribution of the species along the reservoir. This is the case for instance when linear alkanes are involved. Gravity tends to increase the longest chains concentration in the bottom of the reservoir whereas the effect of thermodiffusion is opposite (because temperature increases with depth).

In this work, for the first time ever to the best of our knowledge, it is proposed to use molecular dynamics (MD) simulations on Lennard-Jones spheres in order to study gravitational segregation in non-isothermal "isotopic" fluids (thermogravitation) i.e. analyse the coupling between the gravity field and thermodiffusion influences on the composition profiles in simple mixtures.
Such a molecular dynamics approach is interesting at three levels:

- first, it does not assume the underlying formalism to describe this process and so allows a true "test" of the phenomelogical macroscopic theory usually applied.
- second, it permits the description of not only the stationary state but also the transient toward this state (which is not possible using equilibrium thermodynamic models).
- third, because of the vertical size involved (typically ten nanometers), even when heating strongly from below, the Rayleigh number is always largely smaller than its critical value i.e. the fluid column remains always in a purely diffusive regime (no convection occur).

2 Theory and Modelling

2.1 Non-isothermal gravitational segregation

When an isothermal fluid mixture is subject to the gravity field, directed along the *z*-axis, after a transient state (with, *a priori*, a characteristic time associated to the mass diffusion coefficient), at equilibrium the distribution of the species *i* can be obtained using [3]:

$$\frac{d\mu_i}{dz} = M_i g \tag{1}$$

where μ_i is the chemical potential, M_i the molecular weight and g the gravitational acceleration.
In a binary "ideal" mixture ($\mu_1 = RT \ln x_1 + const$, where T is the temperature and x_1 the molar fraction of component 1), assuming that the pressure gradient, dp/dz, is equal to the hydrostatic one ρg, we have simply:

$$\frac{d\mu_1}{dz} = \frac{\partial \mu_1}{\partial p}\frac{dp}{dz} + \frac{\partial \mu_1}{\partial x_1}\frac{dx_1}{dz} = \left(x_1 M_1 + x_2 M_2\right) g + \frac{RT}{x_1}\frac{dx_1}{dz} \tag{2}$$

Combining eqs (1) and (2) leads to:

$$\frac{g}{RT}\left(M_2 - M_1\right)dz + \frac{dx_1}{x_1\left(1 - x_1\right)} = 0 \tag{3}$$

which allows to determine the equilibrium isothermal concentration profiles.

When the system is subject to a thermal gradient along the z axis (but non convective), one should take into account an extra term due to thermodiffusion in eq. (3) which leads, at equilibrium, the following relation:

$$\frac{g}{RT}\left(M_2 - M_1\right)dz + \frac{dx_1}{x_1\left(1 - x_1\right)} - \frac{\alpha_T}{T}dT = 0 \tag{4}$$

where α_T is the thermal diffusion factor (=TD_{12}/D_T, where D_{12} and D_T are respectively the mutual diffusion and the thermal diffusion coefficients). Assuming that α_T does not depend on x_1 and T which is acceptable in "isotopic" mixtures [4], and that g is constant, after integration of eq. (4), one arrives to an explicit formulation of the non isothermal equilibrium molar fraction in function of the depth relatively to a reference (noted with a superscript 0):

$$x_1 = \frac{\frac{x_1^0}{1-x_1^0}\exp\left[\frac{g}{RT^0}(M_1 - M_2)(z - z^0) + \alpha_T \ln\frac{T}{T^0}\right]}{1 + \frac{x_1^0}{1-x_1^0}\exp\left[\frac{g}{RT^0}(M_1 - M_2)(z - z^0) + \alpha_T \ln\frac{T}{T^0}\right]} \quad (5)$$

2.2 Molecular dynamics

To describe interaction between fluid particles (spheres), the classical truncated Lennard-Jones 12-6 potential has been used, $U_{LJ} = 4\varepsilon\left[(\sigma/r)^{12} - (\sigma/r)^6\right]$, where σ is the distance at which the potential is equal to zero (the "atomic diameter"), ε the potential depth and r the intermolecular distance. A cutoff radius equals to 2.5σ has been used. For sake of simplicity, in the following, all variables have been expressed in reduced units, noted with a star as superscript, using ε as the energy scale, σ as the length one and M as the mass one.

The simulation box is noncubic (L_x^*=L_y^*=10 and L_z^*=30) and contains 1800 particles. Two smoothly repulsive walls (using a WCA potential) are located at both ends along the z direction (z-axis is oriented downward) and periodic boundary conditions are applied along x and y directions. A timestep of 0.004 with the velocity Verlet algorithm have been used. To maintain the overall temperature a Berendsen thermostat has been applied.
To induce the gravitational segregation, first the system is equilibrated without external field, then, during 10^4 timestep the gravity acceleration is progressively increased from zero to its final value. Finally, discarding the transient state (roughly 10^7 timesteps), under a constant gravity field (and temperature gradient when applied) data have been collected during very long runs of 1.5-5 10^7 timesteps. The temperature gradient is imposed by applying a Gaussian thermostat at the desired temperatures at both end of the simulation box (along z-axis). The analysis of the various profile is done by divided the simulation box into 20 slabs perpendicularly to the z-axis, discarding the four slabs located near the walls (number 1,2 and 19,20) where the system is perturbed both by the walls presence and the thermostatisation.

All simulations have been performed at, on average, T^*=2.0 and ρ^*=0.64 (in the bulk), which corresponds to a dense supercritical fluid consistent with thermodynamic conditions encountered in petroleum reservoirs.

3 Results and Discussion

3.1 Gravitational segregation

The first step of this work is to verify that the proposed MD procedure yields the correct final equilibrium distribution, compared to eq.(5), in a binary isothermal equimolar "isotopic" mixture (σ_1=σ_2, ε_1=ε_2, M_2/M_1=10) subject to a gravitational field. To do so, MD

simulations have been performed for various values of the external field, g^*=0.01, 0.02, 0.04, 0.08, 0.16, 0.32. Results are shown on figure 1.

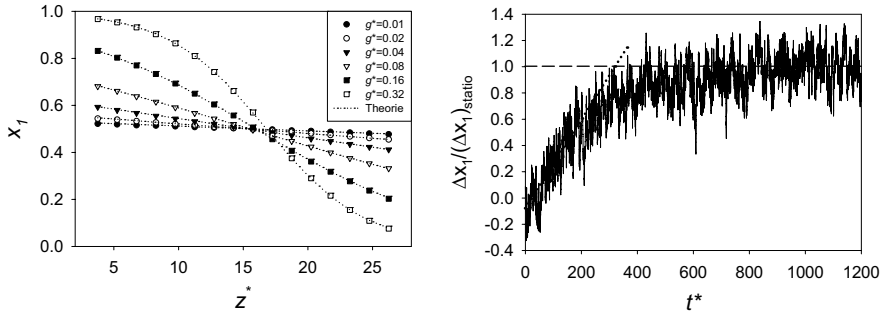

Fig. 1: *Right, comparisons between MD and theoretical, eq.(5), molar fraction profiles when segregated along the vertical extension for various external gravity field amplitude. Left, concentration evolution in a binary equimolar "isotopic" mixture during segregation.*

As expected, because of segregation, in all cases the lightest species, component 1, is enriched at the top of the column (smallest values of z^*), see figure 1. In addition, as it appears clearly from figure 1 (left), the MD procedure proposed here is able to yield the correct equilibrium vertical distribution of the species compared to the theory (eq. (5) with α_T=0). This is the case even for huge gravity fields where a non linear molar fraction distribution appears.

Concerning the gravitational characteristic time, the evolution of the difference between the molar fraction at $L_z^*/4$ and at $3L_z^*/4$, for g*=0.08, is shown on figure 1 (right). From this figure it can be estimated that the characteristic time is of the order of 300. This value is consistent with the mass diffusion characteristic time [5] estimated from $L_z^{*2}/\left(\pi^2 D_{12}^*\right)$, which yields 258.5. Thus, this result confirms that the characteristic time of gravitational segregation is related to the mass diffusion one, even if the precise dynamic should be studied further.

3.2 Thermogravitation

For the same equimolar configuration than above, with g^*=0.02, the influence of a thermal gradient (through the thermodiffusion) has been analyzed. To compare the concentration profiles obtained by MD with those predicted by eq. (5), the thermal diffusion factor has been estimated using the correlation provided in ref. [4] which yields α_T=2.085. So, for different ΔT^* between the two walls (ΔT^* is positive when the system is heated from below), the concentration profiles have been computed by MD simulations and are shown on figure 2.

It should be mentioned that for the largest ΔT^*, the Rayleigh number ($\alpha^* g^* L_z^{*3} \Delta T^* / (\upsilon^* \kappa^*)$, where α^* is the thermal expansion coefficient, ν^* the kinematic viscosity and κ^* the thermal diffusivity) is of the order of 25. This value is roughly two orders of magnitude below its critical value, and therefore all systems studied here are in a diffusive regime (stable without convection).

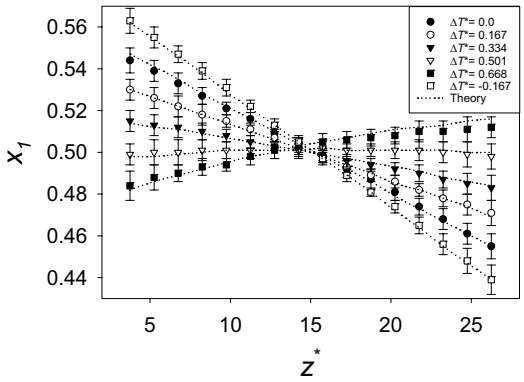

Fig. 2: *Comparisons between MD and theoretical, eq.(5), molar fraction profiles when segregated along the vertical extension for various external thermal field.*

It is worth to note that, from the results shown on Fig. 2, MD results are consistent with those yielded by eq. (5) whatever the external thermal field. In addition, for this mixture, because of the opposite effects of the two external fields (gravitational and thermal), it is possible to obtain a nearly homogeneous systems when $\Delta T^* = 0.501$, and even a system where the top of the column is enriched in the heaviest species due to thermodiffusion!

Nevertheless, it should be mentioned that a usual geothermal gradient of 0.03K/m, would correspond to ΔT^*=0.068 in this study (two times less than the lowest value tested). Thus, it seems that the thermodiffusion effect only due to the mass effect between species may only slightly affect the vertical distribution of the component in a petroleum reservoir. However, the situation may be different in systems close to critical conditions (where thermodiffusion diverge) and in more complex mixtures.

4 Conclusions

In this work, a simple scheme is proposed to study gravitational segregation (isothermal or not) thanks to MD simulations on LJ spheres. For an isothermal binary equimolar "isotopic" mixture (M_2/M_1=10), it is shown that the scheme proposed is able to yield the correct equilibrium distribution (enrichment of the lighter species at the top) when compared to the macroscopic theory, even under extreme gravity field. In addition, it is

shown that the gravitational segregation characteristic time seems to be related to the mass diffusion one.
In non isothermal "isotopic" systems, where thermodiffusion occurs, it is shown that the MD simulations results of the concentration profile at equilibrium can be well described by the theory and that, because of thermodiffusion, under extreme thermal gradient the heaviest species can be enriched at the top of the column.

References

[1] F. Montel, J. Bickert, A. Lagisquet and G. Galliero, J. Pet. Sci. and Eng. **58**, 391 (2007).

[2] H. Nasrabadi and A. Firoozabadi, SPE 95804 (2005).

[3] A. Firoozabadi, *Thermo. of Hydrocarbon Reservoirs*, McGraw-Hill, New York (1999)

[4] G. Galliero, M. Bugel and B. Duguay, J. of NonEqui. Thermo. **32**, 251 (2007).

[5] S.R. de Groot, P. Mazur, *Non-Equilibrium Thermodynamics*, Dover, New-York, 1984.

Single particle thermodiffusion by molecular dynamics simulations: application to simple Lennard-Jones mixtures and nanofluids

Guillaume Galliero[1], Sebastian Volz[2]

[1] *Laboratoire des Fluides Complexes (UMR-5150), Université de Pau et des Pays de l'Adour, BP 1155, F-64013 PAU Cedex, France.*
[2]*Laboratoire d'Energétique Moléculaire et Macroscopique, Combustion, Ecole Centrale Paris, Grande Voie des Vignes, F-92295 Chatenay-Malabry Cedex, France*

E-mail: guillaume.galliero@univ-pau.fr

Abstract

A new scheme is proposed to compute single particle (infinite dilution) thermodiffusion in model systems using Non-Equilibrium Molecular Dynamics simulations through the estimation of the thermophoretic force that applies on a solute particle. This approach enables, assuming a Stokesian behavior of the system, the direct knowledge of the single particle thermal diffusion factor which is not accessible using standard Molecular Dynamics schemes. For one liquid and one supercritical state, this scheme is shown to provide consistent results for simple "isotopic" Lennard-Jones fluids (m_1/m_2=10), even if, for such systems, the underlying assumptions are questionable. In addition, this new Molecular Dynamics scheme is applied to nanofluids (spherical non-metallic nanoparticles + Lennard-Jones fluid) and is shown to provide results in agreement with extrapolation from finite concentrations results. In addition, for such model nanofluids, it is shown that nanoparticles tend to migrate towards the cold areas, whatever the concentration, and that the thermodiffusion amplitude decreases with nanoparticles concentration for both nanoparticles sizes tested.

1 Introduction

Among the possible alternatives to improve the modeling and the knowledge of the microscopic mechanisms underlying the thermodiffusion process is the use of molecular dynamics (MD) simulations on model systems. Such an approach has already proved its efficiency, at least concerning the microscopic mechanism responsible of thermodiffusion on rather simple systems [1-4]. Nevertheless, thermodiffusion in dilute systems (infinite dilution), which is of high relevance for the modeling because it reduces considerably the complexity of the problem, is not directly accessible by molecular dynamics simulations. This is mainly due because of the too poor statistics in such systems when using usual equilibrium or non-equilibrium MD algorithms. In addition, when the solute particle is large compared to those of the solvent, as it is the case in macromolecular systems (polymer solution, colloids …), the mass diffusion process becomes particularly slow. So, in addition to the intrinsic limitations of the system sizes accessible by MD (10^4-10^5 atoms at most), the simulation duration needed to perform the computation of thermodiffusion using MD becomes too large ($>10^7$ timesteps) and so inaccessible

Therefore, in this work, the main aim is to provide a new MD procedure to allow the computation of infinite dilution (single particle) thermodiffusion in a reasonable amount of CPU time. The new non equilibrium molecular dynamics (NEMD) scheme, called Single Particle Thermodiffusion Algorithm (SPTA), relies on the estimation of the thermophoretic force on a solute particle induced by a fluid subject to a thermal gradient. This enables, assuming a Stokesian behavior of the system, the direct knowledge of the single particle thermal diffusion factor. This scheme is first applied on simples Lennard-Jones (LJ) mixtures and second on model nanofluids and compared to what can be extrapolated from finite molar fraction results using a classical NEMD approach [5].

2 Theory and Modelling

2.1 Fluid/nanoparticles description

To model the fluid-fluid interaction, the usual truncated Lennard-Jones 12-6 (LJ) potential is used on spheres:

$$U_{ij}^{LJ} = 4\varepsilon\left[\left(\frac{\sigma}{r_{ij}}\right)^{12} - \left(\frac{\sigma}{r_{ij}}\right)^{6}\right] \tag{1}$$

where σ is the distance at which the potential is equal to zero (the “atomic diameter”), ε the potential depth and r_{ij} the distance between atoms i and j.

The nanoparticles, when present, are modelled by quasi-spheres composed of atoms, having the same molecular parameters than those of the solvent, distributed on a FCC crystal. Nanoparticle atoms are linked to their nearest neighbours through a Finite Extensible Nonlinear Elastic (FENE) bonding potential:

$$U_{ij}^{FENE} = -0.5\kappa R_0^2 \ln\left[1-\left(\frac{r_{ij}}{R_0}\right)^2\right] \quad (2)$$

where R_0 is a finite extensibility and κ a spring constant. In this work the FENE parameters were set to R_0=1.5σ and κ=30ε/σ^2.

2.2 Single Particle Thermodiffusion

Let us consider a single particle (solute) in a fluid (solvent) subjected to an established thermal gradient. If we assume that this particle experiences a thermophoretic forces, $\mathbf{F}_T$, linearly related to the temperature gradient, and that the velocity drift, $\mathbf{v}_T$, induced by this force is small enough (and related to a Stokes drag), it is possible to deduce that [6]:

$$\mathbf{v}_T = \frac{\mathbf{F}_T}{\xi} \quad (3)$$

where ξ is the friction coefficient.

Moreover, if we assume that a Stokes-Einstein law relates the single particle mass diffusion, D_{12}^{SP}, and the friction, we can deduce that the single particle thermal diffusion factor, α_T^{SP}, in such systems can be expressed as:

$$\alpha_T^{SP} = -\frac{\mathbf{F}_T}{k_B \nabla T} \quad (4)$$

Such an expression implies that the measurement of the thermophoretic force acting on the particle for a given thermal gradient provides a straightforward estimation of the thermal diffusion amplitude in such dilute systems.

In order to measure the thermophoretic force, $\mathbf{F}_T$, acting on the particle using molecular dynamics simulations, a simple scheme, described on Fig. 1, is proposed.

First, an initial system composed of two particles and the fluid is constructed. The two particles are centred at L_x/4 and 3L_x /4, L_x being the size along x of the simulation box. These two particles are attached to the reference frame of the simulation box thanks to a harmonic potential. Then, the Non Equilibrium MD scheme proposed in Ref. [2] is used to generate a bi-periodical thermal gradient in the simulation box in the direction x.

After a transient state, the location of the centres of mass of the two particles will be displaced relatively to their point of fixation because of the thermophoretic force induced by the thermal gradient in the fluid. The measure of this displacement for both particles, Δx, provides a direct estimation of the amplitude of the thermophoretic force.

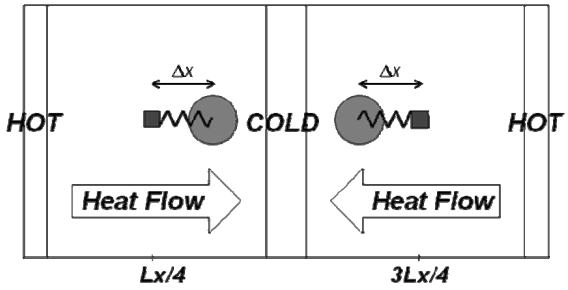

Fig. 1: *Scheme of the proposed setup to measure the thermophoretic force that applies on nanoparticles in a nonisothermal fluid.*

3 Results and Discussion

3.1 Lennard-Jones mixture

The first mixture tested is composed of species having the same molecular parameters except that m_1/m_2=10 (isotope like mixtures) i.e. ideal ones in the thermodynamic sense. Two thermodynamic conditions have been studied, one corresponding to a dense liquid at T^*=1 and ρ^*=0.8 and the second one to a dense supercritical gas at T^*=1.686 and ρ^*=0.477.

Results shown on figure 1 clearly reveal that, the proposed approach to compute the single particle values of α_T is consistent with what could be extrapolated from the values obtained by classical NEMD simulations for both molar fraction limits ($x_1 \rightarrow 0$ and $x_1 \rightarrow 1$) and for both states (with perhaps a slight underestimation). This is rather surprising as long as the underlying assumptions leading to eq. (4) are valid, *a priori*, only for a solute particle large compare to that of the solvent, which is not the case here (they have the same size), and only for the liquid state.

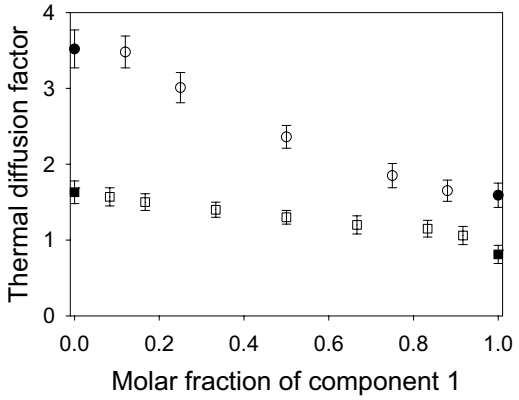

Fig. 2: *α_T in "isotopic" LJ mixtures for two states (○ :T^*=1, ρ^*=0.8, □ : T^*=1.686, ρ^*=0.477). Open symbols have been obtained using a usual NEMD approach* [4] *and full symbols through the SPTA.*

3.2 Nanofluids

To test the validity of the SPTA when applied on nanofluids, have been simulated various nanoparticles volume fraction for d_{NP}/σ=2.4 and 4.03, where d_{NP} is the nanoparticle diameter, at T^*=1 and P^*=1 (dense liquid).

The first interesting result is that, see Fig. 3, for such model nanofluids, in all cases the thermal diffusion factor, α_T, is positive which means that nanoparticles tend to migrate toward the cold areas relatively to the solvent. Furthermore, it appears that the amplitude of thermodiffusion tends to decrease with the concentration of the nanoparticles without any sign change for the concentrations accessible.

In addition, results provided on Fig. 3 confirm that the proposed SPTA is able to provide an estimation of α_T^{SP} which is consistent with what could be extrapolated from classical NEMD results and therefore enables the estimation of single particle thermodiffusion for larger nanoparticles. This is true even if it seems, as in the LJ mixture, see Figs. 2-3, that the SPTA values slightly underestimate extrapolated values. This possible underestimation may come from the fact that for very low concentration α_T becomes independent of concentration as particles do not see each other (reaching a plateau) or because of a weakness in the underlying theory [7].

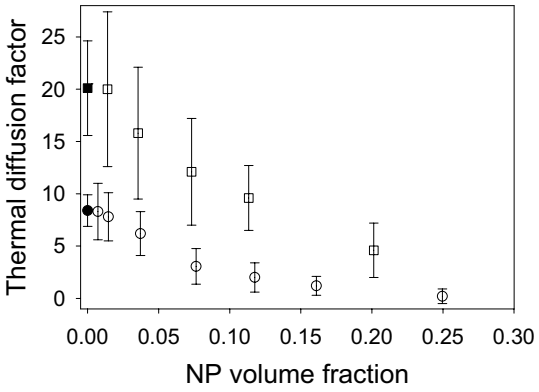

Fig. 3: *α_T versus nanoparticles volume fraction for two nanoparticle sizes (○: d_{NP}/σ = 2.4, □: d_{NP}/σ = 4.03). Open symbols have been obtained using the usual NEMD approach and full symbols through the SPTA.*

4 Conclusions

In this work, we provide a new simple scheme to compute, using Non Equilibrium Molecular Dynamics simulations, the single particle (infinite dilution) thermal diffusion factor in fluids which is not accessible in a reasonable amount of time using standard MD schemes.

By a comparison with extrapolations from finite concentration results using standard NEMD simulations, this scheme is shown to be efficient for "isotopic" Lennard-Jones binary mixtures for one liquid and one supercritical state (for which the underlying theory does not apply *a priori*) as well as in model nanofluids. These last being described by a LJ fluid + quasi-spherical nanoparticles composed of atoms distributed on a FCC crystal and interacting through LJ potential plus FENE bonding with the nearest neighbours.

In addition, for such nanofluids, it appears that, first, whatever the concentration, nanoparticles tend to migrate towards the cold areas, and that the thermodiffusion amplitude decreases with nanoparticles concentration for both nanoparticles sizes tested.

Acknowledgment

We gratefully acknowledge computational facilities provided by TREFLE laboratory, which supercomputer has been financially supported by the Conseil Régional d'Aquitaine.

References

[1] B. Hafskjold, T. Ikeshoji and S. Ratkje, Mol. Phys. **80**, 1389 (1993).

[2] P. Bordat, D. Reith and F. Müller-Plathe, J. Chem. Phys. **115**, 8978 (2001).

[3] G. Galliero, Fluid Phase Equi. **224,** 13 (2004).

[4] P.A. Artola and B. Rousseau, Phys. Rev. Let. **98**, 125901 (2007).

[5] G. Galliero, B. Duguay, J.-P. Caltagirone and F. Montel, Phil. Mag. **83**, 2097 (2003).

[6] G. Galliero and S. Volz, J. Chem. Phys. **38**, 064505 (2008).

[7] E. Brinquier and A. Bourdon, Physica A **385**, 9 (2007).

Schriften des Forschungszentrums Jülich
Reihe Schlüsseltechnologien / Key Technologies

1. **Soft Matter**
   From Synthetic to Biological Materials
   Lecture manuscripts of the 39th IFF Spring School March 3 – 14, 2008
   Jülich, Germany
   edited by J.K.G. Dhont, G. Gompper, G. Nägele, D. Richter, R.G. Winkler (2008),
   c. 1000 pages
   ISBN: 978-3-89336-517-3

2. **Structural analysis of diblock copolymer nanotemplates using grazing incidence scattering**
   by D. Korolkov (2008), III, 167 pages
   ISBN: 978-3-89336-522-7

3. **Thermal Nonequilibrium**
   Lecture Notes of the 8th International Meeting on Thermodiffusion,
   9 – 13 June 2008, Bonn, Germany
   edited by S. Wiegand, W. Köhler, J.K.G. Dhont (2008), 300 pages
   ISBN: 978-3-89336-523-4

Solid State Research

Institute of Solid State Research

Institut für Festkörperforschung

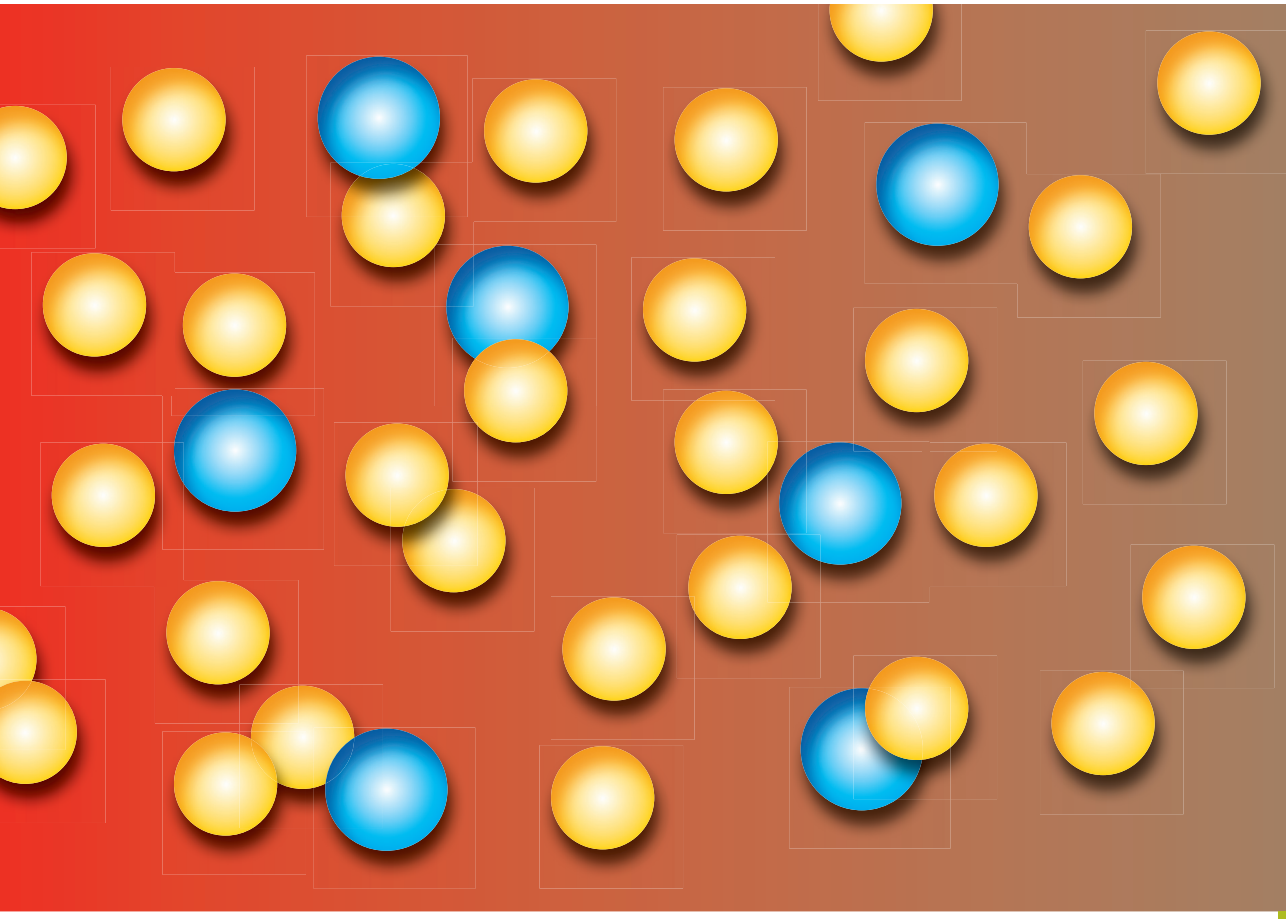

UNIVERSITÄT BAYREUTH

JÜLICH FORSCHUNGSZENTRUM

Band | Volume 3
ISBN 978-3-89336-523-4